UNIVERSITÉ DE STRASBOURG

ÉCOLE DOCTORALE DES SCIENCES CHIMIQUES

Laboratoire de Chimie Moléculaire, UMR 7509
Laboratoire d'Innovation Moléculaire & Applications, UMR 7042

THÈSE

présentée par :

Angéline CHERBONNEL

soutenue le : **02 février 2018**

pour obtenir le grade de : **Docteur de l'université de Strasbourg**

Discipline/ Spécialité : Chimie / Chimie Analytique

Study of the Mechanism of Action of Metallic Active Oxygen Barriers Applied in Polymers for Food and Drinks Preservation

THÈSE dirigée par :

M. ELHABIRI Mourad	Directeur de Recherches, Université de Strasbourg

RAPPORTEURS :

M. SIRI Olivier	Directeur de Recherches, Aix-Marseille Université
M. TRIPIER Raphaël	Professeur, Université de Bretagne Occidentale

---

AUTRES MEMBRES DU JURY :

M. DECORTES Antonello	Docteur, Clariant
Mme HUBSCHER Véronique	Professeur, Université de Strasbourg
M. SAHL Mike	Docteur, Clariant
Mme VICTORIA RODRIGUEZ Maria	Docteur, Clariant

UNIVERSITÉ DE STRASBOURG

ÉCOLE DOCTORALE DES SCIENCES CHIMIQUES

Laboratoire de Chimie Moléculaire, UMR 7509
Laboratoire d'Innovation Moléculaire & Applications, UMR 7042

THÈSE

présentée par :

Angéline CHERBONNEL

soutenue le : **02 février 2018**

pour obtenir le grade de : **Docteur de l'université de Strasbourg**

Discipline/ Spécialité : Chimie / Chimie Analytique

Study of the Mechanism of Action of Metallic Active Oxygen Barriers Applied in Polymers for Food and Drinks Preservation

THÈSE dirigée par :	
M. ELHABIRI Mourad	Directeur de Recherches, Université de Strasbourg
RAPPORTEURS :	
M. SIRI Olivier	Directeur de Recherches, Aix-Marseille Université
M. TRIPIER Raphaël	Professeur, Université de Bretagne Occidentale

---

AUTRES MEMBRES DU JURY :	
M. DECORTES Antonello	Docteur, Clariant
Mme HUBSCHER Véronique	Professeur, Université de Strasbourg
M. SAHL Mike	Docteur, Clariant
Mme VICTORIA RODRIGUEZ Maria	Docteur, Clariant

Remerciements

Je tiens tout d'abord à remercier les membres du jury qui ont accepté de juger mon travail de thèse : le **Dr. Olivier SIRI** (Aix-Marseille Université), le **Pr. Raphaël TRIPIER** (Université de Bretagne Occidentale) et le **Pr. Véronique HUBSCHER** (Université de Strasbourg).

Je tiens ensuite à remercier particulièrement mon encadrant, le **Dr. Mourad ELHABIRI**, qui m'a donné l'occasion de réaliser ma thèse au sein du laboratoire et de travailler sur un projet multidisciplinaire très enrichissant. Je souhaite également le remercier pour ses conseils, son temps, son aide, et nos discussions toujours intéressantes et enrichissantes. Merci également de m'avoir laissé la possibilité d'enseigner, d'encadrer deux stagiaires et de participer à des congrès.

Je souhaite également remercier le **Dr. Elisabeth DAVIOUD-CHARVET**, responsable de l'équipe de Chimie Bio(in)organique et Médicinale, de m'avoir accueillie dans son équipe pour mon stage de Master 2 puis pour réaliser ma thèse. Merci également à tous les stagiaires, doctorants, post-doctorants que j'ai pu croiser au laboratoire : **Didier**, **Don Antoine**, **Elena**, **Didier**, **Max**, **Jérémy**, **Saravanan**, **Gwen**, **Xavier**, **Sabah**, **Parastoo**, **Malika**, **Aurélia**, **Birgit**, **Jose**, **Mouhamad**, **Liwen**, **Leandro** ; ainsi que **Maxime** et **Mickaël**, même si on n'a pas eu beaucoup le temps de se connaître. Je tiens à remercier particulièrement les personnes qui ont travaillé avec moi sur ce projet :

- le **Dr. Dhanya JINO** ;
- **Hasret DOGANAY**, que j'ai encadré lors de son stage de D.U.T. Chimie ;
- **Nicolas PYTHOUD** qui a réalisé son stage de fin d'études sur ce projet. Merci pour tout le travail réalisé mais surtout pour ta bonne humeur tous les jours au labo.

Cette thèse a été réalisée dans le cadre d'une collaboration industrielle entre le CNRS et la société Clariant. I would like to warmly thank Clariant members, who were involved in this project, and with whom I had the chance to work and to have very interesting discussions: **Dr. Pascal STEFFANUT**, who initiated the collaboration for my master internship; **Dr. Angelica MARSON**, who was leading this project for months during my Ph.D.; **Dr. Thierry MULLER**, for his knowledge in organic and inorganic chemistry; **Dr. Jan SUELTEMEYER**, who is the head of Global Innovation and I had the chance to meet; and finally the three remaining Clariant members involved in the collaboration at the end of my Ph.D. : **Dr. Mike SAHL**, **Dr. Maria VICTORIA RODRIGUEZ**, **Dr. Antonello DECORTES**. Thank you for our interesting discussions, your advices.

Je tiens également à remercier toutes les personnes avec qui j'ai pu travailler lors de cette thèse et qui m'ont apporté leur aide pour mener à bien ce projet :

- Le responsable de la plateforme d'analyses de l'UMR : **Matthieu CHESSE** (LIMA, Université de Strasbourg). Merci de m'avoir laissé la possibilité d'utiliser à souhait l'infra-rouge et la LC-MS.
- Le service commun d'analyses élémentaires, mesures physiques et spectroscopie de l'Université de Strasbourg, et plus particulièrement **Noémie BOURGEOIS** (Institut de Chimie) pour les microanalyses élémentaires.
- Le **Dr. Sylvie CHOUA** (Institut de Chimie, Université de Strasbourg), pour les analyses RPE. Merci de m'avoir fait découvrir cette technique d'analyse, et de m'avoir fait assister aux mesures ainsi qu'aux traitements de résultats.
- Le **Dr. Geneviève POURROY** (IPCMS, Université de Strasbourg) et le **Dr. François ROULLAND** (IPCMS, Université de Strasbourg) de m'avoir permis d'utiliser la tamiseuse ainsi que le granulomètre de leur laboratoire.
- Le service commun de spectroscopie de masse de l'Université de Strasbourg ainsi qu'**Estelle MOTSCH** (Institut de Chimie) pour tous ses conseils lors de l'utilisation et la maintenance du spectromètre de masse.

- Le responsable de la résonance magnétique nucléaire au sein de l'unité : **Dr. Emeric WASIELEWSKI** (LIMA, Université de Strasbourg).
- Le **Dr. Anne HEBRAUD** et **Céline PIRAS** (ICPEES, Université de Strasbourg) ainsi que le **Dr. Mélanie LEGROS** et **Catherine FOUSSAT** (ICS, Université de Strasbourg) pour les analyses de chromatographie d'exclusion stérique.
- **Thierry ROMERO** (ICPEES, Université de Strasbourg) pour les images obtenues par microscopie électronique à balayage.
- Le **Dr. Vasiliki PAPAEFTHYMIOU** (ICPEES, Université de Strasbourg) pour les analyses par spectrométrie photoélectronique X.

Après avoir passé toutes ces années à Strasbourg, comment ne pas parler de tous les amis rencontrés à l'ECPM : **Antoine M.**, **Antoine V.**, **Audrey**, **Chloé**, **Clément, Eric M.**, **Flo**, **Franck**, **Gwen**, **Julien, Lara**, **Quentin**, **Sam**, **Sarah**, **Vincent**. Même si la distance nous a éloignés pendant la thèse avec certains d'entre vous, c'est toujours un plaisir de se retrouver pour faire la fête !!! Merci à Quentin et Chloé pour leur soutien au quotidien ! Merci aux Strasbourgeois/Colmariens pour les soirées en tout genre (coinche, pétanque, jeux, ou juste une grosse soirée) pour décompresser !!!

Je tiens également à remercier **Daisy**, **Elodie**, **Laurence** et **Marie**, mes amies du lycée avec qui j'ai gardé contact malgré la distance pendant toutes ces années. C'est toujours un plaisir de se retrouver autour d'une galette (ou autre) et j'espère que ça continuera comme ça. Merci également à **Nico & Lucie** pour leur amitié malgré la distance.

Je souhaite également remercier ma famille, **mes parents** et **Thibaud**, mon frère dont le soutien m'a été indispensable pour réaliser mes études. Merci à eux d'avoir accepté mes choix.

Enfin, je souhaite à remercier **Eric**, qui partage ma vie depuis un petit bout de temps maintenant. Merci pour ton soutien avant et surtout pendant la thèse. Merci pour tes conseils avisés, nos discussions, ton aide (surtout pendant la rédaction, malgré la distance). Ça n'a pas toujours été facile mais on a réussi ensemble. Tu espérais pouvoir m'aider autant que je l'avais fait pour ta thèse, et tu l'as largement fait ! Merci pour tout !!!

Table of Contents

Abbreviations..1

Résumé en français 7

General introduction 35

I. Food products packaging: a problematic since the ancient times 41

I.1. A brief history of the food packaging materials 41

I.1.1. Main functions of the food packaging materials 42

I.1.2. Plastic packaging: modulating properties for food and drinks preservation 43

I.2. An innovative solution: active packaging 49

I.2.1. A key parameter for an adequate goods preservation: oxygen barriers.......................50

I.2.1.1. Iron-based oxygen scavengers.. 51

I.2.1.2. Acid ascorbic-based oxygen scavengers 52

I.2.1.3. Enzyme-based oxygen scavengers.. 52

I.2.1.4. Photosensitive dye-based oxygen scavengers.. 53

I.2.1.5. Ethylenic-unsaturated hydrocarbons-based oxygen scavengers 54

I.2.1.6. Polymers-based oxygen scavengers 54

I.2.2. Metal complexes: a key role in the polymers-based oxygen barriers 57

I.2.2.1. Metal centres and their oxygenation properties... 57

I.2.2.2. Influence of ligand design on oxygenation 58

I.3. Metal complexes and organic/polymeric additives: on the way to a deeper understanding of the mechanism of action of metal oxygen barriers 63

II. Synthesis, characterization & physico-chemical investigation of the metal catalysts 71

II.1. A plethora of analytical tools to unravel the physico-chemical properties of the ligands and the metal complexes 71

II.2. Synthesis, stability and protonation constants of the Schiff base ligands 72

II.2.1. Preparation of the ligands 72

II.2.2. Stability of the ligands in solution under acidic and basic conditions 74

II.2.3. Protonation constants of the Schiff base ligands 79

II.3. Synthesis and physico-chemical properties of the metal complexes 82

II.3.1. Preparation of the cobalt(II) and manganese(II) complexes 82

II.3.1.1. Classical strategy.. 82

II.3.1.2. Innovative strategy 85

II.3.1.3. Characterization of commercially available complexes.. 86

II.3.2. Affinity of the different Schiff base ligands with cobalt(II) and manganese(II) 91

II.4. Oxygenation/activation properties of the metal catalysts 94

II.4.1. Oxygenation/activation monitored by absorption spectrophotometry 94
II.4.2. Oxygenation/activation monitored by oximetry coupled to UV-visible absorption 96
II.4.3. Oxygenation/activation monitored by ESI-MS 101
II.4.4. Oxygenation/activation monitored by ^{1}H NMR 104
II.4.5. Oxygenation/activation monitored by UV-visible absorption spectrophotometry using a chromophoric probe 107
II.4.6. Electrochemical properties of the metal catalysts..111
II.5. Experimental section..116
II.5.1. Analytical equipments used in this study..116
II.5.1.1. Nuclear Magnetic Resonance spectroscopy - NMR.. 116
II.5.1.2. Fourier Transform Infrared Spectroscopy - FTIR 116
II.5.1.3. Liquid Chromatography-Mass Spectrometry Analyses - LC-MS 116
II.5.1.4. Electrospray Ionization-Mass Spectrometry analyses - ESI-MS............................ 117
II.5.1.5. Automated potentiometry.. 117
II.5.1.6. UV-visible absorption spectrophotometry coupled to potentiometry 119
II.5.1.7. UV-visible absorption spectrophotometry 120
II.5.1.8. UV-visible absorption spectrophotometry with DPPH 120
II.5.1.9. Oximetry 121
II.5.1.10. Electrochemistry 123
II.5.1.11. Microanalysis 124
II.5.1.12. High Resolution Mass Spectrometry - HRMS... 125
II.5.1.13. Electron Paramagnetic Resonance spectroscopy - EPR..................................... 125
II.5.2. Synthesis and characterization of the ligands and metal catalysts 125
II.5.2.1. Synthesis and characterization of the ligands 125
II.5.2.2. Synthesis and characterization of the metal complexes 130
III. Oxidation of organic additive models 151
III.1. Oxidation of substrates with either metal catalysts or strong oxidants 151
III.1.1. Metal-catalysed aerobic oxidation 151
III.1.1.1. Acetylacetonate complexes.. 152
III.1.1.2. Schiff bases complexes 153
III.1.1.3. Stearate complexes.. 155
III.1.2. Oxidation of organic additives of interest 155
III.2. Absorption spectrophotometry: a tool to monitor the oxidation of organic additives by oxidants 156
III.2.1. Oxidation of additives with H_2O_2 and TBHP 156
III.2.2. Another alternative for the oxidation of the additives 157
III.2.2.1. Synthesis of the oxidized additives with meta-chloroperoxybenzoic acid 159

III.2.2.2. Oxidation of additives with m-CPBA: kinetics monitoring by absorption spectrophotometry ... 161

III.3. Assisted-oxidation of organic additives with metal complexes ... 164

III.4. Experimental section ... 165

III.4.1. Analytical equipments used in this study ... 165

III.4.1.1. Nuclear Magnetic Resonance spectroscopy - NMR ... 165

III.4.1.2. Electrospray Ionization-Mass Spectrometry - ESI-MS ... 165

III.4.1.3. UV-visible absorption spectrophotometry ... 165

III.4.1.4. Microanalysis ... 166

III.4.1.5. Electron Paramagnetic Resonance spectroscopy - EPR ... 166

III.4.2. Oxidation of organic additive models by strong oxidants (H_2O_2, TBHP) monitored by UV-visible absorption spectrophotometry ... 166

III.4.3. Oxidation kinetics of organic additive models by strong oxidant (*m*-CPBA) monitored by UV-visible absorption spectrophotometry ... 167

III.4.4. Synthesis of the oxidized organic additive models ... 168

III.4.5. Oxidation of organic additive models by metal catalyst ... 172

IV. Polymeric additives oxidation ... 177

IV.1. Analytical approach for polymeric additives oxidation monitoring and selection of metal catalysts ... 178

IV.2. Investigation on Dercolyte S 125 14 oxidation ... 181

IV.2.1. Preliminary investigations of oxidation in the solid state ... 181

IV.2.2. Particle size: a key role on the oxidation process? ... 183

IV.2.2.1. Influence of the additive particle size distribution ... 184

IV.2.2.2. Influence of the catalyst particle size distribution ... 187

IV.2.3. "Extrusion" process: an activation stage for the metal catalysts? ... 188

IV.2.4. Potential coordination of the catalyst along the oxidation process with the oxidized polymeric additive or one of its precursors ... 194

IV.2.5. Catalyst impurities poisoning of the oxidation reaction? ... 195

IV.2.6. Elucidation of the nature of the oxidized product(s) ... 198

IV.3. Study of the oxidation of polyTHF 15 ... 204

IV.3.1. Oxidation of polyTHF 15 monitored by FTIR ... 204

IV.3.1.1. Optimization of the catalyst:additive ratio ... 206

IV.3.1.2. Influence of the temperature on the metal-catalysed oxidation process of 15 ... 207

IV.3.2. Elucidation of the nature of the oxidation product(s) ... 209

IV.4. Experimental section ... 215

IV.4.1. Analytical equipments used in this study ... 215

IV.4.1.1. Nuclear Magnetic Resonance spectroscopy - NMR ... 215

IV.4.1.2. Fourier Transform Infrared spectroscopy - FTIR ... 215

IV.4.1.3. Microanalysis 215

IV.4.1.4. Electron Paramagnetic Resonance spectroscopy - EPR....................................... 215

IV.4.1.5. Laser diffraction granulometry 215

IV.4.1.6. Scanning Electron Microscopy - SEM 216

IV.4.1.7. Size Exclusion Chromatography - SEC... 217

IV.4.1.8. X-ray Photoelectron Spectroscopy - XPS 217

IV.4.2. General experimental protocols for setting up FTIR measurements 218

IV.4.2.1. Preparation of the KBr pellets for FTIR measurements....................................... 218

IV.4.2.2. Use of glass strips for FTIR measurements.. 219

IV.4.2.3. Oxidation of the polymeric additives monitored by FTIR spectroscopy 219

IV.4.2.4. Sieving of the samples 219

IV.4.2.5. Mimicking the “extrusion” process of the samples... 220

IV.4.2.6. Interpretation of the FTIR data... 221

IV.4.3. Setting up of experiments for Dercolyte S 125 14 oxidation monitored by FTIR 221

IV.4.3.1. Preliminary experiments with polymeric additives in the presence of metal catalyst 221

IV.4.3.2. Influence of the particle size distribution of the samples 222

IV.4.3.3. Influence of the “extrusion” process 223

IV.4.3.4. Evaluating whether a coordination of the metal catalyst occurs during the oxidation process with the oxidized polymeric additive or one of its precursors? 225

IV.4.3.5. Influence of the potential impurities arising from the metal catalyst on the oxidation process 226

IV.4.4. Setting up of experiments for the oxidation of the polytetrahydrofuran derivative (polyTHF) additive 15 monitored by FTIR 227

IV.4.4.1. Preliminary experiments with the polymeric polyTHF additive in the presence of metal catalyst.. 227

IV.4.4.2. Influence of the catalyst/additive ratio on the efficiency and speed of the additive oxidation 228

IV.4.4.3. Influence of the temperature on the oxidation process of the polyTHF additive 15 with or without metal catalyst.. 228

IV.4.5. Characterization of the polymeric additives and their oxidation products 229

IV.4.5.1. Characterization of Dercolyte S 125 14 and its oxidation products 229

IV.4.5.2. Characterization of the polyTHF 15 and its oxidation products 231

General conclusion...237

List of molecules 243

Abbreviations

Uncertainty are given in brackets

acac: acetylacetone *or* acetylacetonate

A.D.: *anno Domini* (after Christ)

ar: aryl

asym.: asymmetric

B.C.: before Christ

CV: cyclic voltammetry

δ: NMR chemical shift

d: doublet

Đ: dispersity

DCE: 1,2-dichloroethane

DCM: dichloromethane

dd: doublet of doublets

DET: dynamic equivalent point titration

DMF: dimethylformamide

DMSO: dimethylsulfoxide

DPPH: 2,2-diphenyl-1-picrylhydrazyl

ECE: electron exchange-chemical reaction-electron exchange

EDS: energy dispersive X-ray spectroscopy

EDTA: ethylenediaminetetraacetic acid

E_{pa}: anodic peak potential

E_{pc}: cathodic peak potential

EPR: electron paramagnetic resonance

ESI-MS: electrospray ionisation-mass spectrometry

EtOAc: ethyl acetate

EtOH: ethanol

EVOH: ethylene-vinyl alcohol

FDA: food and drug administration of the USA

FTIR: Fourier transform infrared spectroscopy

HDPE: high density polyethylene

HPLC: high performance liquid chromatography

HRMS: high resolution mass spectrometry

IR: infrared

J: coupling constant

LC-MS: liquid chromatography coupled to mass spectrometry

LDPE: low density polyethylene

m: multiplet

$\overline{\mathrm{M}}\mathrm{n}$: number average molecular weight

$\overline{\mathrm{M}}\mathrm{w}$: weight average molecular weight

m-CPBA: *meta*-chloroperoxybenzoic acid

m/z: mass-to-charge ratio

MeOH: methanol

MET: monotonous equivalent point titration

MS: mass spectrometry

MXD6: poly(*meta*-xylylene adipamide)

NHE: normal hydrogen electrode

NMR: nuclear magnetic resonance

OTR: oxygen transmission rate

PDA: photodiode array detector

PE: polyethylene

PEG: polyethylene glycol

PET: polyethylene terephthalate

pK_a: logarithmic acid dissociation constant

PP: polypropylene

ppm: part per million

PS: polystyrene

PTHF: polytetrahydrofuran

PVC: polyvinyl chloride

PVOH: polyvinyl alcohol

q: quartet

rpm: revolutions per minute

r.t.: room temperature

s: singlet

SCE: saturated calomel electrode

SEC: size exclusion chromatography

SEM: scanning electron microscopy

sym.: symmetric

t: triplet

$t_{1/2}$: half-life time

TBHP: *tert*-butylhydroperoxide

TEMPO: (2,2,6,6-tetramethylpiperidin-1-yl)oxyl

THF: tetrahydrofuran

TMP: 2,2,6,6-tetramethylpiperidine

TMS: trimethylsilane

TOF: time of flight

UV: ultraviolet

v/v: volume/volume

vs.: *versus*

w/w: weight/weight

XPS: X-ray photoelectron spectrometry

Résumé en français

Résumé en français

1. Chapitre I : L'emballage des produits alimentaires : une problématique depuis l'antiquité

1.1. Historique des matériaux utilisés pour l'emballage alimentaire

Suite au développement des civilisations et au début des échanges commerciaux dans la Méditerranée, les matériaux d'emballage ont subi une évolution : aux matériaux les plus rudimentaires (céramiques, amphores et verres) utilisés durant les Empires Grecs et Romains ont été tout d'abord ajoutés l'utilisation de papiers (papyrus et papier Chinois) avant notre ère et jusqu'aux XIV et XV$^{\text{ème}}$ siècles, puis des matériaux plus récents tels que le métal et le plastique découverts au début du XIX$^{\text{ème}}$ siècle.

Les produits alimentaires sont les biens les plus consommés chaque jour et leur emballage représente de nos jours environ 50% en poids des ventes mondiales d'emballage.

Bien que les plastiques demeurent plus ou moins perméables aux gaz et aux vapeurs, ils restent le meilleur compromis pour l'emballage alimentaire, et représentent le matériau le plus utilisé. En effet, ils sont pour la plupart transparents, réutilisables et/ou recyclables, légers et non fragiles. De plus, un grand nombre de différents polymères est actuellement disponible et ce chiffre ne cesse d'augmenter, permettant de moduler à souhait les propriétés de ces matériaux. Enfin, ils présentent des coûts moins élevés et beaucoup d'avantages fonctionnels (thermo-soudables, résistance aux micro-ondes, propriétés optiques, légers, difficiles à casser, formes et tailles non limitées…) en comparaison avec le verre ou le métal. Par ailleurs, les problèmes de perméation des plastiques peuvent être améliorés en modifiant la composition de ces derniers.

Comme démontré précédemment, les plastiques sont les matériaux les plus adaptables (c'est-à-dire, emballages souples ou rigides, modulation de la transparence, des propriétés barrières vis-à-vis des gaz…) ; c'est pour cela que notre intérêt sera particulièrement porté sur ces matériaux dans la suite de cette introduction.

Pour le conditionnement, cinq polymères (des thermoplastiques) sont privilégiés : le polyéthylène (PE) (c'est-à-dire, le polyéthylène basse densité (PEBD) et le polyéthylène haute densité (PEHD)) représentant environ 56% du marché européen de l'emballage ; le polypropylène (PP), le polyéthylène téréphtalate (PET), le polystyrène (PS) et le chlorure de polyvinyle (PVC), représentant à eux quatre les 44% restants (en poids).

Le PE présente une faible transparence ainsi qu'une faible barrière aux gaz, ce qui le rend inapproprié pour l'emballage de produits sensibles aux gaz ou pour des applications nécessitant des emballages transparents. Le PP est également faiblement transparent, mais ses propriétés barrières vis-à-vis des gaz sont améliorées, en comparaison au PE. Le PS a l'avantage d'être transparent mais présente d'autres désavantages : une faible barrière aux gaz ou encore une faible solidité. En comparant maintenant le PET et le PVC, ils sont tous les deux caractérisés par une excellente transparence et des propriétés barrières vis-à-vis de la vapeur d'eau comparables. Cependant, le PET présente une meilleure solidité, des propriétés barrières vis-à-vis des gaz améliorées et un coût moindre.

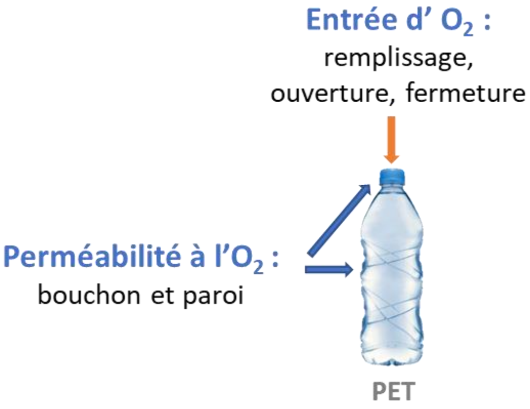

Figure 1 : Voies de pénétration potentielles de l'oxygène.

Il convient de noter que la perméabilité (aux vapeurs, aux gaz) des polymères les plus communs est d'une importance cruciale dans le domaine de l'emballage alimentaire. En effet, la vapeur d'eau et l'oxygène, en particulier, peuvent migrer à travers l'emballage et modifier continuellement l'atmosphère interne du contenant. Bien que le PET présente les meilleures propriétés barrières vis-à-vis des gaz, ce paramètre doit être significativement amélioré. En effet, diverses portes d'entrée pour l'oxygène sont présentes sur une bouteille en plastique. La façon la plus simple pour l'oxygène de pénétrer à l'intérieur est pendant l'ouverture et la fermeture de la bouteille. La deuxième source évidente d'oxygène est représentée par les petites quantités d'oxygène résiduel dans l'espace de tête de la bouteille, durant le remplissage de la bouteille avec les denrées alimentaires, et cela même après le processus d'élimination de l'air. Enfin, la dernière cause est la perméabilité du bouchon et des parois de la bouteille (Figure 1).

Parmi les nombreux gaz qui peuvent pénétrer dans un emballage alimentaire, l'oxygène est responsable de nombreux effets indésirables, qui doivent être évités par l'industrie agro-alimentaire : l'oxydation des lipides ou des graisses, aussi nommée rancissement oxydant des acides gras insaturés, qui conduit à des odeurs indésirables, et dans des circonstances extrêmes, à des produits finaux toxiques ; l'accélération du processus de respiration des fruits et des légumes ; l'apparition d'odeurs de rassissement dans les produits de boulangerie ; l'éclosion d'œufs d'insectes puis leur croissance ; l'oxydation des saveurs d'huiles aromatiques contenues dans les boissons telles que le thé ou le café ; la détérioration du goût de la bière ; le noircissement ou le brunissement des pigments de viande fraîche. De plus, si l'on considère différentes denrées alimentaires, leur tolérance à l'oxygène varie grandement (Figure 2).

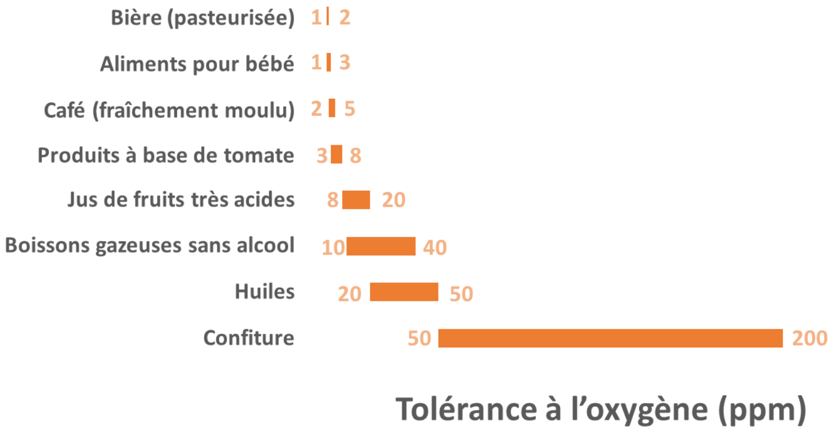

Figure 2 : Tolérance maximale estimée à l'oxygène de certaines denrées alimentaires.

Un paramètre permettant d'évaluer le caractère barrière à oxygène d'un matériau est le taux de transmission d'oxygène, qui est caractéristique pour chacun des cinq polymères les plus utilisés pour l'emballage (Tableau 1). Cette mesure correspond à la quantité de gaz qui peut pénétrer à travers le polymère sur une période d'une journée. Plus la valeur est basse, plus le matériau est imperméable à l'oxygène. Il apparaît donc que le PET présente les meilleures capacités de barrière à oxygène.

Tableau 1 : Taux de transmission d'oxygène de différents polymères utilisés pour l'emballage.

Polymère	PET	PVC	PEHD	PP	PEBD	PS
Taux de transmission d'oxygène (en $cm^3.m^{-2}.jour^{-1}$)	60	150	600	860	4000	6000

Grâce à toutes ses propriétés, le PET présente donc le meilleur compromis possible. En effet, il est transparent, relativement bon marché, présente une bonne solidité et de bonnes propriétés barrières vis-à-vis de la vapeur d'eau et aux gaz (et en particulier à l'oxygène). Bien que son imperméabilité aux gaz soit de loin la plus élevée, comparée aux quatre autres polymères couramment utilisés, cette propriété doit être significativement améliorée.

Un des problèmes majeurs pour les industriels est d'innover en créant de nouveaux matériaux plastiques avec des propriétés barrières améliorées. Depuis quelques années, beaucoup de travaux de recherche sont centrés sur l'amélioration des propriétés barrières du PET vis-à-vis de l'oxygène. De plus, les améliorations des propriétés barrières du PET vis-à-vis de l'oxygène doivent permettre de prolonger la durée de conservation des denrées alimentaires.

1.2. Une solution innovante : les emballages actifs

Pour répondre à la problématique de barrière à oxygène, les industriels ont développé des matériaux innovants tels que les emballages actifs et les emballages intelligents.

Un emballage actif est défini comme un emballage dans lequel des constituants complémentaires ont été délibérément ajoutés dans ou sur le matériau d'emballage ou dans l'espace de tête du contenant, pour améliorer les performances du système d'emballage. Ceci inclut différents systèmes tels que les absorbeurs d'oxygène, d'éthylène ou d'humidité, les absorbeurs ou émetteurs de dioxyde de carbone, les émetteurs d'éthanol, les emballages antimicrobiens, les adsorbeurs d'odeurs…

Un emballage actif ne doit cependant pas être confondu avec un emballage intelligent qui est décrit comme un emballage qui contient un indicateur, externe ou interne, permettant de fournir des informations à propos de l'historique de l'emballage et/ou la qualité des denrées et qui a pour but d'indiquer la qualité du produit (indicateur de fraîcheur ou de qualité, indicateurs de temps ou de température, indicateurs de concentration de gaz, identification de radio fréquence, biosenseurs, …). En résumé, un emballage intelligent peut être considéré comme un emballage actif équipé avec des dispositifs de suivi qui peuvent être directement inclus dans le matériau ou fixé à l'extérieur de l'emballage.

Les piégeurs à oxygène représentent la majeure partie des emballages actifs. Bien que l'oxygène puisse être retiré de l'emballage durant son remplissage avec les denrées alimentaires ou que ces dernières peuvent être stockées dans un emballage avec une atmosphère modifiée, un très faible taux d'oxygène résiduel peut induire des dommages néfastes, en particulier sur les produits très sensibles à l'oxygène.

1.2.1. Un paramètre clé pour une préservation adéquate des produits : les barrières à oxygène

Les absorbeurs d'oxygène, aussi nommés barrières à oxygène ou piégeurs d'oxygène, sont pour certains déjà commercialisés et sont basés sur différentes technologies : poudre de fer, acide ascorbique, enzymes, colorants photosensibles, hydrocarbures insaturés ou polymères…

Ces derniers sont émergents dans le secteur et sont très prometteurs. On peut citer dans cette catégorie, les polyamides (par exemple le poly(méta-xylylène-adipamide) ou MXD6) ou l'éthylène-alcool vinylique qui peuvent être pris en sandwich respectivement entre deux couches de PET ou deux couches de polyoléfines. Pour les différents matériaux multicouches, il est difficile de trouver un équilibre approprié entre la forme, les propriétés barrières vis-à-vis des gaz et la transparence. C'est pourquoi de nouveaux matériaux monocouches ont alors été développés par Clariant et d'autres sociétés et utilisent des polymères sacrificiels et des catalyseurs métalliques pour initier et/ou améliorer la cinétique de réaction.

1.2.2. Les complexes métalliques : un rôle clé dans les barrières à oxygènes basées sur les polymères

Les barrières à oxygène basées sur les polymères représentent une grande opportunité, comme le nombre de polymères et/ou de combinaisons de polymères est quasiment illimité. Pour cette technologie, des catalyseurs métalliques sont utilisés. Ils doivent répondre à plusieurs critères, dont leur propriété à s'oxygéner facilement et aussi leur non toxicité. C'est pour ces raisons que le cobalt(II) et le manganèse (II) ont été choisis dans le cadre de ces travaux.

Le nombre de ligands pouvant être coordinés à ces centres métalliques est très important et notre intérêt s'est porté sur les bases de Schiff, l'acétylacétone et les carboxylates.

1.3. Complexes métalliques et additifs organiques/polymériques : sur la voie d'une compréhension plus approfondie du mécanisme d'action des barrières à oxygène de nature métallique

Dans le but d'obtenir une connaissance plus approfondie du mécanisme d'action de barrières à oxygène potentielles, des composés organiques simples et des additifs polymériques, qui se comportent comme des dérivés sacrificiels, seront étudiés en présence de catalyseurs métalliques durant cette thèse. Comme décrit précédemment, ce travail s'est centré sur deux ions métalliques d'intérêt dans le contexte de l'emballage alimentaire, le cobalt(II) et le manganèse(II). Bien que de nombreux systèmes aient été déjà développés et commercialisés pour certains d'entre eux, leur mécanisme d'action reste pour l'heure encore peu compris, ce qui limite leur développement.

Ce travail de thèse a été réalisé dans le cadre d'une collaboration industrielle entre le CNRS et la société Clariant. L'objectif principal de cette thèse était d'élucider le mécanisme d'action de barrières à oxygène de nature métallique contenues dans les plastiques pour la préservation d'aliments et de boissons. Il est d'une importance cruciale de réaliser une étude fondamentale pour valider le mécanisme d'action ainsi que les (sous)-produits formés pour répondre aux exigences des instances de régulation (par exemple, la *Food and Drug Administration of the United State*) et à plus long terme, être capable d'affiner la composition des barrières à oxygène (nature du centre métallique et des additifs, variation du ratio des différents composants, utilisation potentielle d'autres composés…) permettant d'atteindre les propriétés souhaitées. Pour cela, différents catalyseurs métalliques et additifs ont été considérés au cours de ces recherches.

Les cinétiques d'oxygénation et d'activation des catalyseurs métalliques sont intimement dépendantes de la nature et de la stabilité des espèces catalytiques de cobalt(II) et manganèse(II). D'une part, la cinétique d'oxygénation est plus rapide, par exemple, en conditions basiques en raison de la formation d'espèces hydroxylées qui stabilisent la liaison de l'oxygène. D'autre part, l'étape d'activation résulte des propriétés redox des complexes métalliques. Un mécanisme putatif de réaction des complexes métalliques de cobalt(II) est décrit dans le Schéma 1.

Durant les équilibres **1** et **1'** (Schéma 1), la formation de chélates hydroxylés peut avoir lieu. Par réaction avec l'oxygène, ces espèces réagissent pour former des dimères bimétalliques présentant un pont dioxygène (étape **2**, Schéma 1, correspondant à l'étape d'oxygénation menant aux espèces µ-hydroxo ou bis-hydroxo). Ces espèces peuvent alors subir un transfert électronique intramoléculaire menant aux complexes de cobalt(III) avec un pont (µ-)peroxo (c'est-à-dire, étape d'activation **3**, Schéma 1). Ces espèces activées peuvent alors :

- Oxyder différents substrats tels que des additifs ou des matrices polymériques (étape **6**, Schéma 1).
- Subir une réduction dans des conditions acides (étape **4**, Schéma 1).
- Subir une dégradation irréversible (étape **5**, Schéma 1, qui est en principe inactive envers des propriétés efficaces de barrière à oxygène).

Le même mécanisme est applicable aux chélates monomériques (Schéma 1) avec la formation ultérieure d'espèces dioxo-cobalt(II) et de dérivés superoxo-cobalt(III).

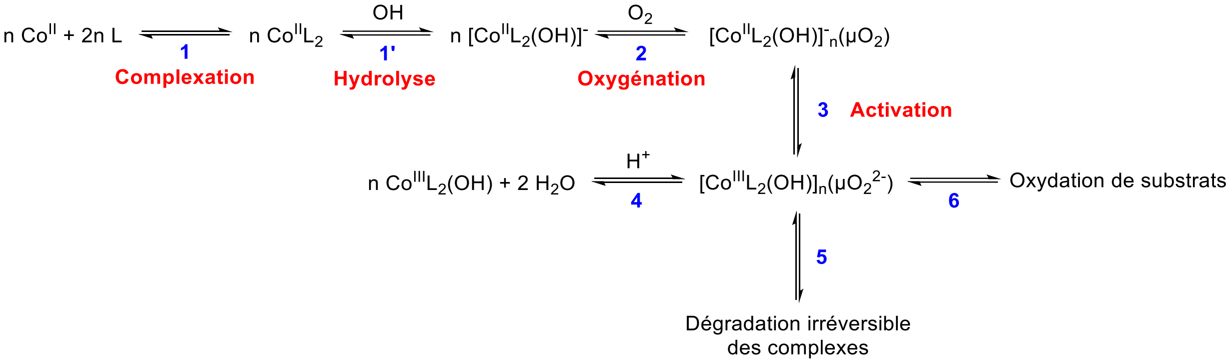

Schéma 1 : Mécanisme putatif de complexation, oxygénation et activation de complexes de cobalt(II).

Ce projet a été divisé en trois objectifs principaux : (*i*) la synthèse et la caractérisation de plusieurs catalyseurs métalliques, (*ii*) l'étude de leurs propriétés d'oxygénation et d'activation, et (*iii*) l'étude du rôle des additifs sacrificiels.

Synthèse et Caractérisation des Catalyseurs Métalliques

Différents catalyseurs métalliques ont été considérés durant cette thèse : le cobalt(II) et le manganèse(II) *bis*(acétylacétonate) comme catalyseurs modèles, plusieurs complexes de cobalt(II) et de manganèse(II) avec des bases de Schiff comme ligands, certains connus, d'autres non reportés, et le cobalt(II) et le manganèse(II) *bis*(stéarate).

Premièrement, différentes bases de Schiff ont été synthétisées (**L^1-L^7**, Schéma 2 et Tableau 2). Leur stabilité (processus d'hydrolyse dans une large gamme de pH) en solution a été étudiée par spectrométrie de masse en mode d'ionisation électrospray (ESI-MS) ou par spectrophotométrie d'absorption UV-visible, et leurs constantes de protonation ont été évaluées par potentiométrie pure ou par spectrophotométrie d'absorption UV-visible couplée au pH.

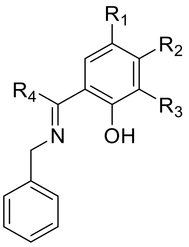

Schéma 2 : Bases de Schiff utilisées comme ligands dans le cadre de ce travail de thèse.

Tableau 2 : Différentes bases de Schiff utilisées comme ligand dans ce travail de thèse.

Ligand	R_1	R_2	R_3	R_4
L^1	H	H	H	H
L^2	H	OH	H	Ph
L^3	Br	H	Br	H
L^4	Me	H	H	H
L^5	NO_2	H	H	H
L^6	OMe	H	H	H
L^7	H	OH	H	H

Dans une seconde partie, l'affinité de ces ligands pour le cobalt(II) et le manganèse(II) a été déterminée potentiométrie pure ou par spectrophotométrie d'absorption UV-visible couplée à la potentiométrie. Les complexes de cobalt(II) et de manganèse(II) correspondants (Schéma 3 et Tableau 3) ont été synthétisés et caractérisés. Enfin, leurs propriétés redox ont été déterminées par voltampérométrie cyclique.

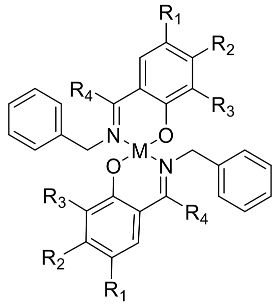

Schéma 3: Complexes métalliques étudiés dans le cadre de ce travail de thèse.

Tableau 3 : Différents complexes de cobalt(II) et de manganèse(II), avec des bases de Schiff comme ligands, étudiés dans ce travail de thèse et leur nomenclature correspondante.

					Complexes	
Ligand	**R$_1$**	**R$_2$**	**R$_3$**	**R$_4$**	**M = Co(II)**	**M = Mn(II)**
L^1	H	H	H	H	**1Co**	**1Mn**
L^2	H	OH	H	Ph	**2Co**	**2Mn**
L^3	Br	H	Br	H	**3Co**	**3Mn**
L^4	Me	H	H	H	**4Co**	**4Mn**
L^5	NO_2	H	H	H	**5Co**	**5Mn**
L^6	OMe	H	H	H	**6Co**	**6Mn**
L^7	H	OH	H	H	**7Co**	**7Mn**

Propriétés d'Oxygénation/d'Activation des Catalyseurs Métalliques

Les propriétés d'oxygénation et d'activation de notre série de catalyseurs de cobalt(II) et de manganèse(II) (c'est-à-dire, avec des bases de Schiff comme ligands **1Co**-**7Co** et **1Mn**-**7Mn**, Schéma 3 et Tableau 3 ; avec l'acétylacétonate **8Co** et **8Mn** ; et avec le stéarate **9Co** et **9Mn**) ont été étudiées en utilisant une combinaison de techniques analytiques complémentaires (par exemple l'ESI-MS, la résonance magnétique nucléaire du proton (RMN ^{1}H), la spectrophotométrie d'absorption UV-visible, l'oxymétrie couplée à la spectrophotométrie d'absorption UV-visible…). En particulier, deux principaux aspects ont été finement examinés : (*i*) les cinétiques des étapes d'oxygénation et d'activation et (*ii*) la caractérisation des (sous-)produits formés durant les processus d'oxygénation.

Rôle des Additifs

L'oxydation des additifs organiques modèles (**10**-**13**, Schéma 4) a été étudiée en solution en présence d'oxydants organiques forts et les processus ont été suivis et quantifiés par spectrophotométrie d'absorption UV-visible. Une fois que l'additif organique modèle le plus actif a été selectionné en utilisant cette approche, l'oxydation de ce dernier a été examinée en présence des catalyseurs métalliques les plus efficaces.

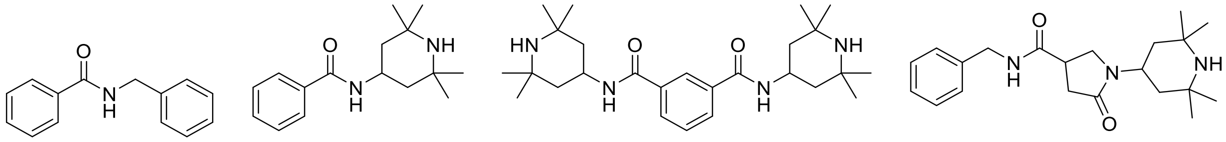

10 **11** **12** **13**

Schéma 4 : Additifs organiques modèles étudiés dans le cadre de ce travail de thèse.

Une part importante de ce travail (c'est-à-dire, mimer les conditions réelles utilisées lors de la mise en œuvre par les divisions *Masterbatches* et *Additifs* de Clariant) a été centrée sur l'investigation minutieuse de l'oxydation d'additifs organiques modèles (**10**-**13**, Schéma 4) et d'additifs polymériques (**14**-**15**, Schéma 5) à l'état solide en présence de différents catalyseurs métalliques. Le processus d'oxydation (cinétique et caractérisation des produits d'oxydation) a été principalement suivi par spectroscopie infrarouge à transformée de Fourier (IRTF) mais aussi avec différentes techniques d'analyses à l'état solide, qui seront développées plus en détails au long de ce manuscrit.

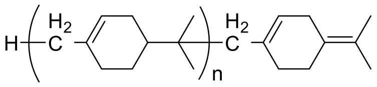

Dercolyte S 125

14

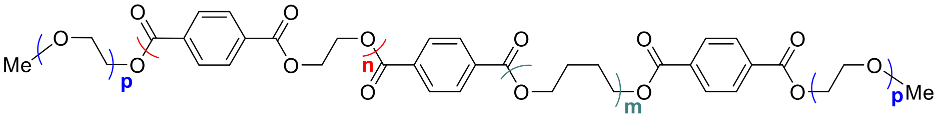

Dérivé polytétrahydrofurane

15

Schéma 5 : Additifs polymériques étudiés durant ce travail de thèse.

2. Chapitre II : Synthèse, caractérisation et investigations physico-chimiques des catalyseurs métalliques

2.1. Une multitude de techniques analytiques pour déterminer les propriétés physico-chimiques des ligands et de leurs complexes métalliques

Avant d'étudier plus en détail les capacités de piège à oxygène des catalyseurs métalliques et des additifs dans les plastiques, il a été d'abord nécessaire d'entreprendre une investigation sur les complexes métalliques, d'évaluer leurs propriétés physico-chimiques (stabilité, résistance en solution, constantes de protonation…). Ces paramètres sont très importants pour comprendre l'efficacité de l'oxygénation des complexes métalliques. Concernant les complexes de cobalt(II), il a été reporté que leurs stabilités sont intimement liées aux propriétés acido-basiques des ligands correspondants. De plus, le processus de liaison de l'oxygène est aussi étroitement relié à la stabilité et aux propriétés rédox des complexes de cobalt(II). Il nous a donc semblé approprié d'étudier les propriétés acido-basiques des ligands libres ainsi que les constantes de stabilité des complexes de cobalt(II) et de manganèse(II) correspondants.

2.2. Synthèse, stabilité et constantes de protonation des bases de Schiff, utilisées comme ligands

2.2.1. Préparation des ligands

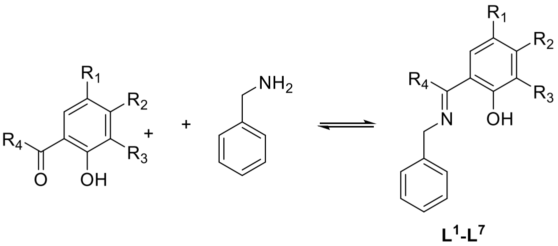

Schéma 6 : Synthèse des bases de Schiff.

Les bases de Schiff sont des ligands bien connus en chimie de coordination et leur préparation résulte d'une condensation réversible entre une amine (la benzylamine dans notre cas) et un carbonyle (c'est-à-dire, un aldéhyde pour les systèmes considérés dans cette étude) pour former la fonction imine.

Les différentes bases de Schiff ont été synthétisées avec succès (Schéma 6 et Tableau 4) et caractérisées par RMN ^{1}H et ^{13}C, par spectroscopie IRTF et ESI-MS. Leur pureté a été confirmée par chromatographie liquide couplée à la spectrométrie de masse.

Il est à noter que les ligands **L^1** et **L^6** ont également été synthétisés sans solvant et obtenus avec les mêmes rendements.

Tableau 4 : Rendements obtenus lors de la synthèse des bases de Schiff.

Base de Schiff	R_1	R_2	R_3	R_4	Rendement (%)
L^1	H	H	H	H	quantitatif
L^2	H	OH	H	Ph	17
L^3	Br	H	Br	H	80
L^4 *	Me	H	H	H	94
L^5	NO_2	H	H	H	75
L^6	OCH_3	H	H	H	quantitatif
L^7	H	OH	H	H	48

2.2.2. Détermination des constantes de protonation des bases de Schiff, utilisées comme ligands

Les différentes constantes de protonation des bases de Schiff (**L^1**-**L^7**) ont été déterminées par potentiométrie pure ou par spectrophotométrie d'absorption UV-visible couplée à la potentiométrie. Les résultats sont présentés dans le Tableau 5 (pour les ligands présentant deux sites de protonation) et dans le Tableau 6 (pour les ligands présentant trois sites de protonation).

*Tableau 5 : Constantes de protonation de **L^1**, **L^3**, **L^4**, **L^5** et **L^6** déterminées par spectrophotométrie d'absorption UV-visible couplée à la potentiométrie et par potentiométrie pure.*

	Potentiométrie		Absorption UV-vis. *versus* pH	
Ligand	pK_{a_1}	pK_{a_2}	pK_{a_1}	pK_{a_2}
L^1	*n.a.*	*n.a.*	*n.d.*	11,87(5)
L^3	6,0(2)	9,5(1)	6,5(6)	9,7(5)
L^4	*n.d.*	*n.d.*	*n.d.*	12,1(1)
L^5	5,80(8)	9,30(5)	5,98(9)	9,91(7)
L^6	*n.d.*	*n.d.*	*n.d.*	12,11(7)

n.a. : non applicable

n.d. : non déterminé en raison de l'hydrolyse trop rapide

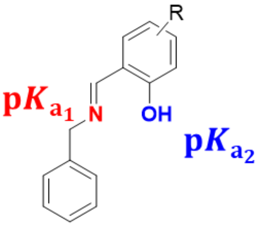

*Tableau 6 : Constantes de protonation de **L^2** et **L^7** déterminées par spectrophotométrie d'absorption UV-visible couplée à la potentiométrie et par potentiométrie pure.*

	Potentiométrie			Absorption UV-vis. *versus* pH		
Ligand	pK_{a_1}	pK_{a_2}	pK_{a_3}	pK_{a_1}	pK_{a_2}	pK_{a_3}
L^2	3,9(2)	8,7(2)	10,4(1)	3,8(3)	8,5(1)	9,74(6)
L^7	3,7(2)	10,85(7)	8,3(1)	4,6(2)	11,4(1)	8,4(1)

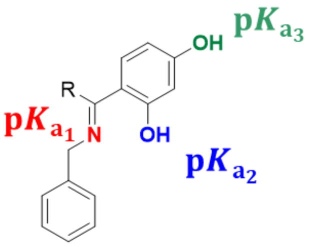

2.3. Synthèse et propriétés physico-chimiques des complexes métalliques

2.3.1. Préparation des complexes de cobalt(II) et de manganèse(II)

2.3.1.1. Stratégie classique

Il a été tout d'abord tenté de synthétiser les complexes de cobalt(II) ou de manganèse(II) avec les différentes bases de Schiff en utilisant une approche synthétique classique ligand/métal, c'est-à-dire que les ligands sont mis à réagir avec le sel métallique (cobalt(II) ou manganèse(II)) pour former le complexe souhaité. Bien que décrite dans la littérature pour les complexes **3Co** et **4Co**, cette stratégie ne nous a pas permis d'obtenir les complexes souhaités.

Une stratégie one-pot a alors été envisagée. Pour cela, l'aldéhyde et la benzylamine réagissent pour former la base de Schiff, puis, sans aucune purification, le sel métallique est ajouté au milieu réactionnel. Bien que des conditions expérimentales variées (nature de l'anion du sel métallique, solvant, température, durée, …) aient été testées, seul le complexe **1Co** a été obtenu par cette approche avec un rendement de 87%.

2.3.1.2. Stratégie innovante

Dans le but de synthétiser les autres complexes de cobalt(II) et de manganèse(II), une autre approche a dû être développée. Dans cette approche, dite « approche *Template* », l'aldéhyde est d'abord complexé au cobalt(II) ou manganèse(II) acétate pour former les complexes intermédiaires, qui ont été isolés et caractérisés. Par réaction de la benzylamine avec ces précurseurs, les complexes finaux de cobalt(II) et de manganèse(II) ont été obtenus. Cependant, malgré nos efforts, tous les complexes de cobalt(II) et de manganèse(II) n'ont pas pu être obtenus (Tableau 7).

Tableau 7 : Préparation des complexes intermédiaires et finaux de cobalt(II) et de manganèse(II).

Complexe intermédiaire de Co(II)	Rdt (%)	Complexe final de Co(II)	Rdt (%)	Complexe intermédiaire de Mn(II)	Rdt (%)	Complexe final de Mn(II)	Rdt (%)
1aCo	54	1Co	15	1aMn	71	1Mn	*n.o.*
2aCo	*n.o.*	2Co	*n.t.*	2aMn	*n.t.*	2Mn	*n.t.*
3aCo	73	3Co	96	3aMn	*n.t.*	3Mn	*n.t.*
4aCo	33	4Co	*n.o.*	4aMn	*n.t.*	4Mn	*n.t.*
5aCo	80	5Co	92	5aMn	49	5Mn	88
6aCo	67	6Co	22	6aMn	23	6Mn	*n.o.*
7aCo	*n.o.*	7Co	*n.t.*	7aMn	*n.t.*	7Mn	*n.t.*

n.o. : non obtenu ; *n.t.* : non testé ; Rdt : rendement

2.3.2. Affinité des différentes bases de Schiff, utilisées comme ligands, avec le cobalt(II) et le manganèse(II)

L'affinité des différentes bases de Schiff pour le cobalt(II) ou le manganèse(II) a été déterminée par spectrophotométrie d'absorption UV-visible couplée à la potentiométrie ou par potentiométrie pure.

Grâce à un traitement statistique des données, les différentes constantes de complexation peuvent ainsi être déterminées. Les données thermodynamiques sont données en constantes globales $\log\beta_{\mathrm{mlx}}$ (où *m* représente le nombre de centre(s) métallique(s) dans le complexe ; *l* correspond au nombre de ligands coordinés au centre métallique ; et *x* relate le nombre de groupes hydroxyles (valeur négative) ou de protons (valeur positive)).

Les complexes peuvent être classés en deux catégories : ceux subissant une hydroxylation et dont les constantes de complexation sont présentées dans le Tableau 8 ; et ceux subissant une ou plusieurs protonations et dont les résultats sont rassemblés dans le Tableau 9.

*Tableau 8 : Constantes de complexation globales déterminées pour **1Mn**, **1Co**, **3Co**, **4Co**, **5Co** et **6Co**.*

	Absorption UV-vis. *versus* pH		
Système	**logβ_{110}**	**logβ_{120}**	**log$\beta_{12\text{-}1}$**
1Mn	*n.d.*	12,8(2)	*n.d.*
1Co	*n.d.*	13,9(2)	3,9(4)
3Co	6,47(3)	11,3(2)	*n.d.*
4Co	8,15(8)	13,9(6)	*n.d.*
5Co	7,30(6)	11,8(4)	*n.d.*
6Co	*n.d.*	14,3(2)	3,7(4)

n.d. : non déterminée

*Tableau 9 : Constantes de complexation globales pour les systèmes subissant des protonations successives (**2Co** et **7Co**).*

	Absorption UV-vis. *versus* pH		
Système	**logβ_{120}**	**logβ_{121}**	**logβ_{122}**
2Co	16,8(1)	25,9(1)	33,3(1)
7Co	14,9(1)	20,15(8)	36,06(9)

Il a été précédemment démontré que les constantes de complexation sont intimement liées aux propriétés acido-basiques des ligands correspondants. En utilisant nos résultats pour la série les ligands N-benzylés et les données de la littérature pour la série les ligands N-arylés, la constante globale de formation du bischelate de cobalt(II) peut être représentée en fonction de la constante de protonation du phénol (site de complexation) (Figure 3). Il apparaît très nettement une relation linéaire entre ces deux constantes pour les deux séries. Les complexes exhibant les plus faibles stabilités (**3Co** et **5Co**) sont ceux étant substitués par des groupements électro-attracteurs (respectivement Br et NO_2).

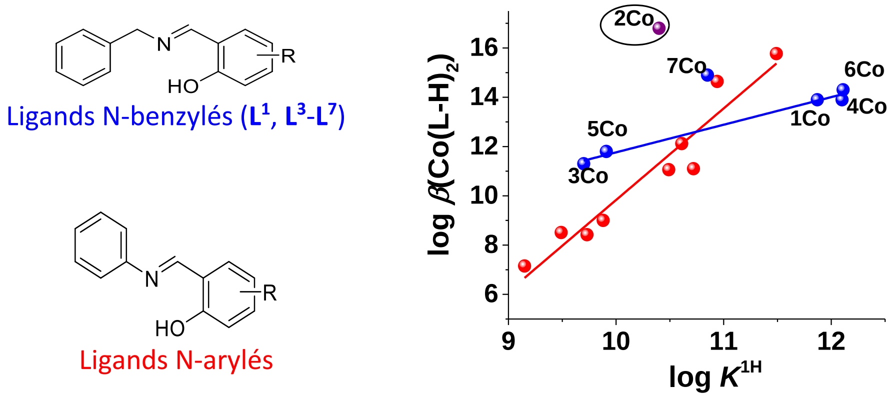

Figure 3 : Relation entre la constante globale de stabilité des complexes de cobalt(II) et les propriétés acido-basiques d'une large gamme de bases de Schiff, incluant celles d'intérêt dans cette étude.

2.4. Propriétés d'oxygénation/d'activation des complexes métalliques

Les propriétés d'oxygénation et d'activation des différents complexes métalliques ont été évaluées grâce à différentes techniques analytiques : la spectrophotométrie d'absorption UV-visible, l'oxymétrie couplée à la spectrophotométrie d'absorption UV-visible, l'ESI-MS, la RMN ^{1}H et l'électrochimie.

2.4.1. Oxygénation/activation suivies par spectrophotométrie d'absorption

Bien que les variations spectrales observées soient faibles (Figure 4), elles mettent clairement en évidence un processus en trois étapes : la première, très rapide (le temps de demi-vie $t_{1/2} \sim 19$ min), pourrait être attribuée à l'oxygénation ; la seconde, plus lente (jusqu'à environ 40 h de suivi), serait liée à l'étape d'activation ; et enfin la dernière (entre environ 40 h de suivi et la fin du suivi) pourrait laisser suggérer une dégradation du complexe.

Pour s'assurer de la nature de la première étape, des mesures d'oxymétrie couplée à la spectrophotométrie d'absorption UV-visible ont été réalisées.

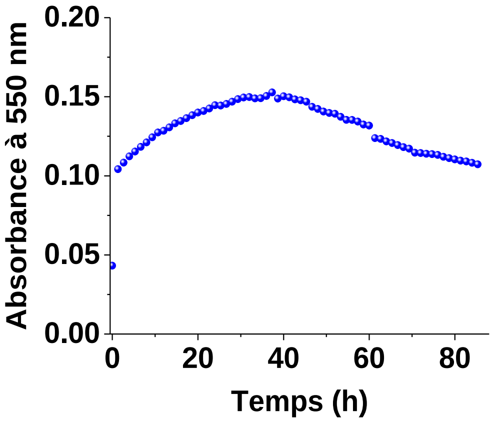

Figure 4 : Variations de l'absorbance à 550 nm de ***1Co*** *au cours du temps ; [****1Co****] = 2,51 x* 10^{-3} *M, solvant : dioxane:*H_2O *(1:1 v/v), l = 1 cm.*

2.4.2. Oxygénation/activation suivies par l'oxymétrie couplée à l'absorption UV-visible

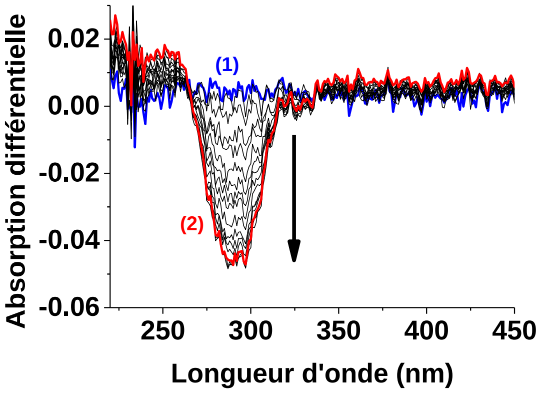

Figure 5 : Spectres d'absorption différentielle mesurés à intervalles réguliers durant la première phase d'oxygénation de ***8Co*** *;* ***(1)*** *t = 0,* ***(2)*** *t = 2 h, [****8Co****] = 2 x* 10^{-4} *M, solvant : dioxane:*H_2O *(1:1 v/v), l = 1 cm.*

Ces expériences ont permis de mettre en lumière que la première phase du processus était bien liée à l'oxygénation du complexe. En effet, la Figure 5 qui décrit les différents spectres d'absorption différentielle mesurés au cours de la première phase d'oxygénation met en évidence des variations spectrales caractéristiques de l'oxygénation. De plus, la longueur d'onde à laquelle ont lieu les variations spectrales permet de déterminer la nature de l'espèce oxygénée.

En outre, en faisant subir à la même solution, une deuxième phase d'oxygénation (consécutive à une phase de désoxygénation, par barbotage de gaz inerte), la réversibilité de l'oxygénation peut être démontrée. En effet, si les deux courbes d'oxygénation (correspondant à la première et la seconde étape d'oxygénation) sont superposables, alors l'oxygénation est dite réversible (Figure 6, pour le système **8Co**) ; a contrario, si elles ne peuvent être superposées, l'oxygénation est dite irréversible (Figure 7, pour le système **1Co**).

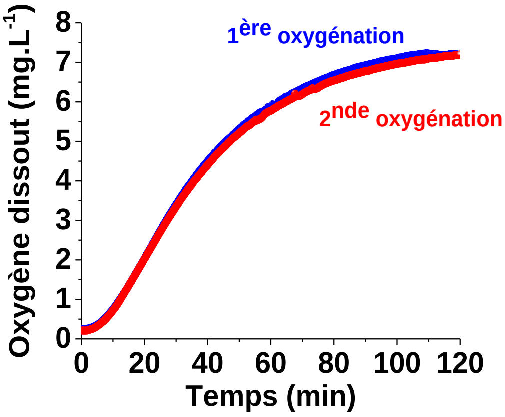

*Figure 6 : Superposition des deux courbes d'oxygénation de **8Co** durant les deux phases d'oxygénation ; [**8Co**] = 2 x 10^{-4} M, solvant : dioxane:H_2O (1:1 v/v).*

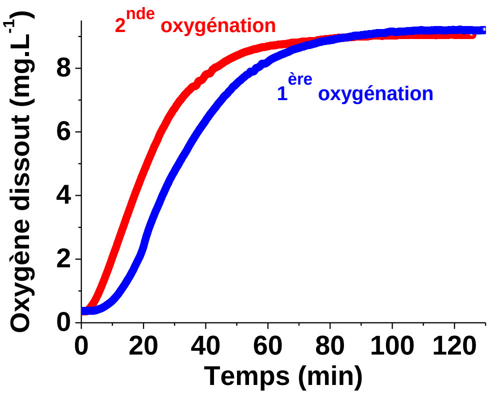

*Figure 7: Superposition des deux courbes d'oxygénation de **1Co** durant les deux phases d'oxygénation ; [**1Co**] = 6 x 10^{-4} M, solvant : dioxane:H_2O (1:1 v/v).*

Maintenant que la nature de la première étape a été démontrée comme étant l'oxygénation des complexes, la caractérisation des produits obtenus a été ensuite effectuée.

2.4.3. Oxygénation/activation suivies par ESI-MS

Une solution de complexes de cobalt(II) **1Co** a été analysée par ESI-MS pendant environ dix jours. Le profil isotopique du pic d'intérêt centré à *m/z* = 480,2 (Figure 8) correspondant à l'espèce $[\mathrm{Co^{II}}(\mathbf{L^1}\text{-H})_2\text{+H}]^+$ (pic monoisotopique) est continuellement altéré au cours du temps (déplacement vers les plus petites masses). Le nouveau pic centré à *m/z* = 479,2 correspond à un degré d'oxydation plus élevé du métal : $[\mathrm{Co^{III}}(\mathbf{L^1}\text{-H})_2]^+$. Ceci peut être interprété par une oxydation du centre métallique (cobalt(II) en cobalt(III)). La cinétique d'oxydation du centre métallique peut être suivie et quantifiée (Figure 9). Le temps de demi-vie du processus d'oxygénation calculé précédemment par spectrophotométrie d'absorption UV-visible ($t_{1/2}$ ~ 19 min) peut être comparé à celui des phases d'activation et d'oxydation quantifiées par ESI-MS ($t_{1/2}$ ~ 1000 min ~ 17 h). L'oxygénation des complexes est donc environ 50 fois plus rapide que son activation/oxydation.

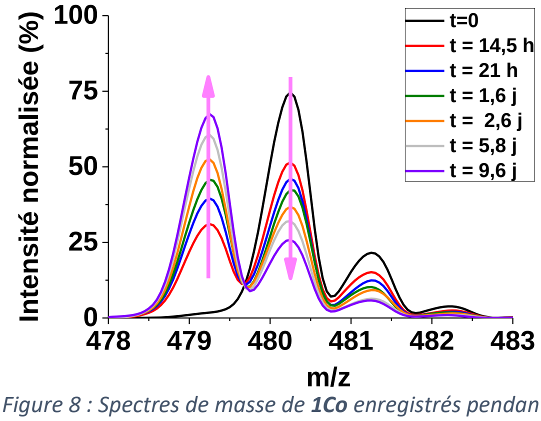

*Figure 8 : Spectres de masse de **1Co** enregistrés pendant 10 jours – zoom entre m/z = 478 et 483 ; [**1Co**] = 1,0 x 10^{-4} M, solvant : CH_3CN:H_2O (1:1 v/v), + 170 V.*

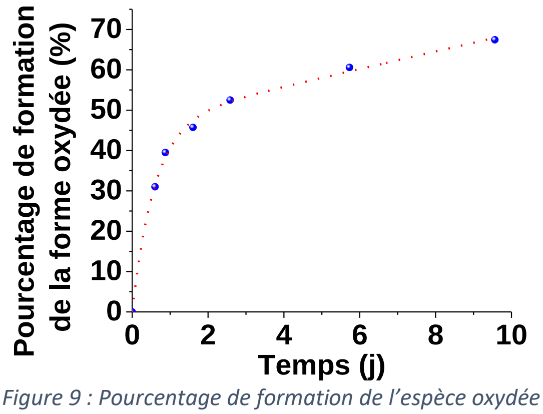

*Figure 9 : Pourcentage de formation de l'espèce oxydée de **1Co** pendant 10 jours.*

La même approche a également été utilisée pour suivre le comportement des différents ligands. Aucune oxydation ou dégradation n'a été détectée dans ces conditions expérimentales.

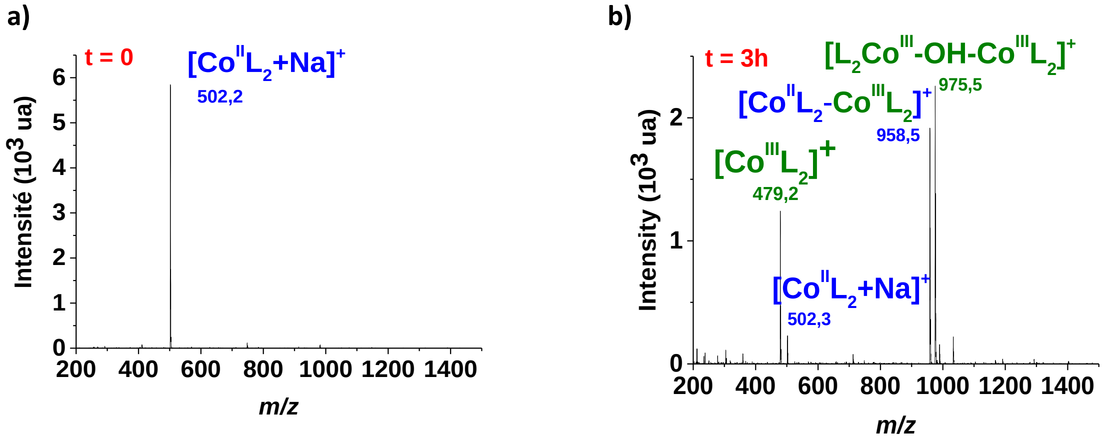

Nos efforts se sont alors portés sur la caractérisation des espèces oxygénées/activées/oxydées. Pour cela, l'expérience a été réitérée sur une journée. Le bischélate de cobalt(II) peut clairement être mis en évidence initialement (Figure 10a). Après trois heures passées en solution, la formation d'espèces bischélates de cobalt(III) peut être observée (Figure 10b), correspondant aux espèces activées, ainsi que des espèces portant un pont hydroxy, mettant en évidence l'étape d'oxygénation. Après un jour (Figure 10c), la formation d'espèces trischélates de cobalt(III) ainsi que la présence de ligand libre peut être observé, suggérant une lente réorganisation des bischélates de cobalt(III).

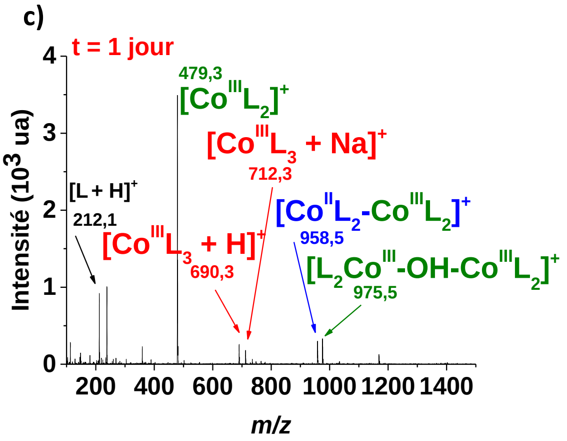

*Figure 10 : Spectres de masse de **1Co** enregistrés pendant une journée : **a)** t = 0 , **b)** t = 3 h, **c)** t = 1 jour, [**1Co**] = 6,97 x 10^{-4} M, solvant : dioxane, + 100 V.*

2.4.4. Oxygénation/activation suivies par RMN ^{1}H

La RMN ^{1}H a également été utilisée pour examiner d'une façon simple la réactivité des différents catalyseurs métalliques. En effet, tandis que les bischélates de cobalt(II) sont paramagnétiques, les complexes de cobalt(III) sont diamagnétiques et leur apparition peut être facilement suivie par RMN.

Les protons benzyliques peuvent être observés sous la forme d'un large singulet dans l'espèce bischélate de cobalt(II) **1Co** (4,85 ppm, Figure 11). Cependant, dans l'espèce trischelate de cobalt(III), ces protons sont magnétiquement non équivalents et la formation de six doublets bien séparés (3,95 – 4,93 ppm, Figure 11) peut être observée. La cinétique de formation de l'espèce oxydée peut être ainsi mesurée (Figure 12).

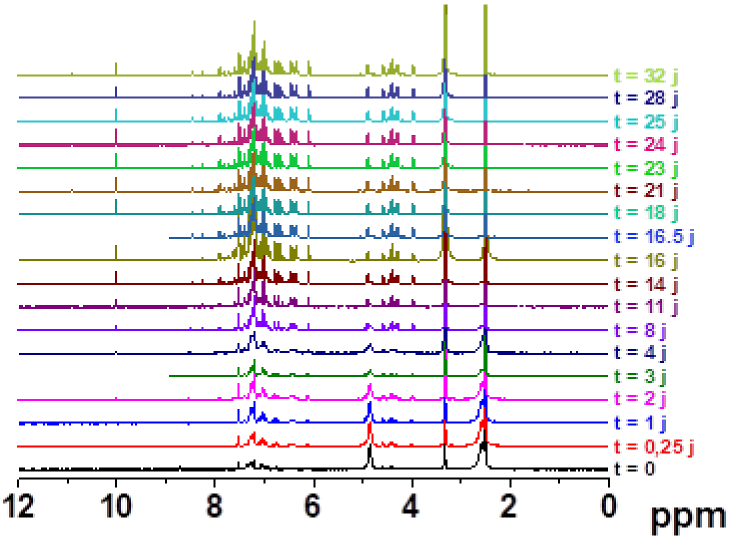

*Figure 11 : Spectres RMN ^{1}H de **1Co** enregistrés au cours du temps ; solvant : (CD$_3$)$_2$SO.*

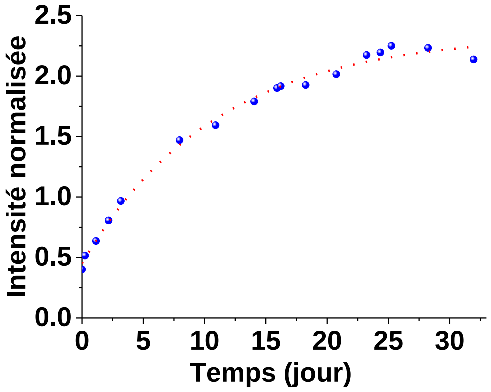

*Figure 12 : Cinétique d'oxydation de **1Co** et de conversion en trischélate de cobalt(III) suivie par RMN ^1H ; solvant : $(CD_3)_2SO$.*

Les différents catalyseurs ont été testés dans différents solvants, en fonction de leur solubilité. Les temps de demi-vie des processus d'oxydation (et de conversion quand elle a lieu) ont été déterminés et sont présentés dans le Tableau 10. Les différents catalyseurs peuvent être classés en deux catégories : ceux subissant uniquement une oxydation sans conversion, c'est-à-dire que les espèces finales sont des bischélates de cobalt(III) (*en orange* dans le Tableau 10) et ceux subissant une oxydation puis une conversion conduisant aux espèces trischélates de cobalt(III) (*en vert* dans le Tableau 10).

Tableau 10 : Temps de demi-vie ($t_{1/2}$) en jours des processus d'oxydation/(de conversion) des centres métalliques (cobalt(II) en cobalt(III)) des différents catalyseurs métalliques dans différents solvants déterminés par RMN ^1H.

Solvant Catalyseur	$(CD_3)_2SO$	$CDCl_3$	$(CD_3)_2CO$	CD_3OD	CD_3CN
1Co	7,7(7)	2,5(7)	*n.t.*	*n.t.*	*n.t.*
2Co	0,44(2)	*n.t.*	0,53(8)	*n.t.*	*n.t.*
3Co	~ 45	*n.d.*	*n.d.*	*n.d.*	*n.d.*
5Co	6,87(6)	*n.d.*	*n.d.*	*n.d.*	*n.d.*
6Co	3,10(3)	*n.d.*	*n.d.*	*n.d.*	*n.d.*
8Co	> 34	*n.d.*	*n.d.*	*n.d.*	*n.d.*
9Co	> 18	*pas de réaction*	0,35(1)	*trop rapide*	*pas de réaction*

n.d. : non déterminé en raison de la faible solubilité du catalyseur dans ce solvant ; *n.t. :* non testé
pas de réaction : aucune réaction n'a été observée dans ces conditions expérimentales
trop rapide : la cinétique de réaction était trop rapide pour être mesurée
en vert : l'espèce finale est $Co^{III}(L\text{-}H)_3$; *en orange :* l'espèce finale est $Co^{III}(L\text{-}H)_2$

2.4.5. Oxygénation/activation suivies par spectrophotométrie d'absorption UV-visible en utilisant une sonde chromophore

La RMN ^1H a permis d'examiner le comportement des catalyseurs métalliques dans différents solvants. Cependant, les concentrations requises en RMN et le nombre limité de solvants deutérés, communément disponibles dans les laboratoires, limitent significativement cette approche. C'est pourquoi la spectrophotométrie d'absorption UV-visible a été de nouveau reconsidérée. Cependant, comme décrit dans le paragraphe 2.4.1, les variations spectrales centrées sur les centres métalliques sont relativement faibles. C'est pourquoi l'utilisation d'un chromophore utilisé comme sonde est nécessaire. Le radical 2,2-diphényl-1-picrylhydrazyle (DPPH) est très stable en solution et a été sélectionné pour cette raison. Les étapes d'oxygénation et d'activation des différents catalyseurs ont été étudiées grâce à cette approche. Une consommation de DPPH au cours de la réaction traduit un mécanisme de nature radicalaire. Quelles que soient les conditions expérimentales utilisées (catalyseur, ratio catalyseur/DPPH, solvant...), la nature radicalaire du mécanisme d'oxygénation/activation des catalyseurs a été toujours démontrée. Pour un même système, le **1Co**, l'influence du solvant sur les étapes d'oxygénation et d'activation a ensuite été étudiée (Figure 13), permettant d'établir une séquence de réactivité en fonction du solvant utilisé. De plus, cette approche a permis de comparer, dans les mêmes conditions expérimentales, les étapes d'oxygénation/d'activation des différents catalyseurs, aussi bien au niveau de la cinétique des processus que de leurs efficacités (Figure 14).

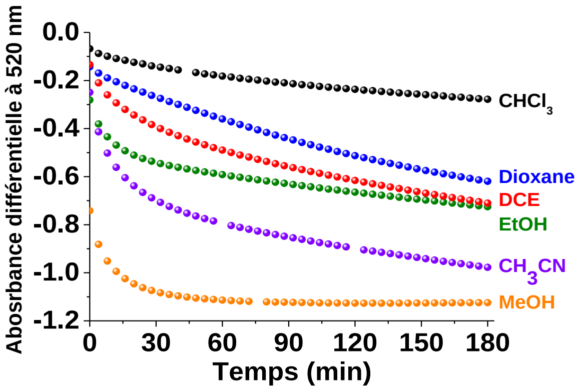

*Figure 13 : Cinétique d'oxygénation/d'activation du complexe **1Co** suivi en présence de DPPH dans différents solvants ; [**1Co**] ~ 3 x 10^{-4} M, [**1Co**]/[DPPH] = 1,0, l = 1cm, T = 25,0(2) °C.*

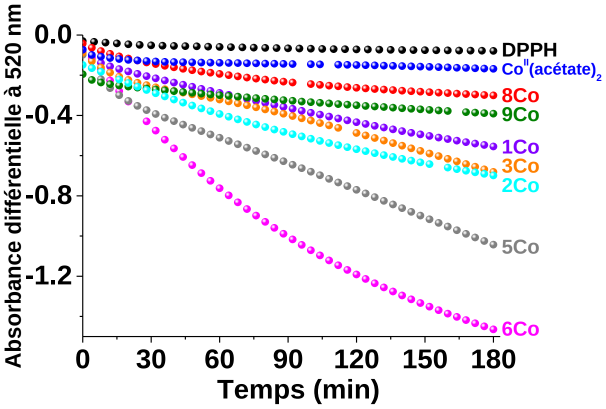

Figure 14 : Réactivité (oxygénation/activation) des différents complexes de cobalt(II) en présence de DPPH ; [Complexe] ~ 3 x 10^{-4} M, [Complexe]/[DPPH] = 1,0, solvant : dioxane, l = 1 cm, T = 25,0(2) °C.

Pour le complexe **1Co**, **c**ette méthode nous a permis de déterminer une séquence de réactivité en fonction du solvant utilisé : méthanol >> acétonitrile >> éthanol > dichloroéthane > dioxane >> chloroforme. Pour un même solvant (le dioxane), la réactivité des différents catalyseurs métalliques a pu être également évaluée : **6Co** >> **5Co** >> **2Co** ~ **3Co** ~ **1Co** > **9Co** > **8Co** > Co^{II}(acétate)$_2$.

2.4.6. Propriétés électrochimiques des catalyseurs métalliques

Enfin, les propriétés électrochimiques des différents catalyseurs métalliques ont été étudiées par voltampérométrie cyclique. Les différents processus d'oxydation et de réduction ont été examinés et la séquence de réactivité suivante peut être proposée (séquence basée sur le potentiel d'oxydation du cobalt(II) en cobalt(III)) (Figure 15).

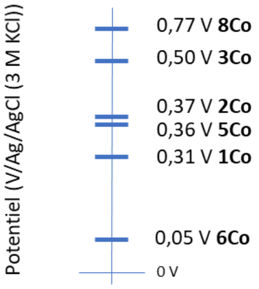

Figure 15 : Potentiels d'oxydation (versus Ag/AgCl/3 M KCl) des complexes de cobalt(II) (processus d'oxydation du cobalt(II) en cobalt(III)).

En résumé, dans le cadre de ce chapitre, les différentes étapes du mécanisme proposé ont été étudiées grâce à l'utilisation de nombreuses techniques analytiques (Schéma 7).

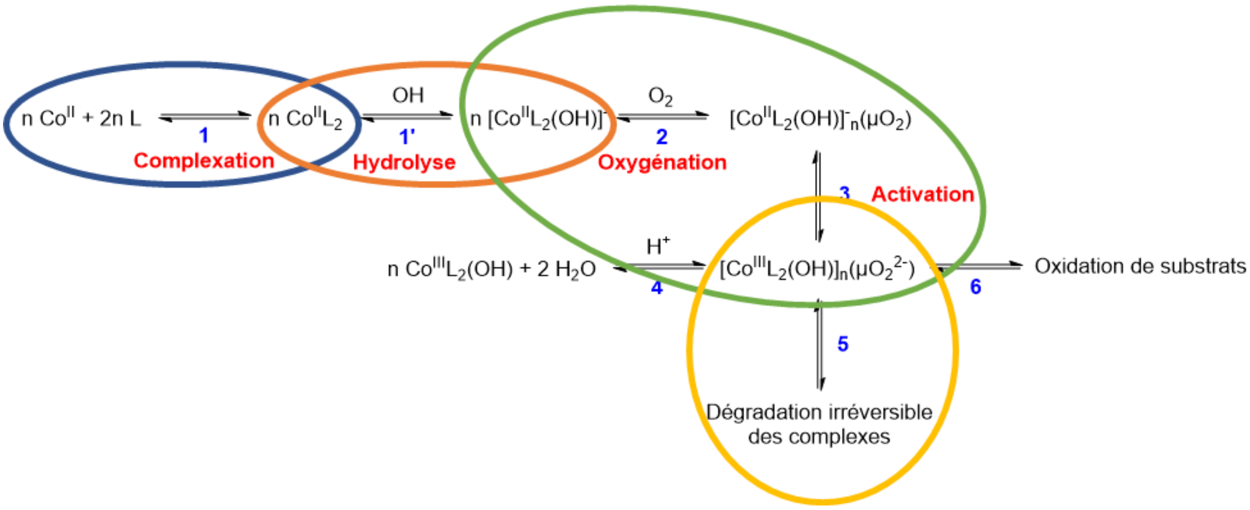
$n\,Co^{II} + 2n\,L$
1
Complexation
$n\,Co^{II}L_2$
OH
1'
Hydrolyse
$n\,[Co^{II}L_2(OH)]^-$
O_2
2
Oxygénation
$[Co^{II}L_2(OH)]^-{}_n(\mu O_2)$
3
Activation
$n\,Co^{III}L_2(OH) + 2\,H_2O$
H^+
4
$[Co^{III}L_2(OH)]_n(\mu O_2{}^{2-})$
6
Oxidation de substrats
5
Dégradation irréversible des complexes

Schéma 7 : Mécanisme putatif de complexation, oxygénation et activation des complexes de cobalt(II).

3. Chapitre III : Oxydation des additifs organiques modèles

Après avoir étudié les premières étapes du mécanisme réactionnel des complexes de cobalt(II) en solution dans le Chapitre II, cette section sera dédiée à l'étude de l'oxydation des substrats (étape 6, Schéma 8).

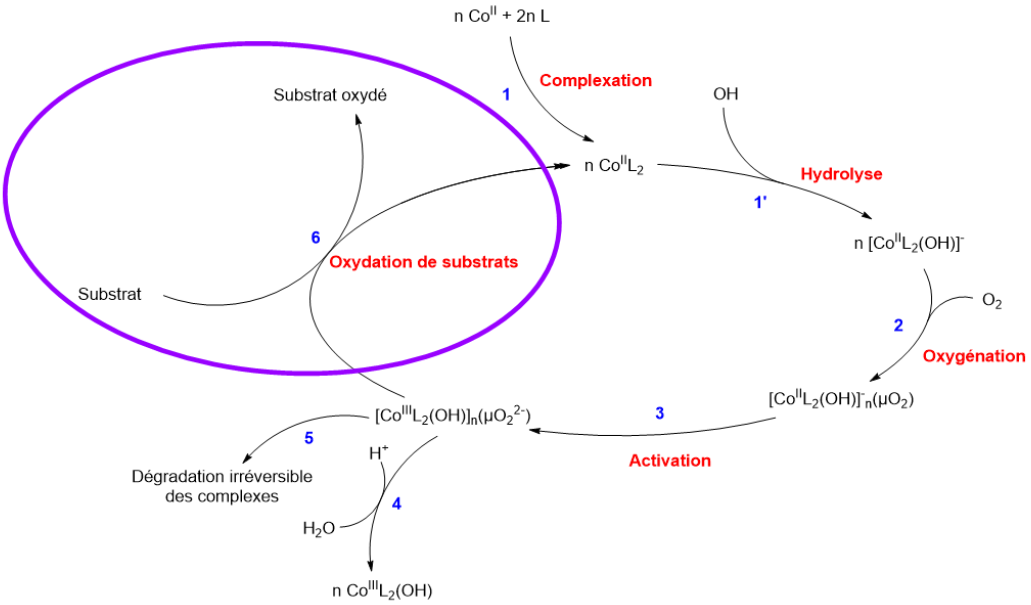
$n\,Co^{II} + 2n\,L$
Complexation
1
Substrat oxydé
OH
$n\,Co^{II}L_2$
Hydrolyse
1'
6
$n\,[Co^{II}L_2(OH)]^-$
Oxydation de substrats
Substrat
O_2
2
Oxygénation
$[Co^{II}L_2(OH)]^-{}_n(\mu O_2)$
$[Co^{III}L_2(OH)]_n(\mu O_2{}^{2-})$
3
5
Activation
H^+
Dégradation irréversible des complexes
4
H_2O
$n\,Co^{III}L_2(OH)$

Schéma 8 : Mécanisme putatif de complexation, oxygénation et activation des complexes de cobalt(II).

Avant d'étudier l'oxydation des additifs polymériques, l'oxydation d'additifs organiques modèles (Schéma 9) a d'abord été abordée.

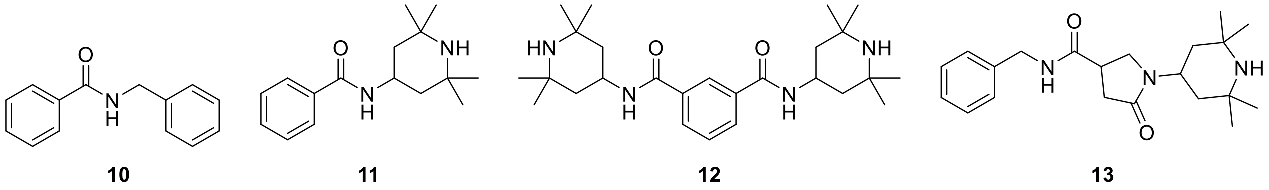

Schéma 9: Additifs organiques modèles étudiés dans le cadre de ce travail de thèse.

3.1. Spectrophotométrie d'absorption : un moyen pour suivre l'oxydation des additifs organiques

Préalablement à l'étude de l'oxydation des additifs par les catalyseurs métalliques, leur oxydation, en solution, par des oxydants organiques classiques a d'abord été effectuée pour caractériser les produits d'oxydation formés ainsi que leur cinétique de formation. Pour cela, trois oxydants organiques ont été employés : le peroxyde d'hydrogène, l'hydroperoxyde de *tert*-butyle et l'acide *méta*-chloroperbenzoïque (*m*-CPBA). Il a été montré que selon les conditions expérimentales employées, seul le *m*-CPBA permettait d'oxyder les différents additifs organiques modèles.

La spectrophotométrie d'absorption UV-visible a également été employée pour suivre les cinétiques de formation des différents produits. Les résultats sont donnés dans le Tableau 11.

*Tableau 11 : Rendements et paramètres cinétiques des oxydations de **11**, **12** and **13** en présence de* m-CPBA *dans différents solvants suivies par spectrophotométrie d'absorption UV-visible.*

Solvant	*m*-CPBA (éq.)	11		12*		13	
		Rdt (%)	$t_{1/2}$ (min)	Rdt (%)	$t_{1/2}$ (min)	Rdt (%)	$t_{1/2}$ (min)
MeOH	25	5	6,9(2)	17	6,7(3)	5	2,5(3)
EtOH	3	*n.t.*	*n.t.*	0,7	231(77)	*n.t.*	*n.t.*
	5	28	1,8(2)	2	24(2)	2	0,30(4)
	10	31	2,6(2)	3	36(4)	2	0,19(5)
DCE	3	9	2,10(2)	5	~ 3500 (~ 58 h)	*n.t.*	*n.t.*

n.t. : non testé

** mécanisme en deux étapes : la première étape étant trop rapide pour déterminer les paramètres cinétiques correspondants, les rendements donnés sont les rendements globaux pour les deux étapes ; les paramètres cinétiques sont donnés pour la seconde étape*

3.2. Oxydation assistée des additifs organiques avec des complexes métalliques

L'objectif étant d'oxyder les additifs en présence de catalyseurs métalliques, ceci a tout d'abord été testé pour un additif organique modèle (**11**) en présence de chacun des deux catalyseurs choisis (**1Co** et **9Co**). Avec chacun des catalyseurs métalliques, l'oxydation de **11** a eu lieu. Ces résultats établissent donc une preuve de concept de l'oxydation d'additifs par un catalyseur métallique. Il ne faut pas perdre de vue que ces expériences ont été menées en solution et devront être transposées à l'état solide pour mimer le comportement dans des polymères.

4. Chapitre IV : Oxydation des additifs polymériques

Afin de se rapprocher au plus près des conditions réelles, des additifs polymériques ont été examinés (Schéma 10). Leur oxydation à l'état solide, en présence ou en l'absence de catalyseur métallique a été suivie.

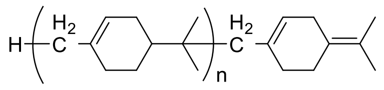

Dercolyte S 125

14

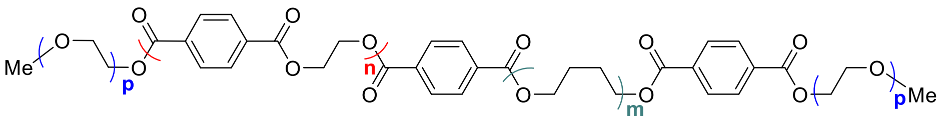

Dérivé polytétrahydrofurane

15

Schéma 10 : Additifs polymériques étudiés durant ce travail de thèse.

4.1. Approche analytique pour le suivi de l'oxydation des additifs polymériques et la sélection de catalyseurs métalliques

La spectroscopie IRTF a été sélectionnée comme la méthode la plus simple à mettre en œuvre et la moins coûteuse pour suivre l'oxydation des additifs à l'état solide.

Une étude préliminaire utilisant le Dercolyte S 125 **14** et plusieurs catalyseurs métalliques a permis de sélectionner les catalyseurs métalliques ayant le plus fort potentiel d'oxydation à l'état solide (Figure 16). Il apparait que le stéarate de cobalt(II) **9Co** présente la meilleure activité. C'est donc pourquoi ce catalyseur et son analogue de manganèse(II) **9Mn** ont été sélectionnés pour les études ultérieures.

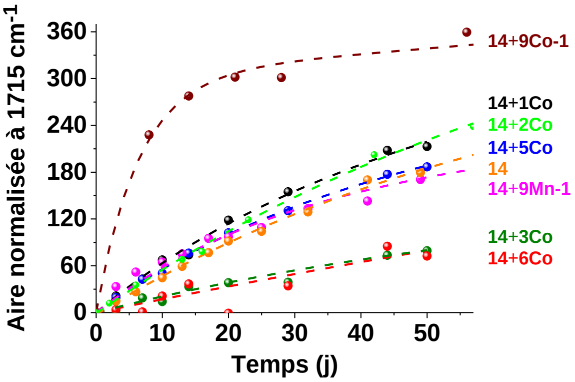

*Figure 16 : Aire normalisée à 1715 cm^{-1} représentant l'oxydation de **14** à 70 °C en présence des différents catalyseurs métalliques.*

Il convient de noter que le pic centré à 1715 cm^{-1} ($\nu_{C=O}$) a été normalisé et utilisé pour suivre le processus d'oxydation au cours du temps, quel que soit l'additif polymérique considéré (Dercolyte S125 **14**, Figure 17 **a)** ou polyTHF **15**, Figure 17 **b)**).

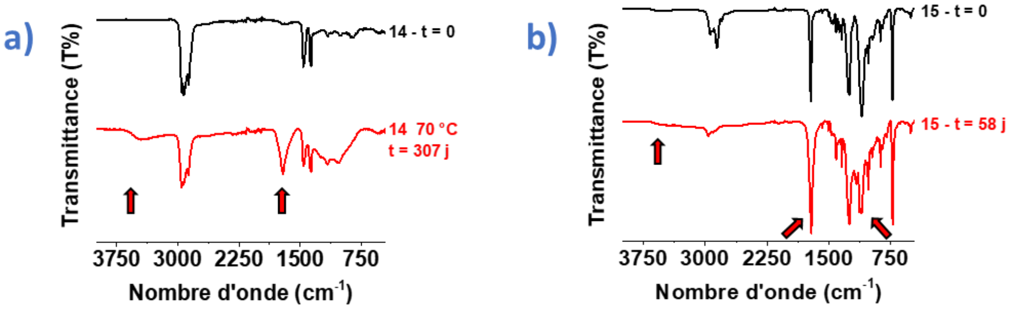

*Figure 17 : Spectres IRTF de **14** (**a**) et **15** (**b**) initialement et après 307 et 68 jours d'oxydation à 70 °C respectivement.*

4.2. Etude de l'oxydation du Dercolyte S 125 14

4.2.1. Oxydation du Dercolyte S 125 14 suivie par spectroscopie IRTF

Des analyses d'échantillons à l'état solide ont été effectuées par microscopie électronique à balayage et ont montrées une hétérogénéité des échantillons en termes de taille de particule. Il a donc été nécessaire d'évaluer l'influence de la distribution de taille des particules (aussi bien de l'additif **14** que des catalyseurs métalliques (**9Co** ou **9Mn**)). Cette étude a montré que ce paramètre n'influençait que peu la cinétique d'oxydation ou son efficacité.

Lors de la mise en œuvre des polymères, ces derniers sont extrudés, c'est-à-dire qu'ils sont chauffés pendant un temps court à haute température et sous atmosphère inerte. Il nous a donc semblé important de mimer ces conditions au laboratoire en chauffant sous atmosphère inerte l'additif seul ou les mélanges additif/catalyseurs pendant un temps défini à une température de 100 °C. Les résultats pour l'additif **14** en présence de stéarate de cobalt(II) **9Co** sont présentés en Figure 18 et ceux pour l'additif **14** en présence de stéarate de manganèse(II) **9Mn** en Figure 19.

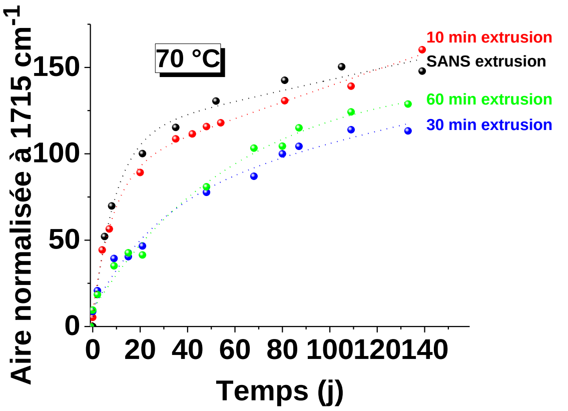

*Figure 18 : Aire normalisée à 1715 cm^{-1} illustrant l'oxydation de **14** avec **9Co-2** à 70 °C après 0, 10, 30 et 60 minutes d'extrusion.*

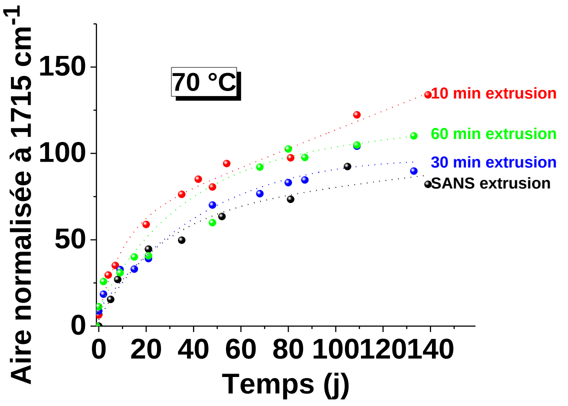

*Figure 19 : Aire normalisée à 1715 cm^{-1} illustrant l'oxydation de **14** avec **9Mn-2** à 70 °C après 0, 10, 30 et 60 minutes d'extrusion.*

Les premières observations, complétées par les paramètres cinétiques (Tableau 12) permettent de conclure que le temps optimal d'extrusion, dans les conditions expérimentales données, est de dix minutes, aussi bien en termes d'efficacité d'oxydation que de cinétique, quel que soit le catalyseur considéré (**9Co** ou **9Mn**).

Tableau 12 : Temps de demi-vie (donnés en jours) des différentes réactions d'oxydation à 70 °C après 0, 10, 30 et 60 minutes d'extrusion.

Conditions / **Echantillon**	**$t_{1/2}$ (jour)** Sans *"extrusion"* **70 °C**	**$t_{1/2}$ (jour)** 10 min *"extrusion"* **70 °C**	**$t_{1/2}$ (jour)** 30 min *"extrusion"* **70 °C**	**$t_{1/2}$ (jour)** 60 min *"extrusion"* **70 °C**
14-F1'	36(2)	46(3)	58(10)	43(3)
14-F1'+**9Co-2**-F4	6(1)	6,3(6)	17(9)	35(17)
14-F1'+**9Mn-2**-F4	10(3)	7(1)	~ 35*	~ 35*

* Valeur estimée

4.2.2. Elucidation de la nature des produits d'oxydation

Les spectres infrarouges enregistrés durant les différentes études impliquant le Dercolyte S 125 **14** à l'état solide ont montré la formation d'une bande centrée vers 1715 cm^{-1}, caractéristique des groupes carbonyles, et une autre centrée vers 3450 cm^{-1} qui reflète la formation de fonctions alcool. Il a donc été initialement proposé que l'oxydation de l'additif **14** s'effectue en position α de la double liaison carbone-carbone (c'est-à-dire une oxydation allylique) menant à des fonctions alcools et/ou carbonyles (Schéma 11).

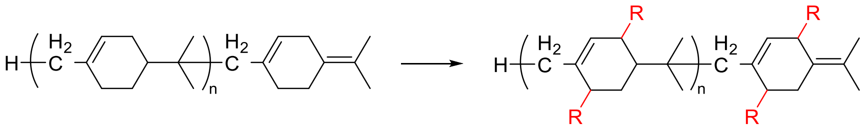

14

R : =O ou -OH

*Schéma 11 : Oxydation aérobie assistée par catalyse métallique proposée pour l'additif polymérique **14**.*

La présence de fonctions carbonyles et alcools a également été évaluée par XPS. Les échantillons de l'additif **14** présentent un enrichissement en oxygène démontrant très clairement que l'oxydation a bien eu lieu. En regardant l'analyse portant sur l'oxygène (O 1s, Tableau 13), l'échantillon initial, **14**, contribue à 92% pour l'échantillon oxydé. Cependant, la même analyse centrée sur le carbone (C 1S, Tableau 13), les simples et les doubles liaisons carbone-oxygène contribuent à 57% et 31% respectivement pour l'échantillon oxydé pendant dix mois.

Tableau 13 : Contribution relative des différentes fonctions dans l'échantillon oxydé analysé par XPS.

	C 1s		**O 1s**		
Echantillon	**14** (initial)	**C**-O	**14** (initial)	C-**O**-C, CO**O**H ou C-**O**H	**O**=C ou O-C=**O**
14 (après 10 mois d'oxydation)	92%	8%	12%	57%	31%

De plus, l'enrichissement en oxygène des échantillons **14** au cours de l'oxydation a également été démontré par microanalyse (Tableau 14).

*Tableau 14 : Résultats de microanalyses pour les échantillons **14** au cours du processus d'oxydation.*

	%N	**%C**	**%H**	**%O**
14 frais	0	86,7	11,5	**1,8**
14 après 10 jours d'oxydation à 70 °C	0	83,9	11,0	**5,2**
14 après 4,5 mois d'oxydation à 70 °C	0	77,0	9,6	**13,4**

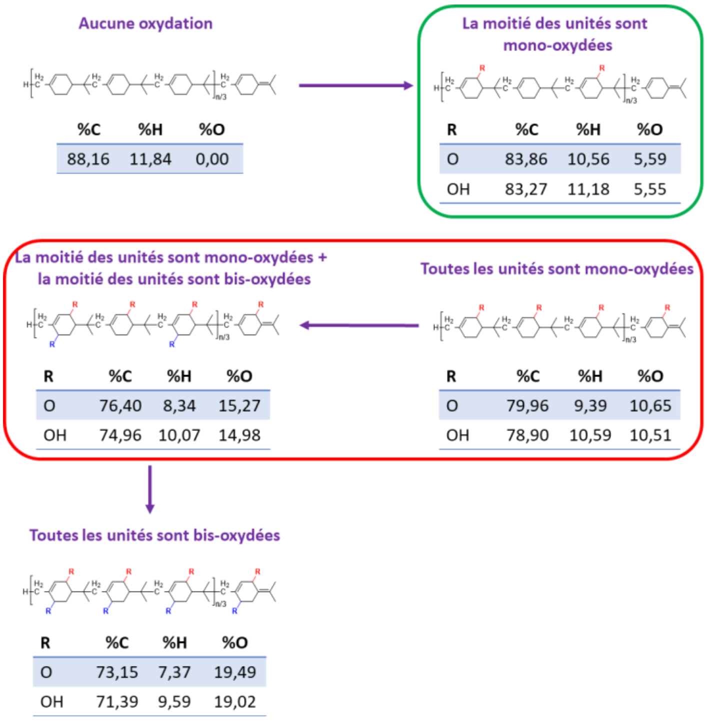

Aucune oxydation

%C	%H	%O
88,16	11,84	0,00

La moitié des unités sont mono-oxydées

R	%C	%H	%O
O	83,86	10,56	5,59
OH	83,27	11,18	5,55

Toutes les unités sont mono-oxydées

R	%C	%H	%O
O	79,96	9,39	10,65
OH	78,90	10,59	10,51

La moitié des unités sont mono-oxydées + la moitié des unités sont bis-oxydées

R	%C	%H	%O
O	76,40	8,34	15,27
OH	74,96	10,07	14,98

Toutes les unités sont bis-oxydées

R	%C	%H	%O
O	73,15	7,37	19,49
OH	71,39	9,59	19,02

*Figure 20 : Modèles pour les calculs des analyses élémentaires théoriques des espèces oxydées supposées de l'additif polymérique **14**.*

Afin d'estimer le nombre de positions oxydées ainsi que la nature des produits d'oxydation (alcools et/ou cétones), une approche théorique a été utilisée en supposant une mono-oxydation de la moitié des unités, une mono-oxydation de toutes les unités, et une double oxydation de la moitié ou de toutes les unités. Ceci laisse suggérer qu'après dix jours d'oxydation (%O : 5,2%, Tableau 14), la moitié des unités sont mono-oxydées (encadré vert, Figure 20). Après quatre mois et demi d'oxydation, le produit oxydé semble être une moyenne entre la mono-oxydation de toutes les unités, et la mono-oxydation de toutes les unités et la bis-oxydation de la moitié des unités polymériques (encadré rouge, Figure 20).

D'autre part, la chromatographie d'exclusion stérique a permis d'écarter l'hypothèse d'un clivage oxydatif du polymère durant le processus d'oxydation et la RPE a indiqué l'absence de caractère radicalaire des produits formés. Enfin, la RMN ^{1}H a permis de mettre en évidence une disparition du signal des protons vinyliques laissant suggérer une oxydation de ce site.

En combinant l'ensemble de ces données, la formation d'alcools/cétones en position α de la double liaison carbone-carbone ne peut pas conduire aux seuls produits d'oxydation suggérés. L'époxydation de la double liaison carbone-carbone doit également être envisagée comme décrit dans le Schéma 12.

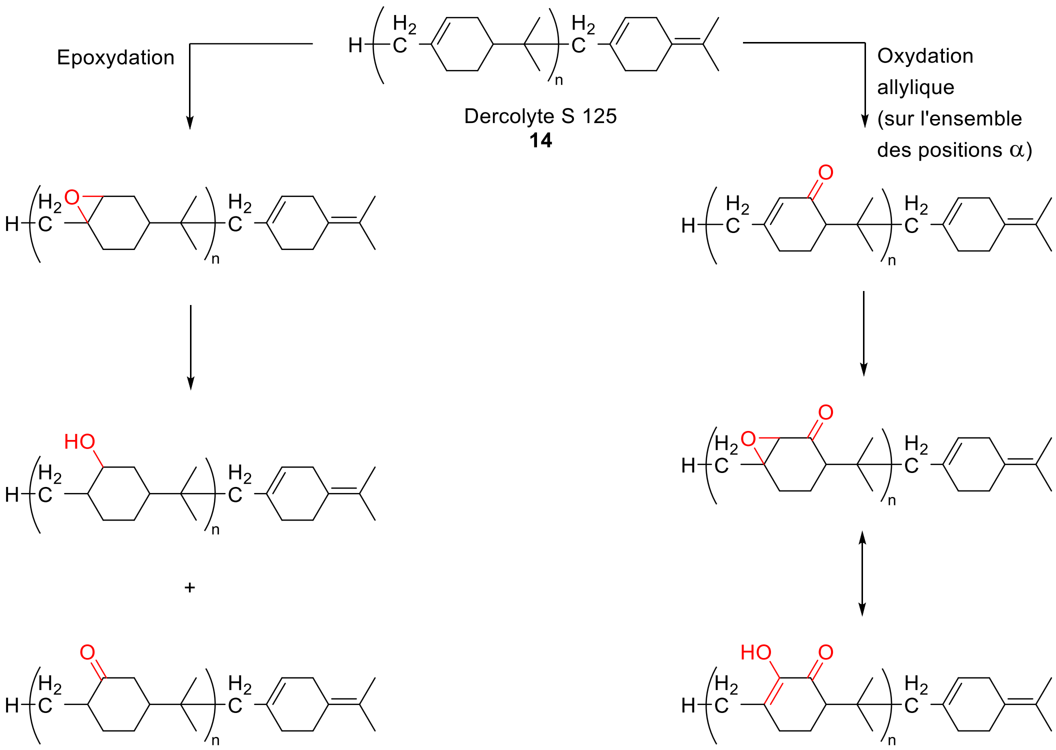

Schéma 12 : Produits d'oxydation suggérés et leur mécanisme de formation putatif. Pour l'oxydation allylique, les deux positions α peuvent être impliquées, seuls les produits d'oxydation résultant d'une position α sont décrits ici.

4.3. Etude de l'oxydation du polyTHF 15

L'oxydation d'un autre additif polymérique, le polyTHF **15**, a également été étudiée.

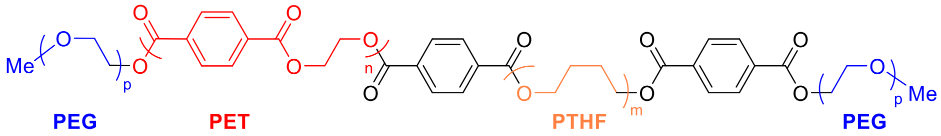

polyTHF

15

*Schéma 13 : Structure chimique de l'additif polymérique **15***
(PEG : polyéthylène glycol ; PET : polyéthylène téréphtalate ; PTHF : polytétrahydrofurane)

4.3.1. Oxydation du polyTHF 15 suivie par spectroscopie IRTF

Comme pour le Dercolyte S125 14, l'oxydation du polyTHF 15 a été suivie par spectroscopie IRTF. Contrairement au Dercolyte S125 14, le polyTHF 15 s'oxyde à température ambiante, en présence ou en absence de catalyseur métallique (Figure 21). Les temps de demi-vie des différentes réactions sont donnés dans le Tableau 15.

Tableau 15 : Temps de demi-vie (donnés en jours) des différentes réactions d'oxydation à température ambiante.

Echantillon	$t_{1/2}$ (jour)
15-2-F1'	~ 17
15-2-F1'+**9Co-2**-F4	5(1)
15-2-F1'+**9Mn-2**-F4	~ 69
15-2-F1'+**9Mn-3**-F4	~ 58

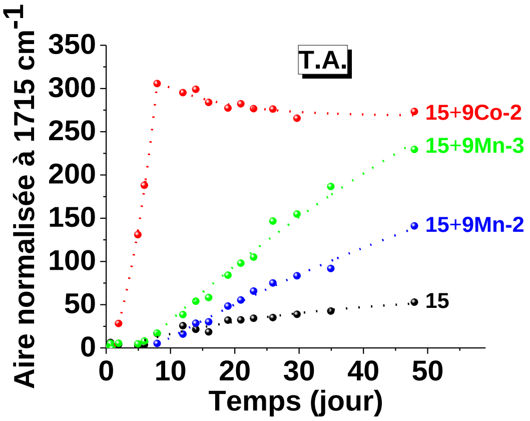

*Figure 21 : Aire normalisée à 1715 cm⁻¹ démontrant l'oxydation de l'additif **15** à température ambiante que ce soit seul ou en présence de catalyseur métallique.*

4.3.1.1. Optimisation du ratio catalyseur/additif

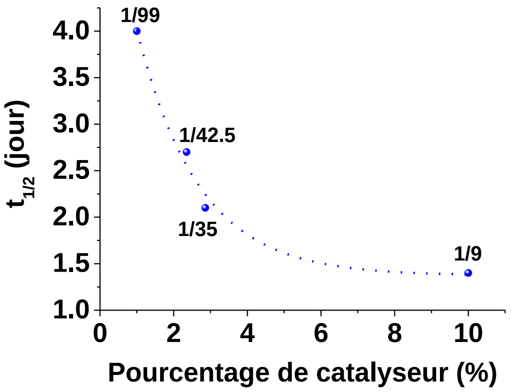

*Figure 22 : Temps de demi-vis de la réaction d'oxydation de l'additif **15** en présence de cobalt(II) stéarate **9Co-2** à température ambiante en fonction du ratio catalyseur/additif.*

L'influence du ratio entre le catalyseur métallique (seul le cobalt(II) stéarate **9Co** a été considéré dans cette étude) et l'additif polymérique **15** a été évalué en faisant varier celui-ci : additif/catalyseur 9/1, 35/1, 42,5/1 et 99/1 (masse/masse). Il apparaît que plus la proportion de catalyseur est élevée, plus le temps de demi-vie de la réaction d'oxydation est faible, comme illustré dans la Figure 22. Cependant, pour des questions de cinétique et économique, le ratio 35/1 a été conservé.

4.3.1.2. Influence de la température sur le processus d'oxydation avec des catalyseurs métalliques de l'additif 15

L'impact de la température sur la cinétique et l'efficacité de l'oxydation de l'additif **15** a également été évalués. Quelles que soient les combinaisons considérées (avec ou sans catalyseur métallique, nature du catalyseur métallique), les réactions d'oxydation de l'additif **15** se sont avérées être plus efficaces (Figure 23) et plus rapides (Tableau 16) à 70 °C qu'à température ambiante (Figure 21 et Tableau 16).

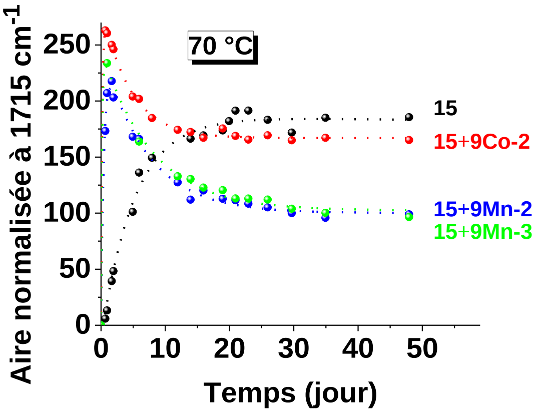

*Figure 23 : Aire normalisée à 1715 cm^{-1} représentant l'oxydation de l'additif **15** seul ou avec **9Co-2**, **9Mn-2** ou **9Mn-3** à 70 °C.*

*Tableau 16 : Temps de demi-vies des différentes réactions d'oxydation de l'additif **15** à température ambiante et à 70 °C (donnés en jours)*

	$t_{1/2}$ (jour)		
	T.A.	70 °C	
Echantillon		1ère étape	2ème étape
15-2-F1	~ 17	3,6(4)	
15-2-F1+**9Co-2**-F4	5(1)	0,13(2)	3,3(2)
15-2-F1+**9Mn-2**-F4	~ 69	0,32(3)	5,1(5)
15-2-F1+**9Mn-3**-F4	~ 58	<< 0,2	8,3(8)

4.3.2. Elucidation de la nature des produits d'oxydation

Comme pour le Dercolyte S125 **14**, une investigation sur les produits oxydés de l'additif **15** a été menée afin de déterminer leur nature/structure. Les spectres infrarouges enregistrés durant les différentes études impliquant le polyTHF **15** à l'état solide ont montré la formation d'une bande centrée vers 1715 cm^{-1}, caractéristique des groupes carbonyles, et une autre centrée vers 3450 cm^{-1} qui reflète la formation de fonctions alcool. Ces observations ont été confirmées par XPS (Tableau 17).

Tableau 17 : Contribution relative des différentes fonctions dans l'échantillon oxydé analysé par XPS.

Echantillon	**C 1s**			**O 1s**		
	15 (initial)	**C**-C	O-**C**=O	**15** (initial)	C-**O**-C, CO**O**H ou C-**O**H	**O**=C ou O-C=**O**
15 (après 26 jours d'oxydation)	68%	17%	15%	27%	31%	42%

De plus, l'enrichissement en oxygène des échantillons **15** au cours de l'oxydation a également été démontré par microanalyse (Tableau 18).

*Tableau 18 : Résultats de microanalyses pour les échantillons **15** au cours du processus d'oxydation.*

	%N	**%C**	**%H**	**%O**
15 frais	0	62,4	7,8	**29,8**
15 après 26 jours d'oxydation à 70 °C	0	55,9	5,3	**38,8**

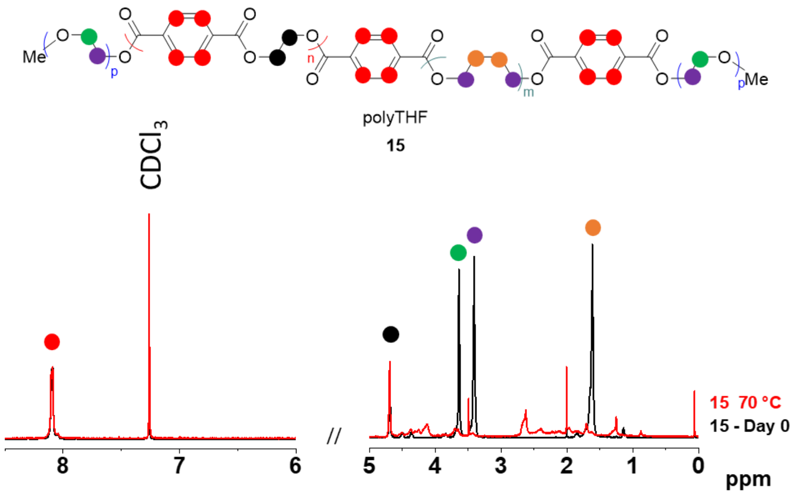

*Figure 24 : Spectres RMN ^{1}H du polyTHF **15** avant (**noir**) et après (**rouge**) une oxydation prolongée à 70 °C, enregistrés dans le CDCl$_3$ à 500 MHz.*

Contrairement à ce qui a été observé lors de l'étude menée sur le Dercolyte S125 **14**, la RMN (^{1}H et ^{13}C) s'est révélée interprétable pour les échantillons de polyTHF **15**. Ces analyses nous ont permis d'observer la disparition de certains signaux (protons en *violet*, Figure 24, portés par les unités PTHF et PEG ; protons en *vert*, Figure 24, portés par les unités PEG et protons en *orange*, Figure 24, portés par les unités PTHF) et ainsi de déterminer les différents sites d'oxydation ou de clivage de la molécule.

Les analyses réalisées par chromatographie d'exclusion stérique ont également permis de mettre en évidence un clivage oxydatif du polymère durant le processus d'oxydation (Tableau 19), confirmant l'hypothèse effectuée à partir des résultats de la RMN ^{1}H.

*Tableau 19 : Résultats de chromatographie d'exclusion stérique pour les différents échantillons de l'additif **15**.*

Echantillon	**$\overline{\mathrm{M}}\mathrm{n}$ (g.mol^{-1})**	**$\overline{\mathrm{M}}\mathrm{w}$ (g.mol^{-1})**	**Đ**
15 frais	18 800	46 100	49,8
15 après oxydation à 70 °C	2 700	4 500	1,6

Contrairement au Dercolyte S125 **14**, l'intégrité du polyTHF **15** n'est pas conservée durant son oxydation (catalysée ou non par des complexes métalliques). En combinant l'ensemble de ces analyses, il peut donc être suggéré le mécanisme d'oxydation suivant (Schéma 14).

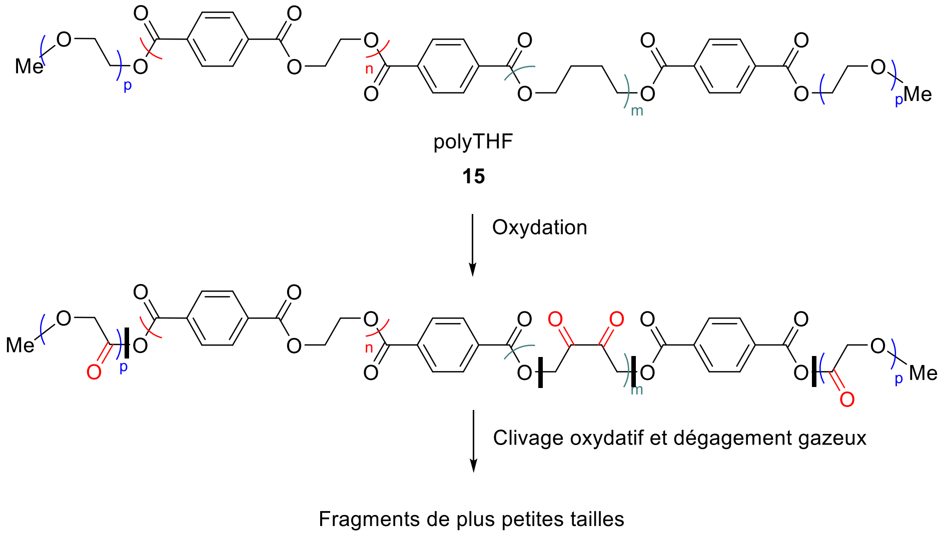
polyTHF
15
Oxydation
Clivage oxydatif et dégagement gazeux
Fragments de plus petites tailles

*Schéma 14 : Sites d'oxydation putatifs et produits formés à partir du clivage oxydatif de l'additif **15**. Les lignes noires indiquent les potentiels points de clivage.*

5. Conclusion générale

L'objectif principal de ce travail de doctorat était d'acquérir une connaissance plus profonde du mécanisme d'action des barrières à oxygène dans les plastiques (c'est-à-dire, catalyseurs métalliques et additifs sacrificiels) pour la préservation de denrées alimentaires.

Les propriétés physico-chimiques des catalyseurs métalliques ont été étudiées en solution. Les bases de Schiff de cobalt(II) (**1Co**-**7Co**) et de manganèse(II) (**1Mn**-**7Mn**), ainsi que les stéarates de cobalt(II) **9Co** et de manganèse(II) **9Mn** ont été sélectionnés. Les constantes de protonation et la stabilité des ligands ont été déterminées par spectrophotométrie d'absorption UV-visible en fonction du pH, et ont clairement été reliées à leurs affinités pour le centre métalliques (c'est-à-dire, cobalt(II)). **1Co** apparaissait comme l'un des systèmes les plus prometteurs pour l'oxygénation et l'activation de l'oxygène. La synthèse de ces bases de Schiff de cobalt(II) a été réalisée au moyen de stratégies de synthèse originales, comme la synthèse sans solvant et en une seule étape, ou en utilisant une approche « *Template* ».

Les étapes d'oxygénation et d'activation de ces catalyseurs métalliques ont été étudiées par diverses techniques analytiques (par exemple, spectrophotométrie d'absorption UV-visible, oxymétrie, ESI-MS, RMN ^{1}H, voltampérométrie cyclique) pour suivre leurs processus, évaluer leurs cinétiques, et déterminer la nature de leurs produits. Tandis que le complexe de base de Schiff de cobalt(II) substitué avec un groupement méthoxy **6Co** présentait l'oxygénation et l'activation la plus rapide en solution, une espèce trischelate de cobalt(III) (c'est-à-dire un catalyseur inactif) était formée durant les étapes d'oxygénation et d'activation. Il a été montré que ces espèces trischelates de cobalt(III) ne sont plus actives envers la liaison/activation de l'oxygène. Bien que leurs activités d'oxygénation et d'activation ne soient pas parmi les plus efficaces, il a clairement été démontré que **2Co** et **9Co** sont les systèmes les plus prometteurs du fait de la formation des seules espèces bischelates de cobalt(III) en solution dans des conditions aérobie.

Après avoir étudié les propriétés physico-chimiques de ces catalyseurs métalliques en solution, l'oxydation d'additifs organiques modèles a été évaluée en solution en utilisant des oxydants organiques classiques (par exemple, le peroxyde d'hydrogène, l'hydroperoxyde de *tert*-butyle ou le *m*-CPBA) et leurs produits d'oxydation ont été caractérisés. Afin d'avoir une évaluation plus précise de leur réactivité en solution, leurs paramètres cinétiques d'oxydation ont été déterminés en utilisant la spectrophotométrie d'absorption UV-visible. Enfin, l'oxydation en solution de l'additif organique le plus prometteur **11** en présence de l'un des deux catalyseurs de cobalt(II) sélectionnés (**1Co** et **9Co**) a été réalisée avec succès, établissant une preuve de concept de l'oxydation aérobie, en solution, d'additifs par des catalyseurs métalliques.

Bien que la faisabilité de l'oxydation d'additifs en solution par des catalyseurs métalliques a été établie, le principal objectif constituait néanmoins de se placer au plus près des conditions réelles (c'est-à-dire des films ou des bouteilles en plastique) et c'est pourquoi des études d'oxydation des additifs à l'état solide ont été entreprises. Pour suivre cette étape d'oxydation, la spectroscopie IRTF a été mise en évidence comme un moyen analytique pertinent. L'oxydation aérobie (c'est-à-dire thermiquement assistée ou non) de deux additifs polymériques (l'homopolymère Dercolyte S 125 **14** et le copolymère **15** également nommé polyTHF (polytétrahydrofurane)) a été étudiée en l'absence ou en présence de catalyseurs métalliques sous diverses conditions expérimentales (par exemple, influence de la température, de la distribution de taille des particules du catalyseur et/ou de l'additif, de la pré-activation des échantillons avec un processus dit d'« extrusion », de la pureté des catalyseurs métalliques, …). Contrairement à l'homopolymère Dercolyte S 125 **14**, le copolymère **15** subissait une oxydation que ce soit à température ambiante ou à 70 °C. Il a été démontré que sa cinétique d'oxydation était plus rapide que celle de l'homopolymère **14**, spécialement quand il était associé avec le catalyseur métallique **9Co** à température ambiante ou à 70 °C.

Point d'orgue de ce travail de thèse, des études ont été entreprises pour élucider les produits d'oxydation des additifs **14** et **15**. Bien qu'un large spectre de techniques analytiques complémentaires ait été employé (par exemple, spectroscopie IRTF, analyse élémentaire, XPS, chromatographie d'exclusion stérique, RMN), leur caractérisation reste un challenge. Il a été démontré que l'homopolymère **14** ne subit pas de clivage oxydatif même après une oxydation intensive. Il a été également montré que l'insaturation constituait un site réactionnel important d'oxydation. Concernant le copolymère **15** hautement dispersé, son oxydation catalysée par les stéarates de cobalt(II) **9Co** ou manganèse (II) **9Mn** s'effectue sur différents sites réactionnels et mène ultérieurement à des clivages oxydatifs et la génération de fragments plus petits.

Il apparaît donc que la vitesse et l'efficacité de l'oxydation des additifs polymériques étaient hautement dépendantes de la nature du catalyseur métallique sélectionné (c'est-à-dire **9Co** était plus efficace que son analogue **9Mn**). Du fait de la sensibilité différente de l'oxygène pour les produits alimentaires, l'optimisation de la combinaison catalyseur/additif et la formulation (c'est-à-dire le catalyseur métallique sélectionné, la nature de l'additif, le ratio catalyseur/additif, …) pourraient permettre de répondre aux besoins spécifiques des différents types de produits alimentaires. En perspective pour ce projet, une étude intensive pourrait être orientée vers les conditions réelles (c'est-à-dire, emballage rempli de produits alimentaires) où les effets des barrières à l'oxygène pourraient être directement évalués sur les produits alimentaires affichant un spectre large de sensibilité à l'oxygène (par exemple, vitamine, lipide, graisse, houblon, …).

General introduction

General introduction

From the ancient times, the civilisations have been faced to foodstuff storage issues and have tried to find appropriate containers that are still undergoing improvements. While the packaging materials evolved significantly from amphoras to plastics *via* glass, metal or paper; from local to global trade, the central question remained the same: find an appropriate container to store and transport food products.

In our globalised world, crops are grown in a continent, food are processed in a second one, and consumed in a third one. The food packaging is therefore increasingly necessary. Plastics packaging emerged on the market during the last century and are now becoming the most used and developed material. Indeed, due to the broad spectrum of chemical functions, the properties of plastic packaging can be modulated at will. From its production till its use by the consumers, the packaged food products could suffer various aggressions of different types: physical, chemical or microbiological to cite a few. While protecting the packaging from physical damages, *e.g.* shocks, consists to basically improve the physical properties and resistance of the material, tackle the chemical or microbiological attacks is more challenging. In that case, the composition of the material has to be optimized to address these issues. Responsible of numerous oxidation reactions in the food products, oxygen has to be eliminated from the inner atmosphere of the food packaging.

It is in this context that oxygen scavengers have been proposed and developed; they have to react with oxygen before it enters the packaging or to remove oxygen already present within the packaging. By developing and improving these innovative plastic materials, the shelf-life of processed foods will be prolonged, and wastes significantly reduced.

To achieve this goal, oxygen scavengers of different types have been developed and some of them are already available on the market. They are based on various technologies, such as iron powder, acid ascorbic, enzymes, photosensitive dyes or sacrificial polymers to cite a few. A wide spectrum of polymers is available and broadens every day; the possibilities are therefore endless, making this oxygen barriers technology as the best promising one. However, it became apparent that addition of metal catalysts in the composition of these polymer oxygen barriers is required to enhance the oxygen scavenging properties of these polymers (Figure 25). Even though the effect of the metal catalysts in such systems has been clearly demonstrated, the mechanistic (re)action is not yet well understood and the fundamental investigations are extremely scarce.

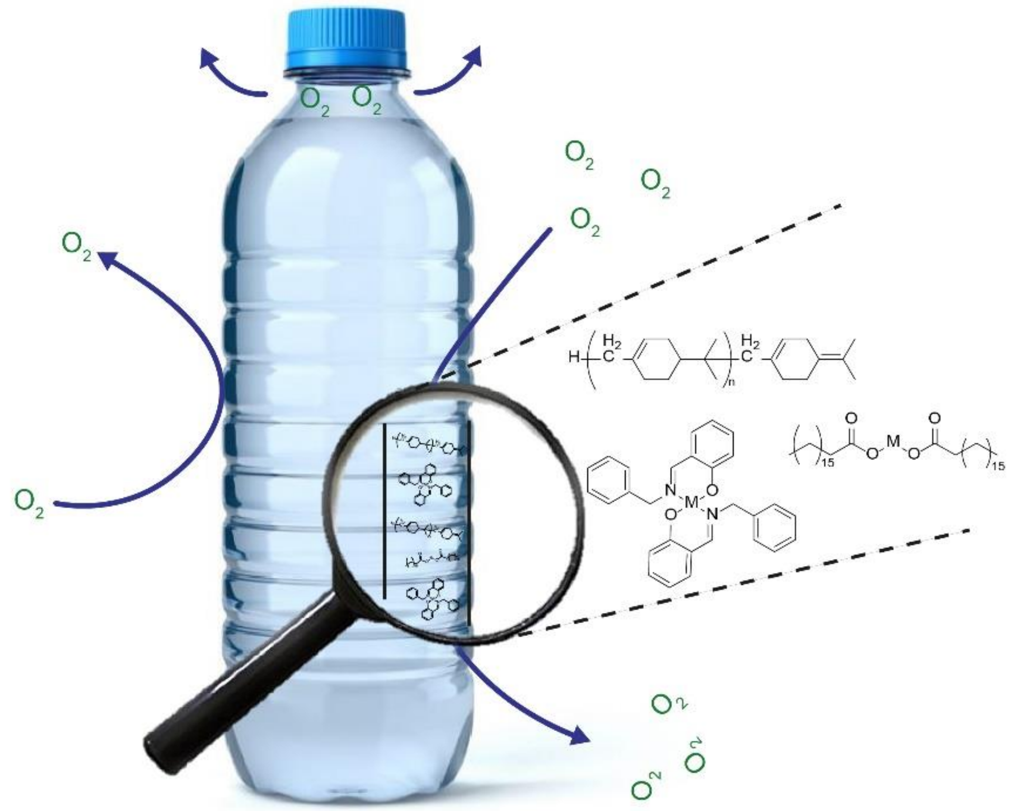

Figure 25: General principle of polymer-based oxygen barriers

It is in this context that this Ph.D. work was carried out within the framework of an industrial research collaboration between CNRS and Clariant. The main objective of this Ph.D. thesis was to unravel the mechanism of action of metallic active oxygen barriers devoted to plastics for food and drinks preservation.

In the introductory chapter, we will first describe a brief history of the different food packaging materials with a special focus on the plastic-based ones. The problematic of oxygen in the food packaging will be then discussed together with some approaches to solve this issue. A particular attention will be paid on a very promising and high potential solution, the combination of metal catalyst with sacrificial polymeric additives as versatile and efficient oxygen barriers devices.

The synthesis and full characterization of several metal catalysts of interest will be detailed in the second section of this manuscript. Their physico-chemical properties will be thoroughly described taking into account their use as metal catalysts for oxygen barriers applications. The protonation constants and stability in solution of the different ligands have been evaluated. It has been indeed shown that these acido-basic properties are intimately linked to the affinity of these ligands for the metal centres (*e.g.* cobalt(II) or manganese(II)). A significant part of this chapter will be dedicated to the oxygenation and activation properties of the different metal catalysts of interest. For that, complementary analytical means have been set up and the analytical strategy will be described.

The third chapter will describe the oxidation capacities of model organic additives in solution that have been originally considered in this project. Following a brief description of their oxidation reactions by classical organic oxidants (*i.e.* kinetics, spectroscopy, yield, characterization…), their oxidation in solution by metal catalysts of interest will be detailed.

Finally, the last chapter will be focused on solid-state approaches to be as close as possible to the real conditions (*i.e.* plastic films or bottles). The solid-state behaviour of two polymeric additives will be investigated under various experimental conditions in the presence or in the absence of metal catalysts. For each of the studied polymeric additives, a section will be dedicated to the tentative elucidation of the nature of the oxidation products that are generated along the oxidation process.

The data acquired during this Ph.D. work will be then discussed as a whole in the conclusion part.

Chapter I:

Food products packaging: a problematic since the ancient times

I. Food products packaging: a problematic since the ancient times

I.1. A brief history of the food packaging materials

Historically, leaves, skins and shells were used as the first hard packaging materials to store goods. From 6000 B.C., reed baskets and earthenware were produced and replaced progressively the less developed materials. With the development of the civilization and the beginning of the commercial exchange in the Mediterranean area, new containers, such as ceramics and amphoras, were developed to store and transport wine and other products between the ancient Greek and Roman empires. They were mainly used between 1500 B.C. and 500 A.D.. Glass materials were traced back to 7000 B.C. but the industrialisation of glass really began in 1500 B.C. in Egypt. The glass material composition did not vary so much until now, but significant advances were realized in the fabrication process. On the other hand, paper was the oldest flexible packaging; it was used from ancient Egypt with the papyrus and was progressively substituted by Chinese paper from 200-100 B.C. to 1300-1400 A.D., which is made from sheets of treated mulberry bark. The two newest materials, which appeared more recently, are metal and plastics. The first metal can was discovered in 1812, and metal containers use grew exponentially with the discovery of the can opener in 1875 and the pop top/tear tab can in the 1950's. Finally, plastics were developed from the 19th century with the discovery of the polystyrene by Eduard Simon in 1839. The discovery of all the other types of plastics and the rise of the plastic containers use was achieved from the 20th century onwards.[1]

With the evolution of the civilizations, food packaging materials evolved also; however, the main roles of the packaging remained the same: store, preserve and transport foods. In fact, foods should be preserved from the external environment, such as moisture, oxygen, mould…

Food is the most consumed product every day in the world and its packaging represents nowadays about 50% (by weight) of global packaging sales.[2] Therefore, this sector is very attractive and competitive for industrialists.

In Table I-1 are gathered the main different properties[2,3,4] of each type of material. Paper is a natural packaging which is light, not so much fragile and can be easily recycled. However, it is not adapted to every type of foods, such as liquid foods or drinks for example. On the other side, glass is an effective material which is not permeable, recyclable or directly reusable, but it suffers of its heavy weight and its weakness. Metal shares the same properties with glass, with, however, the main advantages to be lighter and not fragile. Nevertheless, it is not transparent, which can lead to marketing issues. Even though plastics are more or less permeable to gases or vapours, they remain one of the best choices for packaging. In fact, numerous types of plastics are nowadays available, allowing modulating packaging properties at will. In addition, they display lower costs and many functional advantages (thermosealability, microwave-resistant, optical properties, lightweight, difficult to break, unlimited shapes and sizes…) with respect to glass or metal. Moreover, the permeation issue of plastics can be improved with modification of the plastic composition.

---

[1] Raheem, D. *Emir. J. Food Agric.* **2012**, *25* (3), 177–188.

[2] Marsh, K.; Bugusu, B. *J. Food Sci.* **2007**, *72* (3), R39–R55.

[3] Coles, R.; McDowell, D.; Kirwan, M. J. *Food Packaging Technology*, Blackwell Publishing Ltd.; 2003.

[4] http://www.bbc.co.uk/schools/gcsebitesize/design/foodtech/packaginglabellingrev_print.shtml (accessed Sept 20, 2017).

Table I-1: Different materials for packaging - comparison of their primary properties.

Property / Material	Permeability	Transparency	Reusability/recyclability	Weight	Fragile
Glass	No	Yes	Yes	Heavy	Yes
Metal	No	No	Yes	Light	No
Aluminium	*No*	*No*	*Yes*	*Light*	*No*
Tinplate	*No*	*No*	*Yes*	*Light*	*No*
Paper	Yes	No	Yes	Light	No
Plastics	Yes	Yes	Yes	Light	No

Plastics (both rigid and flexible ones) are the most used materials nowadays, representing 37% of the global packaging market, as depicted on Figure I-1.[2]

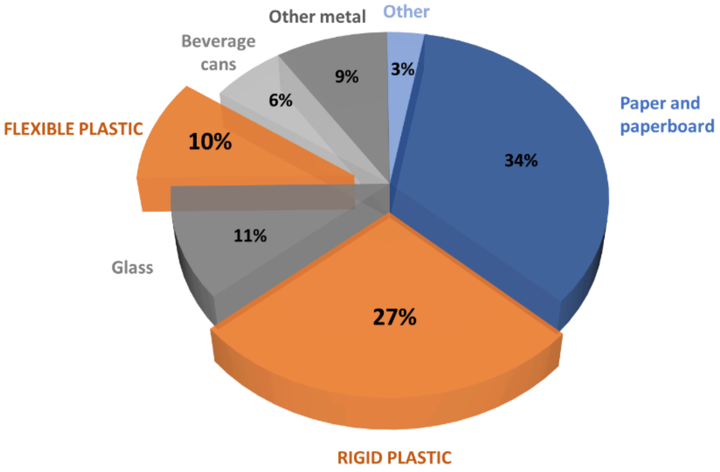

Figure I-1: Segmentation of packaging material.

I.1.1. Main functions of the food packaging materials

Each of the packaged goods owns a nutritional value and physical, chemical and microbiological states. The main role of any food packaging material is therefore to preserve these product properties from ambient environment aggressions (*e.g.* gases and vapours such as oxygen, carbon dioxide and moisture, temperature variations, relative humidity, light, pressure, mechanical impacts…). Packaging should also meet macro-environment requirements, such as the local or international legislations for food content packaging, but also marketing criteria (*e.g.* the price, ingredients and nutritional information to the consumers, the design), or transport, handling and distribution convenience. The environmental impact of the packaging material is also taking an increasingly layer place. (Figure I-2).[2,3,4]

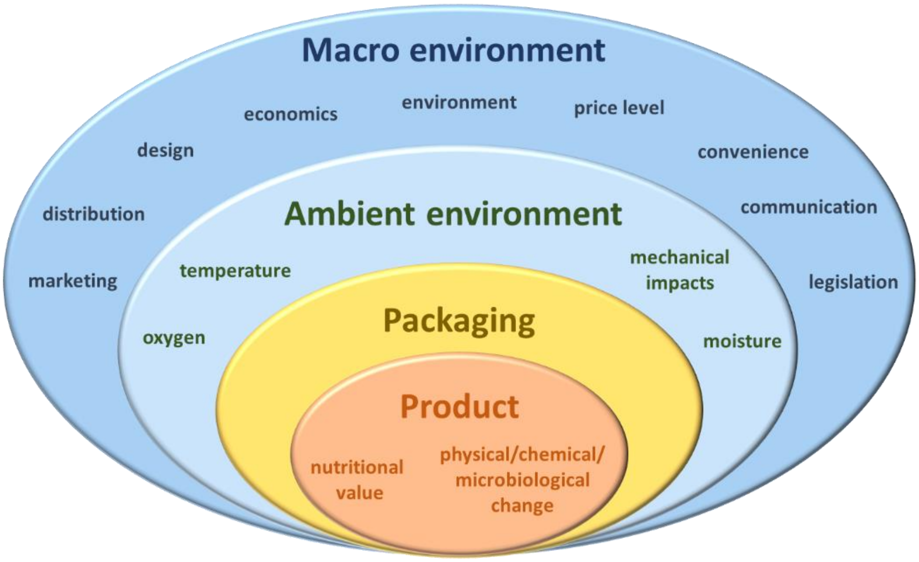
Macro environment
economics
environment
price level
design
convenience
distribution
communication
marketing
legislation
Ambient environment
temperature
mechanical impacts
oxygen
moisture
Packaging
Product
nutritional value
physical/chemical/ microbiological change

Figure I-2: Interaction of food with its environment - role of the packaging.[5]

Packaging also presents secondary functions as traceability, convenience, presentation, brand communication and tamper indication.

Three types of packaging can be defined:[3,4]

- The primary packaging, which is in direct contact with the beverage or the food (*e.g.* glass, plastic, metal, paper…).
- The secondary packaging, which is the middle layer of packaging and contains the primary packages (*e.g.* plastic film, carton…).
- The tertiary packaging, which is of importance for transport and handling (*e.g.* pallet, stretch-wrap…).

Attention will be paid on the food protection by the primary packaging from external influences, which can be grouped in three different categories:

- The chemical barriers allowing decreasing influence, on the contents, of gases (*e.g.* oxygen, carbon dioxide), moisture or light exposure.
- The biological barriers (*e.g.* bacterial, fungal, viral, parasitic).
- The physical protection against shocks.

I.1.2. Plastic packaging: modulating properties for food and drinks preservation

As mentioned above, plastic is the most versatile material (*i.e.* rigid or flexible containers, modulation of the transparency, of the gas barrier properties…); that is the reason why the following sections will be primarily focused on plastic materials for foods and drinks packaging.

Notwithstanding the stability of the European plastics production over the last fifteen years, the world plastics production is continuously increasing (Figure I-3), thus demonstrating the increasing use of plastics in our society.[6,7]

---

[5] International Association of Packaging Research Institutes. 2013.

[6] PlasticsEurope - Association of Plastics Manufacturers. 2015.

[7] PlasticsEurope - Association of Plastics Manufacturers. 2016.

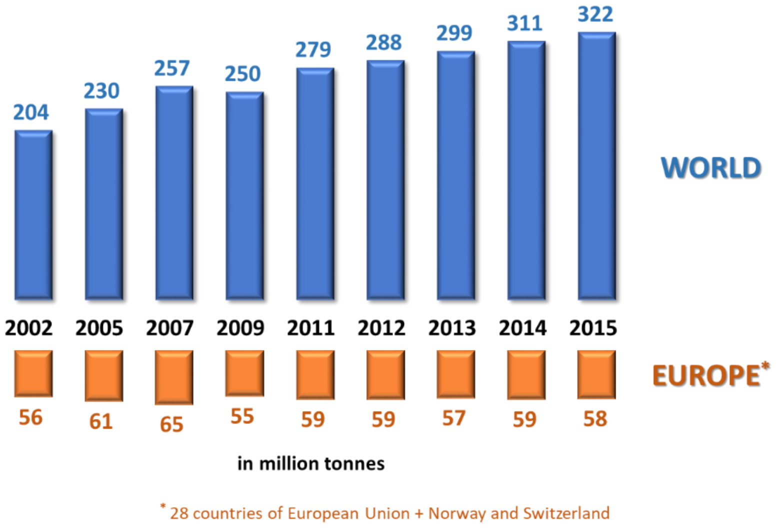

Figure I-3: World and European Union plastics production.

Regarding the European plastic market, 58 million tonnes are needed each year whose about 40% are required for packaging applications (Figure I-4) thus, representing the most important sector user.[6,7,8]

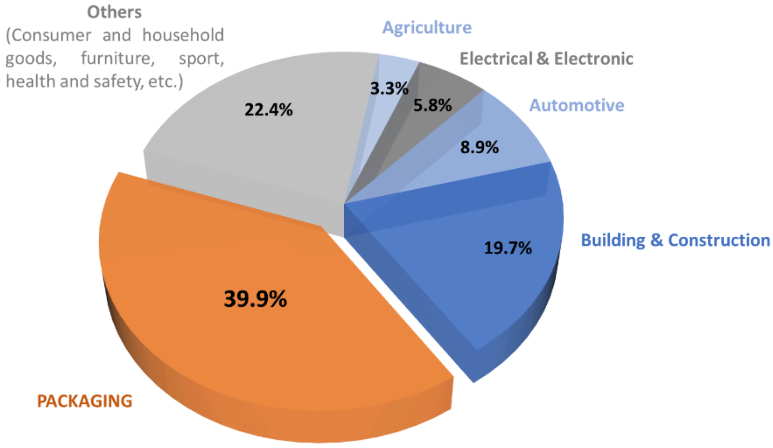

Figure I-4 : European plastic demand by market sector.

Plastics can be divided into two categories: the thermosets and the thermoplastics. Thermosets refer to polymers that cannot be remoulded after heating, whereas thermoplastics designate polymers that come back to their initial condition after heating. Due to these intrinsic properties, thermosets are principally used for automobiles and construction sectors, while thermoplastics can be ideally used for packaging purposes.

Five types of thermoplastics are commonly used nowadays for packaging applications: the polyethylene (PE) (*i.e.* representing both low density polyethylene (LDPE) and high density polyethylene (HDPE)) with about 56% of the European packaging market (by weight); both polypropylene (PP), polyethylene terephthalate (PET), polystyrene (PS) and polyvinyl chloride (PVC) representing the remaining 44% (by weight).[3] The repartition for the worldwide market slightly differs

---

[8] Silvestre, C.; Duraccio, D.; Cimmino, S. *Prog. Polym. Sci.* **2011**, *36* (12), 1766–1782.

in numbers but follows the same trend: PE (LDPE and HDPE) represents 56% of the worldwide market, followed by PET with 18%, PP with 14%, PS with 8% and PVC with only 2% (Figure I-5).[9]

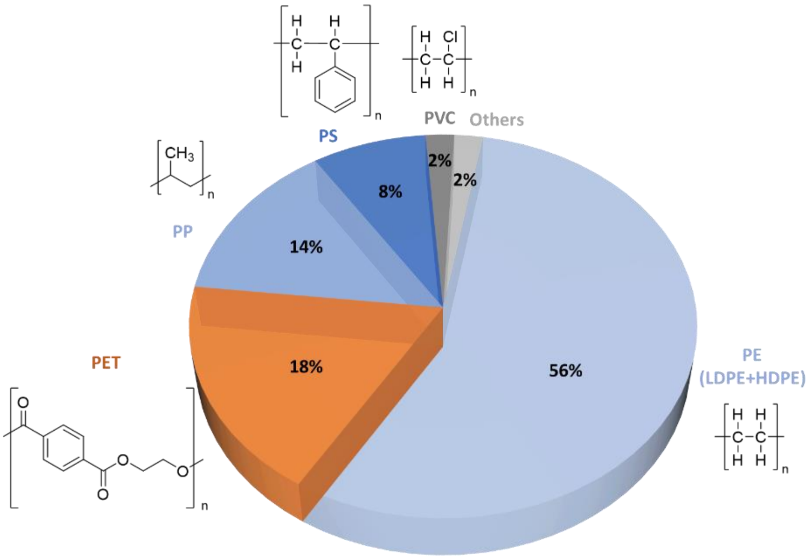

Figure I-5: Worldwide repartition of different plastics for packaging.

The main properties of the five thermoplastics mainly used for food packaging are presented in Table I-2.[2,3,10,11] PE (LDPE and HDPE) presents poor transparency and gas barrier properties, which makes this plastic material not suitable for gas sensitive products or for transparent packaging applications. PP remains not transparent but demonstrates improved gas barrier property with respect to PE. PS has the advantage to be transparent but displays some drawbacks such as poor gas barrier property and poor strength. If PET and PVC are now compared, both of them are characterized by excellent transparency and comparable water vapour barrier property. An additional advantage of PET with respect to PVC is its strength and its good gas barrier property. Last but not least for the industrialists is the lower cost of PET, as compared to that of PVC.

Table I-2 : Properties of mainly used polymers for food packaging.

Property / Polymer	Transparency	Cost (€/tonne)*	Strength	Water vapour barrier	Gas barrier	Granules aspects
PE (LDPE / HPDE)	Poor	1300-1410	Good	Excellent	Poor	
PP	Poor	1260-1400	Fair	Good	Fair	
PET	Excellent	1075-1115	Good	Good	Good	
PS	Excellent	1790-1930	Poor	Fair	Poor	
PVC	Good	1400-1550	Fair	Good	Fair	

* *August 2017 prices varying according to the market and quality.*[11]

---

[9] Alavi, S., Thomas, S., Sandeep, K. P., Kalarikkal, N., Varghese, J., Yaragalla, S. *Polymers for packaging applications*; lo; Apple Academic Press: Toronto, 2015.

[10] http://www.alphap.com/bottle-basics/plastics-comparison-chart.php (accessed Sept 20, 2017).

[11] http://www.plasticsnewseurope.com/ (accessed Sept 20, 2017).

It is worth noting that food requires different types of packaging and this economic sector reaches almost 50% (by weight) of the packaging sales.[2] The five most used polymers for food packaging applications (*e.g.* PE, PP, PET, PS and PVC), tiered with respect to their different properties, are indeed used for different food packaging applications. Table I-3 describes some applications of thermoformed and, films or bags packaging for each of the main used polymers.[1,2,12] Thermoplastic packaging are mainly used for semi-rigid to rigid containers applications (PE, PET or PVC bottles for milk and sauces, beverages, or beverages and oils respectively; PP and PS are used for yoghurt or ice cream containers…); whereas films and bags are mainly used for flexible packaging applications (*e.g.* PE for bread bags, PP for biscuit sachets, PVC for fruits, vegetables or cheese containers).

Table I-3: Mainly used plastics and their applications in food packaging.

Use **Polymer**	**Thermoformed**	**Films/bags**
PE (LDPE/HPDE)	- Bottles (milk) - Food storage containers - Sauces	- Household bags - Wrapping films - Bread bags - Food wraps
PP	- Sweet and snack wrappers - Screw caps - Food storage containers - Yoghurt, ice cream and butter pots	- Biscuits - Snacks - Sugar - Vegetables - Metalized films
PET	- Bottles (beverages) - Ready-meal trays	- Boil-in-the-bag packs - Metallized snack bags
PS	- Egg trays - Meat trays - Hot drink cups - Yoghurt - Ice cream - Jam - Syrup - Take-home boxes	- Wrapping films for sugar sweets
PVC	- Bottles (beverages, oils) - Tubes - Trays	- Shrink wrapping films for meat - Inserts in chocolate boxes - Fruits - Vegetables - Cheese

In addition, it is worth noting that permeability to vapour, gases… of common plastics is of crucial importance in the context of food packaging. In fact, water vapour and oxygen, in particular, can migrate through the package and modify continuously the inner atmosphere.

Although PET displays the best oxygen barrier properties of the five mainly used polymers for packaging, this property should be significantly improved. In fact, diverse entrance doors for oxygen are present on a plastic bottle. The simplest way is throughout opening and closing the bottle. The second most obvious purpose is small amounts of oxygen remaining in the headspace of packaging during bottle filling with food or drink, even after the air removal process. Finally, the last cause is the permeability of the plastic bottle cap and the walls (Figure I-6).

---

[12] Johansson, C. Functional barriers against migration for food packaging. In *Multifunctional and Nanoreinforced Polymers for Food Packing*; Lagarón, J.-M. Eds, 2011; pp 316–344.

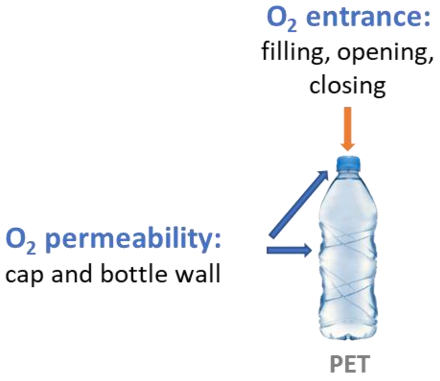

Figure I-6: Possible oxygen ingress.

Among the numerous gases and vapours that can penetrate into a food container, oxygen is responsible of numerous adverse effects, that have to be avoided in the food and drink industry:[3,13,14]

- Lipid or fat oxidation, also called oxidative rancidity of unsaturated fats that leads to undesirable flavours, and in extreme circumstances, to toxic end-products. It is the primary cause of food deterioration. The rancidity development can be inhibited by removal of oxygen or replacement of oxygen by inert gases such as nitrogen or carbon dioxide.
- Acceleration of fresh fruit and vegetable respiration processes. In fact, respiration and transpiration rates of these types of products are dependent on numerous parameters: such as temperature, relative humidity, gas composition (*e.g.* ethylene, oxygen and carbon dioxide), light, mechanical/physical damage or inclusion of food additives and treatments, to cite a few. A narrow range of oxygen level should be therefore maintained to avoid too low oxygen content (*e.g.* anaerobic respiration, production of off-flavours and off-odours, or anaerobic bacterial growth…) but also too high oxygen environment leading to undesired processes (*e.g.* maturation, chemical and microbial injuries…).
  High level of oxygen can also lead to other processes that can affect the fresh fruits and vegetables: loss of ascorbic acid or vitamin C, discoloration of pigments or enzymatic and non-enzymatic phenolic browning…
- Staling odours in soft bakery goods.
- Hatching of insect eggs followed by their growth.
- Oxidation of aromatic flavour oils beverages such as coffee and tea.
- Flavour deterioration of beer. Indeed, hops can be oxidized in the presence of oxygen and lead to off-flavour. To avoid this phenomenon, oxygen scavenger bottles are needed.[15]
- Darkening or browning of fresh meat pigments. The purple myoglobin can be either oxygenated under high oxygen concentration into red oxymyoglobin, responsible of the red colour of fresh beef meat; or be oxidized under low oxygen concentration in brown metmyoglobin, which is not able to bind oxygen anymore and not valued by consumers (Figure I-7).[16] It is why a high level of oxygen (70 to 80%) should be maintained in fresh meats packaging.

---

[13] Peterson, K.; Nielsen, P. V.; Bertelsen, G.; Lawther, M.; Olsen, M. B.; Nilsson, N. H.; Mortensen, G. *Trends Food Sci. Technol.* **1999**, *10*, 52–68.

[14] Brody, A. L.; Strupinsky, E. P.; Kline, L. R. *Active packaging for food applications*; CRC press, 2001.

[15] Kuchel, L.; Brody, A. L.; Wicker, L. *Packag. Technol. Sci.* **2006**, *19* (1), 25–32.

[16] Lee, S. Y.; Lee, S. J.; Choi, D. S.; Hur, S. J. *J. Sci. Food Agric.* **2015**, *95* (14), 2799–2810.

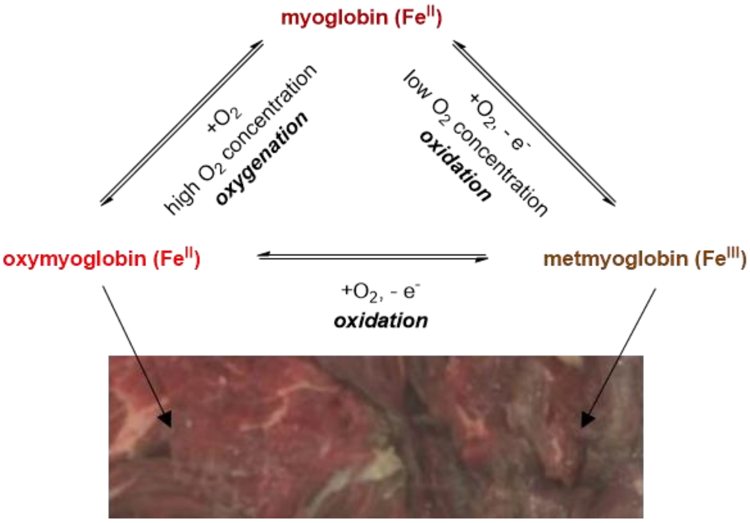

Figure I-7: Colour cycle of fresh meat.

One parameter allowing evaluating the oxygen barrier character of a material is the oxygen transmission rates (OTR), which is characteristic for each of the five major plastic materials (Figure I-8).[9,10,17,18] This measurement corresponds to the quantity of gas that can go through a material over an one day period. Measurements are performed at a standard temperature (23°C) and 0% relative humidity (*i.e.* according to ASTM D3985 standard for film measurement).[19] The lower the value is, the more impermeable to oxygen the material is. Compared to LDPE and PS, which present the lowest oxygen barrier property, Figure I-8 clearly demonstrates that PET is characterized by the best oxygen barrier property among the five most used polymers for plastic packaging.

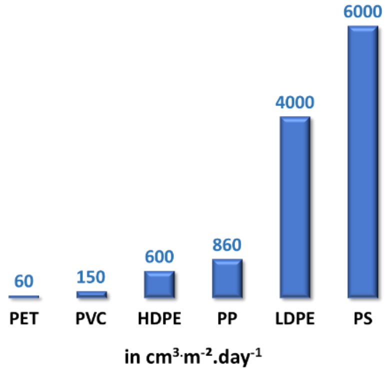

Figure I-8: OTR of some plastics packaging.

Compared to the four other polymers, PET presents the best compromise possible between the properties. Indeed, it is transparent, relatively cheap, has a good strength and good water vapour and gas barrier properties (Table I-2). Even though its gas impermeability is far above the other four mainly used polymers (Table I-2 and Figure I-8), this property has to be significantly improved.

One of the major issues for industrialists is therefore to innovate by creating new plastics materials with improved barrier properties. Since a few years, many research works have been focused on the improvement of oxygen barrier property of PET. As a reminder, PET belongs to polyesters polymers,

---

[17] http://www.evergreen-packaging.com/ (accessed Sept 6, 2017).

[18] Siracusa, V.; Rocculi, P.; Romani, S.; Rosa, M. D. *Trends Food Sci. Technol.* **2008**, *19* (12), 634–643.

[19] Cros, S. *Techniques de l'Ingénieur* **2007**, *am3160*

which are resulting from the condensation of carboxylic acids with alcohols.[20] For instance, PET can be prepared from terephthalic acid or dimethyl terephthalate with ethylene glycol.[21]

Considering the various foods and drinks, their tolerance to oxygen widely varies. For example, Figure I-9 demonstrates that jams are by far less sensitive to oxygen than pasteurised beer, baby foods or freshly ground coffee. As the properties of plastics materials can be modulated at will, a special effort has to be done on the improvement of the oxygen barrier property of plastic packaging for these very sensitive products.[3]

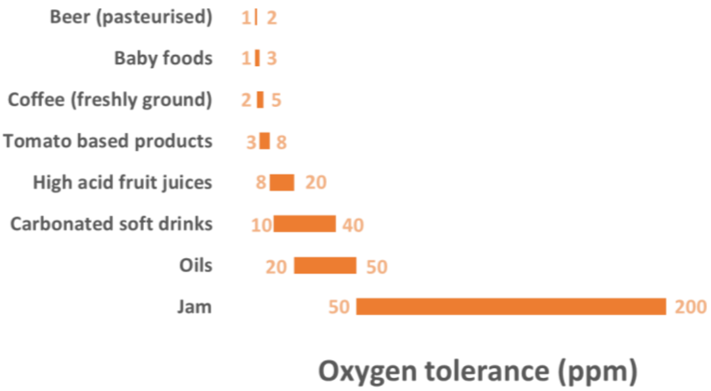

Figure I-9: Estimated maximum oxygen tolerance of food and drinks.

Moreover, the improvements of the gas barrier properties of PET would extend the shelf-life of food products.

I.2. An innovative solution: active packaging

To meet the demand related to this oxygen barrier issue, industrialists have developed innovative plastic materials such as active and intelligent packaging.

To extend the shelf-life of the food products, packaging is not the only tool and efforts have to be focused on different related parameters,[14] the four most important being:

- Process the food or drink itself in a way to prevent enzymatic, microbiological and biochemical activity.
- Protect the product (usually by hermetic sealing) from active biological contamination.
- Use hermetically closed high gas-barrier packaging.
- Control and minimize oxygen quantity in the sealed package (*i.e.* oxygen can be present in the headspace of the package, in the package material itself and in the foods).

In the following section, the solution of gas-barrier package use will be discussed in detail.

According to Robertson[22] an "*active*" packaging is defined as a "*packaging in which subsidiary constituents have been deliberately included in or on either the packaging material or the package headspace to enhance the performance of the package system*". It includes different systems like oxygen, ethylene or moisture absorbers, carbon dioxide absorbers or emitters, ethanol emitters, antimicrobial packaging, flavour/odour adsorbers, self-heating and self-cooling or changing gas permeability.

---

[20] Quentin, J.-P. *Dossier Techniques de l'Ingénieur* **2004**, *j5850*.

[21] Quentin, J.-P. *Dossier Techniques de l'Ingénieur*; **2004**, *j6488*.

[22] Robertson, G. L. Active and Intelligent Packaging. In *Food packaging: principles and practice*; CRC press, 2013; p 686.

Active packaging should not be confused with "*intelligent*" or "*smart*" packaging, which is described as "*packaging that contains an external or internal indicator to provide information about aspects of the history of the package and/or the quality of the food*" and is aimed at indicating the product quality (quality or freshness indicators, time-temperature indicators, gas concentration indicators, radio frequency identification, biosensors…), supplying convenience (thermochromic inks, microwave doneness indicators…) or providing protection against theft, counterfeiting and tampering. In brief, "*intelligent*" packaging can be considered as an "*active*" packaging equipped with monitoring devices, which can be directly included into the package or attached outside the material.[23]

Oxygen scavengers represent the most used category of active packaging. Although oxygen can be removed during filling of the package or the foodstuff can be stored under modified atmosphere packaging, a very small level of residual oxygen can induce deleterious damages to highly sensitive foods. It is therefore of crucial importance to innovate and develop new oxygen scavengers that preserve and extend the shelf-life of food products.

I.2.1. A key parameter for an adequate goods preservation: oxygen barriers

After vacuum or gas flushing, 0.3 to 3.0% of residual oxygen is still remaining in the headspace. To decrease considerably this value, embedding oxygen absorbers, also designated as "*oxygen scavengers*", in the packaging material became evident and necessary. Their main role is to lower the oxygen level in the packaging headspace below 100 ppm. Throughout the last years, different oxygen scavengers have been developed and some of them are already available and are based on various technologies, that can be used alone or in combination (Table I-4): *e.g.* iron (Entries 1-12), ascorbic acid (Entries 13-14), enzyme (Entry 15), photosensitive dye (Entry 16), sulphite, catechol, nylons (Entry 17), unsaturated hydrocarbons, ligands….[23,24,25,26,27,28,29,30,31] They can be found through different forms, such as sachets in the headspace of the packaging or directly incorporated into the package materials for example (Table I-4). The systems gathered in Table I-4 are some of the already commercially available oxygen scavengers, many others are still in the development stage.

---

[23] Brody, A. L.; Bugusu, B.; Han, J. H.; Sand, C. K.; McHugh, T. H. *J. Food Sci.* **2008**, *73* (8), R107–R116.

[24] Rooney, M. L., *Active Food Packaging* Ed.; Springer US: Boston, MA, 1995.

[25] Tarver, T. *Food Technology* October **2008**, 54–59.

[26] Cruz, R. S.; Camilloto, G. P.; dos Santos Pires, A. C. In *Structure and Function of Food Engineering*; Eissa, A. A., Ed.; InTech, 2012.

[27] Wyrwa, J.; Barska, A. *Eur. Food Res. Technol.* **2017**, *243* (10), 1681-1692.

[28] Ahvenainen, R.; Hurme, E. *Food Addit. Contam.* **1997**, *14* (6–7), 753–763.

[29] Vermeiren, L.; Devlieghere, F.; van Beest, M.; de Kruijf, N.; Debevere, J. *Trends Food Sci. Technol.* **1999**, *10* (3), 77–86.

[30] Biji, K. B.; Ravishankar, C. N.; Mohan, C. O.; Srinivasa Gopal, T. K. *J. Food Sci. Technol.* **2015**, *52* (10), 6125–6135.

[31] de Kruijf, N.; van Beest, M.; Rijk, R.; Sipiläinen-Malm, T.; Losada, P. P.; de Meulenaer, B. *Food Addit. Contam.* **2002**, *19* (sup1), 144–162.

Table I-4: Trade and company names, type and active substance of some commercially available oxygen scavengers.

Entry	Trade Name	Company	Type	Active substance
1	**Ageless®**	Mitsubishi Gas Chemical Co., Ltd. (Japan)	Sachets, Labels	Iron based
2	**ATCO®**	Standa Industrie (France)	Sachets, Labels	Iron based
3	**Freshilizer®**	Toppan Printing Co. Ltd. (Japan)	Sachets	Iron based
4	**FreshMax®**	Multisorb technologies Inc. (US)	Labels	Iron based
5	**FreshPax®**	Multisorb technologies Inc. (US)	Sachets	Iron based
6	**O-Buster®**	Dessicare Ltd. (US)	Sachets	Iron based
7	**Oxycap**	Standa Industrie (France)	Bottle crowns	Iron based
8	**OxyGuard®**	Toyo Seikan Kaisha Ltd. (Japan)	Plastic trays	Iron based
9	**Sanso-cut**	Finetec Co. (Japan)	Sachets	Iron based
10	**Seaqul**	Nippon Soda Co. (Japan)	Sachets	Iron based
11	**Shelfplus® O_2**	Ciba Specialty chemicals (Switzerland)	Plastic film	Iron based
12	**Vitalon**	Toagosei Chem. Industry Co. (Japan)	Sachets	Iron based
13	**Darex**	W.R. Grace and Co. (US)	Bottle crowns	Ascorbate/sulphite
14	**PureSeal**	W.R. Grace and Co. (US)	Bottle crowns	Ascorbate/metallic salts
15	**Bioka**	Bioka Ltd. (Finland)	Sachets	Enzyme based
16	**OS1000™, OS2000™**	Cryovac Sealed Air Co. (US)	Plastic film	Light activated scavenger/cobalt catalyst
17	**Oxbar**	Carnaud-Metal Box Technologies	Plastic bottle	Cobalt catalyst/ nylon-MXD6 polymer

Although sachets or films are both able to remove oxygen from the inter packaging, the main difference between is that only films are also able to block the polymer wall permeation of oxygen.

As mentioned above, different technologies can be used as oxygen scavenging systems. These technologies that are based on different active principles will be detailed in the following sections.

I.2.1.1. Iron-based oxygen scavengers

Iron-based oxygen scavengers are based on the reaction given in Scheme I-1.[26] Iron powder is firstly oxidized into its ferrous cation with the production of two electrons. These electrons will reduce oxygen under presence of water into hydroxide anions, which will react with the ferrous cation to form ferrous hydroxide. This latest will be able to react with oxygen and water to generate ferric hydroxide. In global, one molecule of iron powder will consume 0.75 molecule of oxygen.

$$\mathrm{Fe} \longrightarrow \mathrm{Fe}^{2+} + 2\,e^-$$

$$1/2\ \mathrm{O_2} + \mathrm{H_2O} + 2\,e^- \longrightarrow 2\ \mathrm{OH^-}$$

$$\mathrm{Fe}^{2+} + 2\ \mathrm{OH^-} \longrightarrow \mathrm{Fe(OH)_2}$$

$$\mathrm{Fe(OH)_2} + 1/4\ \mathrm{O_2} + 1/2\ \mathrm{H_2O} \longrightarrow \mathrm{Fe(OH)_3}$$

$$\mathbf{Fe + 3/4\ O_2 + 1/2\ H_2O \longrightarrow Fe(OH)_3}$$

Scheme I-1: Iron-based oxygen scavenger principle.

Using this technology, a level of oxygen lower than 0.01% can be reached.[32] However, the main drawback lies in the fact that iron-containing plastics are not transparent. In addition, iron can alter the mechanical properties of the polymer, leading to troubles during the processing. Migration of compounds and/or oxidation products can be observed as well, leading to governmental regulations issues.[33] Because of the difficulty to process iron, iron-based oxygen scavengers are mainly used in sachets and are not directly incorporated within the plastic films. In addition, for all these reasons, the use of iron-based scavengers is prevented for transparent plastic bottles applications.

I.2.1.2. Acid ascorbic-based oxygen scavengers

Another type of oxygen scavenger is based on the oxidation of ascorbic acid to dehydroascorbic acid (Scheme I-2). This oxidation reaction is known to be slow and light or a metal catalyst, such as copper or cobalt, is usually employed to speed up the reaction rate. Ascorbic acid will reduce cupric cation into its cuprous state and will be concomitantly converted into dehydroascorbic acid. The cuprous cation will react with oxygen to regenerate the cupric ion and induce the formation of the superoxide anion. The latter will react with cupric anion leading to the formation of oxygen and hydrogen peroxide, which will then be reduced into water in the presence of ascorbic acid and cupric ion. Overall, two molecules of ascorbic acid will thus consume one molecule of oxygen as evidenced in the following equations (Scheme I-2), the cupric cation playing the role of a catalyst.[26,33]

$$\begin{array}{l}
\mathrm{AA} + 2\,\mathrm{Cu}^{2+} \longrightarrow \mathrm{DHAA} + 2\,\mathrm{Cu}^{+} + 2\,\mathrm{H}^{+} \\
2\,\mathrm{Cu}^{+} + 2\,\mathbf{O_2} \longrightarrow 2\,\mathrm{Cu}^{2+} + 2\,\mathrm{O_2}^{-} \\
2\,\mathrm{O_2}^{-} + 2\,\mathrm{H}^{+} + \mathrm{Cu}^{2+} \longrightarrow \mathbf{O_2} + \mathrm{H_2O_2} + \mathrm{Cu}^{2+} \\
\mathrm{H_2O_2} + \mathrm{Cu}^{2+} + \mathrm{AA} \longrightarrow \mathrm{Cu}^{2+} + \mathrm{DHAA} + 2\,\mathrm{H_2O} \\
\hline
\mathbf{AA + 1/2\ O_2 \longrightarrow DHAA + H_2O}
\end{array}$$

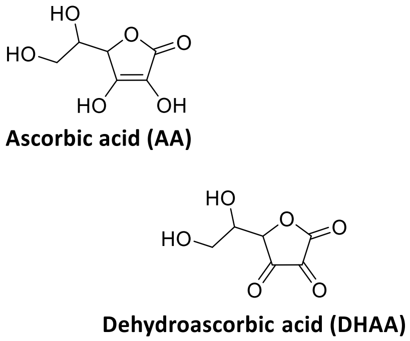

Ascorbic acid (AA)

Dehydroascorbic acid (DHAA)

Scheme I-2: Ascorbic acid-based oxygen scavenger principle.

I.2.1.3. Enzyme-based oxygen scavengers

Oxygen scavengers can also be based on the use of enzymes. Two main categories of enzymes are frequently used in these systems: glucose oxidase/catalase and alcohol oxidase/catalase.[16,26,33]

In the presence of glucose oxidase (Scheme I-3), glucose will consume oxygen and water to form gluconic acid and hydrogen peroxide. Hydrogen peroxide will be reduced into water and oxygen in the presence of glucose catalase. Overall, two molecules of glucose will consume one molecule of oxygen (Scheme I-3) with the help of glucose oxidase and catalase enzymes.

---

[32] Pereira de Abreu, D. A.; Cruz, J. M.; Paseiro Losada, P. *Food Rev. Int.* **2012**, *28* (2), 146–187.

[33] López-Rubio, A.; Almenar, E.; Hernandez-Muñoz, P.; Lagarón, J. M.; Catalá, R.; Gavara, R. *Food Rev. Int.* **2004**, *20* (4), 357–387.

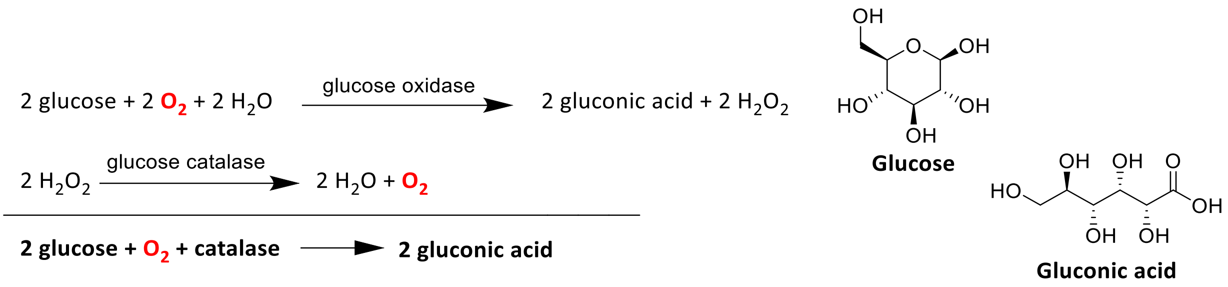

$$2\ \text{glucose} + 2\ O_2 + 2\ H_2O \xrightarrow{\text{glucose oxidase}} 2\ \text{gluconic acid} + 2\ H_2O_2$$

$$2\ H_2O_2 \xrightarrow{\text{glucose catalase}} 2\ H_2O + O_2$$

$$\mathbf{2\ glucose + O_2 + catalase \longrightarrow 2\ gluconic\ acid}$$

Scheme I-3: Enzyme-based oxygen scavenger principle (glucose oxidase/catalase).

Similarly, in the presence of ethanol oxidase (Scheme I-4), oxygen will react with water to form hydrogen peroxide, which in turn will be reduced into water in the presence of ethanol and ethanol catalase with the concomitant formation of acetaldehyde. Overall, one molecule of ethanol is consuming one molecule of oxygen (Scheme I-4).

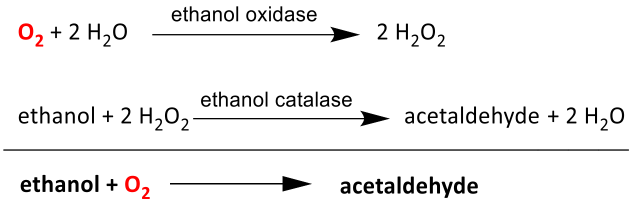

$$O_2 + 2\ H_2O \xrightarrow{\text{ethanol oxidase}} 2\ H_2O_2$$

$$\text{ethanol} + 2\ H_2O_2 \xrightarrow{\text{ethanol catalase}} \text{acetaldehyde} + 2\ H_2O$$

$$\mathbf{ethanol + O_2 \longrightarrow acetaldehyde}$$

Scheme I-4: Enzyme-based oxygen scavenger principle (ethanol oxidase/catalase).

Glucose oxidase and catalase enzymes are the most used enzymatic systems for this type of applications. These enzymes are usually immobilized on the polymers (PS, PE, PP…). However, by immobilizing the enzymes on the polymeric material, these can be in close contact with the food products and lead to several drawbacks such as the consumption of glucose that is contained in the foods and also to undesirable by-products.

In the case of ethanol oxidase/catalase enzymes, acetaldehyde is also formed, which is responsible of off-flavours.

If the immobilization of enzymes turns out to be an ideal and efficient strategy, these enzymes should not be in direct contact with the food products but sandwiched between two films (*i.e.* one gas impermeable and one gas permeable).

Furthermore, this technology is more expensive than the iron-based scavenging approach, because of the increased costs of enzymes.[34] Moreover, the enzyme-based oxygen scavengers have limited applications as they are very sensitive to temperature, pH, water activity and the nature of the solvent or the substrate. In addition, because of their temperature sensitivity, enzymes cannot be extruded and so be included into the plastic composition.

I.2.1.4. Photosensitive dye-based oxygen scavengers

When a plastic material containing a photosensitive dye is exposed to ultraviolet light, the excited dyes activate oxygen from its triplet (O_2, $^3O_2$, S = 1) to its singlet (O_2^*, $^1O_2$, S = 0) state, which in turn is able to react easily with an acceptor (Scheme I-5). Oxygen is therefore removed from the container after light-induced activation of its singlet state and subsequent reaction with an appropriate acceptor. One molecule of acceptor will then react with one molecule of oxygen.[26,29,33]

---

[34] Ozdemir, M.; Floros, J. D. *Crit. Rev. Food Sci. Nutr.* **2004**, *44* (3), 185–193.

$$\text{photon} + \text{dye} \longrightarrow \text{dye}^*$$

$$\text{dye}^* + O_2 \longrightarrow \text{dye} + O_2^*$$

$$O_2^* + \text{acceptor} \longrightarrow \text{acceptor oxide}$$

$$\mathbf{photon} + \mathbf{O_2} + \mathbf{acceptor} \longrightarrow \mathbf{acceptor\ oxide}$$

Scheme I-5: Photosensitive dye-based oxygen scavenger principle.

I.2.1.5. Ethylenic-unsaturated hydrocarbons-based oxygen scavengers

Ethylenic-unsaturated hydrocarbons (such as squalene, fatty acids, polybutadiene…) can be used as oxygen scavenger as well. They are easy to process (especially with polyester, PE, PP or PS). However, they should be functionalized with an appropriate terminal group to be compatible with the polymeric bulk.[33,35,36,37]

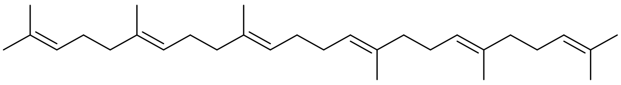

squalene

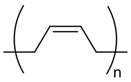

polybutadiene

One of the most investigated and used system is the polybutadiene, which is characterized by a natural high oxygen-scavenging capacity. It is transparent and possesses good mechanical properties and displays the same processing characteristics than PE. Interestingly, it has been reported that combining cobalt(II) catalyst (cobalt(II) neodecanoate or octoate)[38] with polybutadiene increases its oxidation reaction rate; photoinitiator (or a mixture of photoinitiators) can also facilitate and control the initiation of the oxygen scavenging processes.

The main issue of using ethylenic-unsaturated hydrocarbons is the generation of by-products (*e.g.* organic acids, aldehydes, ketones…), which can possibly alter the sensorial quality of the food products and lead to regulatory restrictions. To solve this problem, one layer has to be added between the food product and the scavenger layer and should display the combined properties to be both a barrier to organic compounds (to avoid migration) and permeable to oxygen to allow it reacting.

I.2.1.6. Polymers-based oxygen scavengers

In addition to the oxygen scavengers described until now, the packaging industry has also developed, since a few years, oxygen scavenging polymers. It is now becoming an emerging market and it will be described herein in more detail.

Oxygen scavenging polymers are in most cases laminated (composed of different layers). In fact, a single polymer cannot satisfy all the requirements (transparency, flexibility, barrier properties, heat resistance…).[39] Therefore, a core layer displaying gas barrier properties can be sandwiched between two inner and outer common polymer layers; this type of structure is commonly characterized as

---

[35] Speer, D., V.; Roberts, W., P. Improved Oxygen Scavenging Compositions for Low Temperature Use. WO9407379, 1994.

[36] Speer, D. V.; Roberts, W., P. Oxygen scavenging compositions for low temperature use. US005310497A, 1994.

[37] Speer, D. V.; Roberts, W., P.; Morgan, C. R.; Ebner, C. L. Packaging articles suitable for scavenging oxygen. US005700554A, 1997.

[38] Cahill, P. J.; Richardson, J. A.; Rotter, G. E.; Smyser, G. L.; Barski, R. F.; Wass, R. V.; Nyderek, W. M. Active oxygen scavenger compositions and their use in packaging articles. US006346308B1, 2002.

[39] Rachidi, S.; Damsir, H. Additive for the improvement of the barrier properties of polymers, MateriaNova Mai 18, 2010.

"*passive barrier*". "*Passive oxygen barrier*" is defined as a physical barrier that blocks small molecules movement (such as carbon dioxide, oxygen…) whereas "*active oxygen barrier*" is a technology that consumes oxygen by a chemical reaction.

This generation of new polymers presents higher oxygen barrier properties with respect to the above-mentioned system, even though there are not yet comparable to glass or metal one, but introduces recycling issues. In this category can be mentioned polymers such as polyamide (*e.g.* poly(*meta*-xylylene adipamide), MXD6) or ethylene-vinyl alcohol (*i.e.* EVOH), that can be sandwiched between two PET layers or two polyolefin layers, respectively.

Oxygen scavenging (OS1000™ and OS2000™) polymers commercialized by Cryovac Sealed Air Co. can scavenge oxygen without cleavage into smaller fragments and undesirable sub-products. One-tenth of the polymer is in fact either a photoinitiator or a metal catalyst, which allow the system to not react with oxygen in the absence of ultraviolet irradiation. The reaction is only initiated by the energy brought by UV light absorption by the photoinitiator. Then, the oxidable polymer will react with oxygen and scavenge it. The role of the catalyst in this system is to reduce the activation energy of the reaction and favour it. It is also noteworthy that this oxygen scavenging system is co-extruded with the polymer.[33,40]

In the vein of the polymers developed by Cryovac Sealed Air Co., the Oxbar system developed by Carnaud-Metal Box Technologies contains nylon MXD6 (1 to 5%) which is mixed with PET (95 to 99%). One nylon MXD6 layer is inserted between two PET layers. A cobalt complex (50 to 200 ppm) is also used as catalyst for that system. This system is used especially in the manufacturing of rigid PET bottles for packaging of wine, beer, flavoured alcoholic beverages and malt-based drinks. MXD6 presents the most efficient gas barrier property (*i.e.* compared to other resins) and can be co-extruded or co-injection-molded with thermoplastics (*e.g.* PET or PP). However, the multilayer products containing nylon MXD6 display thickness irregularities and whitening. Moreover, incompatibility of nylon MXD6 with polyesters in monolayer material was evidenced.[33,41] Fava also patented in 2013 the use of nylon MXD6 as an additive in the oxidation reaction for oxygen scavenging.[42]

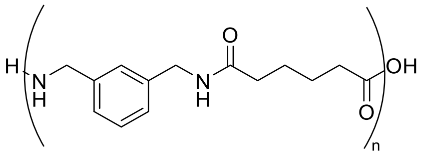

Nylon MXD6

Hydroxy-alkylene polymers gather ethylene-vinyl alcohol (EVOH) or polyvinyl alcohol (PVOH) copolymers. These units (EVOH and PVOH) are known to possess valuable oxygen barrier properties.[33,43,44,45,46] EVOH is defined as a polymer containing 10 to less than 100% (preferably 75 to

---

[40] Kaufman, J.; LaCoste, A.; Schulok, J.; Shehady, E.; 'Kit'Yam, K. An overview of oxygen scavenging packaging and applications https://www.bakeryonline.com/doc/an-overview-of-oxygen-scavenging-packaging-an-0002 (accessed Aug 23, 2017).

[41] Özen, I.; Bozoklu, G.; Dalgiçdir, C.; Yücel, O.; Ünsal, E.; Çakmak, M.; Menceloglu, Y. Z. *Eur. Polym. J.* **2010**, *46*, 226–237.

[42] Fava, F. Oxygen Scavenging Plastic Material. US2013089686B2, 2013.

[43] Frisk, P. Multilayer, high barrier film. WO9824625, June 1998.

[44] Kröhnke, C. Polymer compositions with improved barrier properties against the permeation of oxygen. WO2010072501A1, 2010.

[45] Kröhnke, C.; Kenyo, C.; Renner, K.; Pukanszky, B. Polymer compositions with improved barrier properties against the permeation of oxygen. EP2204404A1, 2010.

[46] Mokwena, K. K.; Tang, J. *Crit. Rev. Food Sci. Nutr.* **2012**, *52* (7), 640–650.

less than 100%) of hydroxyl ethylene units, while PVOH is characterized as a polymer that contains 100% of hydroxyl ethylene units.[44,45]

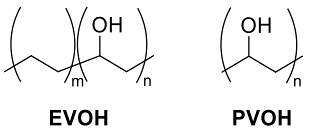

The primary benefit to use EVOH and/or PVOH in the composition is the possibility to process (extrusion, injection molding, film blowing…) this polymer. However, EVOH and PVOH are water sensitive and need in almost all cases to be laminated or coated with moisture-barrier compounds (*e.g.* polyolefins). Moreover, to improve their gas barrier properties, the use of thick films appears preferable but is not favourable because of the cost and the non-transparency of the polymer.

On its side, Airsec has developed a system based on the same technology with the addition of an additive, Nylostab®-SEED® (0.3 to 0.5% *w/w* with respect to the polymer).[47] It is also possible to add polyolefin coating to this system to improve its moisture barrier property, but in that case the thickness of this layer will be lower (*i.e.* than for conventional EVOH and PVOH technology) leading to transparency issue.[44,45]

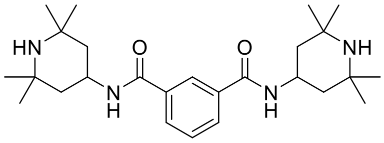

Nylostab®-SEED®

Considered the above-mentioned systems, it thus clearly appears that for multilayer materials, it is usually complex to reach an appropriate balance between shape, gas-barrier property and transparency.

Peters and Cliffton[48] have recently developed new oxygen barrier systems for the PET market. They have reported the use of metallic complexes (cobalt(II) octanoate, acetate or neodecanoate) as catalysts (25 to 500 ppm) for the innovative oxidation of benzyl substituted additives (0.5 to 6.0%) incorporated in PET polyesters (94.0 to 99.5%) for oxygen scavenging applications.

It is in this context that Clariant has developed new mono- or multilayer materials displaying the ability to be both a passive and/or an active barrier (*i.e.* "*passive barrier*" designates the material that is able to remove oxygen at a faster rate than the oxygen permeability of the packaging wall and "*active barrier*" connotes a material that is able to remove oxygen from the packaging headspace). This product can be used in different states (container, film or sheet) and for different structures (flexible: 5 to 250 µm wall thickness, rigid: 100 to 1000 µm wall thickness or semi-rigid materials). In the case of rigid containers, monolayer-based materials are preferred.

Fava, Marson, Steffanut and Johann described in 2014[49,50] an oxygen scavenger composed of a plastic material **A** (polyester, polyolefin, a polyolefin copolymer or PS) which is mixed with:

---

[47] Sahl, M.; Zeissberger, E.; Zäh, M.; Schacker, O.; Steffanut, P. Polymer Additive and a Method for the Production thereof. WO2017005413A1, 2017.

[48] Peters, R. D.; Cliffton, M. D. Polyesters with low molecular weight additives for improved gas barrier properties. US20120199515A1, 2012.

[49] Fava, F.; Marson, A.; Steffanut, P.; Johann, L. Oxygen Scavenging Plastic Material. EP2708574A1, 2014.

[50] Fava, F.; Marson, A.; Steffanut, P.; Johann, L. Oxygen Scavenging Plastic Material. WO2014044366A1, 2014.

- An additive **B** (it can be Nylostab®-SEED® or a mixture of Nylostab®-SEED® and *N*^{1},*N*^{3}-*bis*-(phenylmethyl)-1,3-benzenedicarboxamide…).
- A transition metal catalyst **C** to initiate and increase the oxygen scavenging rate (different metals can be used such as manganese(II) or (III), iron(II) or (III), cobalt(II) or (III), nickel(II) or (III), copper(I) or (II), rhodium(II), (III) or (IV) and ruthenium with a preference for cobalt). Counter anions have to be compatible for food contact materials and the corresponding regulations and should not exhibit migration to the food content. Preference is given to chloride, acetate, propionate, oleate, stearate, palmitate, 2-ethylhexanoate, neodecanoate or naphthenate.
- An aliphatic or partially aromatic polyamide **D**.
- And/or a colorant **E**.

The proportions of the different ingredients of the compositions are given in Table I-5. If the final product is a masterbatch, the composition might differ slightly from the final material.

Table I-5: Composition of oxygen scavenging materials.

	A (%)	B (%)	C (%)	D and E (%)
Masterbatch	14 to 94	5 to 50	1 to 10	0 to 80
Compound	90 to 99.86	0.1 to 0.8	0.04 to 0.3	0 to 8.9

In 2015, Fava and Steffanut,[51,52] and Decortes, Steffanut, Marson, Fava and Muller[53,54] patented the same principle with the use of *N*-phenylmethylbenzamide (for example) as the additive. The composition of the masterbatch and the final compound also slightly differed.

This emerging class of oxygen scavengers based on polymers displays significant benefits with respect to the other developed systems (transparency of the final packaging, possibility to form a monolayer material, recyclability in contrast to multilayer materials…). Nonetheless, significant efforts are still needed to enhance the oxygen barrier properties of these innovative plastic materials.

I.2.2. Metal complexes: a key role in the polymers-based oxygen barriers

As described above, polymers-based oxygen barriers are part of an emerging technology since only a few years. The following section of this chapter will be mainly focused on this oxygen scavenging solution.

In addition to the fruitful used of an organic or a polymeric sacrificial additive, a metal catalyst also enters the final composition to initiate and/or increase the oxidation reaction rate and to accordingly improve the oxygen barrier properties of these new materials.

In this section, we will briefly outline the different types of metal catalysts, that are more prone to be used for oxygenation issues. A first part will be dedicated to the different metals that can be used while the second one will focus on the different ligand types.

I.2.2.1. Metal centres and their oxygenation properties

As described above, polymeric oxygen scavenging solutions based on the oxidation of a sacrificial additive in the presence of a metal catalyst are sparsely related and patented. Generally, the

---

[51] Fava, F.; Steffanut, P. Oxygen Scavenging Composition for Plastic Material. WO2015135635A1, 2015.

[52] Fava, F.; Steffanut, P. Oxygen Scavenging Composition for Plastic Material. EP2915842A1, 2015.

[53] Decortes, A.; Steffanut, P.; Marson, A.; Fava, F.; Muller, T. Oxygen Barrier Plastic Material. WO2015192928A1, 2015.

[54] Decortes, A.; Steffanut, P.; Marson, A.; Fava, F.; Muller, T. Oxygen Barrier Plastic Material. EP2957590A1, 2015.

appropriate metal ions originate from the first, second or third row of transition metals of the periodic table of elements. However, a few metals are often mentioned in the patents, especially, for their catalytic properties in the oxidation of polymeric additives such as manganese, iron, cobalt, nickel, copper, rhodium or ruthenium.[32,40,42,43,44,45,48,49,50,51,52,53,54] To ensure efficient additive oxidation throughout their catalytic cycles, these metals should first exhibit good oxygenation properties.

Besides, the selected metal salts have to fulfil the safety and government requirements[55] (*e.g.* the Food and Drug Administration of the USA (FDA)) and have also to meet the specific industrial and marketing specifications.

For given applications, such as for instance the plastic bottles, the transparency of the final product, and so of the different components, is also of crucial importance.

It is for this reason that iron salts, even though they display valuable oxygenation properties (*e.g.* myoglobin), were not extensively considered in this research area.

On the other hand, nickel and rhodium are not known to behave as efficient oxygen carrier complexes.[56] Even though nickel is a natural and abundant element, it is classified as genotoxic, as rhodium and ruthenium did.[55] For this reason, these metals will be not described further.

On its side, cobalt is naturally occurring in the human body as it is an essential constituent of Vitamin B12; however, it has been classified by the FDA in the category of potential toxic compounds.[55] So far, cobalt it is still tolerated and approved by the FDA for the preparation of plastics for food contact applications, but a risk assessment has to be performed beforehand.

Even though cobalt is characterized by a higher oxygenation capacity than manganese, this latest was also studied as it is considered by the FDA to display low inherent toxicity.[55]

I.2.2.2. Influence of ligand design on oxygenation

Numerous ligands have been described so far for cobalt(II) or manganese(II) complexation. They can be classified into five main categories depending on the nature of the binding sites: N_2O_2, N_2S_2, N_4, O_4 and O_2 ligand types (Scheme I-6). In the following section, we will provide representative examples of ligands displaying such binding patterns.

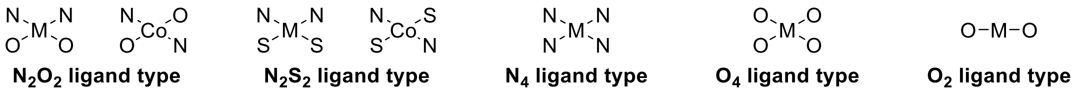

Scheme I-6: N_2O_2, N_2S_2, N_4, O_4 and O_2 ligand types.

I.2.2.2.1. N_2O_2 ligand type

This category of ligands regroups mainly the Schiff base ligands. These latest owe their name to Hugo Schiff, who discovered them. They are analogous to aldehyde or ketone with the replacement of the oxygen by a nitrogen, leading to an imine function (Scheme I-7). The Schiff base ligands are characterized by the fact that the nitrogen R_3 substituent cannot be a hydrogen atom but only an alkyl or an aryl group. The R_1 and R_2 substituents can be an alkyl or an aryl group or a hydrogen atom.

---

[55] U.S. Department of Health and Human Services & Food and Drug Administration & Center for Drug Evaluation and Research (CDER) & Center for Biologics Evaluation and Research (CBER), International Conference on Harmonisation of Technical Requirements for Registration of Pharmaceuticals for Human Use (ICH) – Guideline for Elemental Impurities (Q3D) 2015.

[56] Cabani, S.; Ceccanti, N.; Tiné, M. R. *Pure Appl. Chem.* **1991**, *63* (10), 1455–1464.

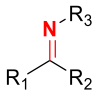

Scheme I-7: General structure of Schiff base.

Schiff base ligands are formed following the condensation of an aldehyde or a ketone with a primary amine (Scheme I-8).

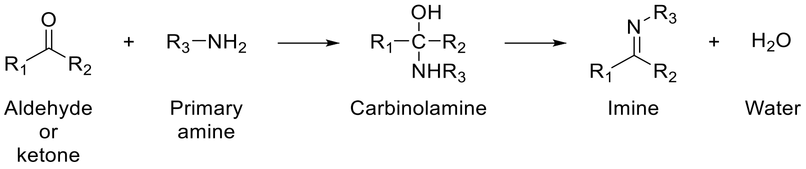

Scheme I-8: Formation of a Schiff base from an aldehyde or a ketone and an amine.

In coordination chemistry, the Schiff base ligands are more related to the types of structures that are depicted in Scheme I-9. The coordination of a metal centre usually requires two ligands of the structure type **a)** (*i.e.* which can be identical in the case of symmetric Schiff base ligands or different for asymmetric Schiff base ligands, Scheme I-9) or one ligand of the structure type **b)**, Scheme I-9. The ligands of the structure type **b)** (Scheme I-9) are commonly defined as salen-type ligands. Salen being an abbreviation arising from the contraction of salicylaldehyde and ethylenediamine (Scheme I-10).[57,58,59,60]

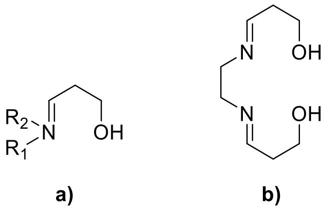

Scheme I-9: Schiff base in coordination chemistry.

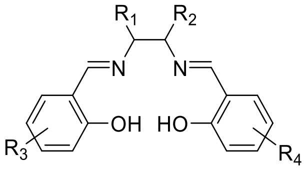

Scheme I-10: Salen-type ligand.

The number and variety of Schiff base compounds is not limited as they can be formed from a wide variety of ketones, aldehydes and primary amines. When coordinated to a metal centre, they might display a multitude of properties that are relevant for various applications. Some of them, the list is not exhaustive, are listed below:

---

[57] Anson, C. W.; Ghosh, S.; Hammes-Schiffer, S.; Stahl, S. S. *J. Am. Chem. Soc.* **2016**, *138* (12), 4186–4193.

[58] Aymes, D. J.; Bollotte, B.; Pâris, M. R. *J. Molecular Catal.* **1980**, *7*, 289–298.

[59] Bailes, R. H.; Calvin, M. *J. Am. Chem. Soc.* **1947**, *69* (8), 1886–1893.

[60] Basolo, F.; Hoffman, B. M.; Ibers, J. A. *Acc. Chem. Res.* **1975**, *8* (11), 384–392

- Catalysts[61,62,63,64] in the oxidation of:
    - Alcohols.[65,66,67,68,69,70,71,72,73,74]
    - Alkanes.[66,75,76]
    - Alkenes.[66,77]
    - Aldehydes.[65,78]
    - Amines.[69,79,80,81,82,83,84]
- Redox active sensors.[85]
- Ionic ferroelectrics.[86]
- Single-molecule-magnet.[87,88,89]
- Luminescent probe.[90]
- Dye.[91]
- Biological activity towards:

---

[61] Simándi, L. I. *Advances in catalytic activation of dioxygen by metal complexes*, Ed.; Kluwer Academic Publishers: Dordrecht; Boston, 2003.

[62] Cozzi, P. G. *Chem. Soc. Rev.* **2004**, *33* (7), 410–421.

[63] Che, C.-M.; Huand, J.-S. *Coord. Chem. Rev.* **2003**, *242* (1–2), 97–113.

[64] Gupta, K. C.; Sutar, A. K. *Coord. Chem. Rev.* **2008**, *252* (12–14), 1420–1450.

[65] Sobkowiak, A.; Sawyer, D. T. *J. Am. Chem. Soc.* **1991**, *113* (25), 9520–9523.

[66] Mandal, A. K.; Khanna, V.; Iqbal, J. *Tetrahedron Lett.* **1996**, *37* (21), 3769–3772.

[67] Bedell, S. A.; Martell, A. E. *J. Am. Chem. Soc.* **1985**, *107* (26), 7909–7913.

[68] Araki, K.; Kuboki, T.; Otohata, M.; Kishimoto, N.; Yamada, M.; Shiraishi, S. *J Chem Soc Dalton Trans* **1993**, No. 24, 3647–3651.

[69] Knaudt, J.; Förster, S.; Bartsch, U.; Rieker, A.; Jäger, E.-G. *Z. Für Naturforschung B - J. Chem. Sci.* **2000**, *55b* (1), 86–93.

[70] Nishinaga, A.; Tomita, H. *J. Mol. Catal.* **1980**, *7* (2), 179–199.

[71] Zombeck, A.; Drago, R. S.; Corden, B. B.; Gaul, J. H. *J. Am. Chem. Soc.* **1981**, *103* (25), 7580–7585.

[72] Bozell, J. J.; Hames, B. R.; Dimmel, D. R. *J. Org. Chem.* **1995**, *60* (8), 2398–2404.

[73] Türk, H.; Çimen, Y. *J. Mol. Catal. Chem.* **2005**, *234* (1–2), 19–24.

[74] Nishinaga, A.; Tojo, T.; Matsuura, T. *J. Chem. Soc. Chem. Commun.* **1974**, *21*, 896–897.

[75] Soobramoney, L.; Bala, M. D.; Friedrich, H. B. *Dalton Trans* **2014**, *43* (42), 15968–15978.

[76] Mac Leod, T. C. O.; Kirillova, M. V.; Pombeiro, A. J. L.; Schiavon, M. A.; Assis, M. D. *Appl. Catal. Gen.* **2010**, *372* (2), 191–198.

[77] Bailey, C. L.; Drago, R. S. *Coord. Chem. Rev.* **1987**, *79*, 321–332.

[78] Watanabe, E.; Kaiho, A.; Kusama, H.; Iwasawa, N. *J. Am. Chem. Soc.* **2013**, *135* (32), 11744–11747.

[79] Saliu, F.; Putomatti, B.; Rindone, B. *Tetrahedron Lett.* **2012**, *53* (28), 3590–3593.

[80] Bolzacchini, E.; Meinardi, S.; Orlandi, M.; Rindone, B. *J. Mol. Catal. Chem.* **1996**, *111*, 281–287.

[81] Liu, J.-M.; Peng, X.-G.; Liu, J.-H.; Zheng, S.-Z.; Sun, W.; Xia, C.-G. *Tetrahedron Lett.* **2007**, *48* (6), 929–932.

[82] Chen, L.-J.; Bao, J.; Mei, F.-M.; Li, G.-X. *Catal. Commun.* **2008**, *9* (5), 658–663.

[83] Orejón, A.; Castellanos, A.; Salagre, P.; Castillón, S.; Claver, C. *Can. J. Chem.* **2005**, *83* (6–7), 764–768.

[84] Förster, S.; Rieker, A.; Maruyama, K.; Murata, K.; Nishinaga, A. *J. Org. Chem.* **1996**, *61* (10), 3320–3326.

[85] Goze, C.; Leiggener, C.; Liu, S.-X.; Sanguinet, L.; Levillain, E.; Hauser, A.; Decurtins, S. *ChemPhysChem* **2007**, *8* (10), 1504–1512.

[86] Sui, Y.; Li, D.-P.; Li, C.-H.; Zhou, X.-H.; Wu, T.; You, X.-Z. *Inorg. Chem.* **2010**, *49* (4), 1286–1288.

[87] Wernsdorfer, W.; Sessoli, R. *Science* **1999**, *284* (5411), 133–135.

[88] Oshio, H.; Nihei, M.; Yoshida, A.; Nojiri, H.; Nakano, M.; Yamaguchi, A.; Karaki, Y.; Ishimoto, H. *Chem. - Eur. J.* **2005**, *11* (3), 843–848.

[89] Oshio, H.; Hoshino, N.; Ito, T.; Nakano, M. *J. Am. Chem. Soc.* **2004**, *126* (28), 8805–8812.

[90] Imbert, D.; Comby, S.; Chauvin, A.-S.; Buenzli, J.-C. G. *Chem. Commun.* **2005**, *11*, 1432–1434.

[91] Fakhari, A. R.; Khorrami, A. R.; Naeimi, H. *Talanta* **2005**, *66* (4), 813–817.

- Bacteria.[92,93,94,95,96,97,98,99]
- Fungi.[92,93 ,98,100,101,102,103,104]
- Cancer.[105,106]
- Herbicidal.[107]

Some of these Schiff base compounds have been also described to possess valuable oxygenation properties.

I.2.2.2.2. N_2S_2 ligand type

The oxygen atoms of the Schiff base derived ligands can be alternatively replaced by sulfur atoms to lead to the N_2S_2 ligand type. In this category, one can find the so-called sacsacen or bensacacen ligands (Scheme I-11). It is noteworthy that the electronic effects of the ligands are of crucial importance in the strength of the metal-oxygen bond (*i.e.* in the case of oxygen binding). In fact, the more Lewis acid the metal centre, the better affinity to oxygen it will have. This acid Lewis character is strengthened with binding sites presenting high electronegativity. According to the Pauling scale, electronegativity is decreasing from oxygen ($\chi_O = 3.44$) through nitrogen ($\chi_N = 3.04$) to sulfur ($\chi_S = 2.54$). For this reason, a N-O ligand type will have more affinity for the metal centre than N-N and N-S ligand types. It is why ligand containing sulfur atoms on the coordination sites are not the best adapted for oxygen carrier applications.

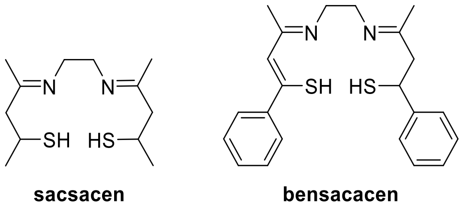

Scheme I-11: Examples of N_2S_2 ligand type.

---

[92] More, P. G.; Bhalvankar, R. B.; Patter, S. C. *J. Indian Chem. Soc.* **2001**, *78* (9), 474–475.

[93] Pandeya, S. N.; Sriram, D.; Nath, G.; De Clercq, E. *Farmaco* **1999**, *54* (9), 624–628.

[94] You, Z.-L.; Shi, D.-H.; Xu, C.; Zhang, Q.; Zhu, H.-L. *Eur. J. Med. Chem.* **2008**, *43* (4), 862–871.

[95] Shi, L.; Fang, R.-Q.; Xue, J.-Y.; Xiao, Z.-P.; Tan, S.-H.; Zhu, H.-L. *Aust. J. Chem.* **2008**, *61* (4), 288–296.

[96] Chohan, Z. H.; Pervez, H. *Synth. React. Inorg. Met.-Org. Chem.* **1993**, *23* (7), 1061–1071.

[97] Malik, Z. A.; Alam, S. *J. Pure Appl. Sci.* **1984**, *17* (1), 69–76.

[98] Mishra, V.; Saksena, D. K.; Jain, M. C. *Synth. React. Inorg. Met.-Org. Chem.* **1987**, *17* (10), 987–1002.

[99] Singh, K.; Barwa, M. S.; Tyagi, P. *Eur. J. Med. Chem.* **2006**, *41* (1), 147–153.

[100] Dash, B.; Mahapatra, P. K.; Panda, D.; Pattnaik, J. M. *J. Indian Chem. Soc.* **1984**, *61* (11–12), 1061–1064.

[101] Rao, N. R.; Rao, P. V.; Reddy, G. V.; Ganorkar, M. C. *Indian J. Chem. Sect. Inorg. Bio-Inorg. Phys. Theor. Anal.* **1987**, *26A* (10), 887–890.

[102] Mishra, P.; Gupta, P. N.; Shakya, A. K. *J. Indian Chem. Soc.* **1991**, *68* (11), 618–619.

[103] Srivastava, V.; Srivastava, S. K.; Mishra, A. P. *J. Indian Chem. Soc.* **1995**, *72* (1), 47–48.

[104] Singh, R. V.; Gupta, N.; Fahmi, N. *Indian J. Chem. Sect. Inorg. Bio-Inorg. Phys. Theor. Anal.* **1999**, *38A* (11), 1150–1158.

[105] Desai, S. B.; Desai, P. B.; Desai, K. R. *Heterocycl. Commun.* **2001**, *7* (1), 83–90.

[106] Sharma, K. P.; Jolly, V. S.; Phatak, P. *Ultra Sci. Phys. Sci.* **1998**, *10* (2), 263–266.

[107] Samadhiya, S.; Halve, A. *Orient. J. Chem.* **2001**, *17* (1), 119–122.

I.2.2.2.3. N_4 ligand type

For N_4 type ligands (*i.e.* oxygen of the Schiff base derived ligands substituted by nitrogen atoms), one can group porphyrins and related derivatives,[60,108] hemoglobin or myoglobin,[60] or polyamines[108,109,110,111,112,113,114] just to cite a few. They have been reported to be good chelating agents for metal centres but suffer the same phenomena as sulfur-based ligands. In fact, the aromatic porphyrin ligand delocalizes the electron density from the metal to the ligand, resulting to lower oxygen binding and carrier capacities.

I.2.2.2.4. O_4 ligand type

The main representative ligand of the O_4 ligand type series is pentane-2,4-dione or acetylacetone ligand (also known as acac). The deprotonated form of acetylacetone is known as acetylacetonate and is a strong and versatile ligand in metal coordination chemistry. For example, the use of metal catalyst containing acac ligands is well known in catalysis (*e.g.* oxidation of alcohols, [115,116,117,118,] alkanes[119,120,] or α-hydroxyketones[121]).

I.2.2.2.5. O_2 ligand type

In this last category of commonly observed O_2-based ligands are gathered carboxylate ligands,[108] such as acetate (*i.e.* ethanoate), propionate, *cis*-octadec-9-enoate (also designated as oleate), hexadecanoate (*i.e.* palmitate), octoate, neodecanoate, octadecenoate (*i.e.* stearate) or cyclam. Metal (*e.g.* cobalt(II)) carboxylate complexes are well known and widespread used as reagents to synthesize intricate metal complexes. The interest is particularly focused on metal stearates and examples of their use in catalysis are given below:[122]

- Oxidation of carboxylic acid[123] or hydrocarbons[124] in the presence of cobalt(II) stearate.
- Oxidation of toluene into benzoic acid in the presence of cobalt(II) stearate.[125]

---

[108] Cabani, S. *React. Funct. Polym.* **1996**, *28* (2), 167–182.

[109] Bencini, A.; Bianchi, A.; Cabani, S.; Ceccanti, N.; Paoletti, P.; Tinè, M. R. *J. Chem. Soc. Dalton Trans.* **1993**, No. 5, 695–702.

[110] Cabani, S.; Ceccanti, N.; Pardini, R.; Tiné, M. R. *Polyhedron* **1999**, *18* (25), 3295–3303.

[111] Cabani, S.; Ceccanti, N.; Tiné, M. R. *J. Chem. Soc. Dalton Trans.* **1988**, *2*, 373–379.

[112] Cabani, S.; Ceccanti, N.; Tiné, M. R. *J. Solut. Chem.* **1986**, *15* (2), 177–187.

[113] Cabani, S.; Ceccanti, N.; Conti, G. *Inorganica Chim. Acta* **1984**, *89* (2), L21–L22.

[114] Cabani, S.; Ceccanti, N.; Conti, G. *J. Chem. Soc. Dalton Trans. Inorg. Chem.* **1983**, *7*, 1247–1251.

[115] Ishii, Y. *J. Mol. Catal. Chem.* **1997**, *117*, 123–137.

[116] Mastrorilli, P.; Suranna, G. P.; Nobile, C. F.; Farinola, G.; Lopez, L. *J. Mol. Catal. Chem.* **2000**, *156*, 279–281.

[117] Cicco, S. R.; Latronico, M.; Mastrorilli, P.; Suranna, G. P.; Nobile, C. F. *J. Mol. Catal. Chem.* **2001**, *165* (1), 135–140.

[118] Mastrorilli, P.; Muscio, F.; Suranna, G. P.; Nobile, C. F.; Latronico, M. *J. Mol. Catal. Chem.* **2001**, *165*, 81–87.

[119] Ishii, Y.; Iwahama, T.; Sakaguchi, S.; Nakayama, K.; Nishiyama, Y. *J. Org. Chem.* **1996**, *61*, 4520–4526.

[120] Han, X.; Zhou, Z.; Wan, C.; Xiao, Y.; Qin, Z. *Synthesis* **2013**, *45*, 615–620.

[121] Dell'Anna, M. M.; Mastrorilli, P.; Nobile, C. F.; Lopez, L. *J. Mol. Catal. Chem.* **1996**, *111*, 33–36.

[122] Opeida, I. A.; Plekhov, A. L.; Kushch, O. V.; Matvienko, A. G. *Russ. J. Phys. Chem. A* **2011**, *85* (7), 1119–1123.

[123] Heaton, F. W.; Uri, N. *J. Lipid Res.* **1961**, *2* (2), 152–160.

[124] Shilov, A. E.; Shul'pin, G. B. Homogeneous Catalytic Oxidation of Hydrocarbons by Molecular Oxygen. In *Oxidation by Molecular Oxygen*; 2002; pp 371–429.

[125] Gizli, A.; Aytimur, G.; Alpay, E.; Atalay, S. *Chem. Eng. Technol.* **2008**, *31* (3), 409–416.

- Degradation of HDPE in the presence of manganese(II) stearate[126] or cobalt(II) stearate.[127]
- Degradation of linear LDPE in the presence of cobalt(II) stearate.[128]

I.3. Metal complexes and organic/polymeric additives: on the way to a deeper understanding of the mechanism of action of metal oxygen barriers

With the aim of getting a deeper understanding of the mechanism of action of potential oxygen barrier devices, simple organic compounds and polymeric additives that act as sacrificial derivatives in the presence of metal catalysts have been investigated in this thesis. More precisely, this work has been focused on two metal centres of interest for industrialists in the context of food products packaging: cobalt(II) and manganese(II). As described in the various patents that were quoted above, cobalt catalyst, in particular, has been widely considered by industrialists to initiate and speed up the oxidation reaction of organic oxygen scavengers. However, if numerous systems have been developed so far, their mechanism of action are poorly understood.[49,50,53,54]

This Ph.D. work was carried out in the frame of an industrial collaboration between CNRS and Clariant. The primary objective of this Ph.D. thesis was to elucidate the mechanism of action of metallic active oxygen barriers contained in plastics for food and drinks preservation. It is of crucial importance to carry out a fundamental approach to validate the mechanism and the (sub-)products formed alongside to the regulatory instances (*e.g.* FDA) and on longer-term, to be able to fine-tune the composition of the oxygen barrier system (nature of the metal catalyst and of the additive; variation of component ratio, potential use of other compounds…) allowing to reach the targeted oxygen barrier properties. For that purpose, different metal catalysts and additives have been considered in this work.

The kinetics of oxygenation and activation of the metal catalysts is seeming intimately dependent on the nature and the stability of the cobalt(II) and manganese(II) catalytic species. On the one hand, the oxygenation kinetics increases, for instance, under basic conditions because of the formation of hydroxylated species that stabilizes the oxygen binding. On the other hand, the activation step (formation of μ-superoxo or μ-peroxo species) results of the redox properties of the metallic complexes. A putative mechanism of reaction for metallic complexes with cobalt(II) was established by S. Cabani[108] and is depicted in Scheme I-12.

During equilibria **1** and **1’** (Scheme I-12), formation of the hydroxylated metal chelates is supposed to occur. By reaction with oxygen, these dimeric species will form the bimetallic dimers displaying a dioxygen bridge (step **2**, Scheme I-12 corresponds to the oxygenation step leading to the μ-hydroxo or the bis-hydroxo species, Scheme I-13 describing the oxygenated and activated species that can be formed along this process).[56,108,129] These species can then undergo an intramolecular electronic transfer leading to cobalt(III) complexes with a (μ-)peroxo bridge (*i.e.* activation stage **3**, Scheme I-12 and Scheme I-13).

These activated species can then:

- Oxidize different substrates such as additives or the polymeric matrix (step **6**, Scheme I-12).
- Undergo a reduction in an acidic environment (step **4**, Scheme I-12).

---

[126] Maryudi; Yunus, R. M.; Nour, A. H.; Beg, M. D. H.; Abidin, M. H. The degradation of high density polyethylene containing manganese stearate under accelerated weathering. In *IC-GWBT2012, Ahmad Dahlan University*; March 23-24, 2012.

[127] Norshafika, B. Y. Effect of cobalt carboxylate on thermal degradation of polyethylene (HDPE), Bachelor Thesis, University Malaysia Pahang, April 2010.

[128] Roy, P. K.; Surekha, P.; Rajagopal, C.; Choudhary, V. *J. Appl. Polym. Sci.* **2008**, *108* (4), 2726–2733.

[129] Tiné, M. R. *Coord. Chem. Rev.* **2012**, *256* (1–2), 316–327.

- Undergo an irreversible degradation (step **5**, Scheme I-12, which is in principle inactive towards efficient oxygen barrier properties).[130]

The same mechanism is applicable to monomeric chelates (Scheme I-12) with subsequent formation of the dioxo-cobalt(II) species (Scheme I-13) and the superoxo-cobalt(III) derivative (Scheme I-13).

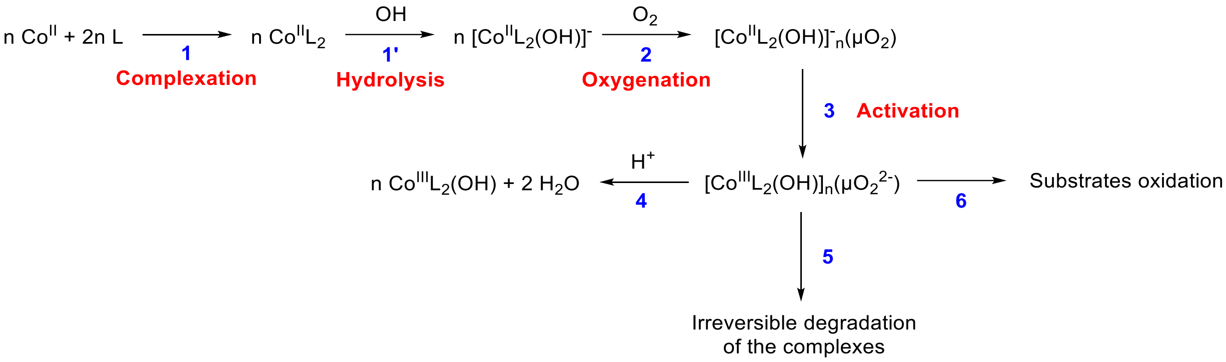
n Co^II + 2n L
1
Complexation
n Co^IIL2
OH
1'
Hydrolysis
n [Co^IIL2(OH)]-
O2
2
Oxygenation
[Co^IIL2(OH)]-n(μO2)
3 Activation
n Co^IIIL2(OH) + 2 H2O
H+
4
[Co^IIIL2(OH)]n(μO2 2-)
6
Substrates oxidation
5
Irreversible degradation of the complexes

Scheme I-12: Putative mechanism of complexation, oxygenation and activation of cobalt(II) complexes. Main steps are noted 1 to 6. Adapted from Cabani.

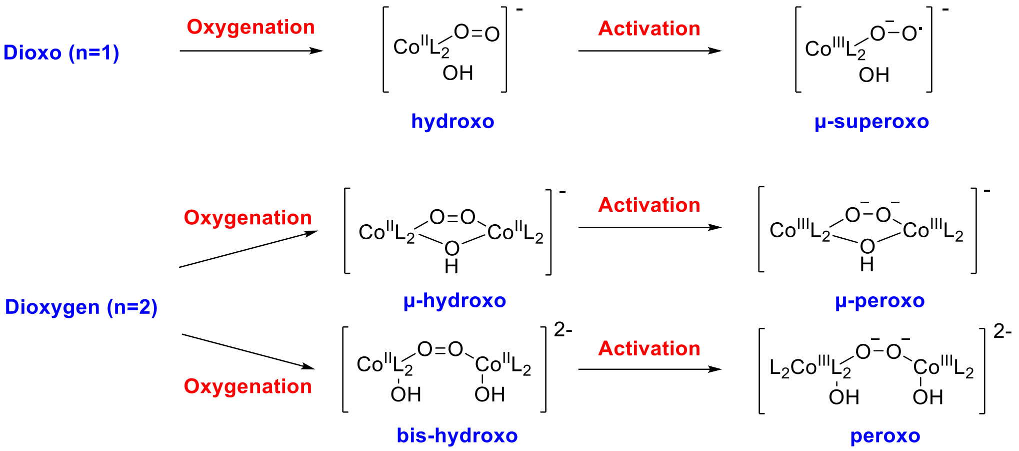
Dioxo (n=1)
Oxygenation
hydroxo
Activation
μ-superoxo
Dioxygen (n=2)
Oxygenation
μ-hydroxo
Activation
μ-peroxo
Oxygenation
bis-hydroxo
Activation
peroxo

Scheme I-13: Chemical structures of the key oxygenated cobalt(II)/cobalt(III) species.

This project is divided into three main objectives: (*i*) the synthesis and the thorough characterization of several metal catalysts, (*ii*) the oxygenation/activation properties of these metal catalysts, and (*iii*) the role of the additives. All these main topics investigated in this work are detailed in the following sections:

Synthesis and Characterization of the Metal Catalysts

As stated above, different metal catalysts have been considered throughout this work: cobalt(II) and manganese(II) *bis*(acetylacetonate) as model catalysts, several cobalt(II) and manganese(II) complexes derived from known and unreported Schiff base ligands, and cobalt(II) and manganese(II) stearate.

Firstly, different Schiff base ligands have been synthesized ($\mathbf{L^1}$-$\mathbf{L^7}$, Scheme I-14 and Table I-6). These ligands were chosen because of their temperature stability (they can so be extruded) and their compatibility towards the polymers. Their stabilities (hydrolysis process within a broad range of pH) in solution have been studied by electrospray ionization-mass spectrometry (ESI-MS) or UV-visible absorption spectrophotometry, and their protonation constants have been assessed by pure potentiometric or UV-visible absorption spectrophotometry *versus* pH titrations.

---

[130] Martell, A. E.; Basak, A. K.; Raleigh, C. J. *Pure Appl. Chem.* **1988**, *60* (8), 1325–1329.

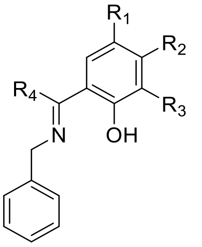

Scheme I-14: Schiff base ligands studied in this work.

Table I-6: Different Schiff base ligands studied in this work.

Ligand	R_1	R_2	R_3	R_4
L^1	H	H	H	H
L^2	H	OH	H	Ph
L^3	Br	H	Br	H
L^4	Me	H	H	H
L^5	NO_2	H	H	H
L^6	OMe	H	H	H
L^7	H	OH	H	H

In a second part, the affinities of those ligands towards cobalt(II) and manganese(II) complexation have been determined by pure potentiometry or by UV-visible absorption spectrophotometry coupled to potentiometry; the corresponding cobalt(II) and manganese(II) complexes (Scheme I-15 and Table I-7) have been synthesized and characterized. Finally, their redox properties have been determined by cyclic voltammetry.

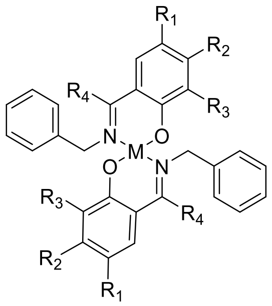

Scheme I-15: Metal complexes studied in this work.

Table I-7: Different cobalt(II) and manganese(II) Schiff base complexes studied in this work and their corresponding nomenclature.

					Schiff base complex	
Ligand	R_1	R_2	R_3	R_4	M = Co(II)	M = Mn(II)
L^1	H	H	H	H	1Co	1Mn
L^2	H	OH	H	Ph	2Co	2Mn
L^3	Br	H	Br	H	3Co	3Mn
L^4	Me	H	H	H	4Co	4Mn
L^5	NO_2	H	H	H	5Co	5Mn
L^6	OMe	H	H	H	6Co	6Mn
L^7	H	OH	H	H	7Co	7Mn

Oxygenation/Activation Properties of the Metal Catalysts

The oxygenation and activation properties of our series of cobalt(II) and manganese(II) catalysts (*i.e.* with Schiff base ligands **1Co-7Co** and **1Mn-7Mn**, Scheme I-15 and Table I-7; with acetylacetonate **8Co** and **8Mn**, Scheme I-16; and with stearate **9Co** and **9Mn**, Scheme I-17) have been investigated using a fruitful combination of complementary analytical techniques (*e.g.* ESI-MS, proton nuclear magnetic resonance (^{1}H NMR), UV-visible absorption spectrophotometry, oximetry coupled to UV-visible absorption spectrophotometry…). In particular, two main aspects have been thoroughly examined: (*i*) the kinetics of the oxygenation and activation steps and (*ii*) the characterization of the (sub-)products that are formed during these oxygenation processes.

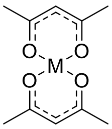

M = Co(II): **8Co**
M = Mn(II): **8Mn**

8

Scheme I-16: Acetylacetonate complexes studied in this work: cobalt(II) bis*(acetylacetonate)* ***8Co*** *and cobalt(II)* bis*(acetylacetonate)* ***8Mn****.*

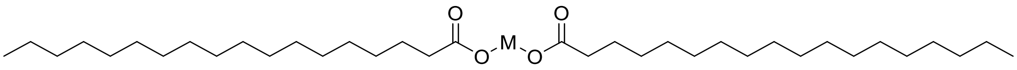

M = Co(II): **9Co**
M = Mn(II): **9Mn**

Scheme I-17: Stearate complexes studied in this work: cobalt(II) bis*(stearate)* ***9Co*** *and manganese(II)* bis*(stearate)* ***9Mn****.*

Role of the Additives

Oxidation of organic additive models (**10**-**13**, Scheme I-18) has been studied in solution in the presence of strong organic oxidants and these processes have been monitored and quantified by UV-visible absorption spectrophotometry. Once the most active organic additive model defined using this approach, its oxidation has been then examined in the presence of the most efficient metal catalysts.

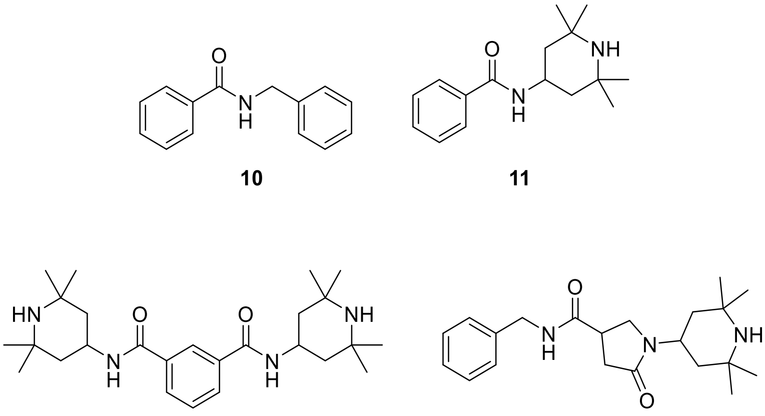

10 **11**

12 **13**

Scheme I-18: Organic additive models studied in this work.

An important part of this work (mimicking the real conditions used during the manufacture process used by the masterbatches and additives division of Clariant) has been then focused on the deep investigation of the oxidation in the solid-state and in the presence of several metal catalysts of organic additive models (**10**-**13**, Scheme I-18) and polymeric additives (**14**-**15**, Scheme I-19). The oxidation process (kinetics and characterization of the oxidation products) has been mainly monitored by Fourier transform infrared spectroscopy (FTIR), but also with a set of complementary solid-state techniques that will be further developed throughout this manuscript. For instance, the initial polymeric additives (before oxidation with/without the metal catalysts) and their oxidized products (thermal oxidation or assisted with metal catalysts) have been analysed and characterized by ^{1}H and ^{13}C NMR spectroscopy, electron paramagnetic resonance (EPR), X-ray photoelectron spectroscopy (XPS), scanning electron microscopy (SEM), size exclusion chromatography (SEC).

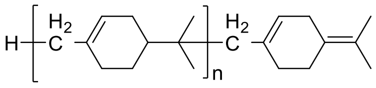

Dercolyte S 125

14

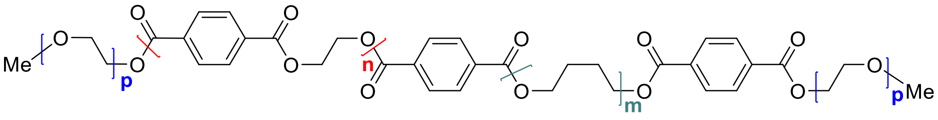

polytetrahydrofuran derivative

15

Scheme I-19: Polymeric additives studied in this work.

Dercolyte S 125 (**14**, Scheme I-19) is obtained from the polymerization of the β-pinene (Scheme I-20) and its use has been already reported for oxygen barrier applications.[131,132] It is well known as a

---

[131] Katsumoto, K.; Ching, T. Y. Multi-component oxygen scavenging composition. US005776361, 1998.

[132] Menozzi, E.; Galfré, E.; Ruggeri, N. Use of metal complexes as oxygen absorber/scavenger elements for packaging applications. US20120263974A1, 2012.

tackifying resin used to improve the adhesive properties (*e.g.* tack, adhesion, heat resistance) of adhesives (*i.e.* hot melt-based or solvent-based).

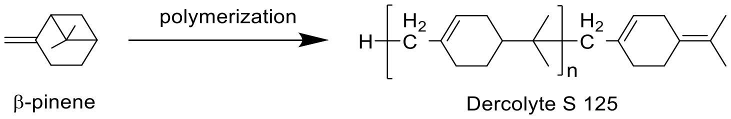

14

Scheme I-20: Synthesis of Dercolyte S 125 ***14****.*

The polymeric additive **15** (Scheme I-19) is a Clariant-made system never described so far with a high potential in oxygen barrier technology. It can be regarded as the repetitive arrangement of "tetrahydrofuran", terephthalate and "ethylene glycol" subunits (*i.e.* copolymer made of PET and PTHF and terminated by PEG residues).

For each of the polymeric additives, a mechanism of action will be proposed and discussed (*e.g.* kinetics parameters, relevant intermediates, (sub-)products, efficiency of the metal catalysts…).

Chapter II:

Synthesis, characterization & physico-chemical investigation of the metal catalysts

II. Synthesis, characterization & physico-chemical investigation of the metal catalysts

II.1. A plethora of analytical tools to unravel the physico-chemical properties of the ligands and the metal complexes

Before going further on the oxygen scavenging capacities of both the metal catalysts and the additives in plastics, it was first necessary to undertake a preliminary investigation on the metal complexes, to evaluate their physico-chemical properties (stability, resistance in solution, protonation constants…). These parameters are indeed of key importance to figure out the oxygenation efficacies of the metal catalysts. Regarding cobalt(II) complexes, it has been indeed reported that their stabilities are intimately linked to the acido-basic properties of the ligands. Furthermore, the oxygen binding processes were also demonstrated to be closely related to the stability[133] and the redox properties[134] of the cobalt(II) complexes. It therefore seemed appropriate to first carefully investigate the acido-basic properties of the free ligands as well as the stability constants of the corresponding cobalt(II) and manganese(II) complexes.

As mentioned previously in Chapter I, ligands displaying more than one heteroatom donor site are very interesting for the preparation of metallic complexes and, in particular, the ligands based on a Schiff base skeleton. Their uses as ligands were shown to display a wide range of applications such as in catalysis, medicine or in materials. They are also well known for their oxygenation properties once coordinated to metal centres, such as cobalt(II), manganese(II) or nickel(II).[129,135,136,137,138,]

To reach these objectives, it was so necessary to first synthesize both the ligands and the metal complexes before starting any physico-chemical characterization. The ligand stability has been then studied by different but complementary means such as UV-visible absorption spectrophotometry and ESI-MS. The ligands properties such as, their protonation constants, have been assessed either by pure potentiometry or by a homemade automatic interfaced system that combines simultaneous measurements done by a UV-visible absorption spectrophotometer and a potentiometer. This later, allowed us saving time, expanding the experiments and gaining repeatability and reliability.

After this thorough physico-chemical characterization of the ligands, interest has been then focused on their cobalt(II) and manganese(II) complexes. The affinities of the synthesized Schiff base ligands for cobalt(II) and manganese(II) have been evaluated by UV-visible absorption spectrophotometry coupled to potentiometry.

As described previously (section I.3), other type of ligands such as, acetylacetonate (*i.e.* acac) and carboxylate (*e.g.* stearate), are also of particular interest in the context of this Ph.D. work. Commercially available complexes have been therefore characterized by using various analytical tools. Elemental analysis allowed ensuring the structure and the purity of the complexes. EPR has been used to determine the paramagnetic character of the compounds as well as the oxidation state of the metal centre. FTIR has been also employed advantageously to confirm the structure and the purity of the investigated complexes. Last but not least, regarding the manganese(II) stearate (*i.e.* the manganese(II) stearate supplied by Clariant was not of high purity), its synthesis and purification has been optimized in the laboratory and its thorough characterization has been realized by using the same analytical means.

---

[133] Martell, A. E. *J. Mol. Catal.* **1988**, *44*, 1–14.

[134] Hanzlik, R. P.; Jun, D. F. S. *J. Chem. Soc., Chem. Commun.* **1974**, 528–529.

[135] Pui, A. *Croat. Chem. Acta* **2002**, *75* (1), 165–173.

[136] Emara, A. A. A.; Ali, A. M.; El-Asmy, A. F.; Ragab, E.-S. M. *J. Saudi Chem. Soc.* **2014**, *18* (6), 762–773.

[137] Huber, A.; Müller, L.; Elias, H.; Klement, R.; Valko, M. *Eur. J. Inorg. Chem.* **2005**, *2005* (8), 1459–1467.

[138] Horwitz, C. P.; Dailey, G. C. *Comments Inorg. Chem.* **1993**, *14* (5), 283–319.

We then turned our efforts on the heart of the matter that is the study of the oxygenation properties of the investigated metal catalysts. These have been studied by combining complementary analytical tools (*e.g.* UV-visible absorption spectrophotometry, oximetry, ESI-MS, NMR). Using UV-visible absorption spectrophotometry, we were able to monitor the oxygenation and activation of the catalysts and accordingly determine the kinetics parameters. When coupled to oximetry, we could relate the UV-visible absorption spectrophotometric variations to the oxygen concentration in solution. Interestingly, the reversibility of the oxygenation process centred on the metal catalysts could be assessed using this approach (*i.e.* absorption *versus* oximetric measurements). To characterize the oxygenation and activation products, ESI-MS and NMR have been used, and kinetics parameters have been determined. In the last part of this work, we have developed a new approach to properly monitor the oxygenation/activation processes of the metal catalysts under a broad range of experimental conditions. Indeed, for a large number of metal catalysts, the spectral variations have been observed to be weak to accurately monitor the corresponding oxygenation and activation processes. A known spectrophotometric probe (*i.e.* 2,2-diphenyl-1-picrylhydrazyl (DPPH)), never used to the best of our knowledge for this type of application, has been successfully employed. In particular, its radical nature allowed identifying whether the oxygenation/activation processes underwent through a radical mechanism or not. Finally, an electrochemical investigation (*i.e.* cyclic voltammetry) has been conducted to complete this extensive study and assess the redox properties of the different metal catalysts.

II.2. Synthesis, stability and protonation constants of the Schiff base ligands

II.2.1. Preparation of the ligands

Schiff base ligands are well known ligands in coordination chemistry and their preparations usually result from a reversible condensation between an amine (the benzylamine) and a carbonyl group (*i.e.* an aldehyde for the systems considered in the present work) to afford an imine function.[139]

The Schiff base ligands (**L**^{1}-**L**^{7}) have been synthesized using a protocol described in the patent published by Sierra Rodriguez *et al.* in 2002 (Scheme II-1) from commercially available corresponding aldehydes and benzylamine.[140]

---

[139] Rotondo, E.; Pietropaolo, R.; Tresoldi, G.; Faraone, F.; Cusmano, F. *Inorganica Chim. Acta* **1976**, *17*, 181–191.

[140] Sierra Rodriguez, M. A.; Gomez Galleco, M.; Alcazar Montero, R.; Ramirez Lopez, P.; Moreno Lozano, J.; Lucena Marotta, J. J. Novel method of preparing hydroxyarylglycines, alcoxyarylglycines and the glycinates thereof. WO02102762A1, 2002.

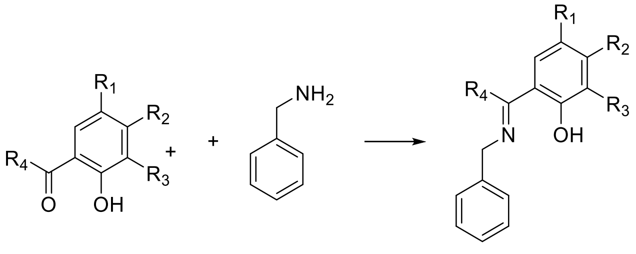

L^1-L^7

Scheme II-1: Synthesis of the Schiff base ligands investigated in this work.

In a first stage, the Schiff base ligands were obtained without any optimization from 17% to quantitative yield (Table II-1).

Table II-1: Yields of the synthesis of the different Schiff base ligands.

Schiff base ligand	R_1	R_2	R_3	R_4	Yield (%)
L^1	H	H	H	H	quantitative
L^2	H	OH	H	Ph	17
L^3	Br	H	Br	H	80
L^4 *	Me	H	H	H	94
L^5	NO_2	H	H	H	75
L^6	OCH_3	H	H	H	quantitative
L^7	H	OH	H	H	48

* for **L^4**, the corresponding aldehyde, 2-hydroxy-5-methylbenzaldehyde, was synthesized from *p*-methylphenol[141,142]

For the sake of simplicity, a different and innovative synthesis way has been also developed. The benzylamine and the aldehyde being both a liquid in some cases, attempt to prepare the corresponding ligands in solvent-free conditions was tested and the ligands were successfully obtained (**L^1**, quantitative yield, **L^6**, quantitative yield).

The ligands were characterized by ^1H and ^{13}C NMR, FTIR, and ESI-MS, and their purity was assessed by liquid chromatography-mass spectrometry (LC-MS). The Schiff base compounds exhibited two characteristics FTIR bands: one centred at ~ 1625 cm^{-1} related to the $\nu_{C=N}$ stretching vibration and the other one centred (*i.e.* ν_{O-H}, sharp and weak intensity) at ~ 3000 cm^{-1} demonstrating the presence of strong intra-molecular hydrogen bond for some of them (*e.g.* **L^4** and **L^6**, Figure II-1). All these analyses confirmed the structure of the synthesized ligands and their high purity.

---

[141] Nakai, Y.; Moriyama, K.; Togo, H. *Eur. J. Org. Chem.* **2014**, *2014* (27), 6077–6083.

[142] Bhatt, S.; Nayak, S. K. *Tetrahedron Lett.* **2009**, *50* (42), 5823–5826.

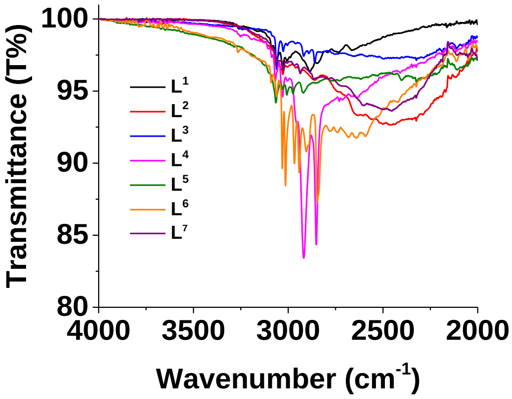

Figure II-1: FTIR spectra - expansion of the 4000 - 2000 cm^{-1} wavenumber range - of the Schiff base ligands investigated in this work.

II.2.2. Stability of the ligands in solution under acidic and basic conditions

The stability of the Schiff base ligands (**L^1**-**L^7**) was evaluated in solution over time. Two representative examples (**L^1** and **L^2**) will be described in detail in this section and the results for the other ligands (**L^3**-**L^7**) will be briefly presented.

A solution of **L^1**, that was freshly prepared in CH_3CN:water (1:1 *v/v*), was first studied over a period of 32.5 hours by ESI-MS. At first glance, no variation was observed, as depicted on Figure II-2. The intensity of each mass spectrum was normalized with respect to the [**L^1**+H]$^+$ peak intensity on each spectrum.

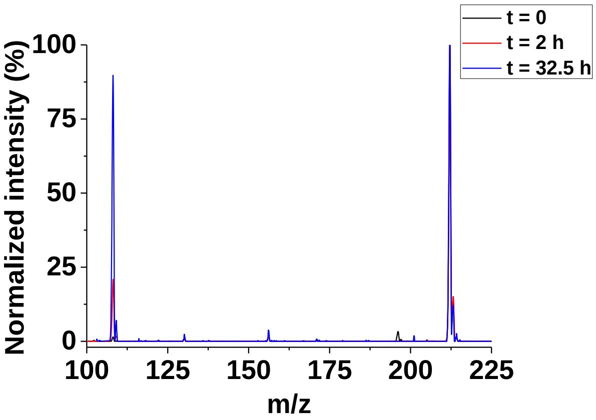

*Figure II-2: Stability of a solution of **L^1** monitored by ESI-MS; [**L^1**] = 1.0 x 10^{-4} M; solvent: CH_3CN:H_2O (1:1 v/v); + 100 V.*

But scrutinizing the two peaks of interest [**L^1**+H]$^+$ (*m/z* = 212.1; Figure II-3) and [benzylamine+H]$^+$ (*m/z* = 108.1; Figure II-4), some marked variations could be observed. In fact, Figure II-3 shows that the ligand did not undergo aerobic oxidation over time and Figure II-4 rather highlights that the intensity of the [benzylamine+H]$^+$ peak was increasing over time. This means that equilibrium between the ligand and the starting amine took place and that the ligand was hydrolysed over time to reinstate the starting amine and the aldehyde. This process was seemingly rather slow.

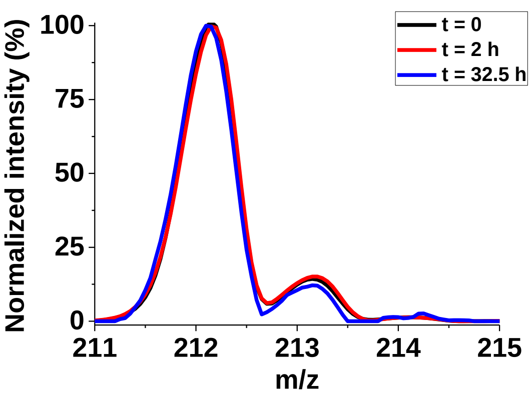

Figure II-3: Stability of a ***L*** ^{1} *solution over time (zoom on the [*$\mathbf{L^1}$*+H]*$^{+}$ *peak centred at* m/z *= 212.1); [*$\mathbf{L^1}$*] = 1.0 x 10*$^{-4}$ *M; solvent: CH*$_3$*CN:H*$_2$*O (1:1* v/v*); + 100 V.*

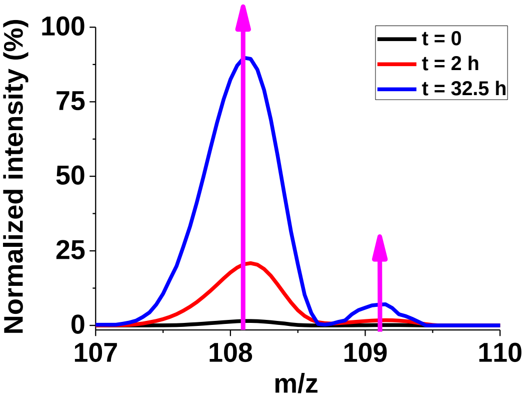

Figure II-4: Stability of a ***L*** ^{1} *solution over time (zoom on the [benzylamine+H]*$^{+}$ *peak centred at* m/z *= 108.1); [*$\mathbf{L^1}$*] = 1.0 x 10*$^{-4}$ *M; solvent: CH*$_3$*CN:H*$_2$*O (1:1* v/v*); + 100 V.*

The corresponding experiment was repeated in dioxane:water (1:1 *v/v*) and monitored by UV-visible absorption spectrophotometry over 16 hours. A spectral variation could be clearly noticed with a hypsochromic shift of the band centred at 400 nm (Figure II-5). The kinetics of the reaction either at 315 or at 397 nm (Figure II-6) illustrated a one-step process, and substantiated the hydrolysis of the ligand previously observed by ESI-MS.

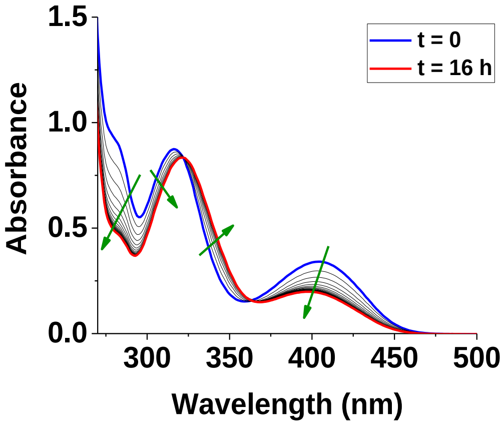

Figure II-5: Stability of a ***L*** ^{1} *solution monitored by UV-visible absorption over 16 hours; [*$\mathbf{L^1}$*] = 2.50 x 10*$^{-4}$ *M, solvent: dioxane:H*$_2$*O (1:1* v/v*), l = 1 cm.*

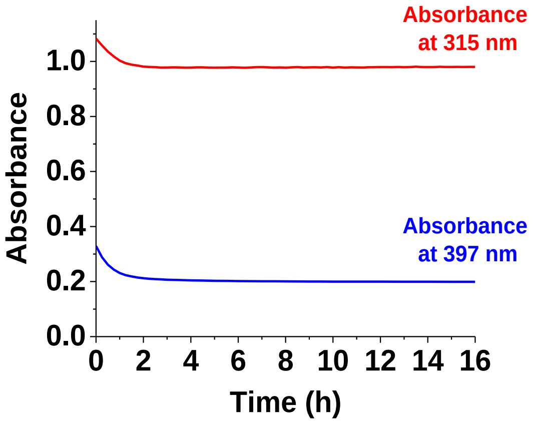

Figure II-6: Kinetics of the hydrolysis reaction of ***L*** ^{1} *solution at 315 and 397 nm; [*$\mathbf{L^1}$*] = 2.50 x 10*$^{-4}$ *M, solvent: dioxane:H*$_2$*O (1:1* v/v*), l = 1 cm.*

The same approach (*i.e.* ESI-MS) was conducted on $\mathbf{L^2}$ over the same time span as for $\mathbf{L^1}$ (*i.e.* 32 h). Even after 32 hours, no obvious evidence of the presence of the corresponding amine or aldehyde was evidenced (Figure II-7, *i.e.* the intensity of each mass spectrum was normalized with respect to the [$\mathbf{L^2}$+H]$^{+}$ peak intensity). Interestingly, $\mathbf{L^2}$ did not undergo any hydrolysis or oxidation in solution over time (Figure II-8).

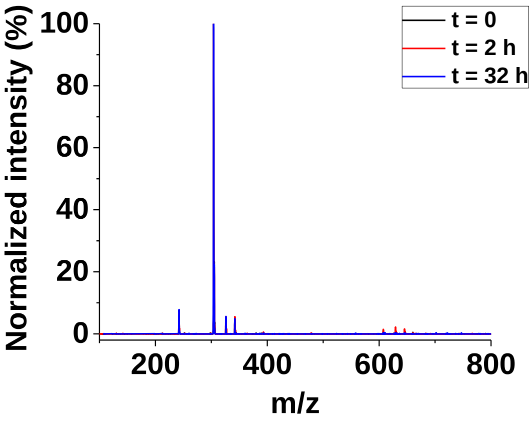

*Figure II-7: Stability of a **L^2** solution assessed by ESI-MS; [**L^2**] = 1.0 x 10^{-4} M; solvent: CH_3CN:H_2O (1:1 v/v); + 100 V.*

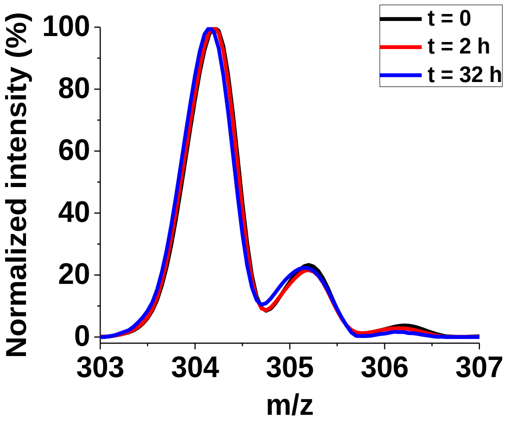

*Figure II-8: Stability of a **L^2** solution over time (zoom on the [**L^2**+H]$^+$ peak centred at m/z = 304.2); [**L^2**] = 1.0 x 10^{-4} M; solvent: CH_3CN:H_2O (1:1 v/v); + 100 V.*

The experiment was repeated in dioxane:water (1:1 *v/v*) and monitored by UV-visible absorption spectrophotometry over 16 hours. No significant absorption variation could be observed (Figure II-9 and Figure II-10), confirming the results previously observed by ESI-MS.

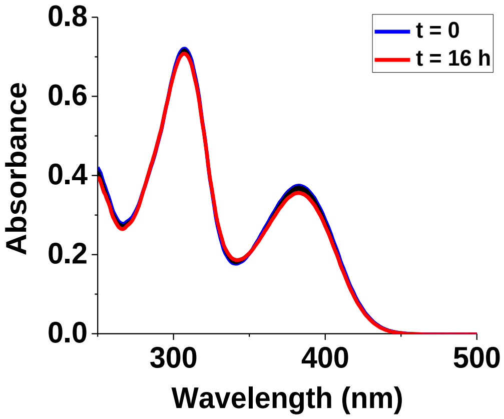

*Figure II-9: Stability of a **L^2** solution monitored by UV-visible absorption spectrophotometry for 16 hours; [**L^2**] = 5.02 x 10^{-5} M, solvent: dioxane:H_2O (1:1 v/v), l = 1 cm.*

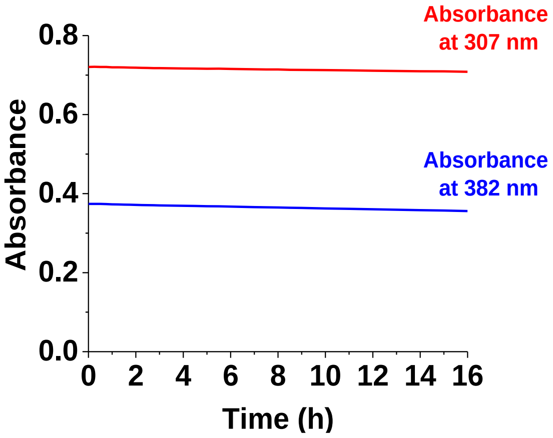

*Figure II-10: Kinetics of the hydrolysis reaction of a **L^2** solution at 307 and 382 nm; [**L^2**] = 5.02 x 10^{-5} M, solvent: dioxane:H_2O (1:1 v/v), l = 1 cm.*

The stability of the other ligands in solution (*i.e.* CH_3CN:water or dioxane:water 1:1 *v/v*) was also investigated by UV-visible absorption spectrophotometry, and it was observed that **L^3**, **L^5** and **L^6** were stable in solution, which means that they were not either hydrolysed or oxidized over time, as already observed for **L^2**.

It is noteworthy that the determination of the protonation constants of the ligands has to be performed in a wide range of pH (*i.e.* from acidic to basic conditions and vice versa). It is the reason why the stability of our ligands was also investigated under acidic and basic conditions, prior to the determination of the protonation constants. As relevant examples, the results obtained for ligands **L^1** and **L^6** are presented below.

Different UV-visible absorption spectra were first recorded on a **L^1** solution at different pHs. The UV-visible absorption spectrum of **L^1** (**(1)**, Figure II-11) was recorded and displayed two absorption maxima at 318 and 404 nm. When this solution was acidified with concentrated perchloric acid (**(2)**, Figure II-11), the absorption maximum at 318 nm underwent a bathochromic shift to 326 nm. When this spectrum was compared to those of benzylamine (**(3)**, Figure II-11) and salicylaldehyde (**(4)**, Figure

II-11), which are the two reactants to synthesize the ligand **L^1**, it clearly appeared that the absorption spectrum of the **L^1** solution recorded under acidic conditions actually corresponded to the salicylaldehyde signature. It thus clearly demonstrated that **L^1** underwent a hydrolysis reaction under acidic conditions.

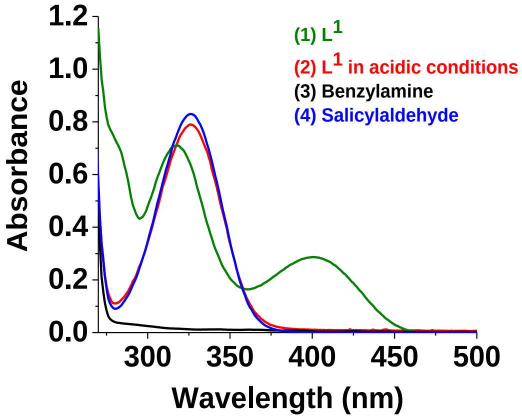

*Figure II-11: UV-visible absorption spectra of **L^1** in neutral and acidic conditions, benzylamine and salicylaldehyde; **(1)** [**L^1**] = 2.26 x 10^{-4} M (pH = 8.6), **(2)** [**L^1**] = 2.20 x 10^{-4} M (pH = 3.9), **(3)** [benzylamine] = 4.94 x 10^{-2} M, **(4)** [salicylaldehyde] = 4.94 x 10^{-4} M, solvent: dioxane:H_2O (1:1 v/v), l = 1 cm.*

These preliminary absorption data obtained for **L^1** were completed by an ESI-MS study (Figure II-12 and Figure II-13). First, an ESI-MS spectrum of **L^1** was recorded in CH_3CN:water (1:1 *v/v*) and the pH of the solution was measured (pH ~ 5-6) (*i.e.* black line on the next figures). The **L^1** ligand could be correctly characterized thank to its mass signal at 212.2 (Figure II-12: [**L^1**+H]$^+$). However, under these conditions, the ligand already began to be hydrolysed (*i.e.* see the previous section) and the characteristic ESI-MS signal related to the free benzylamine at *m/z* = 108.1 was detected (Figure II-13: [benzylamine+H]$^+$). The solution was then basified by adding one drop of concentrated ammonia and the pH of solution was measured to be ~ 10-11. On Figure II-12 and Figure II-13, the hydrolysis of the **L^1** ligand can be substantiated, as an increase of the peak that corresponds to the benzylamine (*m/z* = 108.1, Figure II-13). The initial solution of **L^1** ligand at pH ~ 5-6 was also acidified with one drop of formic acid and the pH of the solution was measured to be ~ 2. Under acidic conditions, the same conclusions, as those deduced from the experiments carried out under basic conditions, can be drawn.

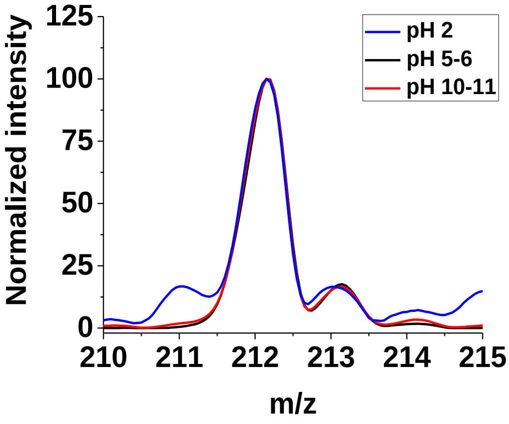

*Figure II-12: Stability of a **L^1** solution over time (zoom on the [**L^1**+H]$^+$ peak centred at m/z = 212.1); [**L^1**] = 9.0 x 10^{-5} M; solvent: CH_3CN:H_2O (1:1 v/v); + 100 V.*

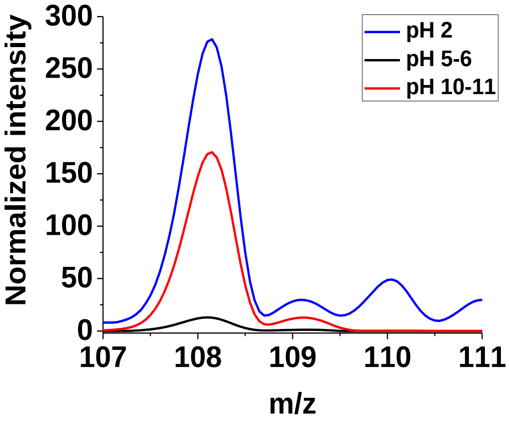

*Figure II-13: ESI-MS spectra of **L^1** at different pH conditions (zoom on the [benzylamine+H]$^+$ peak centred at m/z = 108.1); [**L^1**] = 9.0 x 10^{-5} M, solvent: CH_3CN:H_2O (1:1 v/v), + 100 V.*

Whatever the conditions used (acidic, basic or neutral conditions), **L^1** underwent a hydrolysis as confirmed by the fruitful combination of UV-visible absorption spectrophotometry and ESI-MS. The imine hydrolysis that reinstates the free aldehyde and amine is slow in neutral media, while it is significantly sped up under acidic or basic conditions.

The same approach was conducted by ESI-MS on **L⁶**. A spectrum of the **L⁶** ligand solution at pH ~ 5-6 was first recorded by ESI-MS and the solution was then acidified with one drop of concentrated formic acid to pH ~ 2-3 or basified with one drop of concentrated ammonia to pH ~ 10-11. The different ESI-MS spectra were recorded and are depicted in Figure II-14 and Figure II-15. When the intensities of each observed peaks were normalized with respect to that of the [**L⁶**+H]$^+$ species (Figure II-14), it clearly appeared that hydrolysis of the ligand (*i.e.* originally centred at *m/z* = 242.1, Figure II-14) into the corresponding amine (*m/z* = 108.1, Figure II-15) was enhanced under basic and even more under acidic conditions (Figure II-15).

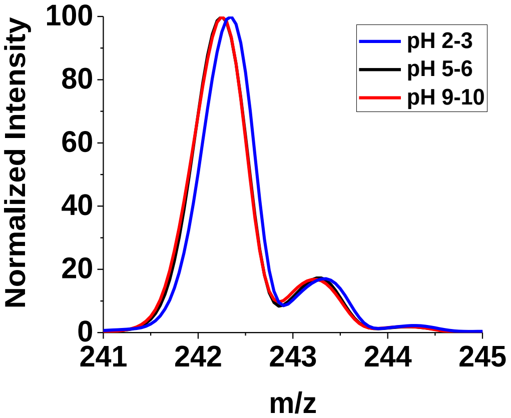

*Figure II-14: ESI-MS spectra of **L⁶** in different pH conditions (zoom on the [**L⁶**+H]$^+$ peak centred at* m/z *= 242.1); [**L⁶**] = 1.06 x 10^{-4} M, solvent: $CH_3CN:H_2O$ (1:1* v/v*), + 150 V.*

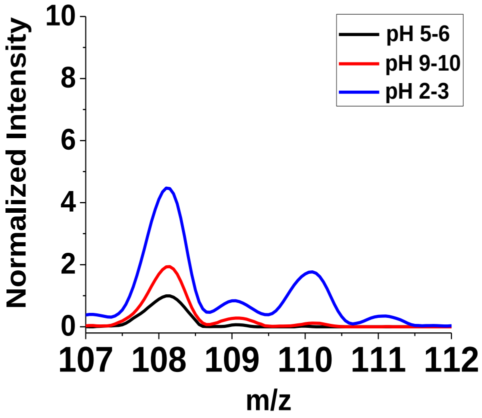

*Figure II-15: ESI-MS spectra of **L⁶** in different pH conditions (zoom on the [benzylamine+H]$^+$ peak centred at* m/z *= 108.1); [**L⁶**] = 1.06 x 10^{-4} M, solvent: $CH_3CN:H_2O$ (1:1* v/v*), + 150 V.*

To conclude on this point, the results obtained from the stability of the different Schiff base ligands are gathered in Table II-2. As anticipated, the two tested ligands examined under various pH conditions (**L¹** and **L⁶**) underwent hydrolysis either under acidic or basic condition. On the other hand, contrary to **L²**, **L³**, **L⁵** and **L⁶** that were found to be stable in solution at neutral pH, **L¹** also underwent hydrolysis under this condition. There are therefore strong indications that **L¹** is the least stable ligand in solution. However, its stability when coordinated to metal centre has to be determined and the system could not be discarded based solely on the stability of the ligand in solution.

Table II-2: Stability of the different Schiff base ligands evaluated under different pH conditions.

Ligand	Stability under standard pH condition	Stability under acidic condition	Stability under basic condition
L¹	Hydrolysis	Hydrolysis	Hydrolysis
L²	Stable	*n.d.*	*n.d.*
L³	Stable	*n.d.*	*n.d.*
L⁴	*n.d.*	*n.d.*	*n.d.*
L⁵	Stable	*n.d.*	*n.d.*
L⁶	Stable	Hydrolysis	Hydrolysis
L⁷	*n.d.*	*n.d.*	*n.d.*

n.d.: not determined

II.2.3. Protonation constants of the Schiff base ligands

The protonation constants of the different ligands (**L^1**-**L^7**) were determined either by automated potentiometry or by UV-visible absorption spectrophotometry coupled to potentiometry.

To exemplify the methodology, the results will be thoroughly described for one ligand (**L^2**), while only the results will be provided for the other systems.

Firstly, the protonation constants were determined by UV-visible absorption *versus* pH titrations. **L^2** displayed absorption properties in the UV region (Figure II-16). An intense absorption band centred at ~ 308 nm could be observed under acidic conditions (pH ~ 4 at which hydrolysis is prevented) while the raise of the pH induced a large bathochromic shift of the latter absorption. The successive protonation constants were calculated after processing the absorption and pH data sets using the *Specfit* program (Table II-3). In addition to these thermodynamic data, the electronic spectra of the different protonated species of **L^2** were calculated as well and are depicted in Figure II-17. The different protonation constants were easily attributed to the potential protonation sites of **L^2** (Scheme II-2).

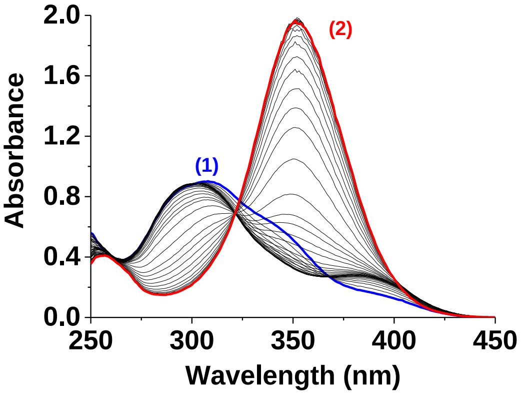

*Figure II-16: UV-visible absorption spectrophotometric titration of the free **L^2** ligand as a function of pH; **(1)** pH: 4.00, **(2)** pH: 12.54, [**L^2**] = 7.31 x 10^{-5} M, solvent: dioxane:H_2O (1:1 v/v), T = 25.0(2) °C, I = 0.1 M ($NaClO_4$.H_2O), l = 1 cm.*

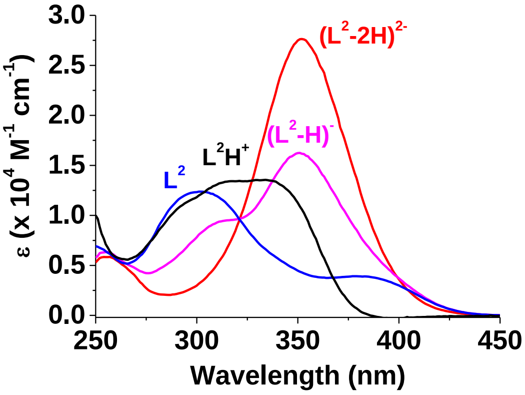

*Figure II-17: Electronic spectra of the protonated **L^2** species; [**L^2**] = 7.31 x 10^{-5} M, solvent: dioxane:H_2O (1:1 v/v), T = 25.0(2) °C, I = 0.1 M ($NaClO_4$.H_2O), l = 1 cm.*

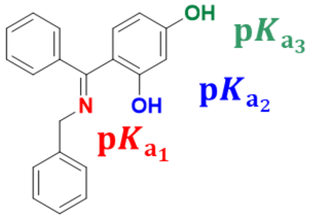

*Scheme II-2: Protonation sites of **L^2**.*

As mentioned previously, the **L^2** protonated species was characterized by a broad absorption band centred at ~ 308 nm (π-π* transitions of the aromatic units). The deprotonation of the imine function induced a large bathochromic shift of ~ 45 nm of this main absorption band.

Surprisingly, the deprotonation of the phenolic function was characterized by much weaker spectral variations. This could be explained by the presence of a strong hydrogen bond between the phenolic proton and the imine function. This feature could be attributable to hydrogen bonding within this (*N,O*)-binding unit as well as resonance effects (Scheme II-3).[143,144] It is noteworthy that the

---

[143] Dudek, G. O.; Dudek, E. P. *J. Am. Chem. Soc.* **1966**, *88* (11), 2407–2412.

[144] Chatziefthimiou, S. D.; Lazarou, Y. G.; Hadjoudis, E.; Dziembowska, T.; Mavridis, I. M. *J. Phys. Chem. B* **2006**, *110* (47), 23701–23709.

salicylideneimine-type compounds could exist in solution under four different tautomeric states (Scheme II-3):

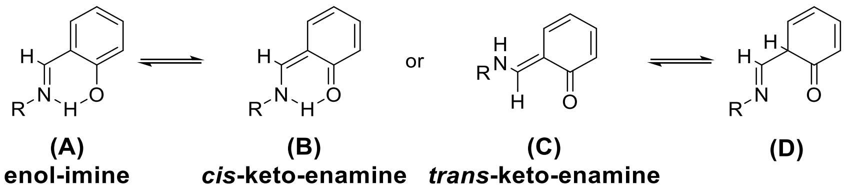

Scheme II-3: Keto-enol equilibrium.

Although **(D)** is a possible tautomer, no evidence of its presence has been proposed until now.[143] Tautomers **(A)** and **(B)** or **(C)** can be characterized by their absorption properties (for **(A)** $\lambda_{max} \sim 300 -$ 380 nm and **(B)** or **(C)** $\lambda_{max} > 400$ nm) and their relative abundance is closely related on the solvent properties. From our spectrophotometric studies, it is likely that $\mathbf{L^2}$ mainly predominates in solution as its enol-imine tautomer **(A)**.

In addition to the protonation constants that were calculated thanks to UV-visible absorption spectrophotometry *versus* pH titrations, we then conducted pure potentiometric experiments to confirm our first determinations. Figure II-18 displays the potentiometric titration curve of $\mathbf{L^2}$. The data have been processed by the *Hyperquad* software. Figure II-19 depicts the distribution diagrams of the protonated species as a function of pH. It shows that the neutral species $\mathbf{L^2}$ predominated in a broad range of pH (*i.e.* $\mathbf{L^2}$ predominated from pH ~ 3.8 to ~ 8.5).

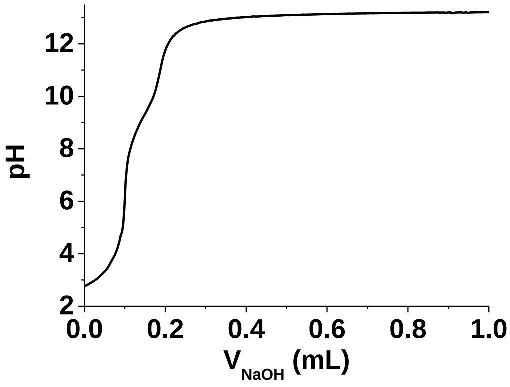

Figure II-18: Potentiometric titration curve of $\mathbf{L^2}$; [$\mathbf{L^2}$] = 1.05 x 10^{-3} M, solvent: dioxane:H_2O (1:1 v/v), T = 25.0(2) °C, I = 0.1 M ($NaClO_4.H_2O$).

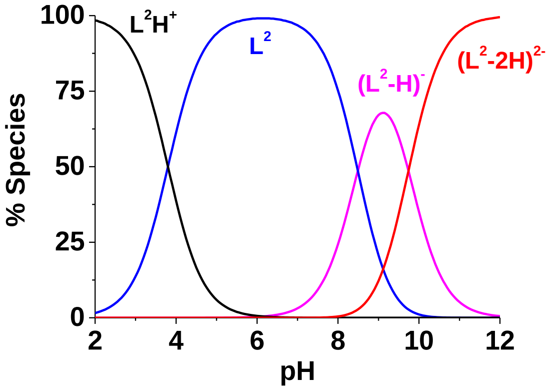

Figure II-19: Distribution diagrams of the protonated $\mathbf{L^2}$ species; [$\mathbf{L^2}$] = 7.31 x 10^{-5} M, solvent: dioxane:H_2O (1:1 v/v), T = 25.0(2) °C, I = 0.1 M ($NaClO_4.H_2O$), l = 1 cm.

The thermodynamic data, which have been calculated from these absorption and/or potentiometric data sets, are gathered in Table II-3. It is noteworthy that they correspond to an average of at least two to three independent experiments conducted under similar conditions. A good agreement can be clearly observed. As anticipated, the $\mathbf{L^2}$ ligand is characterized by two basic pK_as related to the phenolate units and an acidic pK_a that is characteristic of the imine function.

Table II-3: Protonation constants of ***L²*** *determined by UV-visible absorption spectrophotometry coupled to potentiometry and by pure potentiometry.*

Equilibrium	Potentiometry p*K*a	Absorption *versus* pH p*K*a
$(\mathbf{L^2}\text{-}2H)^{2-} + H^+ \overset{K_{11}}{\rightleftharpoons} (\mathbf{L^2}\text{-}H)^-$	10.4(1)	9.74(6)
$(\mathbf{L^2}\text{-}H)^- + H^+ \overset{K_{12}}{\rightleftharpoons} \mathbf{L^2}$	8.7(2)	8.5(1)
$\mathbf{L^2} + H^+ \overset{K_{13}}{\rightleftharpoons} \mathbf{L^2}H^+$	3.9(2)	3.8(3)

The same methodology has been applied for the other Schiff base ligands examined in this work. Their pK_a values are depicted in Table II-4 (*i.e.* for the ligands that display two pK_a values) and Table II-5 (*i.e.* for ligands that are characterized by three pK_a values due to the presence of two phenolates protonation sites). It is noteworthy that some of these ligands underwent hydrolysis under basic conditions which makes the analysis and identification difficult (*i.e.* the hydrolysis under acidic conditions was prevented by starting the titrations at about pH 4). To properly attribute the protonation constants determined to the ligands and not to the hydrolysed species (*i.e.* the benzaldehyde reactants), UV-visible absorption titrations of the free substituted benzaldehydes have been also performed and the pK_a attribution of the ligands was therefore done by comparison of the data.

Table II-4: Protonation constants of ***L¹****,* ***L³****,* ***L⁴****,* ***L⁵*** *and* ***L⁶*** *determined by UV-visible absorption spectrophotometry* versus *pH titrations and by pure potentiometric titrations.*

Ligand	Potentiometry pK_{a_1}	 pK_{a_2}	UV-vis. absorption *versus* pH pK_{a_1}	 pK_{a_2}
L¹	*n.a.*	*n.a.*	*n.d.*	11.87(5)
L³	6.0(2)	9.5(1)	6.5(6)	9.7(5)
L⁴	*n.d.*	*n.d.*	*n.d.*	12.1(1)
L⁵	5.80(8)	9.30(5)	5.98(9)	9.91(7)
L⁶	*n.d.*	*n.d.*	*n.d.*	12.11(7)

n.a.: not applicable
n.d.: not determined due to fast hydrolysis

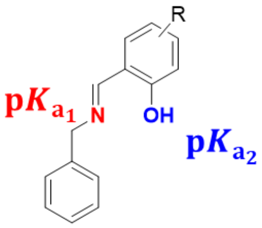

Table II-5: Protonation constants of ***L²*** *and* ***L⁷*** *determined by UV-visible absorption spectrophotometric* versus *pH titrations and by pure potentiometric titrations.*

Ligand	Potentiometry pK_{a_1}	 pK_{a_2}	 pK_{a_3}	UV-vis. absorption *versus* pH pK_{a_1}	 pK_{a_2}	 pK_{a_3}
L²	3.9(2)	10.4(1)	8.7(2)	3.8(3)	9.74(6)	8.5(1)
L⁷	3.7(2)	10.85(7)	8.3(1)	4.6(2)	11.4(1)	8.4(1)

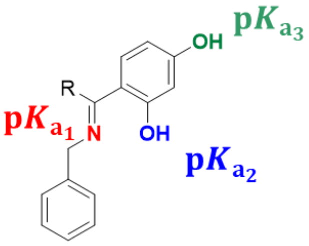

The nature (*i.e.* mesomeric and/or inductive substituent, Table II-6) and the position of substituents have a strong influence on the acidity of the O-H bond. In fact, phenol function with high electronic density will lead to strong hydrogen bond with the adjacent N-imine unit and consequently to high pK_a values. In the case of **L¹** (no substitution), **L⁴** (methyl substitution, inductive electron donor) and **L⁶** (methoxy substitution, mesomeric electron donor), the high pK_a values measured for their phenolate units reflects strong hydrogen bonding. Concomitantly, the pK_a of the imine units could not be determined because of the significant decrease of their pK_a values due to strong hydrogen bonding of the (N,O) moiety.

*Table II-6: Classification of the substituents found in the ligands (**L^1-L^7**) as electron-donor and electron-withdrawal mesomeric and inductive substituents.*

Mesomeric effect		Inductive effect	
Electron-donor	**Electron-withdrawal**	**Electron-donor**	**Electron-withdrawal**
OH, Br, OCH_3	NO_2	Me	OH, Br, NO_2, OCH_3

It should be noticed that the mesomeric effects prevails on inductive effects.

For electron-withdrawing substituents such as Br for **L^3** and NO_2 for **L^5**, one would expect for the same reasons as stated above that decreasing the electron density on the phenol function will impaired the hydrogen bond and consequently decrease the pK_a values of the phenolate units and concomitantly increase the pK_a values of the imine functions. The lower pK_a values attributed to the phenolates of **L^3** and **L^5** as well as the higher pK_a values determined for the corresponding imine sites confirmed this hypothesis thus suggesting weak hydrogen bonding for these two systems.

For **L^1** and **L^3-L^6** ligands, the position of the substituents (*i.e. ortho* and *para* to the phenolate unit) has a significant influence. As shown on Scheme II-4 that represents the possible resonance forms of the phenolate anion, the negative charge can be delocalized within the phenyl ring with formal negative charge in *ortho* and *para* position with respect to the phenolate. The substituents that will strongly influence the acido-basic properties of the phenol group will be those that are substituted in *ortho* and *para* position. The pK_{a3} value (Table II-5) measured for **L^7** was found to be close to that of **L^1** confirming that *meta*-substitution has a negligible impact on the phenolate protonation properties. The protonation properties of **L^2** stand in interesting contrast due to the imine-aryl substituent.

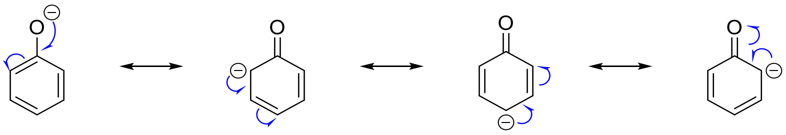

Scheme II-4: Resonance forms of the phenolate anion

As previously mentioned above, the nature and the position of the substituent on the phenol ring strongly influences the pK_a value of the phenol unit. It is generally assumed that the pK_a value of a ligand can be related to its complexation affinity with a given metal centre. Therefore, the higher the pK_a value is, the more stable the corresponding metal complex will be. Furthermore, the pK_a values of the ligands have been also correlated to the oxygenation capacity of the corresponding metal complexes.[130] Following this reasoning, it can be thus anticipated that the cobalt(II) or manganese(II) complexes with **L^1**, **L^4**, **L^6** and **L^7** should be the more efficient in terms of oxygen binding.

II.3. Synthesis and physico-chemical properties of the metal complexes

II.3.1. Preparation of the cobalt(II) and manganese(II) complexes

II.3.1.1. Classical strategy

In this first strategy of synthesis of the metal complexes, two approaches were developed. In one hand, the synthetic attempts were performed using the classical ligand/metal approach. That means that the ligands were allowed to react with the metal salt (cobalt(II) or manganese(II)) to lead to the targeted complex. On the other hand, efforts have been put on a one-pot synthetic strategy. The aldehyde and the amine were allowed to react to form the corresponding Schiff base ligand. Following this reaction and without any further purification, the metal salt was then added to the reaction mixture to afford the targeted metal complex.

II.3.1.1.1. Ligand/metal approach

The first synthetic route to prepare the metal catalysts took place in two classical steps (Scheme II-5). Firstly, the Schiff base ligands were synthesized (see above, II.2.1), based on a patent published by the group of Sierra Rodriguez.[140] The second step consisted of the complexation in solution of these ligands with either cobalt(II) or manganese(II) salt to afford the targeted complexes.

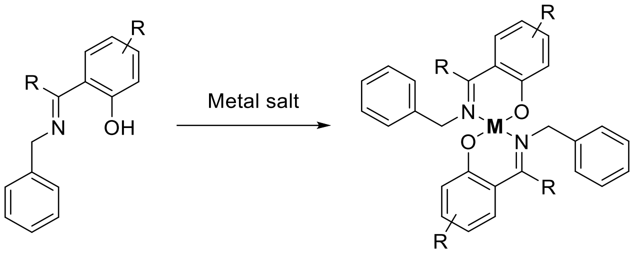

L¹-L⁷

M = Co: **1Co-7Co**
M = Mn: **1Mn-7Mn**

Scheme II-5: Synthetic approach for the preparation of the targeted cobalt(II) and manganese(II) catalysts - ligand/metal version.

If numerous cobalt(II) and manganese(II) complexes derived from Schiff base ligands have been described in the literature so far, scarce data exist for Schiff base ligands prepared from benzylamine. For instance, the groups of Jiang[145] and Dang[146] reported in 2008 the synthesis of the cobalt(II) complexes **3Co** and **4Co**. After the preparation of the corresponding ligand, this latter was stirred with a half equivalent of cobalt(II) chloride in ethanol from half an hour to one hour and the resulting solution was allowed for slow evaporation of the solvent for about 3 to 5 days to afford crystals of the targeted complex. Basically, this strategy was firstly employed to synthesize the corresponding cobalt(II) complexes (**1Co** and **3Co**-**7Co**). Despite numerous efforts at improving the reaction, only the cobalt(III) trischelate species was obtained for each of the attempts. This strategy was also applied to manganese(II) complexes **1Mn** and **2Mn**, starting from manganese(II) chloride. Nevertheless, here again, only the manganese(III) trischelate species were obtained in each case.

A screening of the various experimental conditions (nature of the counter-anion, addition of another reactant such base, nature of the solvent, temperature, reaction time, Table II-7) was then performed for the synthesis of **1Co**, **2Co**, **6Co** or **1Mn** with always the same negative outcome. Either the cobalt(III) trischelate was obtained or no reaction took place.

---

[145] Jiang, W.; Mo, G.-D.; Jin, L. *Acta Crystallogr. Sect. E Struct. Rep. Online* **2008**, *64* (11), m1394–m1394.

[146] Dang, F.-F.; Wang, X.-W.; Zhou, Y.-Z.; Han, G.-P.; Yang, Q.-C. *Acta Crystallogr. Sect. E Struct. Rep. Online* **2008**, *64* (12), m1486–m1486.

Table II-7: Screening of the synthetic conditions for the synthesis of ***1Co, 2Co, 6Co*** *and* ***1Mn.***

Complex	Metal salt (0.5 equiv.)	Other reactants	Solvent	T (°C)	Time	Observation
1Co	Co(acetate)$_2$	$NaHCO_3$ (4 equiv.) - under argon	deg. EtOH	78	15 min	$\mathbf{L^1}$
1Co	$Co(SO_4)_2.7H_2O$	0.1 M NaOH (pH adjusted to 7-8)	H_2O	100	90 min	$Co^{III}(\mathbf{L^1})_3$
2Co	Co(acetate)$_2$	/	EtOH	50	2 h	No isolated product
2Co	Co(acetate)$_2$	/	EtOH	50	16.5 h	No isolated product
6Co	Co(acetate)$_2$	under argon	MeOH	r.t.	10 min	$Co^{III}(\mathbf{L^6})_3$
6Co	Co(acetate)$_2$	under argon	MeOH:H_2O (1:1 *v/v*)	0	10 min	No isolated product
6Co	Co(acetate)$_2$	under argon	MeOH:H_2O (1:0.75 *v/v*)	0	5 min	$\mathbf{L^6}$
6Co	Co(acetate)$_2$	under argon	MeOH	r.t.	5 min	$\mathbf{L^6}$
6Co	Co(acetate)$_2$	under argon	MeOH	r.t.	5 min	$Co^{III}(\mathbf{L^6})_3$
6Co	Co(acetate)$_2$	/	dioxane	r.t.	10 min	$Co^{III}(\mathbf{L^6})_3$
1Mn	$MnCl_2.4H_2O$	/	EtOH:H_2O (9:1 *v/v*)	r.t.	1 h	No isolated product

II.3.1.1.2. One-pot approach

A one-pot strategy was then tried for the synthesis of **1Co**, **6Co** or **1Mn** (Scheme II-6). After the formation of the imine ligand (*i.e.* from the benzylamine and corresponding aldehyde reactants) in solution, a half equivalent of cobalt(II) (or manganese(II)) salt was added and the mixture was allowed to react to lead to the targeted divalent metal bischelate complex.

Various experimental conditions were tested as described in Table II-8. Despite of our efforts, **6Co** or **1Mn** were never obtained. For the cobalt complexes, cobalt(III) trischelate complexes were systematically obtained suggesting a very fast oxidation in solution of the cobalt(II) complexes. For manganese(II), no complexation was evidenced suggesting the lesser reactivity of manganese(II) with respect to cobalt(II). Interestingly, the cobalt(II) bischelate **1Co** was successfully obtained in high yield in the case of a subtle modification of the synthetic route.

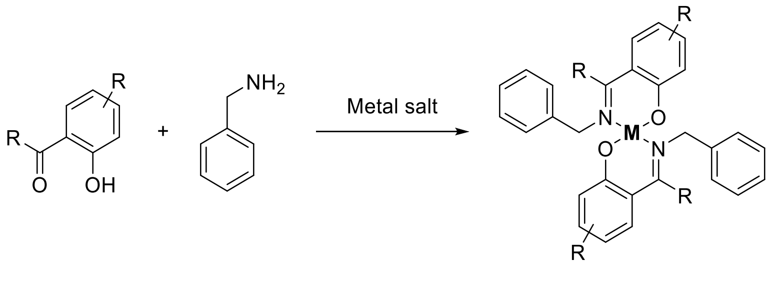

M = Co: **1Co-7Co**
M = Mn: **1Mn-7Mn**

Scheme II-6: Synthetic approach for the preparation of the cobalt(II) and manganese(II) catalysts - one-pot version.

The ligand was first synthesized from the benzylamine and 2-hydroxybenzaldehyde in solvent-free conditions for ~ 2 hours, and was allowed without any further purification to react with a half equivalent of cobalt(II) acetate previously dissolved in a minimum quantity of methanol at r.t. and for 15 minutes. An orange solid spontaneously precipitated. After filtration and washing with cold methanol, the desired complex was obtained with 87% yield. Although the obtained complex is paramagnetic, ^{1}H NMR was systematically used to assess the paramagnetic character of the synthesized complex. The obtained complex was also fully characterized by ESI-MS, HRMS, microanalysis, EPR and FTIR. In fact, in a metal complex containing Schiff base ligands, the FTIR band centred at ~ 3000 cm^{-1} (ν_{O-H}) disappeared in agreement with the subsequent deprotonation of the ligand and coordination of the phenolate to the metal centre. Besides, coordination of the nitrogen imine atom to the metal centre was evidenced by a significant shift of its $\nu_{C=N}$ characteristic band.

*Table II-8: Screening of the synthetic conditions for the one-pot synthesis of **1Co**, **6Co** and **1Mn**.*

Complex	Metal salt (0.5 equiv.)	Solvent	T (°C)	Time	Obtained compounds
1Co	$CoCl_2.6H_2O$	CD_3OD	r.t.		$Co^{III}(\mathbf{L^1})_3$
1Co	Co(acetate)$_2$	EtOH	2 h at 50 °C then 1 h at r.t.		$Co^{III}(\mathbf{L^1})_3$
1Co	Co(acetate)$_2$	EtOH:H_2O (9:1 *v/v*)*	r.t.	1 h	$Co^{III}(\mathbf{L^1})_3$
1Co	$Co(ClO_4)_2.6H_2O$	EtOH	r.t.	55.5 h	$Co^{III}(\mathbf{L^1})_3$
1Co	$Co(SO_4)_2.7H_2O$	EtOH	r.t.	55.5 h	L + $Co^{II}(\mathbf{L^1})_2$ +$Co^{III}(\mathbf{L^1})_3$**
1Co	**Co(acetate)$_2$**	**Solvent-free*** **	r.t.	15 min	**$Co^{II}(L^1)_2$ (87%)**
6Co	Co(acetate)$_2$	Solvent-free***	r.t.	30 min	$Co^{III}(\mathbf{L^6})_3$
1Mn	Mn(acetate)$_2$	EtOH	50	2 h	No isolated product
1Mn	$MnCl_2.4H_2O$	EtOH	50	23 h	$\mathbf{L^1}$
1Mn	$MnCl_2.4H_2O$	EtOH:H_2O (9:1 *v/v*)*	r.t.	1 h	No isolated product
1Mn	$Mn(ClO_4)_2.xH_2O$	EtOH	r.t.	55.5 h	No isolated product
1Mn	$Mn(SO_4)_2.H_2O$	EtOH	r.t.	55.5 h	L + $Mn^{II}(\mathbf{L^1})_2$ + $Mn^{III}(\mathbf{L^1})_3$**

* $\mathbf{L^1}$ was dissolved in EtOH. After complete dissolution, metal salt, previously solubilised in water, was added to the mixture.

** Results confirmed by HRMS

*** The aldehyde and the benzylamine were reacted without solvent to give the corresponding ligand. After 2 hours of reaction, the cobalt(II) salt freshly dissolved in a small volume of MeOH was added to the mixture.

II.3.1.2. Innovative strategy

Even though a significant progress has been accomplished by the preparation of **1Co** complex in high yield (see above, II.3.1.1.2), we have however maintained our efforts to achieve the preparation of the other metal complexes. Another synthetic route was therefore considered to obtain the other metal complexes (**2Co**-**7Co** and **1Mn**-**7Mn**). This second approach (designated as a "*template*" approach), inspired from a report published by the group of Murugesan[147] is also made up of two steps. Firstly, the aldehydes were complexed to cobalt(II) or manganese(II) acetate to afford the intermediate complexes (**1aCo**-**7aCo** and **1aMn**-**7aMn**), that were isolated and fully characterized. Then, benzylamine was reacted with those precursors to lead to the final cobalt(II) or manganese(II) complexes (Scheme II-7).

---

[147] Visuvamithiran, P.; Palanichamy, M.; Shanthi, K.; Murugesan, V. *Appl. Catal. Gen.* **2013**, *462–463*, 31–38.

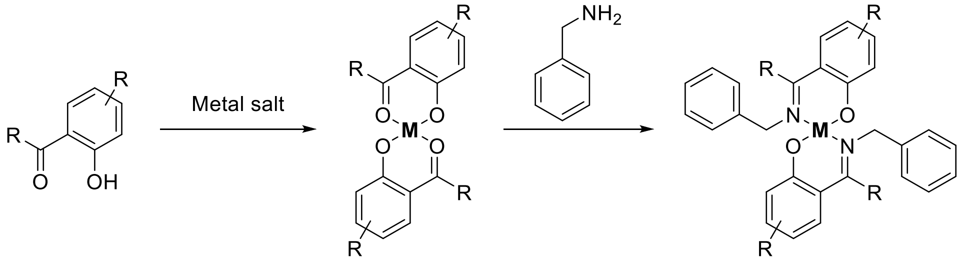

M = Co: **1aCo-7aCo**
M = Mn: **1aMn-7aMn**

M = Co: **1Co-7Co**
M = Mn: **1Mn-7Mn**

Scheme II-7: Second synthetic route for the preparation of the metal catalysts.

The intermediate complexes (**1aCo** and **1aMn**, **3aCo**, **4aCo**, **5aCo** and **5aMn**, **6aCo** and **6aMn**) were successfully obtained with yields ranging from 22 to 80% (Table II-9). Up to now, the two template complexes that were not successfully obtained are the two that display an additional hydroxyl moiety (**2aCo** and **2aMn**, and **7aCo** and **7aMn**), as well as the dibromo- and methyl manganese(II) derivatives (**3aMn** and **4aMn**). These successfully isolated intermediate complexes were found to be paramagnetic as assessed by NMR measurements and were also characterized using FTIR and ESI-MS.

Table II-9: Preparation of the cobalt(II) and manganese(II) intermediate complexes.

Cobalt(II) template complex	Yield (%)	Manganese(II) template complex	Yield (%)
1aCo	54	1aMn	71
2aCo	not obtained	2aMn	*n.t.*
3aCo	73	3aMn	*n.t.*
4aCo	33	4aMn	*n.t.*
5aCo	80	5aMn	49
6aCo	67	6aMn	23
7aCo	not obtained	7aMn	*n.t.*

n.t.: not tested

After further reaction with benzylamine, four cobalt(II) and one manganese(II) final complexes (**1Co**, **3Co**, **5Co**, **6Co** and **5Mn**) were isolated with yields ranging from 15 to 96% for the second step (Table II-10). This yield variation could be explained by the complexes stability, their sensitivity to the oxygenation/oxidation as well as the electronic nature of the substituents. These final complexes were fully characterized by ^{1}H-NMR, FTIR and ESI-MS.

Table II-10: Preparation of the cobalt(II) and manganese(II) complexes.

Cobalt(II) complex	Yield (%)	Manganese(II) complex	Yield (%)
1Co	15	1Mn	not obtained
2Co	*n.t.*	2Mn	*n.t.*
3Co	96	3Mn	*n.t.*
4Co	not obtained	4Mn	*n.t.*
5Co	92	5Mn	88
6Co	22	6Mn	not obtained
7Co	*n.t.*	7Mn	*n.t.*

n.t.: not tested

II.3.1.3. Characterization of commercially available complexes

Having successfully prepared a large series of cobalt(II) Schiff base complexes, we then turned our attention on other metal catalysts from commercial sources, what are also important in this project. Cobalt(II) *bis*(acetylacetonate) **8Co** and cobalt(II) stearate **9Co-1** were used without further purification. A second batch of cobalt(II) stearate **9Co-2** was provided by Clariant. This catalyst was fully characterized by elemental analysis, EPR and FTIR.

Even though metal stearates are often used in industry as metal catalysts for oxygen barrier applications, they have been less studied due to their poor solubilities in aqueous and organic solvents. It is noteworthy that up to now 114 patents are related to the use of cobalt(II) stearate and about half of them (53) are describing its oxygen absorbing/adsorbing properties. Due to their poor solubilities in common solvents, a solid-state tool has to be found. FTIR spectroscopy was selected and metal stearates was characterized by this analytical technique and display an absorbance at 1560 cm^{-1} that is due to the symmetric stretching vibration of the carboxylate group coordinated to the metal ion. Furthermore, the purity of the complex can be also evaluated by FTIR spectroscopy. In fact, if two bands centred at ~ 1560-1590 cm^{-1} (C(O)O$^-$ asymmetric stretching) and ~ 1420-1440 cm^{-1} (C(O)O$^-$ symmetric stretching) are present, it strongly suggests the presence of bridging (*i.e.* polymeric) complexes.[126,148,149] The carboxylate anion can be indeed bound to the metal centre in various ways as described in Scheme II-8: unidentate ligand, chelating ligand, bridging ligand and systems involving both chelation and bridging.[150] By FTIR, one can be distinguished between the chelating and the bridging coordination modes.

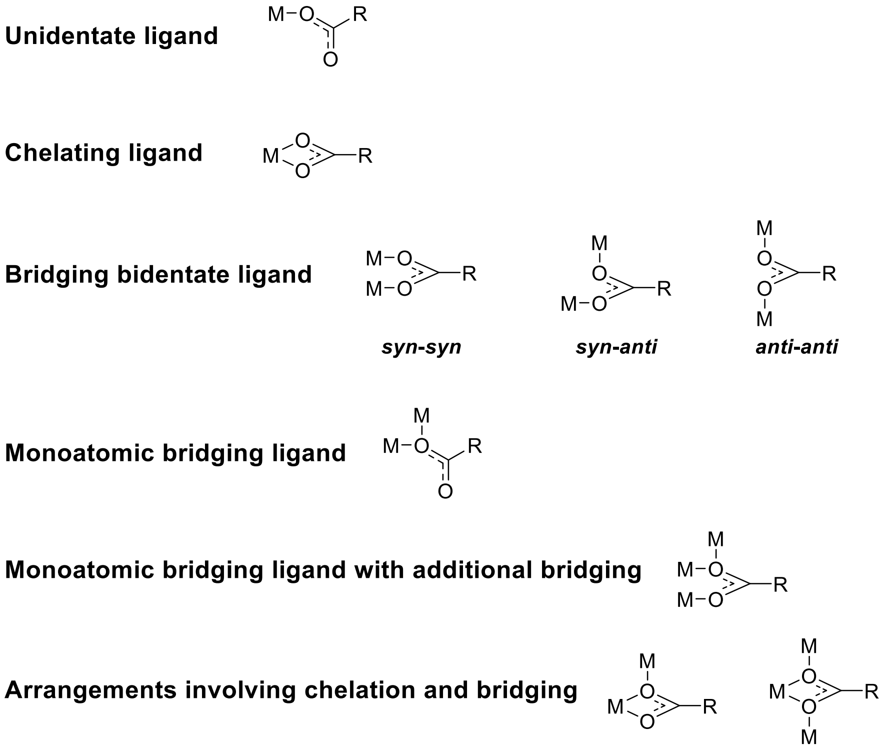
Unidentate ligand
Chelating ligand
Bridging bidentate ligand
syn-syn
syn-anti
anti-anti
Monoatomic bridging ligand
Monoatomic bridging ligand with additional bridging
Arrangements involving chelation and bridging
M
O
R

Scheme II-8: Chelating modes of carboxylate anions to metal centres.

Both cobalt(II) stearate provided by Sigma-Aldrich **9Co-1** and Clariant **9Co-2** were characterized by FTIR (Figure II-20) and their characteristic IR absorptions are gathered in Table II-11.

---

[148] Jóna, E.; Ondrušová, D.; Patjášová, M.; Šimon, P.; Michálek, J. *J. Appl. Polym. Sci.* **2001**, *81* (12), 2936–2943.

[149] Gönen, M.; Egbuchunam, T. O.; Balköse, D.; İnal, F.; Ülkü, S. *J. Vinyl Addit. Technol.* **2014**, 1–10.

[150] Deacon, G. B.; Phillips, R. J. *Coord. Chem. Rev.* **1980**, *33*, 227–250.

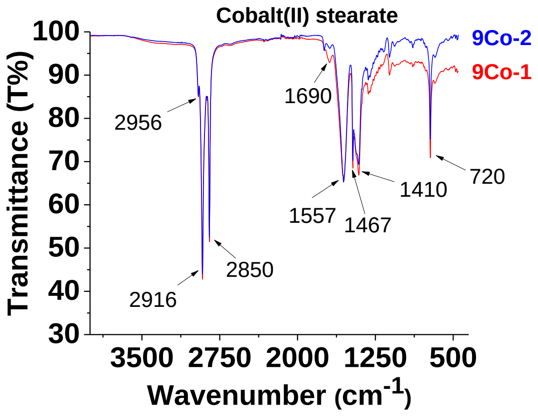

*Figure II-20: FTIR spectra of cobalt(II) stearate **9Co**.*

*Table II-11: Vibrations and corresponding wavenumbers for cobalt(II) stearate **9Co.***

FTIR band (cm^{-1})	Type of molecular vibration
2956	CH_3 stretching
2916	CH_2 asymmetric stretching
2850	CH_2 symmetric stretching
1557	COO^- asymmetric stretching
1467	CH_2 bending
1410	COO^- symmetric stretching
720	CH_2 deformation
1690	*C=O stretching* *(residual stearic acid)*

Surprisingly, the presence of both COO^- asymmetric (*i.e.* 1557 cm^{-1}) and symmetric (*i.e.* 1410 cm^{-1}) stretching vibrations strongly indicated that the carboxylate anions are primarily coordinated to the metal centre through a bridging mode.

Another valuable analytical method employed to characterize paramagnetic compounds (*e.g.* paramagnetic metal centre or radicals) is the EPR spectroscopy. In the frame of this project, X-band EPR measurements were performed to ensure the oxidation state of the metal centre as cobalt(II) and manganese(II) are paramagnetic. This analytical tool was used to ensure the oxidation state of the metal centre in the investigated complexes. No signal was observed at r.t. in the solid state (*i.e.* powder) or in solution (*i.e.* toluene) due to the fast relaxation times of cobalt(II) species at this temperature. However, characteristic signals of high spin (S = 3/2) cobalt(II) species were recorded at lower temperature (4 K) (Figure II-21).

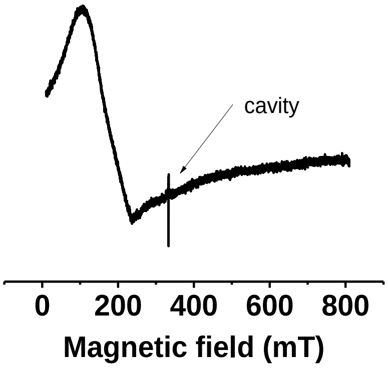

*Figure II-21: EPR spectrum of cobalt(II) stearate **9Co-1** at 4 K.*

Manganese(II) stearate **9Mn-1** was synthesized using a protocol described by the group of Maryudi[151] and another batch **9Mn-2** was provided by Clariant. They were both characterized by elemental analysis to assess the formation of the targeted compound.

FTIR measurements (Figure II-22 and Table II-12) on **9Mn-1** and **9Mn-2** allowed concluding a dominant bridging coordination mode due to the presence of both $C(O)O^-$ asymmetric and symmetric vibrations. Residual free stearic acid was also confirmed (vibration at 1686 cm^{-1}, Figure II-22 and Table II-12).

---

[151] Maryudi; Yunus, R. M.; Nour, A. H.; Abidin, M. H. *J. Appl. Sci.* **2009**, *9* (17), 3156–3160.

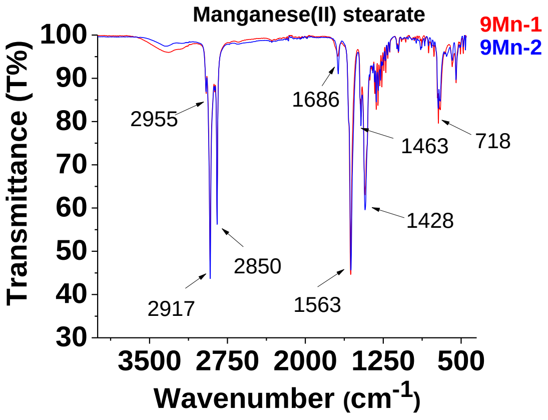

*Figure II-22: FTIR spectra of manganese(II) stearate **9Mn**.*

*Table II-12: Vibrations and their wavenumbers for cobalt(II) stearate **9Mn**.*

FTIR band (cm^{-1})	Type of molecular vibration
2955	CH_3 stretching
2917	CH_2 asymmetric stretching
2850	CH_2 symmetric stretching
1563	COO^- asymmetric stretching
1463	CH_2 bending
1428	COO^- symmetric stretching
718	CH_2 deformation
1686	*C=O stretching (residual stearic acid)*

Despite many attempts, no appropriate solvent to dissolve manganese(II) stearate was found (*i.e.* solvents such as acetone, acetonitrile, 2-butanol, *iso*-butanol, *tert*-butanol, chloroform, *n*-dimethylacetamide, dimethylsulfoxide, dioxane, ethanol, glycerol, methanol, *n*-methylpyrrolidone, 1,2-propanediol, 1,3-propanediol, propanol, tetrahydrofuran or toluene were tested). For this reason, the EPR spectra of **9Mn-1** were only recorded on powder. At r.t. (Figure II-23), a broad line centred at *g* = 2.008 with a line width of 220 G, with an approximately Lorentzian form was recorded. This broad line can be attributed to the low spin state (S = ½) of the manganese(II) species. At low temperature (Figure II-24), the recorded signals were characteristics of a high spin (S = 5/2) manganese(II) species. By decreasing the temperature (from 15 to 4 K), the line width was increasing, and the *g* factor was varying. This comportment was due to a low ferromagnetic coupling with an ordering temperature comprised between 5 and 10 K. This ordering temperature was closely related to the synthesis way.[152]

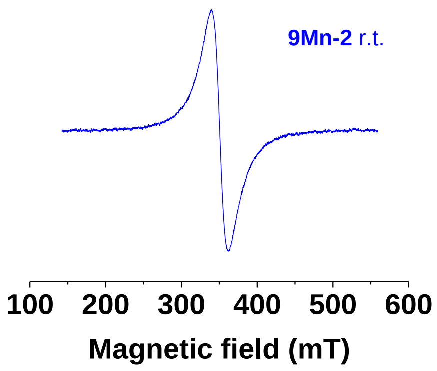

*Figure II-23: EPR spectrum of manganese(II) stearate **9Mn-1** recorded at r.t..*

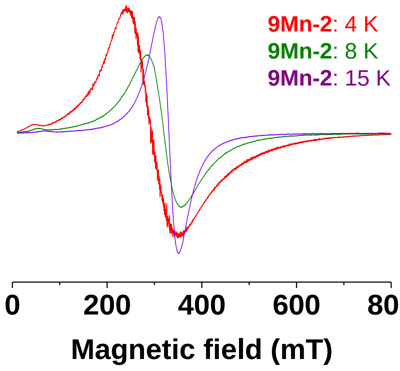

*Figure II-24: EPR spectra of manganese(II) stearate **9Mn-1** recorded at low temperatures.*

With the aim to obtain pure manganese(II) stearate **9-Mn** complex without remaining stearic acid, its synthesis was optimized following the protocol described by the group of Ponti.[153] Stearic acid was reacted with tetramethylammonium hydroxide and manganese(II) chloride to form the manganese(II) stearate complex. This new complex **9-Mn3** was obtained without any remaining stearic acid (Figure II-25) but the elemental analysis indicated the presence of residual tetramethylammonium hydroxide that originates from the synthesis (Table II-13).

---

[152] Pomerantz, M. *Solid State Commun.* **1978**, *27* (12), 1413–1416.

[153] Puglisi, A.; Mondini, S.; Cenedese, S.; Ferretti, A. M.; Santo, N.; Ponti, A. *Chem. Mater.* **2010**, *22* (9), 2804–2813.

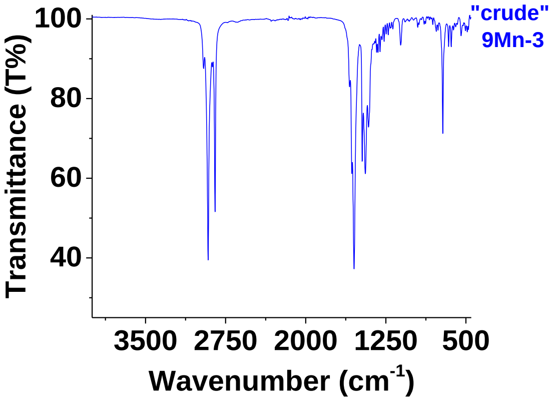

*Figure II-25: FTIR spectrum of the **9Mn-3** complex that was not subjected to any purification step.*

*Table II-13: Elemental microanalysis of the complex **9Mn-3** without any purification.*

	%N	%C	%H
Theoretical value	0.00	69.53	11.35
9Mn-3 without any purification	0.83	66.86	11.09

It therefore appeared that this crude complex had to be purified, and water washing was first envisaged. However, after water washing, the presence of stearic acid was once again observed (Figure II-26) thus indicating a partial decoordination of the stearate anion.

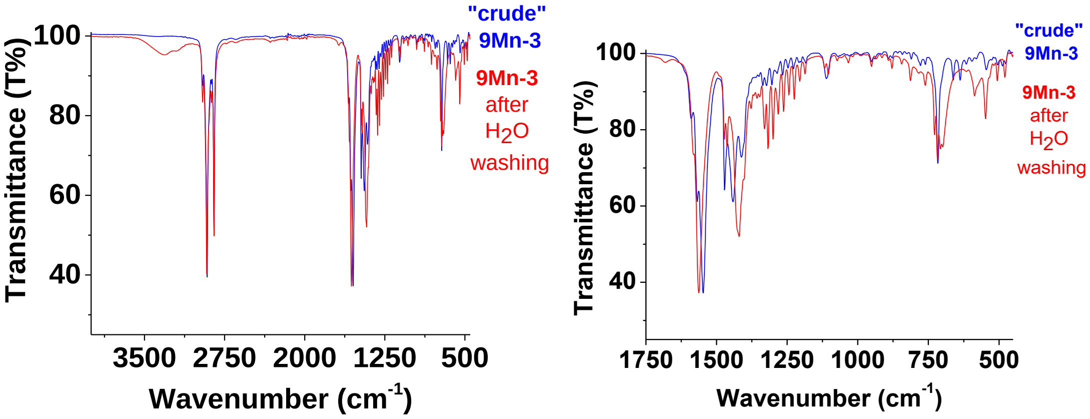

*Figure II-26: FTIR spectra of the complex 9Mn-**3** without any purification and after water washing.*

Another strategy of purification was then considered by changing the solvent from water to methanol. The complex was suspended in methanol and stirred for one hour. After filtration and drying, the purified complex was analysed by FTIR. The process was repeated three successive times until the FTIR spectra clearly indicated the absence of any residual stearic acid (Figure II-27). The characterization of the purified manganese(II) stearate by elemental analysis revealed the absence of remaining tetramethylammonium hydroxide (Table II-14) thus substantiating our synthetic and purification protocols. The **9Mn-3** complex was obtained with a satisfying purity.

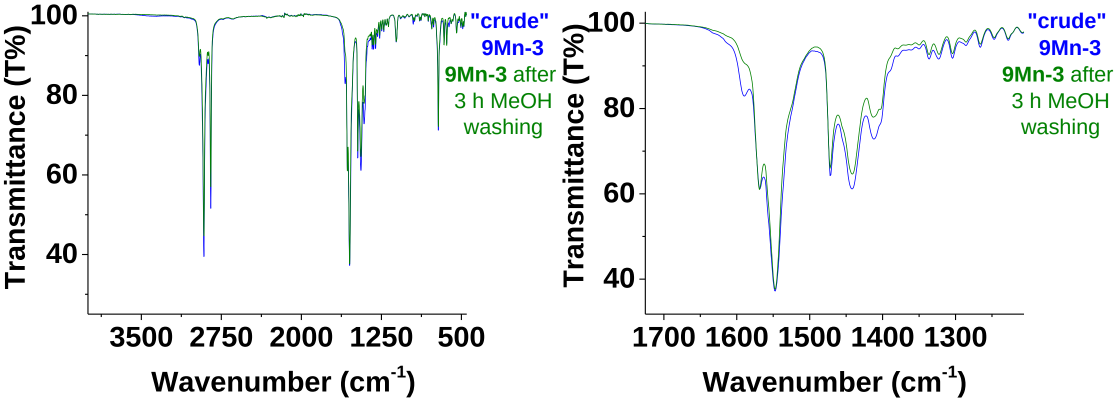

*Figure II-27: FTIR spectra of the complex **9Mn-3** without any purification and after methanol washing.*

*Table II-14: Elemental microanalysis of the complex **9Mn-3** without any purification and after methanol washing.*

	%N	%C	%H
Theoretical value	0.00	69.53	11.35
9Mn-3 without any purification	0.83	66.86	11.09
9Mn-3 after 3 h MeOH washing	0.00	69.20	11.26

II.3.2. Affinity of the different Schiff base ligands with cobalt(II) and manganese(II)

The cobalt(II) and manganese(II) coordination properties of the different Schiff base ligands considered in this work were examined by UV-visible absorption spectrophotometry *versus* pH titrations. The investigation of their thermodynamic parameters allows identifying the stoichiometry of the complexes, their ability to be hydroxylated or protonated, and also establishing a stability sequence.

The UV-visible absorption spectrophotometric *versus* pH titrations were performed on freshly prepared solutions of L:M 2:1 ratio (L: ligand; M: metal ion). The concentrations of cobalt(II) and manganese(II) salts (*i.e.* $Co(ClO_4)_2.6H_2O$ and $Mn(ClO_4)_2.xH_2O$) were previously determined by colorimetric titrations. To exemplify our approach, the results will be thoroughly described for one system (**1Co**), while only the results will be provided for the other systems. Similarly to the protonation of the free ligand, a bathochromic shift of the main absorption band (π-π^* transitions) was observed along the pH titration (Figure II-28) indicating that a complexation process occurred in solution as the pH rose. The absorption and potentiometric data were processed by statistical methods (*i.e.* Specfit program) and allowed calculating the stability constants of two cobalt(II) bischelates, namely Co(**L**^{1}-H)$_2$ and its mono-hydroxylated [Co(OH)(**L**^{1}-H)$_2$]$^-$ homologue, their corresponding electronic spectra (Figure II-29), and their distribution diagram (Figure II-30).

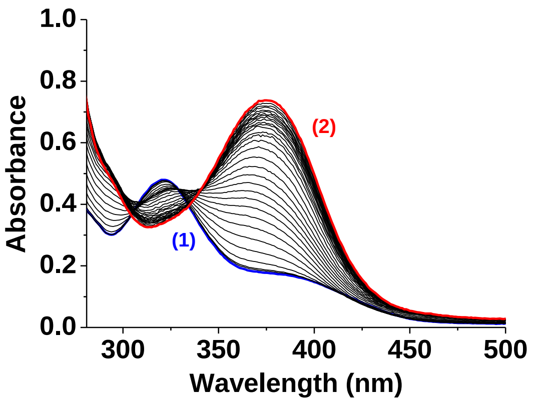

Figure II-28: UV-visible absorption spectrophotometric titration of ***1Co*** *as a function of pH;* ***(1)*** *pH: 7.57,* ***(2)*** *pH: 12.61, [$\mathbf{L^1}$] = 6.89 x 10^{-4} M; [Co] = 3.45 x 10^{-4} M; solvent: dioxane:H_2O (1:1 v/v); T = 25.0(2) °C; I = 0.1 M ($NaClO_4.H_2O$); l = 0.2 cm.*

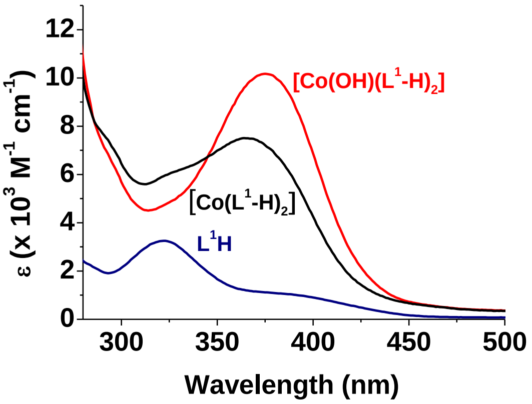

Figure II-29: Electronic spectra of the protonated cobalt(II) $\mathbf{L^1}$ *species; solvent: dioxane:H_2O (1:1 v/v); T = 25.0(2) °C; I = 0.1 M ($NaClO_4.H_2O$).*

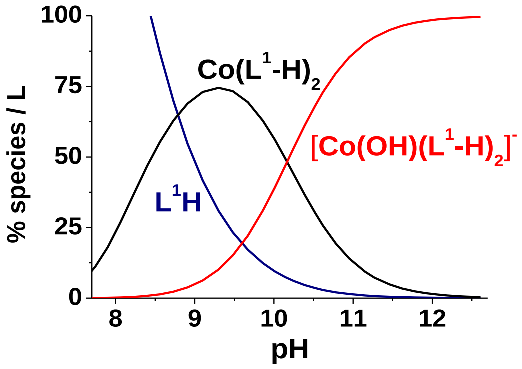

Figure II-30: Distribution diagrams of the protonated cobalt(II) $\mathbf{L^1}$ *species; [$\mathbf{L^1}$] = 6.89 x 10^{-4} M; [Co] = 3.45 x 10^{-4} M; solvent: dioxane:H_2O (1:1 v/v); T = 25.0(2) °C; I = 0.1 M ($NaClO_4.H_2O$).*

The calculated formation constants for the $\mathbf{L^1}$/cobalt system are presented in Table II-15. The same approach was employed for the other systems; mono and bischelate cobalt(II) complexes were observed for **3Co**, **4Co** and **5Co** while only bischelates were characterized for **1Co**, **1Mn** and **6Co** (Table II-15). For **2Co** and **7Co**, cobalt(II) bischelates complexes were observed in addition to two protonated species that likely correspond to the protonation of the additional hydroxy groups (Table II-16). For comparison purpose, the stability constants of **8Co** (*i.e.* using acetylacetonate as ligand) were determined under our experimental conditions by pure potentiometry (Table II-17; *i.e.* the weak absorption prevented the use of absorption *versus* pH titrations). The thermodynamic data are provided as global constant $\log\beta_{mlx}$ (where m stands for the number of metal centre(s) in the complex; l corresponds to the number of ligand(s) coordinated to the metal centre M; and x is related to the number of hydroxyl (negative value) or proton (positive value)).

Table II-15: Global complexation constants determined for ***1Mn**, **1Co**, **3Co**, **4Co**, **5Co*** *and* ***6Co.***

	UV-vis. absorption *versus* pH		
System	$\log\beta_{110}$	$\log\beta_{120}$	$\log\beta_{12-1}$
1Mn	*n.d.*	12.8(2)	*n.d.*
1Co	*n.d.*	13.9(2)	3.9(4)
3Co	6.47(3)	11.3(2)	*n.d.*
4Co	8.15(8)	13.9(6)	*n.d.*
5Co	7.30(6)	11.8(4)	*n.d.*
6Co	*n.d.*	14.3(2)	3.7(4)

n.d.: not determined

*Table II-16: Global complexation constants for the systems which underwent successive protonation (**2Co** and **7Co**) .*

	UV-vis. absorption *versus* pH		
System	**logβ_{120}**	**logβ_{121}**	**logβ_{122}**
2Co	16.8(1)	25.9(1)	33.3(1)
7Co	14.9(1)	20.15(8)	36.06(9)

*Table II-17: Global complexation constants measured for **8Co.***

	Potentiometry		
System	**logβ_{110}**	**logβ_{120}**	**logβ_{12-1}**
8Co	*n.d.*	12.43(3)	2.0(1)

n.d.: not determined

Having established a valuable set of physico-chemical data for cobalt(II) complexes with these Schiff bases, we then investigated their structure-reactivity relationships. The stability constants of the cobalt(II) complexes with the broad range of *N,O*-bidendate ligands can indeed be related to their protonation properties, provided that the considered chelators are structurally related. In our case, the salicylideneimine backbone is preserved whatever the ligand considered and only the benzaldehyde-type moiety has been diversely substituted which allowed evaluating the effects of the substitution on the global stability constants. Figure II-31 illustrates that a clear linear relationship recounts the global stability constants to the corresponding protonation constants of the ionizable phenolic group of the *N,O* binding unit of the ligands. With respect to the series considered (*i.e. N*-arylated *versus N*-benzylated), two clear linear relationships between the global stability constants and the protonation constants can be observed. The chemical structures of the additional systems as well as their thermodynamic data were taken from the literature.[154,155,156,157,158] One of the compounds that is out of the linear variation corresponds to **2Co** that displays an additional phenolic group. For our ligand series, the complexes which display the weakest stabilities are **3Co** and **5Co** that are substituted with electron-withdrawing groups (Figure II-31).

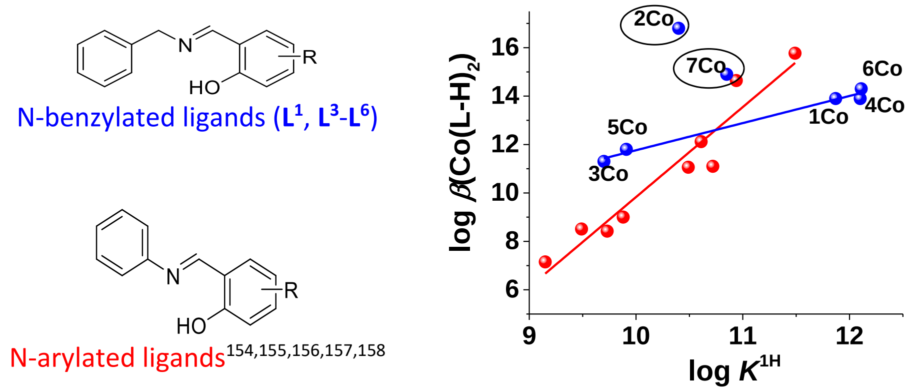

Figure II-31: Relationships between the global stability constants of the cobalt(II) complexes and the acido-basic properties of a broad range of Schiff bases including those of interest in the frame of this study.

Using a set of fruitful analytical methods, we have successfully determined the acido-basic properties of a homogeneous series of *N,O*-bidentate ligands that are closely related to **L^1**. With

---

[154] Shori, N.; Dutt, Y.; Singh, R. P. *J. Inorg. Nucl. Chem.* **1972**, *34* (6), 2007–2014.

[155] Dubey, K. P.; Wazir, B. L. *Indian J. Chem. Sect. Inorg. Bio-Inorg. Phys. Theor. Anal.* **1977**, *15A* (1), 58–60.

[156] Hernández-Molina, R.; Mederos, A.; Gili, P.; Domínguez, S.; Núñez, P. *Polyhedron* **1997**, *16* (24), 4191–4196.

[157] Hernández-Molina, R.; Mederos, A.; Gili, P.; Domínguez, S.; Lloret, F.; Cano, J.; Julve, M.; Ruiz-Pérez, C.; Solans, X. *J. Chem. Soc. Dalton Trans.* **1997**, No. 22, 4327–4334.

[158] Hernández-Molina, R.; Mederos, A.; Gili, P.; Domínguez, S.; Núñez, P.; Germain, G.; Debaerdemaeker, T. *Inorganica Chim. Acta* **1997**, *256* (2), 319–325.

respect to the putative mechanism of oxygenation/activation of cobalt(II) catalysts (Scheme I-12), **1Co** seemingly constitutes one of the most promising systems. It indeed corresponds to one of the most stable cobalt(II) species and displays an ability to undergo hydroxylation reactions that are expecting to favour the oxygenation reaction. We have fully characterized the physico-chemical properties of the two systems of interest (*i.e.* **L**^{1} and **L**^{2} provided by Clariant at the beginning of the project) and have extended this physico-chemical analysis to other closely related chelators (**L**^{3}-**L**^{7}) derivatives that we have synthesized (*i.e.* most of them are unreported systems) to highlight structure/property/reactivity relationships. This being achieved, effort has been then directed to the characterization and quantification of the oxygenation/activation processes of these metal catalysts.

II.4. Oxygenation/activation properties of the metal catalysts

Complementary analytical methods will be hereafter used to assess the oxygenation and activation properties of the different catalysts that have been considered in this work: UV-visible absorption spectrophotometry, oximetry, ESI-MS, ^{1}H NMR and electrochemistry to mention only the most important. In fact, each analytical mean allowed solving the intricate puzzle of the oxygenation/activation behaviour of these metal catalysts and monitoring/determining relevant and informative kinetics parameters.

II.4.1. Oxygenation/activation monitored by absorption spectrophotometry

To get access to a benchmark for the oxygenation properties, free cobalt(II) has been first explored to evaluate its stability with time (24 hours) in solution in open air and its oxygenation capacities. Figure II-32 displays the oxygenation kinetics of the free cobalt(II) in solution and clearly demonstrates that no absorption alteration occurs over 24 hours. Figure II-33 further depicts the absorption changes at 512 nm (maximum of absorption of the d-d transition centred on cobalt(II)) over 24 hours that clearly shows the absence of signal variation. These data demonstrate that free cobalt(II) is stable in solution and is not prone to easy oxygenation. In fact, if oxygen was bound to the metal centre, some variations would be observed on the d-d transitions centred on the metal. This feature is of importance and indicates that potential oxygenation barrier properties of a catalyst originate from the catalyst itself and not from release of free cobalt(II).

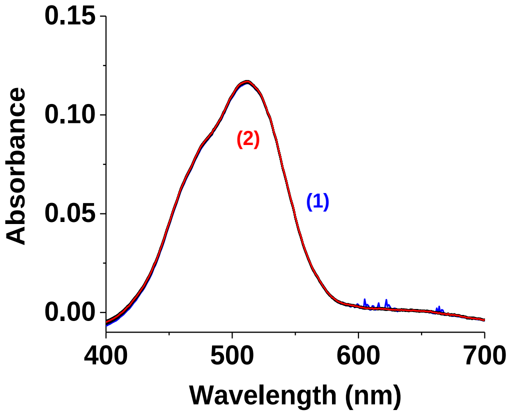

Figure II-32: UV-visible absorption spectra of cobalt(II) perchlorate measured over time; ***(1)*** *t = 0,* ***(2)*** *t = 24 h, [Co(ClO$_4$)$_2$.6H$_2$O] = 2.51 x 10^{-3} M, solvent: dioxane:H$_2$O (1:1 v/v); l = 1 cm.*

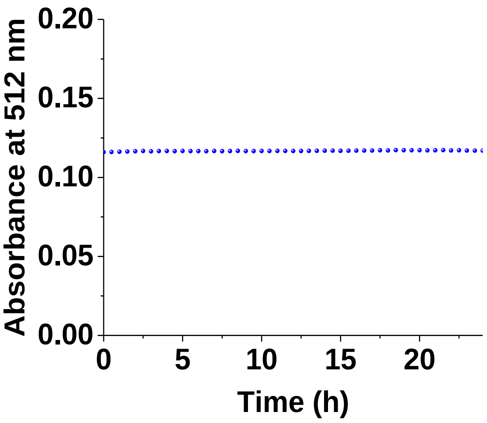

Figure II-33: Absorbance at 512 nm as a function of time; [Co(ClO$_4$)$_2$.6H$_2$O] = 2.51 x 10^{-3} M, solvent: dioxane:H$_2$O (1:1 v/v); l = 1 cm.

Similarly to the previous experiment, the stabilities of cobalt(II) complexes (**1Co**, **3Co**, **5Co**, **6Co**, **8Co** and **9Co**) were examined in solution using UV-visible absorption spectrophotometry over 3 hours. Figure II-34 and Figure II-35 depict the variation of the absorbance centred on the metal centre transitions at 550 nm for these cobalt(II) complexes. The cobalt(II) stearate **9Co** complex was also studied but in *iso*-butanol due to solubility issues. Even weak, significant variations at this wavelength were observed for any of the studied complexes with the exception of **8Co** (cobalt(II) *bis*(acetylacetonate)). These features suggest that these metal complexes underwent somehow rather fast oxygenation/activation reactions under aerobic conditions.

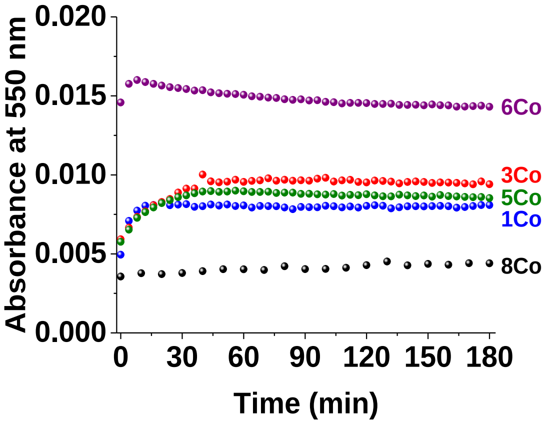

*Figure II-34: Absorbance at 550 nm of **1Co**, **3Co**, **5Co**, **6Co** and **8Co** over time; [**1Co**-**6Co**] ~ 3 x 10^{-4} M, solvent: dioxane, l = 1 cm; [**8Co**] = 8.94 x 10^{-5} M, solvent: dioxane:H_2O (1:1 v/v), l = 1 cm.*

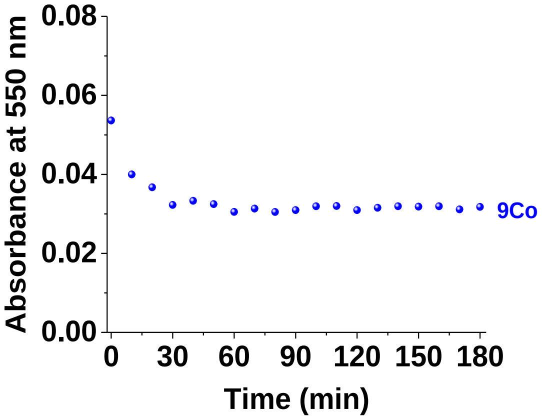

*Figure II-35: Absorbance at 550 nm of **9Co** over time; [**9Co**] = 9.52 x 10^{-4} M, solvent: iso-butanol, l = 1 cm.*

Meanwhile, the same experiments were performed on solutions containing the cobalt(II) catalysts **1Co** and **2Co** that were prepared *in situ* (the ligands and cobalt(II) were mixed in a 2:1 ratio) over a much longer period. Figure II-36 first depicts the variation of the absorbance at 550 nm that seemingly indicated a multi-phase kinetic process with a first fast step followed by much slower steps. The first step might be attributed to the oxygenation reaction of the catalyst most likely followed by activation/degradation reactions. The half-life time ($t_{1/2}$) of the oxygenation process (*i.e.* related to the first step) was calculated for **1Co** to be $t_{1/2}$ ~ 19 min (Figure II-37) in agreement with the first experiments conducted on the isolated cobalt(II) complexes (Figure II-34). In addition, this first step was found to be independent on the catalyst concentration in agreement with a first-order kinetic step (Figure II-38).

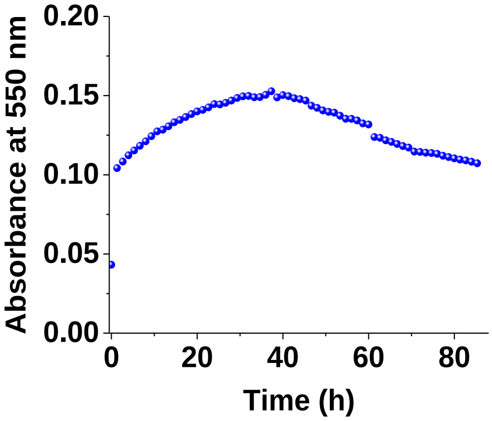

*Figure II-36: Variation of the absorbance at 550 nm of **1Co** as a function of time; [**1Co**] = 2.51 x 10^{-3} M, solvent: dioxane:H_2O (1:1 v/v), l = 1 cm.*

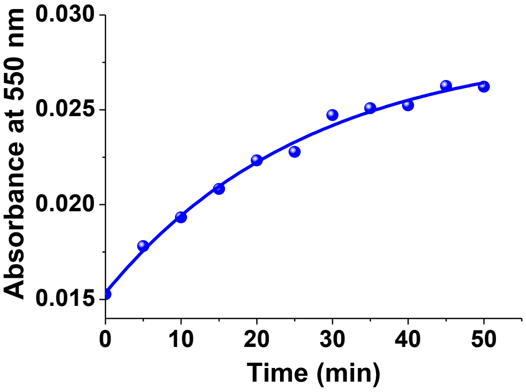

*Figure II-37: Variation of the absorbance at 550 nm of **1Co** as a function of time; [**1Co**] = 5 x 10^{-4} M, solvent: dioxane:H_2O (1:1 v/v), l = 1 cm.*

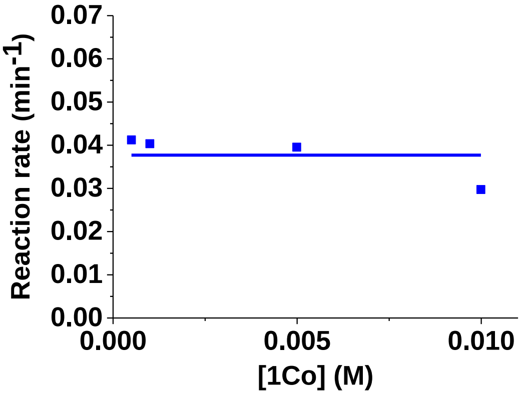

*Figure II-38: Variation of the rate constants associated to the oxygenation of **1Co** as a function of metal catalyst concentrations; solvent: dioxane:H_2O (1:1 v/v), l = 1 cm.*

II.4.2. Oxygenation/activation monitored by oximetry coupled to UV-visible absorption

To get further insight into the oxygenation/activation mechanism, oximetry was coupled to absorption spectrophotometry to ensure that the first fast step is actually related to the oxygenation process. Besides demonstrating the existence of an oxygenation process, oximetry allowed also investigating the reversibility of the oxygenation process for a given metal catalyst. Three cobalt(II) systems were monitored following this approach (**1Co**, **8Co** and **9Co**). For each of the studied systems, two oxygenation steps were successively performed. The system was first degassed and deoxygenated by bubbling argon, and a first oxygenation step was monitored. At the end of this step, the system was re-degassed and re-deoxygenated and a second oxygenation step was followed one more time.

To highlight the spectral variations induced by the oxygenation process, differential absorption spectrophotometry was chosen (*i.e.* the absorption spectrum of starting deoxygenated cobalt(II) complex was taken as the reference spectrum). Figure II-39 and Figure II-40 first show the data recorded for **8Co** that was used as a benchmark of this approach. After a first degassing of the solution (*i.e.* the oxygen concentration was recorded to be less than 0.3 ppm), an UV-visible absorption spectrum of **8Co** was recorded and used as a reference spectrum. The solution was then left to a constant stirring in open air conditions to allow re-oxygenation of the solution while measuring the oxygen content by oximetry. Absorption spectra and oxygen content of the solution were measured at regular intervals.

During the first oxygenation step, a significant variation of the absorbance at 290 nm can be observed (Figure II-39). Figure II-40 further confirmed this phenomenon and interestingly showed that the dissolved oxygen concentration measured as a function of time can be related to the absorption variation indicating that this step likely corresponds to the oxygenation of the cobalt(II) catalyst.

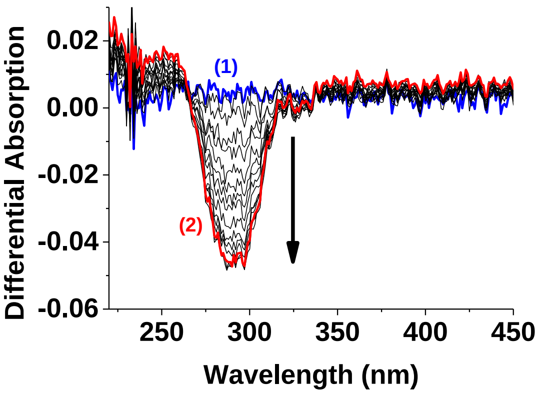

Figure II-39: Differential absorption spectra measured at regular intervals during the first oxygenation stage of ***8Co****;* ***(1)*** *t = 0,* ***(2)*** *t = 2 h, [****8Co****] = 2 x 10^{-4} M, solvent: dioxane:H_2O (1:1 v/v), l = 1 cm.*

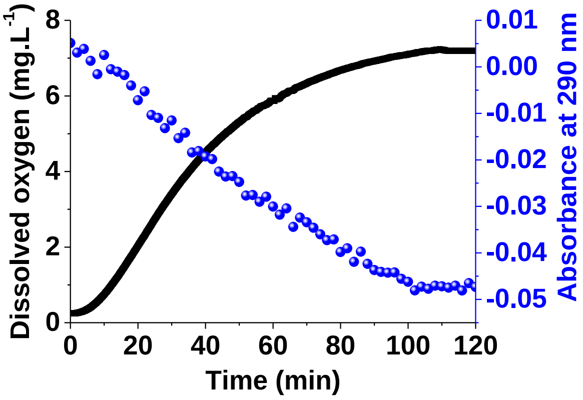

Figure II-40: Dissolved oxygen concentration and absorbance variation at 290 nm as a function of time for the first oxygenation stage of ***8Co****; [****8Co****] = 2 x 10^{-4} M, solvent: dioxane:H_2O (1:1 v/v), l = 1 cm.*

Figure II-41 and Figure II-42 then depict the effect of re-oxygenation on the absorption and oxygen profiles (*i.e.* solution left in open air conditions) of **8Co**. During this second oxygenation stage, the same phenomenon was observed (*i.e.* comparable absorption and oxygenation profiles).

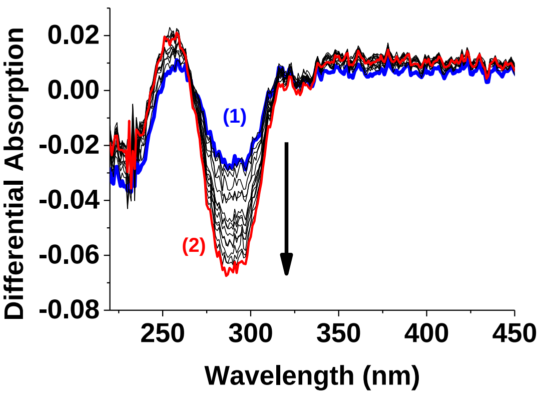

Figure II-41: Differential absorption spectra recorded during the second oxygenation stage of ***8Co****;* ***(1)*** *t = 0,* ***(2)*** *t = 2 h, [****8Co****] = 2 x 10^{-4} M, solvent: dioxane:H_2O (1:1 v/v), l = 1 cm.*

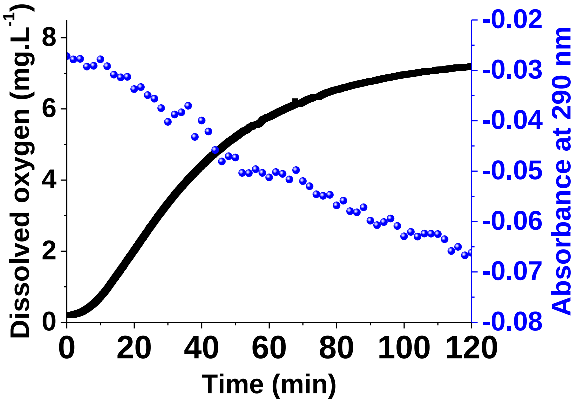

Figure II-42: Dissolved oxygen concentration and absorbance variation at 290 nm as a function of time for the second oxygenation stage of ***8Co****; [****8Co****] = 2 x 10^{-4} M, solvent: dioxane:H_2O (1:1 v/v), l = 1 cm.*

Moreover, differential absorption spectrophotometry allowed determining whether the metallic catalyst binds oxygen and what binding mode to oxygen is. With respect to the literature data, the variation at 290 nm (*i.e.* cobalt(II) to O_2 charge transfer band) is apparently characteristic of a bridged dioxygen species.[56] Taken all together, these analytical data suggested proposing the following oxygenation scheme for **8Co**:

$$\mathrm{Co}(\mathbf{L^8})_2 \xrightarrow{O_2} (\mathbf{L^8})_2\mathrm{Co{-}O{-}O{-}Co}(\mathbf{L^8})_2$$

Scheme II-9: Oxygenation reaction for ***8Co****.*

The two successive and independent oxygenation experiments highlighted relevant feature, *i.e.* a fast and a reversible oxygenation process. If the two successive oxygenation curves of the **8Co** catalyst are compared (Figure II-43), it indeed showed that there are closely similar thus substantiating that the oxygenation process of **8Co** is a reversible process.

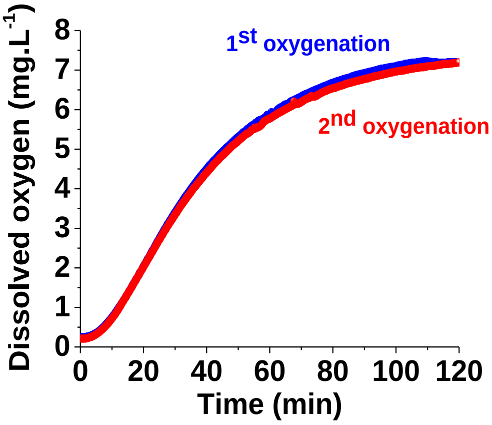

*Figure II-43: Superimposition of the two oxygenation curves of **8Co**; [**8Co**] = 2 x 10^{-4} M, solvent: dioxane:H_2O (1:1 v/v).*

As a partial conclusion, **8Co**, used as a benchmark, reversibly binds oxygen and the oxygenated species of **8Co** is likely an oxygen bridged species. This preliminary study allowed us to set up the experimental conditions and to validate this analytical approach that was further transposed to the catalysts of interest.

The same experiments were thereafter conducted on **1Co** and **9Co**. During the first oxygenation stage of **1Co**, an increase of the absorption signal was observed with a maximum lying at 348 nm (Figure II-44). The absorbance at 348 nm experienced a large increase over a time span of 20 minutes. No significant absorption variation was observed above 20 minutes of reaction (*i.e.* stable absorbance signal). Following a second deoxygenation stage (*i.e.* degassing with argon until a low oxygen concentration is reached), the effect of a second oxygenation stage was evaluated as previously done for our reference **8Co**. During this second oxygenation, different observations could be drawn with respect to the first one. Even though the oxygen concentration obviously increased during the second oxygenation step, the absorbance did not follow the same trend as during the first oxygenation step, but rather gradually decreased (Figure II-45). It can be concluded that a second oxygenation stage has weak to no effect on the absorption profile.

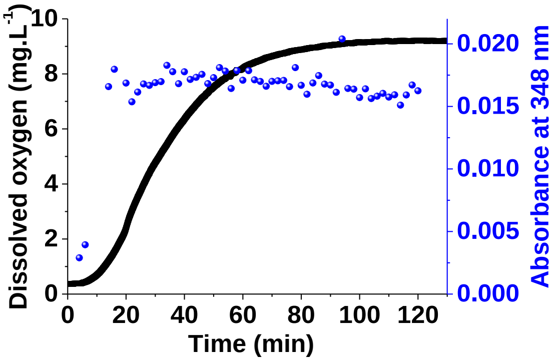

*Figure II-44: Dioxygen concentration and absorbance at 348 nm as a function of time for the first oxygenation stage of **1Co**; [**1Co**] = 6 x 10^{-4} M, solvent: dioxane:H_2O (1:1 v/v), l = 1 cm.*

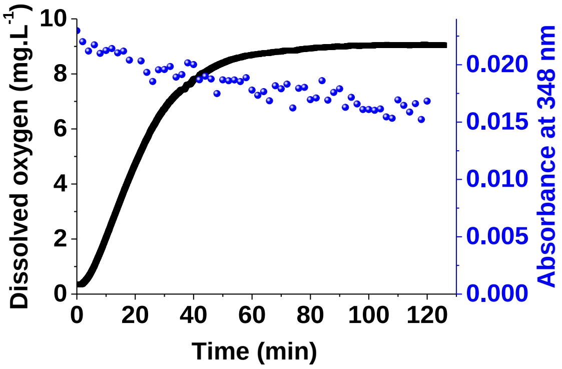

*Figure II-45: Dioxygen concentration and absorbance variation at 348 nm as a function of time for the second oxygenation stage of **1Co**; [**1Co**] = 6 x 10^{-4} M, solvent: dioxane:H_2O (1:1 v/v), l = 1 cm.*

The absorbance variation at 348 nm is likely characteristic of a bridged dioxygen-µ-hydroxo species.[56] The oxygenation equation of **1Co** can thus be written as follow:

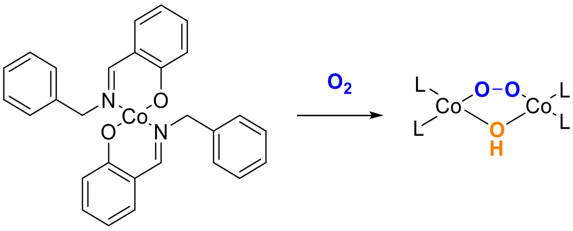

*Scheme II-10: Oxygenation reaction for **1Co**.*

The comparison of the oximetric curves of the two successive oxygenation stages showed marked differences (Figure II-46) as they cannot be properly superimposed. For the first oxygenation stage, a "classical" oxygen concentration profile can be seen with a so-called "retention time" (*i.e.* competitive oxygenation of the catalyst with respect to oxygen dissolution) at the beginning before gradually increasing until a stable value was reached (*i.e.* oxygenation of the hydro-organic solution until oxygen saturation under our experimental conditions). For the second oxygenation stage, the oxygen concentration profile stands in an interesting contrast and behaves as measured for solutions lacking cobalt(II) catalyst (*i.e.* oxygen dissolution). This feature clearly indicated that the oxygenation reaction of **1Co** was most likely irreversible by definition thus suggesting a fast activation by the metal catalyst **1Co**. On the other hand, the oxygenation process of **1Co** was found to be significantly much faster than that measured for **8Co** (Figure II-43 and Figure II-46).

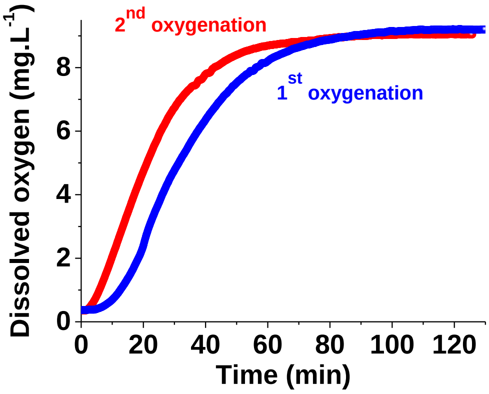

*Figure II-46: Superimposition of the two oxygenation curves of **1Co** during the oxygenation stages; [**1Co**] = 6 x 10^{-4} M, solvent: dioxane:H_2O (1:1 v/v).*

The influence of the solvent on the oxygenation process was investigated for **1Co** by changing the solvent from dioxane:water (1:1 *v/v*) to ethanol. Even though the solvent composition was varying, the same experimental procedure was employed. Figure II-47 depicts the oxygen concentration over time as well as the spectrophotometric variations that were recorded for the first oxygenation stage. In ethanol, the oxygenation of **1Co** seemed to be slower than in dioxane:water mixture (Figure II-47 and Figure II-44). As previously observed, the second oxygenation dissolution curve measured in the presence of **1Co** is not influenced by the catalyst (Figure II-48). The superimposition of the two oxygenation profiles indicated, as previously observed in dioxane:water (1:1 *v/v*), that the oxygenation of **1Co** is irreversible (Figure II-49). In addition, no marked absorption change was observed at 300 nm thus indicating that the catalyst has been oxygenated/activated following the first oxygenation stage and that the oxygenation reaction is accordingly irreversible.

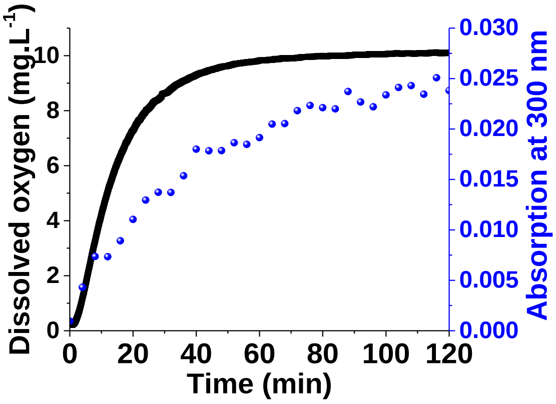

*Figure II-47: Dioxygen concentration and absorbance at 300 nm recorded as a function of time for the first oxygenation stage with **1Co**; [**1Co**] = 4.79 x 10^{-4} M, solvent: EtOH, l = 1 cm.*

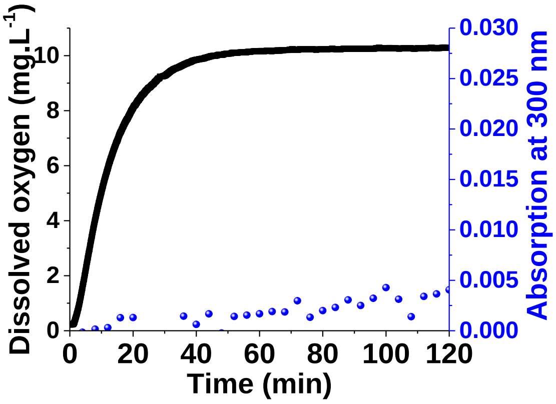

*Figure II-48: Dioxygen concentration and absorbance variation at 300 nm recorded as a function of time for the second oxygenation stage with **1Co**; [**1Co**] = 4.79 x 10^{-4} M, solvent: EtOH, l = 1 cm.*

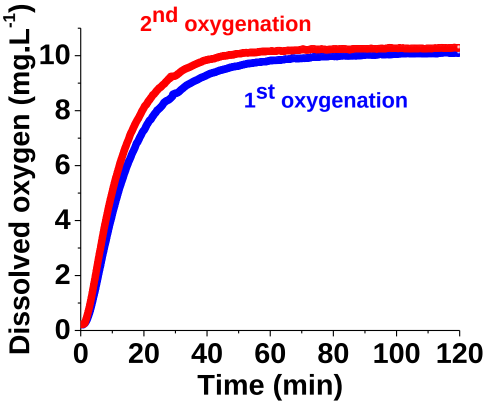

*Figure II-49: Superimposition of the two oxygenation profiles of **1Co** during the oxygenation stages; [**1Co**] = 4.79 x 10^{-4} M, solvent: EtOH.*

The oxygenation of another catalyst of interest, cobalt(II) stearate **9Co**, was then investigated. Figure II-50 depicts the oxygenation profile, as well as the spectrophotometric variations measured during the first oxygenation stage of the cobalt(II) catalyst in *iso*-butanol (*i.e.* solvent imposed by the solubility constraints of **9Co**). The oxygenation seemed to be much slower than for **1Co** in ethanol (Figure II-47 and Figure II-48) and no significant spectral variation could be observed after 80 minutes of reaction. After a deoxygenation stage, a second oxygenation stage was performed and monitored using absorption spectrophotometry and oximetry (Figure II-51). Unlike the observations done for **1Co**, no significant differences could be observed with respect to the spectral variations between the first and the second oxygenation stages. This would indicate a reversible oxygen binding of cobalt(II) stearate **9Co** in *iso*-butanol.

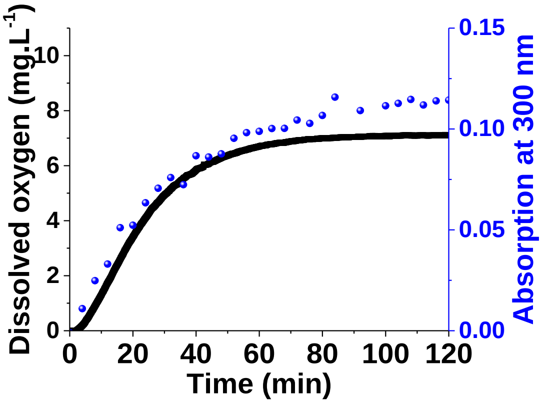

*Figure II-50: Dioxygen concentration and absorbance at 300 nm recorded as a function of time for the first oxygenation stage of **9Co**; [**9Co**] = 5.91 x 10^{-4} M, solvent: iso-butanol, l = 1 cm.*

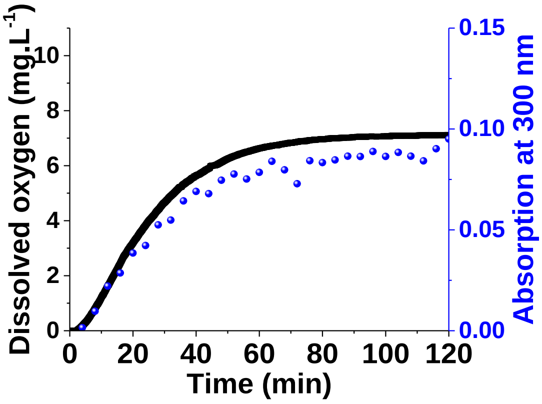

*Figure II-51: Dioxygen concentration and absorbance at 300 nm recorded as a function of time for the second oxygenation stage of **9Co**; [**9Co**] = 5.91 x 10^{-4} M, solvent: iso-butanol, l = 1 cm.*

This observation is further supported by the almost quasi-superimposition of the two oxygenation curves (Figure II-52) that supports a quasi-reversible oxygenation process for **9Co**.

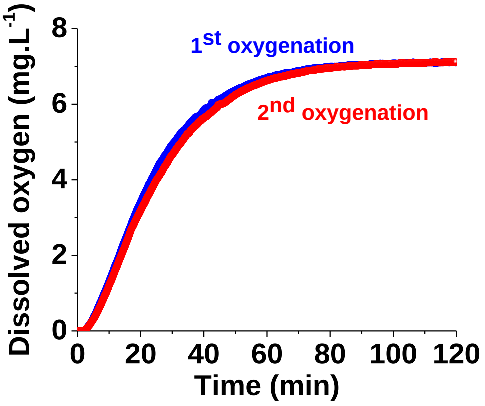

*Figure II-52: Superimposition of the two oxygenation profiles of **9Co** during the oxygenation stages; [**9Co**] = 5.91 x 10^{-4} M, solvent: iso-butanol.*

The three studied complexes (**1Co**, **8Co** and **9Co**) can be grouped into two categories: those whose oxygenation is (quasi)-reversible, and those whose oxygenation is irreversible. Cobalt(II)*bis*(acetylacetonate) **8Co** (*i.e.* in dioxane:water (1:1 *v/v*)) and cobalt(II) *bis*-stearate **9Co** (*i.e.* in *iso*-butanol) belongs to the first category, whereas **1Co** can be grouped into the second one. In the frame of the project, oxygen has to be bound to the metal centre in a way that ensures activation by the redox-active metal centre and the oxidation of a scavenger substrate, also called additive. On the other hand, the metal catalyst has to ensure new catalytic cycles and should not be degraded following oxygen activation.

We have demonstrated by oximetry coupled to UV-visible absorption spectrophotometry that the first step can be related to the oxygenation process. We have then focused our interest on the characterization by ESI-MS of the products formed during the process.

II.4.3. Oxygenation/activation monitored by ESI-MS

The complexes of interest (*i.e.* **1Co** and **2Co** provided by Clariant at the beginning of the project) were prepared *in situ* in solution and characterized by ESI-MS during a few days. During this period, the solutions were let in open air to allow oxygenation/activation.

This experiment was conducted on **1Co** for 32 hours and the kinetics of the oxygenation/activation process was monitored. When scrutinizing the peak of interest centred at *m/z* = 480.2 (Figure II-53) that corresponds to $[\mathrm{Co^{II}}(\mathbf{L^1}\text{-H})_2\text{+H}]^+$ species, the isotopic profile, initially centred on this monoisotopic peak, is gradually altered over time (shifted to smaller masses). After 32 hours, the new peak centred at *m/z* = 479.2 corresponds to a higher oxidation state of the metal: $[\mathrm{Co^{III}}(\mathbf{L^1}\text{-H})_2]^+$. This can be interpreted as an oxidation of the metal centre (*i.e.* cobalt(II) to cobalt(III)). The metal-centred oxidation kinetics can therefore be monitored and quantified (Figure II-54).

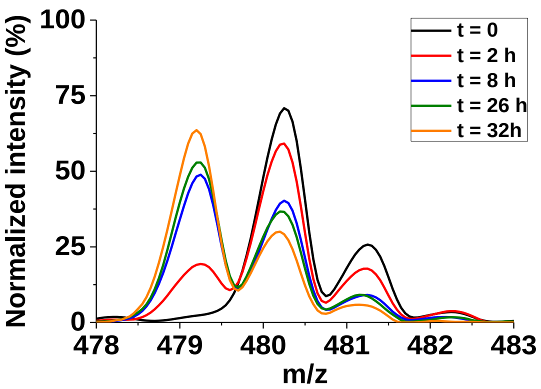

*Figure II-53: ESI-MS spectra of **1Co** recorded over 32 h - zoom between m/z = 478 and 483; [**1Co**] = 1.0 x 10^{-4} M, solvent: $CH_3CN:H_2O$ (1:1 v/v), + 170 V.*

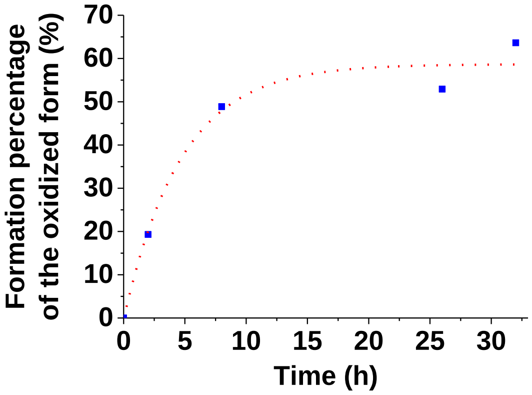

*Figure II-54: Formation percentage of the oxidized form of **1Co** over a time span of 32 h.*

Having demonstrated the valuable help of ESI-MS to characterize and quantify the oxidation process, we have reproduced the same experiment but over a much longer time (about 10 days). On Figure II-55 and Figure II-56, the kinetics of the oxidation reaction can be observed and seemed to be nearly finished.

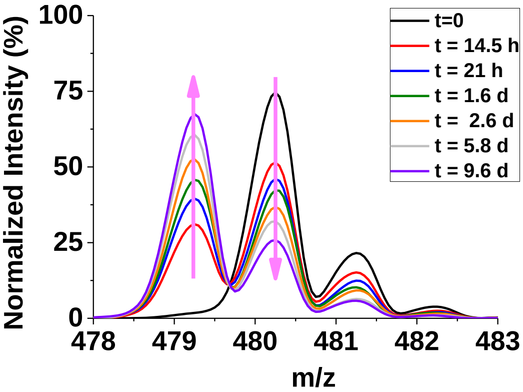

*Figure II-55: ESI-MS spectra of **1Co** recorded over 10 days - zoom between m/z = 478 and 483; [**1Co**] = 1.0 x 10^{-4} M, solvent: $CH_3CN:H_2O$ (1:1 v/v), + 170 V.*

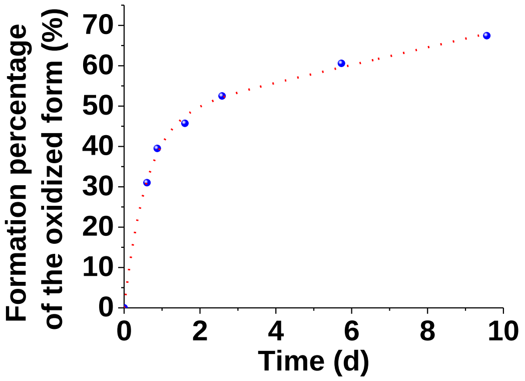

*Figure II-56: Formation percentage of the oxidized form of **1Co** over 10 days.*

The half-life time of the oxygenation process measured previously by absorption spectrophotometry ($t_{1/2}$ ~ 19 min) can be compared to that of the activation/oxidation process (*i.e.* formation of the cobalt(III) bischelate) that was quantified by ESI-MS ($t_{1/2}$ ~ 1000 min ~ 17 h). The oxygenation of the complex is found to be ~ 50 times more rapid than its corresponding activation/oxidation. Moreover, during this experiment, the behaviour of the ligand was also investigated. Neither oxidation nor degradation of the ligand can be observed over the same time span examined.

The ESI-MS analysis of the isolated **1Co** complex in dioxane (*i.e.* spectra recorded from *m/z* = 200 to 1500, Figure II-57) clearly evidenced the same behaviour as discussed above. Initially, the cobalt(II) bischelate complex was mainly observed as a sodium adduct at *m/z* = 502.2. Aerobic oxygenation/oxidation led to the formation of a main species, the cobalt(III) bischelate. Interestingly, other intermediate fleeting species could be characterized such as a hydroxo-bridged species $[Co(III)(\mathbf{L^1})_2]_2(OH)$ (*m/z* = 975.5) giving support to the previous observations (*i.e.* the formation of a bridged dioxygen-µ-hydroxo species was suggested, Scheme II-10). After one day of reaction, a cobalt(III) trischelate as well as free ligand (minor species) can be clearly observed suggesting a very slow reorganisation of the oxidized cobalt(III) bischelate.

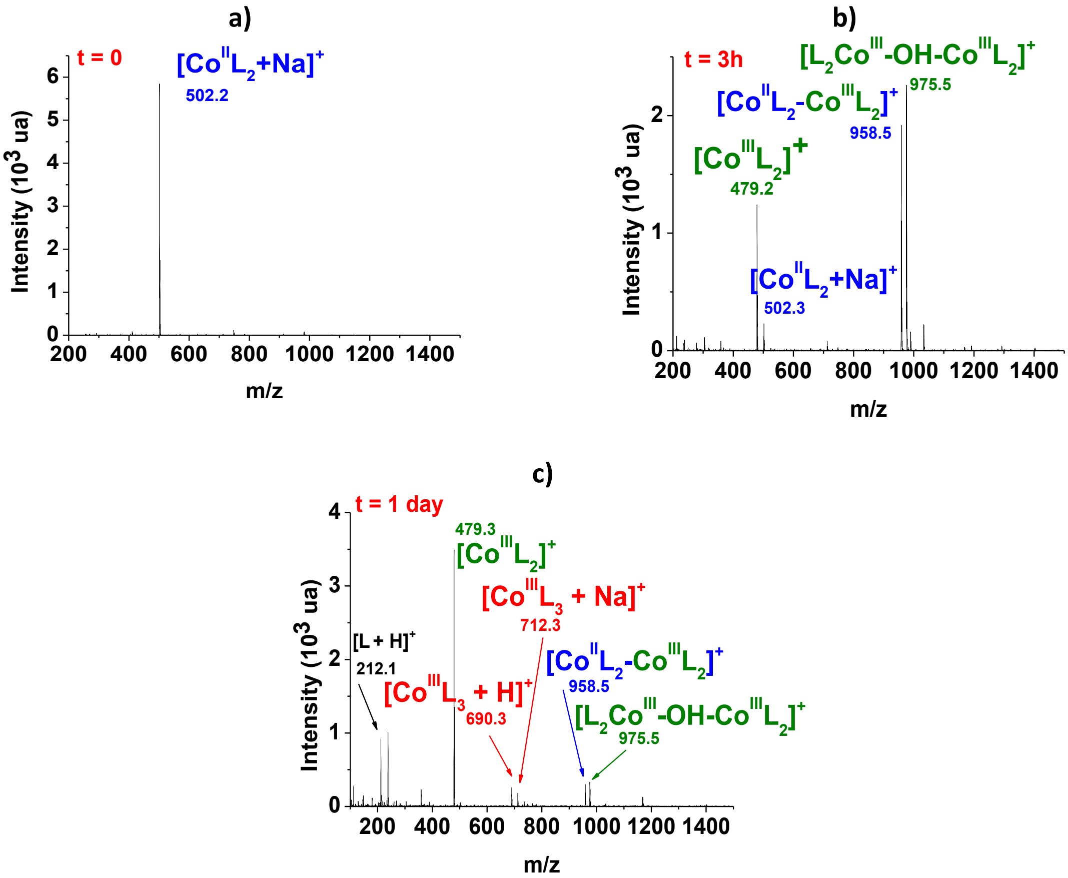

*Figure II-57: Full ESI-MS spectra of **1Co** recorded over one day; **a)** t = 0, **b)** t = 3 h, **c)** t = 1 day, [**1Co**] = 6.97 x 10^{-4} M, solvent: dioxane, + 100 V.*

By contrast with **1Co**, no formation of any other peak than the cobalt(II) bischelate can be evidenced over a large time range for **2Co**. Figure II-58 represents the evolution of the $[Co(\mathbf{L^2}\text{-}H)_2+H]^+$ peak (*m/z* = 304.2) during a 17-day experiment. No major change was observed, except a weak decrease of the intensity of the signal over time (*i.e.* most likely related to instrumental issues). It can be therefore suggested that for **2Co**, contrary to **1Co**, no oxidation of the metal centre and no irreversible degradation of the complex occurred within the time range examined.

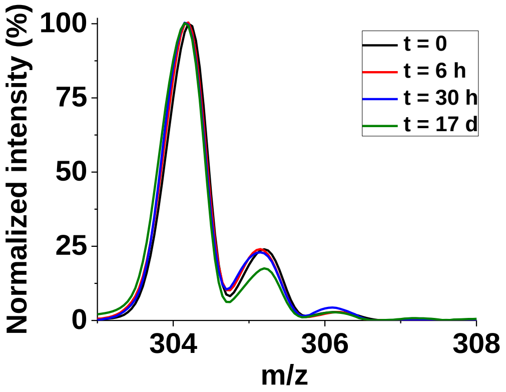

Figure II-58: ESI-MS spectra of ***2Co*** *recorded over 17 d - zoom between* m/z *= 303 and 308;*
*[**2Co**] = 1.0 x 10^{-4} M, solvent: $CH_3CN:H_2O$ (1:1* v/v*), + 225 V.*

Similarly, we have examined the behaviour of cobalt(II) stearate **9Co** by ESI-MS. A freshly prepared solution and a 56-days old solution were analysed by ESI-MS. No oxidation of the metal centre was observed over this time range as depicted in Figure II-59.

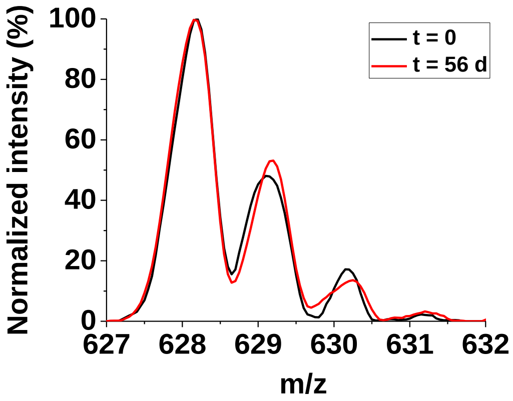

Figure II-59: ESI-MS spectra of ***9Co*** *recorded over 56 d - zoom between* m/z *= 627 and 633;*
*[**9Co**] = 1.0 x 10^{-4} M, solvent: iso-butanol:MeOH (1:1* v/v*), + 150 V.*

By contrast with **1Co,** oximetry coupled to UV-visible absorption spectrophotometry revealed that **8Co** and **9Co** were most likely characterized by (quasi)-reversible oxygenation (*i.e.* no oxygen activation and subsequent metal oxidation was evidenced). Furthermore, the oxygenation/activation processes monitored by ESI-MS allowed concluding that no oxidation under aerobic conditions of **2Co** and **9Co** took place (*i.e.* contrary to **1Co**) suggesting an apparent inertness and stability. We decided to go a step further by analysing these processes with another analytical technique such as ^{1}H NMR.

II.4.4. Oxygenation/activation monitored by ^{1}H NMR

For **1Co**, we have demonstrated the occurrence of at least a two-step (oxygenation and activation) process followed by a very slow conversion of the cobalt(III) bischelate into its trischelate analogue. ^{1}H NMR was then used to screen in a simpler way the reactivity of several metal catalysts in different solvents (*i.e.* suitable for NMR analyses and capable of solubilising the investigated catalysts). In fact, while the cobalt(II) bischelate complexes are paramagnetic species, the cobalt(III) complexes are diamagnetic; their appearance would be therefore easy to monitor by ^{1}H NMR (Figure II-60). For instance we have demonstrated on a solution of the cobalt(III) trischelate (*i.e.* synthesized and fully characterized) that the benzylic protons (*i.e.* circled in red in Figure II-61) became magnetically non-equivalent in the trischelate species leading to the formation of six well separated doublets (ranging from 3.95 to 4.93 ppm (Figure II-61). Originally, the signals of the benzylic protons in the bischelate species were observed to correspond to a broad singlet (4.85 ppm). We therefore anticipated that the formation of the cobalt(III) species over the course of the oxygenation/oxidation of the metal catalysts could be monitored and the corresponding kinetics quantified.

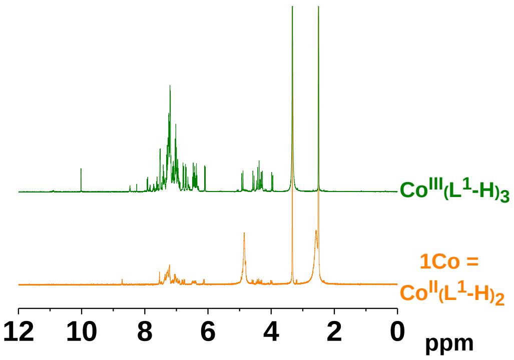

*Figure II-60: ^{1}H NMR spectra of the cobalt(II) bischelate **1Co** and its corresponding cobalt(III) trischelate analogue; solvent: $(CD_3)_2SO$.*

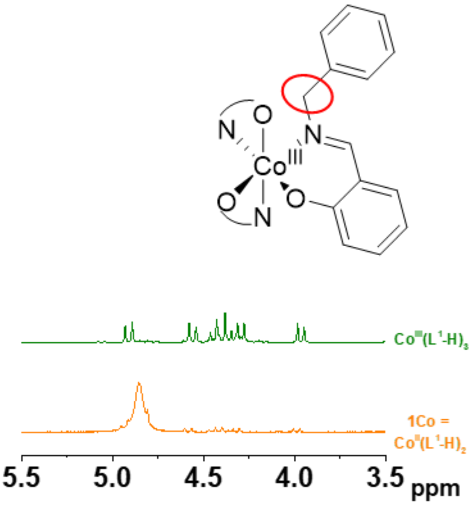

*Figure II-61: ^{1}H NMR spectra of the cobalt(II) bischelate **1Co** and its corresponding cobalt(III) trischelate analogue - zoom between 3.5 and 5.5 ppm; solvent: $(CD_3)_2SO$.*

A NMR tube containing a concentrated solution of **1Co** in DMSO-d_6 was first prepared and ^{1}H NMR spectra were recorded at regular intervals over a time span of about one month (Figure II-62). Interestingly, we observed that the cobalt(II) bischelate left under aerobic conditions in DMSO-d_6 gradually disappeared in favour of a new species, the cobalt(III) trischelate, which thus supposes a major reorganisation of the system. This was already seen by ESI-MS in dioxane with the formation of low levels of cobalt(III) trischelate after one day of aerobic reaction (Figure II-57).

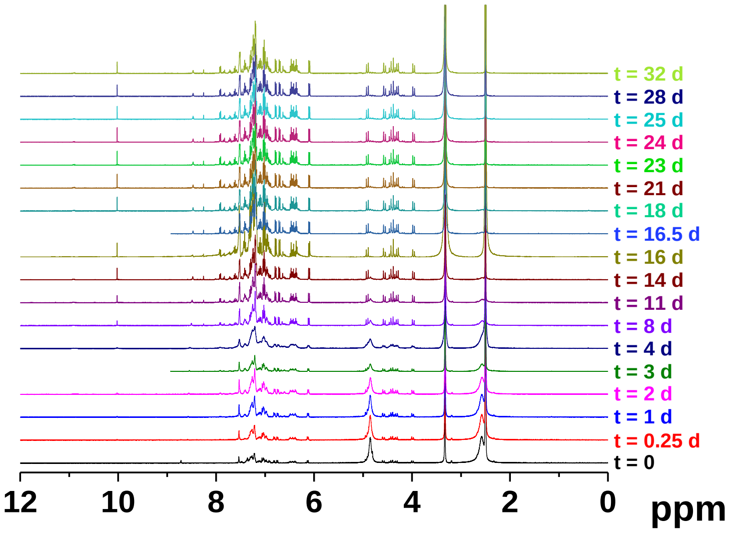

*Figure II-62: ^{1}H NMR spectra of **1Co** recorded over time; solvent: $(CD_3)_2SO$.*

To process the data, the intensity of a benzylic proton was normalized with respect to the solvent peak (*i.e.* we hypothesized that the solvent DMSO peaks were not evolving over time). The kinetics of the conversion into cobalt(III) trischelate species, and so indirectly of the oxidation of the metal centre from cobalt(II) to cobalt(III) can be monitored. The obtained data were processed with the help of

Origin software and the half-life time of the oxidation reaction was calculated to be $t_{1/2}$ = 7.7(7) days in pure DMSO-*d*$_6$ (Figure II-63).

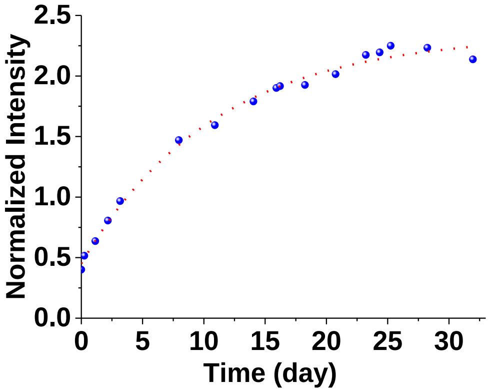

*Figure II-63: Kinetics of oxidation of **1Co** and conversion to its cobalt(III) trischelate monitored by ^{1}H NMR; solvent: $(CD_3)_2SO$.*

For **1Co**, this NMR experiment was extended to other solvents (*e.g.* $CDCl_3$). The cobalt(III) trischelate species was here also the main product of the oxygenation/oxidation/conversion process. Table II-18 depicts the half-life time ($t_{1/2}$) that were calculated for several metal catalysts of interest in different solvent conditions. This NMR approach was very informative since it provided information not only on the kinetics of the oxidation process but also on the nature of the oxidized products. At first glance, by inspecting Table II-18, the catalysts can be grouped into two categories: (*i*) those leading after oxidation of the metal centre to cobalt(III) bischelates (*i.e.* no conversion following oxygenation/oxidation; **2Co** and **9Co**; *in orange* in Table II-18) and (*ii*) those leading to cobalt(III) trischelates (*i.e.* leading to conversion following oxygenation/oxidation; **1Co**, **3Co**, **5Co**, **6Co** and **8Co**, *in green* in Table II-18). Secondly, the effect of the solvent on the oxidation rate can be evaluated. For instance, while the kinetics of cobalt(II) stearate **9Co** was found to be slow in DMSO-*d*$_6$ ($t_{1/2}$ > 18 days), its oxidation was significantly sped up by changing the solvent to acetone-*d*$_6$ ($t_{1/2}$ = 0.35 day) or methanol-*d*$_4$ (*i.e.* the reaction was too fast to be measured). Therefore, according to this oxidation kinetics parameters, the studied catalysts can be now sorted into three other categories: (*i*) fast oxidation kinetics (**1Co**, **2Co**, **5Co** and **6Co**) with half-life time of reaction lower than 10 days; (*ii*) intermediate oxidation kinetics (**9Co**) with half-life time of reaction strongly dependent on the solvent composition; and (*iii*) slow oxidation kinetics (**3Co** and **8Co**) with half-life time of reactions higher than 20 days.

Table II-18: Half-life time ($t_{1/2}$) in days of the oxidation/(conversion) processes of the metal centre (cobalt(II) to cobalt(III)) of different catalysts in various solvents assessed by ^{1}H NMR.

Solvent / Catalyst	$(CD_3)_2SO$	$CDCl_3$	$(CD_3)_2CO$	CD_3OD	CD_3CN
1Co	7.7(7)	2.5(7)	*n.t.*	*n.t.*	*n.t.*
2Co	0.44(2)	*n.t.*	0.53(8)	*n.t.*	*n.t.*
3Co	~ 45	*n.d.*	*n.d.*	*n.d.*	*n.d.*
5Co	6.87(6)	*n.d.*	*n.d.*	*n.d.*	*n.d.*
6Co	3.10(3)	*n.d.*	*n.d.*	*n.d.*	*n.d.*
8Co	> 34	*n.d.*	*n.d.*	*n.d.*	*n.d.*
9Co	> 18	*no reaction*	0.35(1)	*too fast*	*no reaction*

n.d.: not determined due to the low solubility of the catalyst in this solvent
n.t.: not tested
no reaction: no reaction was observed on the time of experiment in these conditions
too fast: the kinetics of the reaction was too fast to be measured
in green: the final species is $Co^{III}(L-H)_3$
in orange: the final species is $Co^{III}(L-H)_2$

This spectroscopic technique was therefore fruitful and allowed characterizing the oxidation products of different cobalt(II) catalysts as well as evaluating the associated kinetics parameters. The effect of the solvent could be also investigated provided good solubilities of the catalysts. This approach was informative since it allowed determining whether the cobalt(III) complex is a bischelate or a trischelate and accordingly if a conversion process took place or not. This is an important aspect to be considered in the development of metal catalysts for oxygenation barriers applications (Scheme I-12).

II.4.5. Oxygenation/activation monitored by UV-visible absorption spectrophotometry using a chromophoric probe

^{1}H NMR allowed screening different catalysts in various solvents. However, the concentrations required for the NMR analyses (*i.e.* consequent low solubilities for many of the investigated metal catalysts) and the number of deuterated solvents usually available in a laboratory significantly restrained this approach. Another analytical method has therefore to be developed to work at much lower concentration in order to screen a wider range of solvents and catalysts. From this point of view, UV-visible absorption spectrophotometry was thus selected. However, as described previously, the observed absorption spectrophotometric variations centred on the catalysts are rather weak, and the use of a chromophoric probe became of importance. For that, the DPPH radical was selected. It is a stable free-radical molecule which does not self-react or react with oxygen. It can scavenge other radicals and in this case, its initial violet colour in solution characterised by a strong absorption at 520 nm is vanished upon reaction to a pale yellow or colourless solution with an obvious decrease of the absorption at 520 nm. Therefore, DPPH can be also employed as a probe to demonstrate the radical nature of a reaction.

The oxygenation/activation mechanism of the ligands (**L**^{1}, **L**^{3}, **L**^{5} and **L**^{6}), the corresponding aldehyde, and template complexes (**1aCo**, **3aCo**, **5aCo** and **6aCo**) and the catalysts (**1Co**, **2Co**, **3Co**, **5Co**, **6Co**, **8Co** and **9Co**) was therefore investigated qualitatively by UV-visible absorption spectrophotometry with the help of DPPH as a chromophoric probe. Differential absorption (*i.e.* the reference cell was filled with only the DPPH solution) was used to emphasize the oxygenation/activation processes. The applied methodology and the results will be first described hereafter in detail for **1Co** as well as for its corresponding aldehyde, ligand (**L**^{1}) and cobalt(II) template (**1aCo**).

The stability of DPPH in dioxane solution was first studied over a time span of 3 hours (*i.e.* that was used for all the other experiments for the sake of comparison). No significant degradation/fading of DPPH was observed thus demonstrating that any absorption variation would originate from the metal catalyst reactivity and DPPH stability in solution. Following the same approach, **1Co** and its precursors (*i.e.* salicylaldehyde, ligand **L**^{1} and cobalt(II) template **1aCo**) were investigated. Figure II-64 depicts the absorption spectral variations recorded over 3 hours. Large and negative variations centred at 520 nm can be clearly seen and originated from the gradual consumption of DPPH over time. This approach allowed us drawing important conclusions: the catalyst **1Co** bound and activated oxygen; the reaction products of the catalyst and oxygen-derived species were of radical nature since DPPH reacts only with radicals and not with oxygen; the oxygenation/activation process of the catalyst **1Co** followed a radical mechanism.

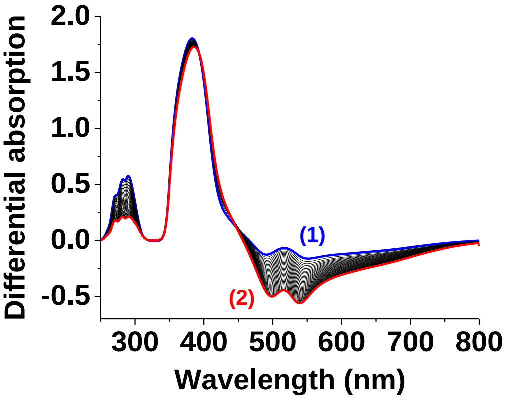

*Figure II-64: Evolution of the UV-visible absorption spectra of **1Co** with DPPH in open air conditions monitored over 3 h; **(1)**: t = 0, **(2)**: t = 3 h, [**1Co**] = 2.92 x 10^{-4} M, [**1Co**]/[DPPH] = 1.0, solvent: dioxane, l = 1 cm, T = 25.0(2) °C.*

After demonstrating the interest of this approach never applied up to now to investigate the reactivity of metal catalysts, the influence of the [compound]/[DPPH] ratio was then evaluated. Figure II-65 depicts the results for **1Co**. It can be clearly evidenced that the higher the [catalyst]/[DPPH] ratio is, the faster and the more efficient the oxygenation/activation processes are.

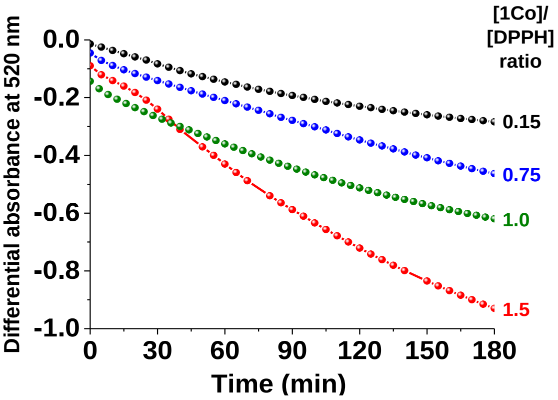

*Figure II-65: Oxygenation/activation kinetics of the compound **1Co** probed by DPPH with various [**1Co**]/[DPPH] ratios; [**1Co**] ~ 3 x 10^{-4} M, [**1Co**]/[DPPH] = 0.15-1.5, solvent: dioxane, l = 1 cm, T = 25.0(2) °C.*

After establishing the influence of the [compound]/[DPPH] ratio, we have then chosen to use a [compound]/[DPPH] ratio = 1.0 in the following experiments. The influence of the solvent on the aerobic reactivity of the catalysts (*i.e.* oxygenation/activation processes) was then investigated (Figure II-66). In methanol, the oxygenation/activation kinetics of **1Co** is very fast, while, in chloroform, the same processes take place slowly. This analytical method allowed establishing a reactivity sequence for **1Co** in different solvents as follows: methanol > acetonitrile > ethanol > 1,2-dichloroethane > dioxane > chloroform.

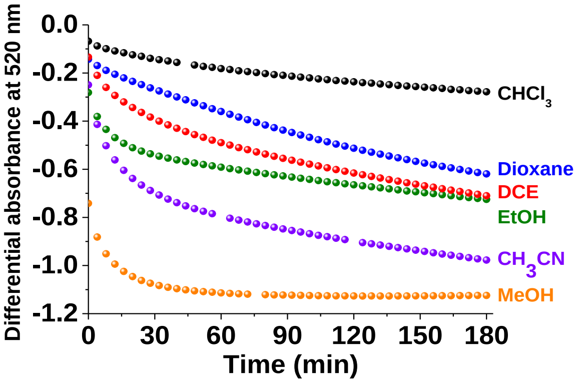

*Figure II-66: Oxygenation/activation kinetics of the complex **1Co** probed by DPPH in different solvents; [**1Co**] ~ 3 x 10^{-4} M, [**1Co**]/[DPPH] = 1.0, l = 1 cm, T = 25.0(2) °C.*

Dioxane was then chosen to compare the oxygenation/activation kinetics of the different cobalt(II) complexes because it ensured a fair solubilisation of all the compounds and complexes investigated in this work (*i.e.* also for **9Co** after a first dissolution in *iso*-butanol). Figure II-67 depicts the differential absorbance variation at 520 nm over 3 hours for a homogeneous series that consisted of the salicylaldehyde, the ligand **L^1**, the cobalt(II) template **1aCo** and the cobalt(II) bischelate **1Co**. Unambiguously, only **1Co** bound and activated rapidly oxygen thus generating radical species that interact with DPPH. The spectral variations observed for the aldehyde, the ligand **L^1** and the template complex **1aCo** were by far less significant. It is noteworthy that the template complexes (*i.e.* cobalt(II) templates with aldehydes) were shown to be of great inertness under aerobic conditions by ^{1}H NMR, thus supporting our observations in the NMR assay (Figure II-68). This feature indicated that complexation with appropriate ligand is primordial for the catalyst role as oxygen barrier.

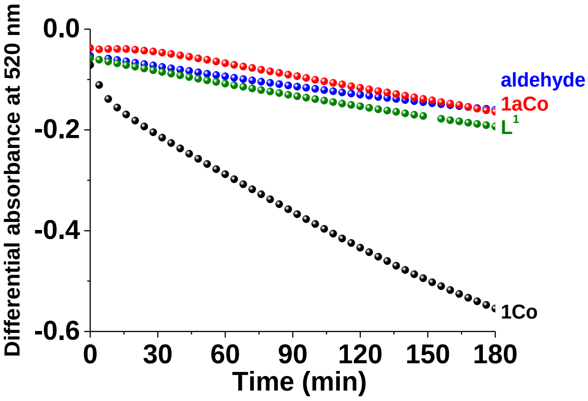

*Figure II-67: Oxygenation/activation kinetics of the **1Co** series probed by DPPH; [Compounds] ~ 3 x 10^{-4} M, [Compounds]/[DPPH] = 1.0, solvent: dioxane, l = 1 cm, T = 25.0(2) °C.*

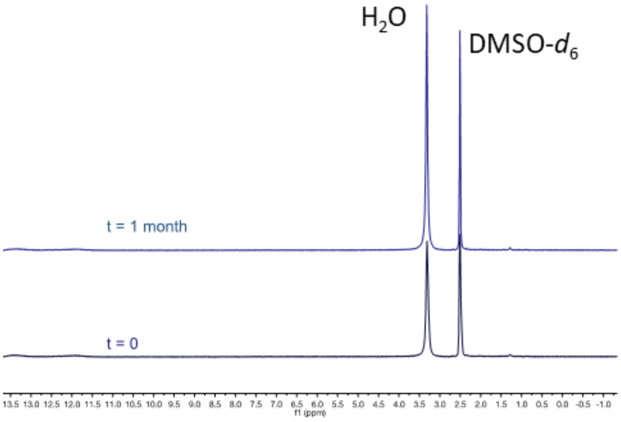

*Figure II-68: ^1H NMR (400 MHz, DMSO-d_6) spectra evolution of complex 1aCo monitoring for one month; [**1aCo**] ~ 10^{-2}M.*

The same methodology was applied to the other series such as **3Co** (Figure II-69), **5Co** (Figure II-70) and **6Co** (Figure II-71). As previously commented for the **1Co** family compounds, the final cobalt(II) catalysts **3Co**, **5Co** and **6Co** presented the most important oxygen binding capacities. They bound and activated oxygen through a radical mechanism as supported by the use of DPPH over time.

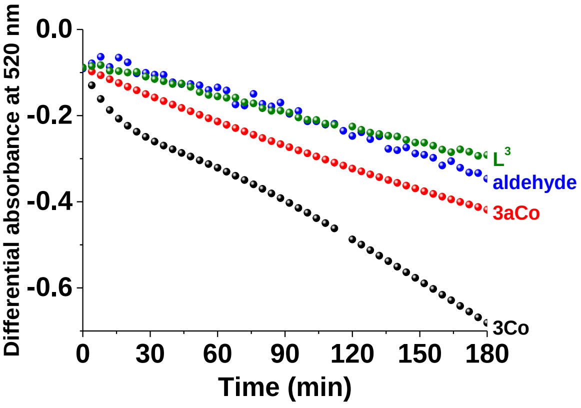

*Figure II-69: Oxygenation/activation kinetics of the compound **3Co** series probed by DPPH; [Compounds] ~ 3 x 10^{-4} M, [Compounds]/[DPPH] = 1.0, solvent: dioxane, l = 1 cm, T = 25.0(2) °C.*

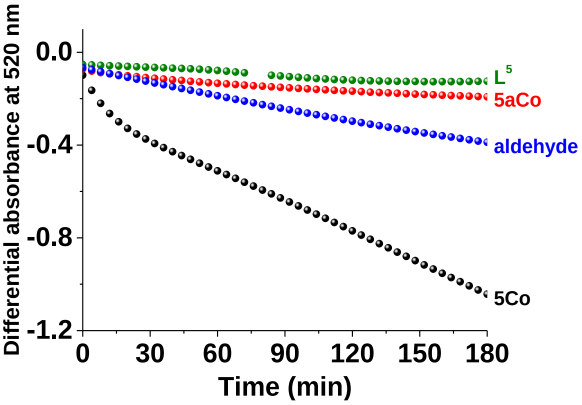

*Figure II-70: Oxygenation/activation kinetics of the compound **5Co** series probed by DPPH; [Compounds] ~ 3 x 10^{-4} M, [Compounds]/[DPPH] = 1.0, solvent: dioxane, l = 1 cm, T = 25.0(2) °C.*

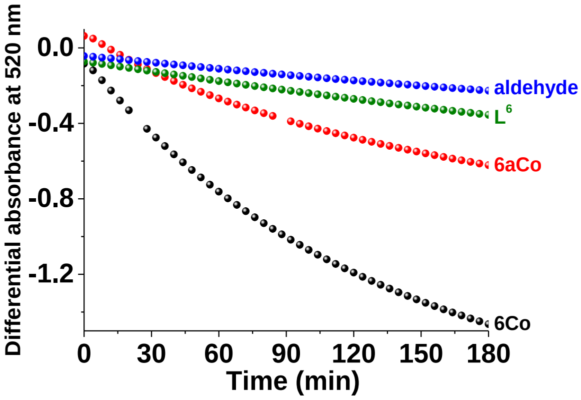

*Figure II-71: Oxygenation/activation kinetics of the compound **6Co** series probed by DPPH; [Compounds] ~ 3 x 10^{-4} M, [Compounds]/[DPPH] = 1.0, solvent: dioxane, l = 1 cm, T = 25.0(2) °C.*

Last but not least, this analytical approach allowed comparing the reactivity of the different cobalt(II) catalysts between them under similar experimental conditions (concentration, solvent and temperature). Figure II-72 depicts the DPPH absorption variations over time for the metal catalysts series that were compared to DPPH alone and cobalt(II) *bis*(acetate) (*i.e.* used as a reagent during the synthesis). Complex **6Co** displayed the fastest kinetics and so the highest reactivity (Figure II-72). Cobalt(II) *bis*(acetate) was found to be almost inert in the presence of oxygen. Furthermore, **8Co** (*i.e.* cobalt(II) *bis*(acetylacetonate) as a reference compound) was also one of the less efficient catalysts compared to the six cobalt(II) complexes synthesized during this work thus substantiating our previous results.

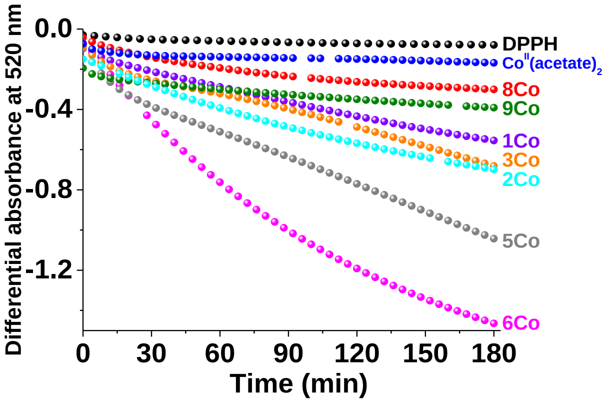

Figure II-72: Reactivity (oxygenation/activation) of the different cobalt(II) complexes probed with DPPH; [Complex] ~ 3 x 10^{-4} M, [Complex]/[DPPH] = 1.0, solvent: dioxane, l = 1 cm, T = 25.0(2) °C.

We have set up an original approach to assess by various complementary analytical methods the oxygenation/activation activities of a homogeneous series of metal complexes. Importantly, to complete this investigation, their redox properties have to be investigated as well to get a broader overview of the oxygenation/activation/conversion properties and mechanism of the cobalt(II) catalysts under aerobic conditions.

II.4.6. Electrochemical properties of the metal catalysts

Cyclic voltammetry (CV) was used to confirm the reactivity sequence of catalysts previously defined using our analytical methodology. The redox potentials were measured under anaerobic conditions using a Ag/AgCl (3 M KCl) reference electrode. This electrochemical analysis allowed quantifying the ease at which a system can be oxidized or reduced. It is important to notice that the interpretation of the voltammograms has been limited to the potential range between -2.0 V and + 0.9 V due to the nature of the solvent. DMSO can be indeed classified as a dipolar aprotic protophilic solvent and is assumed as a suitable solvent[159,160,161] to characterize the electrochemical properties of our metal catalysts (measurable potential limits of + 0.9 V to - 3.9 V with respect to Fc/Fc^+, E = + 0.524 V/Ag/AgCl[160]).

Firstly, free cobalt (cobalt(II) perchlorate) was examined. For the sake of clarity, the CV voltammogram of a mM solution of cobalt(II) perchlorate recorded at a scanning rate of 200 mV.s^{-1} is presented (Figure II-73). An irreversible reduction wave at E_{pc} = - 1.35 V *versus* Ag/AgCl (3 M KCl) can be observed without clear support of re-oxidation of the cobalt complex and that corresponds to the reduction of the cobalt(II) into cobalt(I) species. Instead, an anodic peak characteristic of cobalt(0) to cobalt(II) close to E_{pa} = - 0.2 V *versus* Ag/AgCl (3 M KCl) was observed. This so-called anodic stripping

---

[159] Kolthoff, I. M. In *Treatise on Analytical Chermistry, Part 1 Theory and Practice*; 1993.

[160] Ashnagar, A.; Bruce, J. M.; Dutton, P. L.; Prince, R. C. *Biochim. Biophys. Acta* **1984**, *801* (3), 351–359.

[161] Tsierkezos, N. G. *J. Solut. Chem.* **2007**, *36* (0), 1301–1310.

or redissolution peak (caused by redissolution of metallic cobalt) was a clear signature of cobalt(0) due to disproportionation of dissociated cobalt(I) ions.[162]

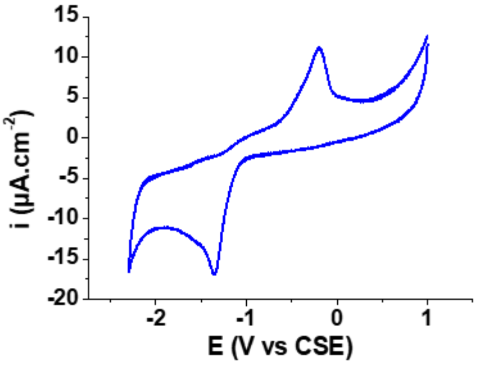

Figure II-73: CV voltammogram of free cobalt (cobalt(II) perchlorate) at 200 mV.s^{-1}
[Co(II)] = 1.13 x 10^{-3} M, solvent: DMSO, I = 0.1 M (n-NBu$_4$PF$_6$).

CV voltammograms of a 10^{-3} M solution of **1Co** was recorded at various scan rates between 50 and 300 mV.s^{-1} (Figure II-74). A quasi-reversible reduction wave at E_{pc} = - 1.71 V *versus* Ag/AgCl (3 M KCl) can be observed and corresponded to the reduction of cobalt(II) to cobalt(I) species with a re-oxidation peak at E_{pa} = - 1.58 V *versus* Ag/AgCl (3 M KCl). It is likely that this redox signal corresponded to a quasi-reversible redox process because of the large $\Delta E \sim 130$ mV and the intensities of the anodic and cathodic peaks that varied with the scan rates (*i.e.* but not the potential values). The anodic peak (i_{pa}) of this process was, however, much weaker than the cathodic peak and can be rationalized by disproportionation of cobalt(I) species even if no clear oxidation peak close to E_{pa} = - 0.2 V *versus* Ag/AgCl (3 M KCl) was observed (*i.e.* value measured for free cobalt, anodic stripping or redissolution peak due to cobalt(0), see above). Moreover, an irreversible reduction wave at E_{pc} = - 0.14 V *versus* Ag/AgCl (3 M KCl) can be observed and likely corresponded to the reduction of the cobalt(III) into the cobalt(II) species while a re-oxidation peak (cobalt(II) to cobalt(III)) at E_{pa} = 0.31 V *versus* Ag/AgCl (3 M KCl) can be observed. Because of its irreversibility character, this redox process was most likely resulting from an ECE (electron exchange-chemical reaction-electron exchange) mechanism. Importantly, no characteristic electrochemical peaks of free cobalt were seen which suggest a strong stability of the metal catalyst whatever its oxidation state.

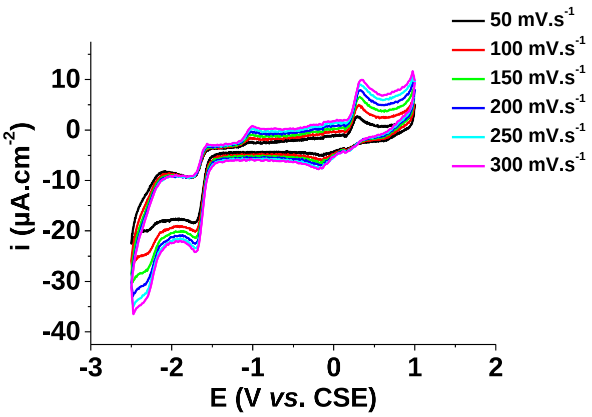

*Figure II-74: CV voltammograms of complex **1Co** measured at different scan rates;*
*[**1Co**] = 9.74 x 10^{-4} M, solvent: DMSO, I = 0.1 M (n-NBu$_4$PF$_6$).*

---

[162] Darko, G.; Batric, P. *Electrochimica Acta* **2002**, *47*, 2901–2912.

Similarly, experiments were carried out for complex **6Co** and same observations can be drawn (Figure II-75). A cathodic signal at E_{pc} = - 1.56 V *versus* Ag/AgCl (3 M KCl) can be observed and likely corresponded to the reduction of the cobalt(II) to the cobalt(I) species, with however no evidence of a re-oxidation process. It was probably due to an efficient disproportionation of cobalt(I) species. A second irreversible reduction wave at E_{pc} = - 0.43 V *versus* Ag/AgCl (3 M KCl) can be observed as well and was attributed to the reduction of the cobalt(III) to cobalt(II) species. In that case, the re-oxidation peak was difficult to evidence. We can however suggest that the re-oxidation peak was centred at E_{pa} = - 0.05 V *versus* Ag/AgCl (3 M KCl) because other visible signals were close to potential limits imposed by the solvent.

The same electrochemical experiments were conducted for complex **5Co** as well (Figure II-75). A reversible reduction peak at E_{pc} = - 1.64 V *versus* Ag/AgCl (3 M KCl) can be observed and was attributed to the reduction of the nitro substituents. The reverse oxidation peak related to this process can be measured at E_{pa} = - 1.54 V *versus* Ag/AgCl (3 M KCl).[163] A second oxidation wave at E_{pa} = 0.36 V *versus* Ag/AgCl (3 M KCl) can be observed and likely corresponded to oxidation of the cobalt(II) to the cobalt(III) species but the reverse reduction wave was difficult to observe. As seen for complex **6Co**, a reduction peak at E_{pc} = - 1.22 V *versus* Ag/AgCl (3 M KCl) can be observed and likely corresponded to the reduction of the cobalt(II) to the cobalt(I) species, but with however no reverse oxidation wave.

In the case of the complex **3Co** (Figure II-75), a cathodic peak at E_{pc} = - 2.01 V *versus* Ag/AgCl (3 M KCl) was observed and was likely attributed to debromination of the complex.[164] A second reduction peak at E_{pc} = - 1.45 V *versus* Ag/AgCl (3 M KCl) can be observed as well and was attributed to the reduction of the cobalt(II) to the cobalt(I) species but with, however, no reverse oxidation peak as seen for complexes **5Co** and **6Co**. Moreover, an oxidation peak (oxidation of the cobalt(II) to the cobalt(III) species) was evidenced at E_{pa} = 0.50 V *versus* Ag/AgCl (3 M KCl) with no obvious evidence of a reduction process.

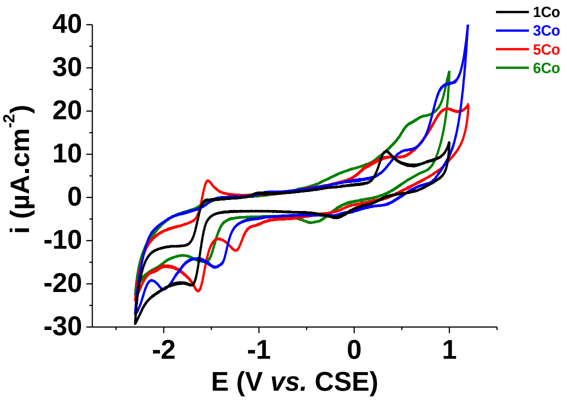

Figure II-75: CV voltammograms of complexes ***1Co***, ***3Co***, ***5Co*** *and* ***6Co***;
[Complex] ~ 1 x 10^{-3} M, solvent: DMSO, I = 0.1 M (n-NBu_4PF_6).

The electrochemical results obtained for the different cobalt(II) catalysts with Schiff base ligands can be compared and a reactivity sequence can be proposed. With respect to Figure II-76 on which the oxidation potentials have been ranked, one can suggest that complex **6Co** is more prone to oxidation (*i.e.* easiness of electron transfer to oxygen than the other complexes). The following sequence can be hence proposed: **6Co** > **1Co** ~ **5Co** ~ **2Co** > **3Co** > **8Co**. This reactivity sequence confirms the results previously obtained by ^{1}H NMR (Table II-18) and UV-visible absorption spectrophotometry with the DPPH probe (Figure II-72).

---

[163] Sidorov, P.; Desta, I.; Chessé, M.; Horvath, D.; Marcou, G.; Varnek, A.; Davioud-Charvet, E.; Elhabiri, M. *ChemMedChem* **2016**, *11* (12), 1339–1351.

[164] Van den Ham, D. M.; Harrison, G. F.; Spaans, A.; Van der Meer, D. *Recl. J. R. Neth. Chem. Soc.* **1975**, *94* (7), 168–173.

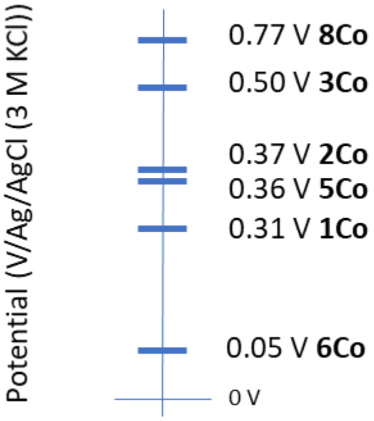

*Figure II-76: Oxidation potentials (*versus *Ag/AgCl/3 M KCl) of cobalt(II) complexes (cobalt(II) to cobalt(III process).*

Electrochemistry and UV-visible absorption spectrophotometry (*i.e.* using DPPH as a chromophoric probe) demonstrated that the cobalt(II) complex **6Co** (bearing methoxy substituent) displayed the most promising oxygenation/oxidation properties. However, once the metal centre was oxidized, **6Co** was found to be prone to a slow conversion process ($t_{1/2}$ = 3 days) that lead to a stable cobalt(III) trischelate as clearly evidenced by ^{1}H NMR experiments (Table II-18). The same feature was observed for all the cobalt(II) complexes investigated in this work (*i.e.* containing Schiff base ligands) with the exception of **2Co**. Although oxidized to its cobalt(III) state, **9Co** (cobalt(II) *bis*(stearate)) remained stable and did not undergo any redox-triggered conversion. This is an important outcome when trying to develop new metal catalysts for oxygen barriers properties. Formation of cobalt(III) trischelate in the course of oxygen binding/activation/scavenging will lead to an inert product that could not cycle anymore. However, the examined catalysts cannot be discarded at this point relying on the basis of this sole aspect since no additive was combined. The reactivity of the metal catalysts could indeed be significantly altered in the presence of exogenous scavengers.

To sum up, Figure II-77 recalls the putative mechanism proposed by Cabani.[108] The first step, that is related to the complexation properties of cobalt(II) by the examined ligands (step **1**), was thoroughly investigated. The corresponding thermodynamic parameters of both the ligands and the metal catalysts were determined by using either a pure potentiometry pH-metric analysis or UV-visible absorption spectrophotometry *versus* pH titrations (*i.e.* **1Co**, **4Co** and **6Co** were found to be the more stable). The stability in solution of both the ligands and the metal catalysts was determined as well either by UV-visible absorption spectrophotometry or by ESI-MS. Hydroxylated (step **1'**) species of several metal catalysts were evidenced during the investigation of the complexation properties. The oxygenation (step **2**) and the activation (step **3**) stages, which are intimately linked, were studied by using UV-visible absorption spectrophotometry alone or coupled with oximetry or a chromophoric probe (*i.e.* DPPH), by ^{1}H NMR and by ESI-MS. The complexes **6Co** and **1Co** were found to be among the most reactive in terms of oxygen binding (*i.e.* irreversible binding demonstrated by oximetry likely due to a fast oxygen activation) and a slow conversion into a more stable cobalt(III) trischelate was clearly evidenced. However, this cobalt(III) trischelate species is not anymore active towards oxygenation and so of less interest in the frame of this project. **2Co** and **9Co** remained the less active catalysts but were not subjected to any conversion in solution once oxidized (*i.e.* that can be considered as a degradation of the complex as seen on step **5**). Once these two catalysts are not forming trischelate species, they are of high interest for this project. However, up to now, **2Co** could not be obtained in pure form. This is the reason why, **9Co** can be considered as the most promising cobalt(II) catalyst for the continuation of this project. Finally, the redox properties of the different metal catalysts were evaluated by cyclic voltammetry. Substrate oxidation was intentionally not studied here (step **6**) and will be the focus of the following chapters either in solution (Chapter III) or in the solid state (Chapter IV).

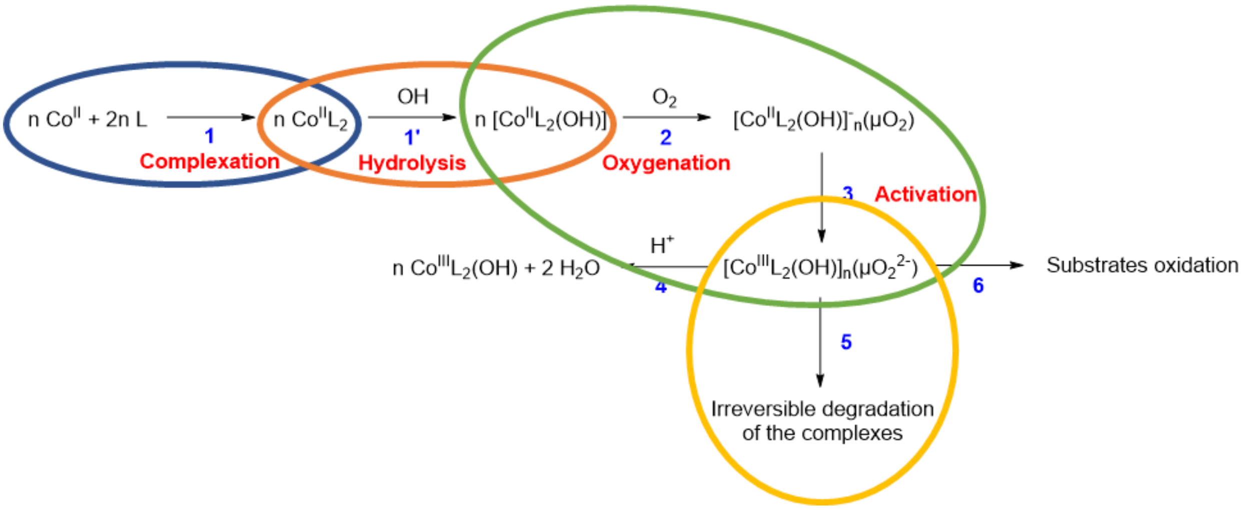
n Co^{II} + 2n L
1
Complexation
n Co^{II}L$_2$
OH
1'
Hydrolysis
n [Co^{II}L$_2$(OH)]
O$_2$
2
Oxygenation
[Co^{II}L$_2$(OH)]^-_n(μO$_2$)
3 Activation
H$^+$
4
n Co^{III}L$_2$(OH) + 2 H$_2$O
[Co^{III}L$_2$(OH)]$_n$(μO$_2^{2-}$)
6
Substrates oxidation
5
Irreversible degradation of the complexes

*Figure II-77: Putative mechanism of complexation, oxygenation and activation of cobalt(II) complexes. Main steps are noted **1** to **6**. Adapted from Cabani.*

II.5. Experimental section

II.5.1. Analytical equipments used in this study

II.5.1.1. Nuclear Magnetic Resonance spectroscopy - NMR

***Objectives and means:** NMR analyses were carried out to characterize the different intermediates, the final compounds and the metal catalysts that were synthesized in this work as well as to monitor the oxygenation/activation stages of the metal catalysts.*

NMR spectra were recorded either on a Bruker Avance I (300 MHz for ^{1}H analyses and 75 MHz for ^{13}C analyses) with a dual ^{13}C decoupled ^{1}H probe, on a Bruker Avance III HD (400 MHz for ^{1}H analyses and 101 MHz for ^{13}C analyses) with BBFO probe or on a Bruker Avance III HD (500 MHz for ^{1}H analyses and 126 MHz for ^{13}C analyses) with "Prodigy" CPPBBO probe spectrometer with solvent peaks as reference. Solvents used for NMR analyses were deuterated solvents (chloroform-*d* ($CDCl_3$, Aldrich, 99.8 atom% D), methanol-d_4 (CD_3OD, Aldrich, ≥ 99.8 atom% D), acetone-d_6 ($(CD_3)_2CO$, Aldrich, 99.9 atom% D) and dimethylsulfoxide-d_6 ($(CD_3)_2SO$, Aldrich, 99.9 atom% D)). Chemical shifts (δ) are expressed in ppm relative to TMS. Multiplicity is indicated as s (singlet), d (doublet), t (triplet), q (quartet), m (multiplet), dd (doublet of doublets). Coupling constants (*J*) values are given in hertz (Hz).

II.5.1.2. Fourier Transform Infrared Spectroscopy - FTIR

***Objectives and means:** FTIR measurements were carried out to characterize the intermediates and the final organic or inorganic products including ligands and metal complexes. The stability over time of the metal catalysts (cobalt(II) and manganese(II)) was also evaluated by FTIR measurements.*

FTIR spectra were recorded neat on a Perkin Elmer FTIR Spectrometer Spectrum Two. Spectra were analysed using *Spectrum* software from PerkinElmer and indexed thanks to Parikh V.M. book.[165]

II.5.1.3. Liquid Chromatography-Mass Spectrometry Analyses - LC-MS

***Objectives and means:** the LC-MS analyses were conducted to evidence the formation of the targeted products and to assess their purities.*

The LC-MS analyses were performed on a Thermo Scientific Liquid Chromatography Accela 600 coupled to PDA and MSQ 20782 detectors.

The column used was a Thermo Scientific Hypersil GOLD 50x2.1 mm with 1.9 µm pore diameter. A Hypersil (2.1 mm intern diameter, filter cartridge 0.2 µm) pre-column was also used. The injection volume was 5 µL and the solvent flow was 600 µL.min^{-1}. A split was performed after the PDA detector and before the entrance of the MS detector. The solvent mixture (water, Sigma Aldrich, CHROMASOLV® Plus, for HPLC and acetonitrile VWR, ≥ 99.95% for HPLC, or Sigma Aldrich, CHROMASOLV® for HPLC) as well as the gradient used are described in Table II-19 below. The cone voltage applied in MS detector was + 30 V.

---

[165] Parikh, V. M. *Absorption Spectroscopy of Organic Molecules*; Addison-Wesley Publishing Company, 1974.

Table II-19: Gradient of solvents used in LC-MS.

Time (min)	Solvent A: H_2O with 0.1% formic acid	Solvent B: CH_3CN with 0.1% formic acid
0	95	5
2	5	95
4	5	95
4.1	95	5
6	95	5

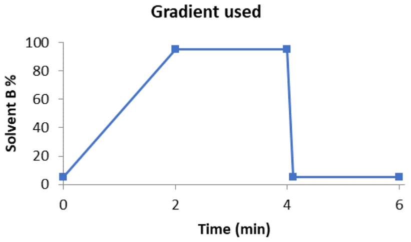

II.5.1.4. Electrospray Ionization-Mass Spectrometry analyses - ESI-MS

Objectives and means: *ESI-MS analyses were carried out to characterize the different ligands and metal catalysts and to monitor the catalyst oxygenation/activation stages as well as the corresponding products. Kinetics of the catalyst oxygenation/activation processes were also investigated by using this analytical technique.*

ESI-MS analyses were carried out on an Agilent Technologies 6120 quadrupole equipped with an electrospray (ESI) interface. The sample solutions were continuously introduced into the spectrometer source with a syringe pump (Kd Scientific) at a flow rate of 800 µL.h^{-1}. For the electrospray ionization, the drying gas was heated at 250 °C and its flow was set at 6 L.min^{-1}. The capillary exit voltage was fixed at 5 kV and the skimmer voltage was varied to optimize the signal responses of the targeted species. The cone voltage values applied for each of the examined samples will be detailed for each experiment. Scanning was usually performed over the maximum scale from *m/z* 100 to 1500. Solvents used for ESI-MS analyses are high quality solvents (methanol, VWR, HPLC grade; ethanol, VWR, > 99.7%, absolute; 1,4-dioxane, Alfa Aesar, ACS, > 99%; and degassed water).

II.5.1.5. Automated potentiometry

Objectives and means: *potentiometry (or pH-metry) was used to evaluate the protonation constants of the examined ligands and to assess their complexation affinities towards cobalt(II) or manganese(II). Potentiometry passively measures the potential of a solution between two electrodes (reference and working electrode) in a non-destructive manner. In our study, a unique glass electrode, that combined both the reference and the working electrodes, was employed. This technique is very accurate and relies on the measurements of the free proton activity along the pH titration but requires high concentrations in solution of the systems to be studied.*

Potentiometric device: the automated potentiometric titrations (calibrations of the electrodes and pH titrations) were performed using an automatic titrator system 794 Basic Titrino (Metrohm) equipped with a combined glass electrode (Metrohm 6.0234.500, Long Life) filled with 0.1 M NaCl (SDS, Carlo Erba, 99-100.5%) in water and an exchange unit with integrated data chip with 1 mL glass cylinder (nominal error of 3 µL for 1 mL) and light protection. The automated potentiometric unit was connected to a microcomputer (*Tiamo light 1.2* program for the acquisition of the potentiometric data). The potentiometric titrations were conducted with the MET-pH method (MET stands for Monotonous Equivalent point Titration) that is available in the *Tiamo light 1.2* software (Metrohm AG Ltd, Herisau, Switzerland) with the following parameters: volume increment 5 µL, maximum flow of the burette 2 mL.min^{-1}, maximum signal drift of 3 mV.min^{-1} and maximum equilibration time of 100 s.

Preparation of degassed water and of dioxane-water mixture: distilled water was further purified by passing it through a mixed bed of ion-exchanger (Fisher Bioblock Scientific R3-83002, M3-83006) and activated carbon (Fisher Bioblock Scientific ORC-83005) and was deoxygenated by CO_2- and O_2-free argon (Sigma Oxiclear cartridge) before use. Due to the rather limited solubility of the cobalt(II) and manganese(II) complexes in water (*ca.* 10^{-3} M), a mixed solvent made of degassed water and of spectroscopic grade dioxane (Alfa Aesar, ACS, >99%) was prepared. This binary solvent represented a good compromise to dissolve both the free ligands (**L^1–L^7**), the cobalt(II) and manganese(II) salts, and the corresponding cobalt(II) and manganese(II) complexes (**1Co**–**7Co** and **1Mn**–**7Mn** respectively) at mM concentration scale.

Calibration of the hydrogen ion probe: the combined glass electrode was calibrated as a hydrogen ion concentration probe by titrating known amounts of perchloric acid ($HClO_4$, ~ 8.9-9.3 x 10^{-2} M, Sigma Aldrich, ~ 70%) in dioxane:water (1:1 *v/v*) with CO_2-free sodium hydroxide solution (NaOH, ~1.26-1.46 x 10^{-1} M, BdH, Analar, ≥ 98%) in the same mixed solvent. Prior to their use, the perchloric acid and sodium hydroxide solutions were titrated with sodium tetraborate decahydrate ($B_4Na_2O_7.10H_2O$, Fluka, ≥ 99.5%, puriss, p.a.) and potassium hydrogen phthalate ($C_8H_5KO_3$, Sigma Aldrich, ≥ 99.5%), respectively, using methyl orange (Reactifs RAL) and phenolphthalein (Sigma Aldrich, ACS reagent) as indicators. During the pH-metric titrations, the titration cell was thermostated at 25.0(2) °C by the flow of a Lauda E200 thermostat. The *Glee* program[166] was applied for the glass electrode calibration (determination of the standard electrode potential $E_0.mV^{-1}$ and of the slope of the electrode $s.mV^{-1}.pH^{-1}$) and to check the carbonate levels of the NaOH solutions that were used.

pH-metric titrations: the pH titrations experiments were realized with 5 mL of solution containing about 10^{-3} M of the ligands (**L^1-L^7**). The ionic strength *I* of the ligands in dioxane:water (1:1 *v/v*) was fixed at 0.1 M using sodium perchlorate ($NaClO_4.H_2O$, Merck, 99.0-102.0%, for analysis). The initial pH of the ligand solutions was decreased to ~ 2-3 with the help of concentrated $HClO_4$ (~ 9 x 10^{-2} M). The pH-metric titration was then realized with a NaOH stock solution freshly prepared (~ 1.08-1.16 x 10^{-1} M in dioxane:water (1:1 *v/v*)) that was placed in the 1 mL exchange unit of the potentiometric apparatus. The titration cell was thermostated at 25.0(2) °C by the flow of a Lauda E200 thermostat. The same methodology was employed for the metal complexes. Potentiometric titrations experiments were performed with solutions containing about 10^{-3} M of the ligand (**L^1-L^7**) and half equivalent of either cobalt(II) or manganese(II) salts.

> *Preparation and colorimetric*[167] *titration of cobalt(II) salt solution:* a solution of cobalt(II) perchlorate ($Co(ClO_4)_2.6H_2O$, Fluka, purum. p.a.) was prepared at about 0.1 M in degassed water. For the titration, 1 mL of this solution was diluted with water and pH was adjusted to 5-6 with ammonium acetate (Riedel-deHaën, > 98%, puriss.). The solution was titrated with standardized EDTA 0.1 M (Titriplex III solution, Merck, 0.1 M) and xylenol orange (Merck) as coloured indicator. The titrations were at least triplicated.
>
> *Preparation and colorimetric*[167] *titration of* manganese*(II) salt solution:* a solution of manganese(II) perchlorate ($Mn(ClO_4)_2.xH_2O$, Aldrich, 99%) was prepared at about 0.1 M in degassed water. For the titration, 2-5 mL of potassium hydrogenotartrate 5% (Sigma Aldrich, ≥ 99.5%) and 1.5-2.0 mL of ammonia 25% (Merck, 25%, EMSURE® for analysis) were added to 1 mL of the metal salt solution. After addition of a very small amount of ascorbic acid (*L*-ascorbic acid, Serva, cryst., research grade), the solution was heated to 70-80 °C. One indicator buffer tablet (indicator buffer tablets for determination of water hardness with Titriplex solutions, Merck) was added and the pH was monitored (it should ranged between 10 and 11).

---

[166] Gans, P.; O'Sullivan, B. *Talanta* **2000**, *51* (1), 33–37.

[167] Merck, E. *Méthodes d'analyses complexométriques avec les Titriplex®*.

The solution was then titrated with standardized EDTA 0.1 M (Titriplex III solution, Merck, 0.1 M). The titrations were at least reproduced in triplicate.

The potentiometric results (~ 200 data) were processed using the *Hyperquad 2000* software.[168,169] These potentiometric data points were weighted by a formula allowing greater pH errors in the region of an end-point than elsewhere. The weighting factor W_i is defined as the reciprocal of the estimated variance of measurements (σ_i^2):

$W_i = \frac{1}{\sigma_i^2} = \frac{1}{\sigma_E^2 + \left(\frac{\delta E}{\delta V}\right)^2 \sigma_V^2}$ where σ_E^2 and σ_V^2 are the estimated variances of the potential and volume readings, respectively. The constants were refined by minimizing the error-square sum, *U*, of the potentials:

$$U = \sum_i^N W_i \; (\mathrm{E}_{\mathrm{obs,i}} - \mathrm{E}_{\mathrm{cal,i}})^2$$

At least three potentiometric titrations were treated either as a single set or as separated entities, for each system, without significant variation in the values of the determined constants. The quality of fit was judged by the values of the sample standard deviation, *S*, and the goodness of fit, χ^2, (Pearson's test). Values of σ_E = 0.1 mV (0.023 σ_{pH}) and σ_V = 0.005 mL were fixed to evaluate the values of sample standard deviation *S*. The scatter of residuals *versus* pH was reasonably random, without any significant systematic trends, thus indicating a good fit of the experimental data. The successive protonation or stability constants were calculated from the cumulative constants determined with the program. The uncertainties in the log*K* values corresponded to the added standard deviations in the cumulative constants.

II.5.1.6. UV-visible absorption spectrophotometry coupled to potentiometry

Objectives and means: *UV-visible absorption spectrophotometry was coupled to potentiometry to also determine the protonation constants of the different ligands as well as their complexation constants towards cobalt(II) or manganese(II). Even though it might offer less accuracy than pure potentiometry, this technique is complementary and requires less concentrated solutions. It relies on the spectral variations of the chromophores upon (de)protonation and/or metal complexation. In addition to the thermodynamic properties (potentiometric values), the UV-visible absorption spectrophotometry allows determining the absorption properties of the system and characterizing the protonation sites, the nature, stoichiometry and structure in solution of the metal complexes.*

The UV-visible absorption spectrophotometric titrations as a function of pH of the ligands ($\mathbf{L^1}$-$\mathbf{L^7}$) and their cobalt(II) and manganese(II) complexes were also performed in dioxane:water (1:1 *v/v*) (1,4-dioxane, Alfa Aesar, ACS, > 99%; degassed water). Stock solutions of ligands ($\mathbf{L^1}$-$\mathbf{L^7}$) were prepared by quantitative dissolution of a solid sample in dioxane:water (1:1 *v/*v) and the ionic strength *I* was adjusted to 0.1 M with $NaClO_4.H_2O$ (Merck, 99.0-102.0%, for analysis). Typically, 40 mL of the solution were introduced into a jacketed cell (Metrohm) maintained at 25.0(2) °C by the flow of a Lauda E200 thermostat and about 0.5 equivalent of cobalt(II) perchlorate ($[Co^{II}] = 2.0 \times 10^{-3}$ M, ($Co(ClO_4)_2.6H_2O$, Fluka, purum p.a.) dioxane:water (1:1 *v/v*)) or manganese(II) perchlorate ($[Mn^{II}] = 2.0 \times 10^{-3}$ M, ($Mn(ClO_4)_2.xH_2O$, Aldrich, 99%) dioxane:water (1:1 *v/v*)) was added. The free hydrogen ion concentration was measured with a combined glass electrode (Metrohm 6.0234.500, Long Life) and an automatic titrator system 794 Basic Titrino (Metrohm) as described above. The initial pH was adjusted to ~ 4 with $HClO_4$ solution (~ 9×10^{-2} M in dioxane:water (1:1 *v/v*), Sigma Aldrich, ~ 70%) and

---

[168] Gans, P.; Sabatini, A.; Vacca, A. *HYPERQUAD2000*; Leeds, UK and Florence, Italy, 2000

[169] Gans, P.; Sabatini, A.; Vacca, A. *Talanta* **1996**, *43* (10), 1739–1753.

the titrations of the ligands (**L^1**-**L^7**) and their cobalt(II) or manganese(II) complexes were then carried out automatically (~ 4 < pH < ~ 12) using the automatic titrator of the 794 Basic Titrino device by adding the NaOH solution (~ 1.08-1.16 x 10^{-1} M in dioxane:water (1:1 *v/v*)). After each addition of the base and subsequent measurement of the potential of the solution by the automated system (DET-pH method (DET stands for Dynamic Equivalent point Titration) in the *Tiamo light 1.2* software (Metrohm AG Ltd, Switzerland) with the following parameters: minimal volume increment: 0.5 µL, maximum flow rate of the burette: 2 mL.min^{-1}, no signal drift and maximum equilibration time depending on the scanning spectral window: 150-200 s, an UV-visible absorption spectrum (200-800 nm) was repeatedly recorded using a Varian CARY 50 spectrophotometer fitted with Hellma optical fibres (Hellma, 041.002-UV) and an immersion probe made of suprasil quartz (Hellma, 661.500-QX), that was interfaced (Cetrib) with the potentiometric unit. The spectrophotometric data were analyzed with *Specfit* program which adjusts the absorptivities and the stability constants of the species formed at equilibrium.[170,171,172]

II.5.1.7. UV-visible absorption spectrophotometry

***Objectives and means:** UV-visible absorption spectrophotometry measurements were carried out to characterize the synthesized ligands, intermediates and metal complexes. In addition to this characterization, UV-visible absorption measurements were carried out to monitor the catalyst oxygenation/activation stages. This method is complementary to the ESI-MS analyses and ^{1}H NMR spectroscopy to unravel the mechanism of action of the metal catalysts in solution.*

UV-visible absorption spectrophotometric spectra were recorded with different solvents of spectrophotometric quality (dioxane, Alfa Aesar, ACS, > 99%; degassed water; *iso*-butanol, VWR, 100%). UV-visible spectra were recorded using either a Varian CARY 50 or an Agilent CARY 5000 spectrophotometer. Stock solutions of complexes (**1Co**-**9Co**), ligands (**L^1**-**L^7**) and the corresponding aldehydes were prepared by quantitative dissolution of solid samples. Measurements were performed in suprasil quartz cells (Hellma) with optical path length of 2 or 10 mm. Prior to any measurement, a baseline correction was recorded in the corresponding solvent. Scanning was usually performed at a scan rate of 200 nm.min^{-1}.

II.5.1.8. UV-visible absorption spectrophotometry with DPPH

***Objectives and means:** UV-visible absorption spectrophotometry measurements were carried out with the DPPH radical (2,2-diphenyl-1-picrylhydrazyl, Sigma Aldrich) to determine the nature of the catalyst oxygenation/activation stages (radical or not) and to monitor the kinetics of these stages in various solvents and with different [catalyst]/[DPPH] ratios. The same analytical instruments as described above were used. Together with the previous analyses (^{1}H NMR, ESI-MS, UV-visible absorption spectrophotometry of the catalysts), this assay allowed getting a deeper insight into the oxygenation/activation stages of the catalysts in solution and also defining a reactivity sequence of the metal catalysts as well as studying the influence of the solvent on their oxygenation/activation properties.*

UV-visible absorption spectrophotometric measurements were performed with spectrophotometric grade solvents (dioxane, Alfa Aesar, ACS, > 99%; methanol, Merck, UVASOL® for spectroscopy; 1,2-dichloroethane, Alfa Aesar, > 99.7%, spectrophotometric grade, stabilized with

---

[170] Gampp, H.; Maeder, M.; Meyer, C. J.; Zuberbühler, A. D. *Talanta* **1985**, *32* (2), 95–101.

[171] Gampp, H.; Maeder, M.; Meyer, C. J. *Talanta* **1985**, *32* (4), 257–264.

[172] Gampp, H.; Maeder, M.; Meyer, C. J.; Zuberbühler, A. D. *Talanta* **1985**, *32* (12), 1133–1139.

amylene; chloroform, Merck, ≥ 99.0%, UVASOL® for spectroscopy; ethanol, VWR, > 99.7%, absolute; acetonitrile, Sigma Aldrich, CHROMASOLV® for HPLC or VWR, ≥ 99.95%, for HPLC; dimethylformamide, Sigma Aldrich, ≥ 99.5% (GC), puriss.). The spectra were recorded using a Agilent CARY 5000 spectrophotometer with the scanning kinetics mode. Stock solutions of complexes (**1Co**, **2Co**, **3Co**, **5Co**, **6Co**, **8Co**, **9Co**), templates complexes (**1aCo**, **3aCo**, **5aCo**, **6aCo**), ligands (**L**^{1}, **L**^{3}, **L**^{5}, **L**^{6}) and corresponding aldehydes were freshly prepared just before each experiment by quantitative dissolution of a solid sample. The solution of DPPH was also freshly prepared by quantitative dissolution of a solid sample in the corresponding solvent ([DPPH] ~ 3.0×10^{-4} M). Measurements were performed with two suprasil quartz cells with an optical path of 1 cm maintained at 25 °C thanks to a Varian CARY Dual Cell Peltier Accessory. A baseline correction was recorded with the sample and reference cells filled with a known volume of DPPH solution. A known volume (Eppendorf pipette) of the stock solution of the catalyst (~ 2.0×10^{-3} M) was then added to the optical cell of the sample compartment and the kinetics of the reaction (differential absorption spectra acquired from 200 to 800 nm) was recorded usually for 3 hours. The following Table II-20 depicts the experimental conditions (solvent, [catalyst]/[DPPH] ratio...) and time for the kinetics performed on **1Co**, **2Co**, **3Co**, **5Co**, **6Co**, **8Co** and **9Co** catalysts.

Table II-20: Kinetics of oxygenation/activation stages monitored by UV-visible absorption spectrophotometry with DPPH ([catalyst]/[DPPH] ratio = 0.15-2.0) in different solvents for different times (80 min and/or 3 h).

Solvent	[Catalyst]/ [DPPH] ratio	1Co	2Co	3Co	5Co	6Co	8Co	9Co
Dioxane	0.15	3 h	*n.d.*	*n.d.*	*n.d.*	*n.d.*	*n.d.*	*n.d.*
	0.75	3 h	*n.d.*	*n.d.*	*n.d.*	*n.d.*	*n.d.*	*n.d.*
	1.0	3 h	3 h	3 h	3 h	3 h	3 h	3 h
	1.5	3 h	*n.d.*	*n.d.*	*n.d.*	*n.d.*	*n.d.*	*n.d.*
MeOH	0.1	80 min	*n.d.*	*n.d.*	*n.d.*	*n.d.*	*n.d.*	*n.d.*
	0.3	80 min	*n.d.*	*n.d.*	*n.d.*	*n.d.*	*n.d.*	*n.d.*
	0.5	80 min	*n.d.*	*n.d.*	*n.d.*	*n.d.*	*n.d.*	*n.d.*
	1.0	80 min + 3 h	*n.d.*	*n.d.*	*n.d.*	*n.d.*	*n.d.*	*n.d.*
	1.5	80 min + 3 h	*n.d.*	*n.d.*	*n.d.*	*n.d.*	*n.d.*	*n.d.*
	2.0	80 min	*n.d.*	*n.d.*	*n.d.*	*n.d.*	*n.d.*	*n.d.*
DCE	1.0	3 h	3 h	*n.d.*	*n.d.*	*n.d.*	3 h	3 h
	1.5	3 h	*n.d.*	*n.d.*	*n.d.*	*n.d.*	*n.d.*	*n.d.*
EtOH	1.0	3 h	*n.d.*	*n.d.*	*n.d.*	*n.d.*	*n.d.*	*n.d.*
$CHCl_3$	1.0	3 h	*n.d.*	*n.d.*	*n.d.*	*n.d.*	*n.d.*	*n.d.*
CH_3CN	1.0	3 h	*n.d.*	*n.d.*	*n.d.*	*n.d.*	*n.d.*	*n.d.*
DMF	1.5	3 h	*n.d.*	*n.d.*	*n.d.*	*n.d.*	*n.d.*	*n.d.*

n.d.: not determined

These experiments ([compound]/[DPPH] ratio = 1.0, dioxane, 3 h) were also performed on:

- 2-hydroxybenzaldehyde, **L**^{1} and **1aCo**
- 2-hydroxy-3,5-dibromobenzaldehyde, **L**^{3} and **3aCo**
- 2-hydroxy-5-nitrobenzaldehyde, **L**^{5} and **5aCo**
- 2-hydroxy-5-methoxybenzaldehyde, **L**^{6} and **6aCo**
- cobalt(II) acetate, tetrahydrate

II.5.1.9. Oximetry

Objectives and means: *oximetry measurements were carried out to monitor the catalyst oxygenation stage. This technique was also coupled to UV-visible absorption spectrophotometry to monitor the oxygen concentration as well as the spectral variations. A Varian CARY 50 equipped with* *optical fibres and an immersion probe was used while the oxygen content of the solution was measured concomitantly with a luminescence oximeter probe.*

A Visiferm^{TM} DO Arc 120 probe (Hamilton) was used for the oxygen concentration measurements. The Visiferm^{TM} DO is based on application of luminescence emitted by oxygen. Blue light excites a fluorescent dye (luminophore) in the sensor cap. In the absence of oxygen, some energy fluoresces as red light. In the presence of oxygen, some fluorescence is quenched by the oxygen molecules and less red light is thus emitted. The partial pressure of oxygen is reliably given by the phase shift between excitation and emission. The principle of the sensor is described in Figure II-78. Prior to any experiment, an auto-calibration in air of the probe was performed.

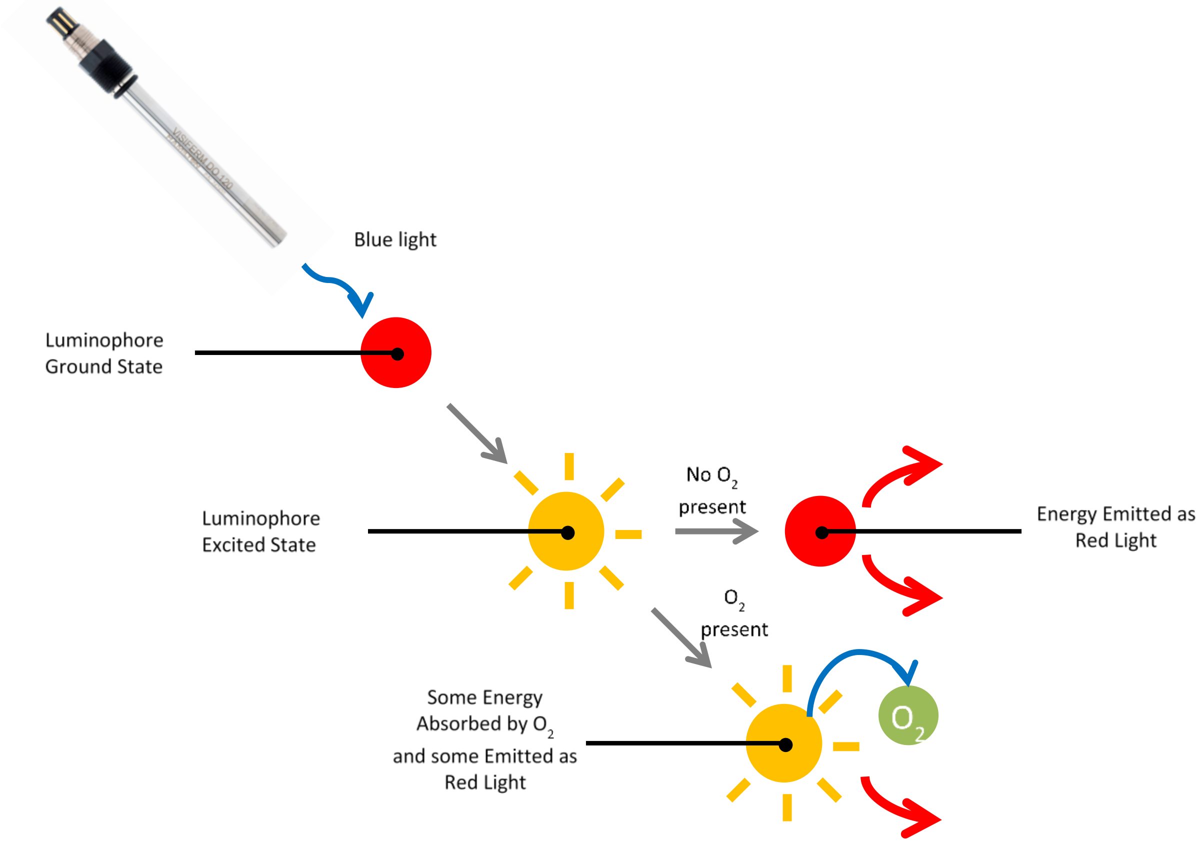
Blue light
Luminophore Ground State
Luminophore Excited State
No O2 present
Energy Emitted as Red Light
O2 present
Some Energy Absorbed by O2 and some Emitted as Red Light
O2

Figure II-78: Principle of the Visiferm™ DO Arc 120 (Hamilton).

The solution of the metal catalyst in a dioxane:H_2O mixture (1:1 *v/v*) (dioxane, Alfa Aesar, ACS, > 99%; degassed water), in ethanol (VWR, > 99.7%, absolute) or in *iso*-butanol (VWR, 100%) was first degassed and deoxygenated by CO_2- and O_2-free argon (Sigma Oxiclear cartridge) until 0.2-0.3 ppm of dissolved O_2 in the solution was measured.

The oxymetric and spectrophotometric measurements were then initiated at this time and the solution was allowed to slowly re-oxygenate by opening the titration vessel: this first measurement step was designated as the first oxygenation step. The spectrophotometric data that were obtained were differential absorption spectra because the baseline was not classically performed with the pure solvents but corresponded to degassed metal catalyst solution prior to oxygenation. The measured absorption spectra then corresponded to the difference between the deoxygenated metal catalyst and the oxygenated/activated one.

When the O_2 concentration reached equilibrium, the solution was then deoxygenated once again using the same methodology as described above and another oxygenation stage was performed (as described above for the first one). This second oxygenation step allowed then confirming the results obtained during the first oxygenation step and concluding whether the oxygenation process of the metal catalysts was reversible or not.

II.5.1.10. Electrochemistry

Objective and means: *electrochemistry measurements were carried out to evaluate the redox properties of the ligands and metal complexes either provided by Clariant or synthesized in the laboratory. The reactivity (oxygenation/activation) of the metal catalysts in solution is intimately related to the redox properties of the metallic centres (i.e. capacity to be oxidized from a +2 to a +3 state). Access to the redox properties of the metallic complexes (Co(II)/Co(III) and Mn(II)/Mn(III)) allowed evaluating their electrochemical behaviour and defining a reactivity sequence.*

Voltammetry is an electrochemical analysis method that consists in disturbing the equilibrium state of a solution by controlling the potential difference between two specific electrodes. The measurement of the current flux, resulting from reduction or oxidation of a compound present in solution, at the surface of the working electrode, allows obtaining the electrochemical profile. This profile allows determining the number of exchanged electrons, the reversibility of the considered redox reaction, as well as the $E_{1/2}$ half-wave potential, in the case of a reversible reaction. Current intensity of electrochemical process results from the competition between two phenomena: electronic transfer resulting from the electrochemical reaction occurring at the working electrode and diffusion of the reactive electrochemical species at that electrode. At constant temperature, convection currents are negligible processes. Presence of a supporting electrolyte prevents any migration current. Absence of stirring during measurements makes diffusion as the only transfer process in the reactive medium.

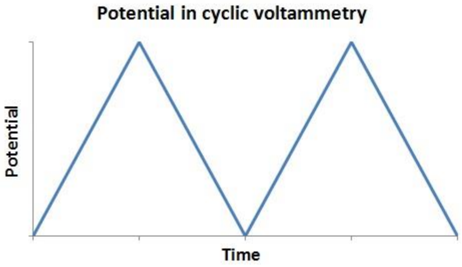

Figure II-79: Potential applied in cyclic voltammetry.

Cyclic voltammetry (CV) is an electrochemical technique consisting in applying a return scanning (varying linearly during time, Figure II-79) of the potential and to observe the intensity which is resulting (*I* = f(E) curves for oxidation and reduction of the same compound). This technique allows studying the kinetics of redox reaction as a function of the measurement time. This technique is more qualitative than quantitative because many parameters are time-dependent. It allows especially rapidly evaluating potentials (oxidation, reduction, half redox) and informs on the nature of the reactions (chemical or electrochemical, physical state of the species, reversibility …). At each time, the [Ox]/[Red] ratio follows the Nernst law (Equation II-1):

$$\mathrm{Ox} + \mathrm{n\,e^-} \leftrightarrow \mathrm{Red} \quad \text{and} \quad \mathrm{E} = \mathrm{E^0} + \frac{\mathrm{R\,T}}{\mathrm{n\,F}} \ln \frac{(\mathrm{Ox})}{(\mathrm{Red})}$$

Equation II-1: Nernst law

E: potential; E°: standard potential; R: ideal gas constant (8.32 $J.K^{-1}.mol^{-1}$); T: temperature (K); n: number of exchanged electrons; F: Faraday constant (96500 C); (Ox) and (Red) are respectively the relative activities of oxidizing and reducing species.

Comparison between cathodic reduction and anodic oxidation curves allows determining if the electronic exchange occurring within the electrode is a reversible process or not. For a reversible system, the separation between the anodic peak and the cathodic peak allows determining the number of transferred electrons n during the electrochemical reactions (Equation II-2):

$$\Delta E_p = E_{pa} - E_{pc} = \frac{0.059}{n}$$

Equation II-2: Derived form of the Nernst equation allowing determining the number of electrons exchanged (n) during the reaction; E_{pa}: anodic peak potential; E_{pc}: cathodic peak potential.

For a quasi-reversible system, ΔE_p is usually found to be higher than $\frac{0.059}{n}$. In the case of irreversible reaction, a single oxidation or reduction peak is observed preventing determination of ΔE_p.

Redox potentials of the cobalt(II) complexes were measured by CV using a potentiosat/galvanostat (Radiometer Analytical MDE150/PST50) and the *Voltamaster 4* software at r.t. (23 ± 1 °C). The measurement of the current was realized between the auxiliary electrode (platinum wire, Radiometer Analytical TM020) and the working electrode (rotating carbon disk electrode, s = 0.071 cm², variable rotation up to 1000 rpm, Radiometer Analytical EDI101). This working electrode might undergo three transport modes: diffusion, convection and/or migration and can generate stationary diffusion currents. The principle is based on the fact that the rotation of the cylinder around its symmetry axis leads to a pumping of the liquid in which it is immerged. This hydrodynamic movement allows controlling the diffusion layer thickness δ as a function of the angular speed ω (s^{-1} or Hz; $\delta = 1.61\ D^{1/3}.\nu^{1/6}.\omega^{-1/2}$ with D: diffusion coefficient; ν: kinematic viscosity, ω=2πf with f in rpm).

The reference electrode (SCE) (Radiometer Analytical TR020) was composed by an Ag/AgCl couple filled with a KCl solution (KCl 3 M and KCl solution saturated with AgCl, Radiometer Analytical S21M011). The measurements were realized in DMSO solvent (used for solubility reasons, Aldrich, ≥ 99.6%) and *n*-NBu_4PF_6 solution (0.1 M, Alfa Aesar, 98%) as the supporting electrolyte. The voltammograms were recorded in the potential range from + 1.5 V to - 2.0 V *versus* KCl(sat.)/Ag/AgCl reference electrode (+ 0.205 V *vs*. NHE).[173] Even though DMSO is an amphiprotic solvent because its autoprotolysis occurs slightly ($pK_{SH} \sim 33$) and the lyate ion ($CH_3SOCH_2^-$) is somehow stable, DMSO has been, however, classified as a dipolar aprotic protophilic solvent and is assumed to be a suitable solvent[174,175] to characterize the electrochemical properties of the cobalt(II) complexes (measurable potential limits of ~ + 1.4 V to ~ - 3.4 V *vs.* NHE). The measurements were performed under anaerobic conditions to prevent any oxidation by dissolved oxygen. The solutions were degassed with an argon flux and a licking was maintained at the surface of the solution during the measurements. Solutions of cobalt(II) complexes, ligands, aldehydes or cobalt(II) metal were prepared by weighing (~ 1 x 10^{-3} M, the ionic strength *I* was maintained at 0.1 M with *n*-NBu_4PF_6).

II.5.1.11. Microanalysis

Objectives and means: *microanalyses (C, H, N) were performed to characterize the synthetic metal complexes.*

Elemental analyses were performed on a Flash 2000 from ThermoFisher Scientific.

---

[173] Sawyer, D. T.; Sobkowiak, A.; Roberts, J. L. *Electrochemistry for Chemists,* Eds., *2nd Edition*; Wiley-Interscience, 1995.

[174] Kolthoff, I. M.; Chantooni, M. K. *Treatise on Analytical Chemistry, Part I, Vol. 2, chap. 19A, 2nd Ed.*, Wiley & Sons.; 1979.

[175] Kolthoff, I. M. *Anal. Chem.* **1974**, *46* (13), 1992–2003.

II.5.1.12. High Resolution Mass Spectrometry - HRMS

Objectives and means: *HRMS analyses were performed to characterize the synthetic metal complexes.*

HRMS experiments were performed on a Bruker Daltonics microTOF spectrometer (Bruker Daltonik GmgH, Bremen, Germany) equipped with an orthogonal electrospray (ESI) interface.

II.5.1.13. Electron Paramagnetic Resonance spectroscopy - EPR

Objectives and means: *EPR measurements were carried out to evaluate the paramagnetic character of cobalt(II) and manganese(II) complexes in the solid state and in solution at r.t., and in the solid state at very low temperature.*

EPR measurements were performed on a Bruker EMX spectrometer at X-band equipped with a 4119 HS-W1 cavity (high sensitivity). An ESR900 cryostat (Oxford Instruments) was used for the low temperature measurements.

II.5.2. Synthesis and characterization of the ligands and metal catalysts

Solvents (provider, quality) used for the syntheses are listed below:

Acetonitrile (CH_3CN), VWR, ≥ 99.95%, for HPLC or Sigma Aldrich, CHROMASOLV® for HPLC
Cyclohexane, VWR, 100%, GPR Rectapur or Sigma Aldrich, ≥ 99.5% (GC), puriss. p.a., ACS reagent
Diethyl ether, VWR, 100.0%, AnalaR Normapur or Sigma Aldrich, ≥ 99.5% (GC)
Dioxane, Alfa Aesar, ACS, > 99%
Ethanol (EtOH), VWR, > 99.7%, absolute or Carlo Erba, ≥ 99.9%, anhydrous
Ethyl acetate (EtOAc), VWR, 99.9%, GPR Rectapur or Sigma Aldrich, ≥ 99.5% (GC), puriss. p.a., ACS reagent
Methanol (MeOH), Sigma Aldrich ≥ 99.6% or 99.8%, anhydrous
Tetrahydrofuran (THF), VWR, 100.0%, AnalaR Normapur
Toluene, VWR, 100%, AnalaR Normapur, ACS reagent or Sigma Aldrich, ≥ 99.7% (GC), puriss. p.a., ACS reagent

II.5.2.1. Synthesis and characterization of the ligands

General procedure **A** for the preparation of Schiff Base ligands:[140]

The aldehyde (1 equiv.) was dissolved in EtOH. Benzylamine (1 equiv., Alfa Aesar, > 98%) was added in one portion and the mixture was refluxed (2-72 hours) and stirred at r.t. until completion of the reaction (0-4.5 hours). The mixture was then evaporated, and toluene was added three times to the solid product. The mixture was evaporated to dryness to remove the remaining water by co-evaporation. Finally, the product was dried under vacuum.

General procedure **B** for the preparation of Schiff Base ligands in solvent free conditions:

The aldehyde (1 equiv.) and benzylamine (1 equiv., Alfa Aesar, > 98%) were heated (2-3 hours) and stirred at r.t. until completion of the reaction (0-2 hours). The mixture was then evaporated, and toluene was added three times to the solid product. The mixture was evaporated to dryness to remove the remaining water by co-evaporation. Finally, the product was dried under vacuum.

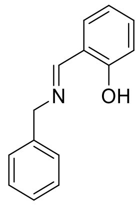

L^1

2-[[(phenylmethyl)imino]methyl]-phenol:

Prepared from the *general procedure **A*** from 2-hydroxybenzaldehyde (Alfa Aeasr, 99%) and benzylamine to give 2-[[(phenylmethyl)imino]methyl]-phenol **L^1** (2.112 g, 10 mmol, **quantitative yield**) as a yellow powder. Reaction time: 2 hours at reflux then 4.5 hours at r.t..

Characterization

^{1}H-NMR (400 MHz, $CDCl_3$) δ (ppm) 4.75 (s, 2H), 6.83 (t, *J* = 7.4 Hz, 1H), 6.91 (d, *J* = 8.0 Hz, 1H), 7.20-7.32 (m, 7H), 8.38 (s, 1H), 13.34 (s, 1H)

^{13}C-NMR (101 MHz, $CDCl_3$) δ (ppm) 63.32, 117.17, 118.75, 118.96, 127.47, 127.88 (2C), 128.79 (2C), 131.54, 132.48, 138.29, 161.24, 165.74

IR: $\nu_{C=N}$ = 1631 cm^{-1}, ν_{C-O} = 1281 cm^{-1}

LC-MS (CH_3CN:H_2O (1:1 *v/v*)): $t_{r\ PDA}$ = 1.89 min, $t_{r\ 254\ nm}$ = 1.89 min; [**L^1**+H]$^+$ m/z_{calc} = 212.1, m/z_{exp} = 212.1

Optimization of the conditions – synthesis in solvent-free conditions

Prepared from the *general procedure **B*** from 2-hydroxybenzaldehyde (Alfa Aeasr, 99%) and benzylamine to give 2-[[(phenylmethyl)imino]methyl]-phenol **L^1** (2.112 g, 10 mmol, **quantitative yield**) as a yellow powder. Reaction time: 2 hours at 50 °C then 2 hours at r.t..

Characterization

^{1}H-NMR (400 MHz, $CDCl_3$) δ (ppm) 4.73 (s, 2H), 6.81 (t, *J* = 7.4 Hz, 1H), 6.89 (d, *J* = 8.0 Hz, 1H), 7.18-7.30 (m, 7H), 8.36 (s, 1H), 13.33 (s, 1H)

^{13}C-NMR (101 MHz, $CDCl_3$) δ (ppm) 63.30, 117.16, 118.73, 118.95, 127.46, 127.87, 128.79, 131.53, 132.48, 138.29, 161.23, 165.73

IR: $\nu_{C=N}$ = 1631 cm^{-1}, ν_{C-O} = 1281 cm^{-1}

LC-MS (CH_3CN:H_2O (1:1 *v/v*)): $t_{r\ PDA}$ = 1.89 min, $t_{r\ 254\ nm}$ = 1.89 min; [**L^1**+H]$^+$ m/z_{calc} = 212.1, m/z_{exp} = 212.1

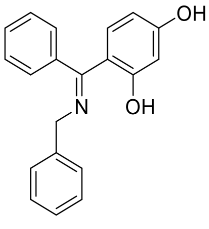

L^2

2-[phenyl[(phenylmethyl)imino]methyl]-5-hydroxy-phenol:

Prepared from the *general procedure **A*** from 2,4-dihydroxybenzophenone (Aldrich, 99%) and benzylamine to give 2-[phenyl[(phenylmethyl)imino]methyl]-5-hydroxy-phenol **L^2** (526.4 mg, 1.74 mmol, **17%**) as a yellow powder. Reaction time: 2 hours at reflux then 2 hours at r.t..

Characterization

^{1}H-NMR (400 MHz, CD_3OD) δ (ppm) 4.48 (s, 2H), 6.00 (d, *J* = 9.0 Hz, 1H), 6.14 (s, 1H), 6.59 (d, *J* = 9.0 Hz, 1H), 7.17-7.39 (m, 7H), 7.53-7.67 (m, 3H)

^{13}C-NMR (101 MHz, CD_3OD) δ (ppm) 52.19, 84.10, 105.81, 107.73, 112.18, 128.48, 128.75, 128.95, 129.38, 129.75, 129.89, 130.01, 131.13, 133.18, 135.54, 138.68, 166.08, 175.53
IR: $\nu_{C=N}$ = 1580 cm^{-1}, $\nu_{C\text{-}O}$ = 1178 cm^{-1}
LC-MS (CH_3CN:H_2O (1:1 *v/v*)): $t_{r\ PDA}$ = 2.02 min, $t_{r\ 254\ nm}$ = 2.02 min; [**L^2**+H]$^+$ m/z_{calc} = 304.1, m/z_{exp} =304.1

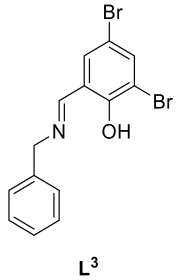

L^3

2-[[(phenylmethyl)imino]phenyl]-4,6-dibromo-phenol:

Prepared from the *general procedure **A*** from 3,5-dibromosalicyladehyde (Aldrich, 98%) and benzylamine under argon atmosphere and in degassed EtOH due to the air sensitivity of this aldehyde. After 2 hours of reflux, the desired product was not obtained.

In a second attempt, the same procedure was used but the aldehyde was introduced with excess (1.2 equiv.). After 72 hours of reflux, the mixture was cooled down to r.t. and the product precipitated. It was recovered by filtration, washed with cold EtOH and dried under vacuum. 2-[[(phenylmethyl)imino]phenyl]-4,6-dibromo-phenol **L^3** was obtained (874 mg, 2.37 mmol, **80%**) as a yellow powder.

Characterization
^{1}H-NMR (400 MHz, $CDCl_3$) δ (ppm) 4.83 (s, 2H), 7.28-7.39 (m, 6H), 7.69 (d, *J* = 2.0 Hz), 8.28 (s, 1H)
^{13}C-NMR (101 MHz, $CDCl_3$) δ (ppm) 62.18, 109.43, 112.69, 119.99, 127.97, 128.0, 129.02, 132.92, 136.87, 137.89, 158.57, 163.70
IR: $\nu_{C=N}$ = 1628 cm^{-1}, $\nu_{C\text{-}O}$ = 1165 cm^{-1}, ν_{Br} = 687 and 698 cm^{-1}
LC-MS (CH_3CN:H_2O (1:1 *v/v*)): $t_{r\ PDA}$ = 2.47 min, $t_{r\ 254\ nm}$ = 2.47 min; [**L^3**+H]$^+$ m/z_{calc} = 367.9, m/z_{exp} = no detection (MS detector out of service at this time)
ESI-MS (MeOH; + 50 V): [**L^3**+H]$^+$ m/z_{calc} = 367.9, m/z_{exp} = 370.0

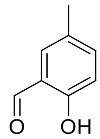

L^{4}a

2-hydroxy-5-methylbenzaldehyde: [141,142]

p-Methylphenol (108 mg, 105 µL, 1 mmol, 1 equiv., Sigma Aldrich, ≥ 99%), paraformaldehyde (90.2 mg, 3 mmol, 3 equiv., Sigma Aldrich, reagent grade) and magnesium chloride $MgCl_2.6H_2O$ (190 mg, 2 mmol, 2 equiv., Prolabo, ultrapure) were dissolved in dry THF (20 mL) under argon atmosphere. After dissolution, triethylamine NEt_3 (305 mg, 0.42 mL, 3.02 mmol, 3.02 equiv., Merck, ≥ 99.0%, for synthesis) was introduced in the solution and the mixture was refluxed for 2 hours. The solution was cooled down to r.t., acidified with aqueous 3 N HCl solution (HCl, Prolabo, 37%) and extracted with diethyl ether. The organic layer was washed with water, brine and dried over $MgSO_4$. Solvent was removed by evaporation. The obtained product was purified by column chromatography (cyclohexane) to lead to 2-hydroxy-5-methylbenzaldehyde **L^{4}a** (29.95 mg, 0.22 mmol, **22%**) as a light-yellow powder.

The reaction was duplicated at a higher scale (*p*-methylphenol (1.0 g, 967 µL, 9.25 mmol, 1 equiv.), paraformaldehyde (833.1 mg, 27.74 mmol, 3 equiv.), magnesium chloride $MgCl_2$ (1.761 g, 18.49 mmol, 2 equiv.), triethylamine NEt_3 (2.823 g, 3.878 mL, 27.9 mmol, 3.02 equiv.)). After 1 hour of reflux, the same work-up and purification were performed and 2-hydroxy-5-methylbenzaldehyde **L^4a** was obtained (577.3 mg, 4.24 mmol, **46%**) as a light-yellow powder.

Characterization

^{1}H-NMR (400 MHz, $CDCl_3$) δ (ppm) 2.34 (s, 3H), 6.88-6.91 (m, 1H), 7.33-7.34 (m, 2H), 9.85 (s, 1H), 10.83 (s, 1H)

^{13}C-NMR (101 MHz, $CDCl_3$) δ (ppm) 20.29, 117.46, 120.42, 129.18, 133.46, 138.09, 159.62, 196.61

IR: $\nu_{C=O}$ = 1645 cm^{-1}, $\nu_{C\text{-}O}$ = 1151 cm^{-1}

LC-MS ($CH_3CN:H_2O$ (1:1 *v/v*)): $t_{r\ PDA}$ = 2.15 min, $t_{r\ 254\ nm}$ = 2.15 min; [**L^4a**+H]$^+$ *m/z*$_{calc}$ = 136.1, *m/z*$_{exp}$ = no detection (MS detector out of service at this time)

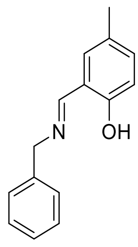

L^4

2-[[(phenylmethyl)imino]phenyl]-4-methyl-phenol:

Prepared from the *general procedure **A*** from 2-hydroxy-5-methylbenzaldehyde **L^4a** and benzylamine to give 2-[[(phenylmethyl)imino]phenyl]-4-methyl-phenol **L^4** (233.4 mg, 1.04 mmol, **94%**) as a yellow powder. Reaction time: 3.5 hours at reflux. Purification: column chromatography (cyclohexane:EtOAc (9:1 *v/v*)).

Characterization

^{1}H-NMR (400 MHz, $CDCl_3$) δ (ppm) 2.30 (s, 3H), 4.81 (s, 2H), 6.88 (d, *J* = 8.4 Hz, 1H), 7.07 (d, *J* = 1.6 Hz, 1H), 7.13 (dd, *J* = 8.4 Hz, *J* = 2.0 Hz, 1H), 7.26-7.38 (m, 5H), 8.39 (s, 1H), 13.14 (s, 1H)

^{13}C-NMR (101 MHz, $CDCl_3$) δ (ppm) 20.47, 63.40, 116.93, 118.64, 127.44, 127.81, 127.90 (2C), 128.79 (2C), 131.59, 133.31, 138.42, 158.98, 165.76

IR: $\nu_{C=O}$ = 1626 cm^{-1}, $\nu_{C\text{-}O}$ = 1158 cm^{-1}, $\nu_{O\text{-}H\ (intramolecular)}$ = 2850-3068 cm^{-1}

LC-MS ($CH_3CN:H_2O$ (1:1 *v/v*)): $t_{r\ PDA}$ = 2.17 min, $t_{r\ 254\ nm}$ = 2.17 min; [**L^4**+H]$^+$ *m/z*$_{calc}$ = 226.1, *m/z*$_{exp}$ = no detection (MS detector out of service at this time)

ESI-MS (MeOH; + 150 V): [**L^4**+H]$^+$ *m/z*$_{calc}$ = 226.1, *m/z*$_{exp}$ = 226.0

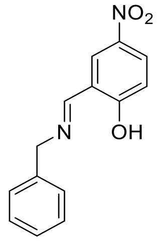

L^5

2-[[(phenylmethyl)imino]phenyl]-4-nitro-phenol:

Prepared from the *general procedure **A*** from 2-hydroxy-5-nitrobenzaldehyde (Aldrich, 98%) and benzylamine to give 2-[[(phenylmethyl)imino]phenyl]-4-nitro-phenol **L^5** (571.4 mg, 2.23 mmol, **75%**) as a yellow powder. Reaction time: 22 hours at reflux.

Characterization

^{1}H-NMR (400 MHz, $CDCl_3$) δ (ppm) 4.87 (s, 2H), 6.98 (d, *J* = 9.2 Hz, 1H), 7.30-7.42 (m, 5H), 8.19 (dd, *J* = 9.2 Hz, *J* = 2.4 Hz, 1H), 8.25 (d, *J* = 2.4 Hz, 1H), 8.44 (s, 1H)

^{13}C-NMR (101 MHz, $CDCl_3$) δ (ppm) 61.93, 117.22, 118.92, 128.1, 128.31, 129.12, 136.50, 139.21, 164.45, 168.71

IR: $\nu_{C=N}$ = 1649 cm^{-1}, ν_{C-O} = 1128 cm^{-1}, ν_{NO_2}= 1246 and 1605 cm^{-1}

LC-MS (CH_3CN:H_2O (1:1 *v/v*)): $t_{r\ PDA}$ = 1.90 min, $t_{r\ 254\ nm}$ = 1.90 min; [**L**^{5}+H]$^+$ *m/z*$_{calc}$ = 257.1, *m/z*$_{exp}$ = no detection

ESI-MS (MeOH; - 100 V): [**L**^{5}-H]$^-$ *m/z*$_{calc}$ = 255.1, *m/z*$_{exp}$ = 255.0

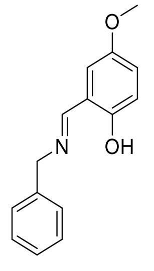

L^6

2-[[(phenylmethyl)imino]phenyl]-4-methoxy-phenol:

Prepared from the *general procedure **B*** from 2-hydroxy-5-methoxybenzaldehyde (Aldrich, 98%) and benzylamine to give 2-[[(phenylmethyl)imino]phenyl]-4-methoxy-phenol **L^6** (859.2 mg, 3.56 mmol, **quantitative yield**) as a yellow powder. Reaction time: 3 hours at 80 °C.

Characterization

^{1}H-NMR (400 MHz, $CDCl_3$) δ (ppm) 3.72 (s, 3H), 4.75 (s, 2H), 6.74 (d, *J* = 2.4 Hz, 1H), 6.84-6.89 (m, 2H), 7.20-7.32 (m, 5H), 8.34 (s, 1H), 12.82 (s, 1H)

^{13}C-NMR (101 MHz, $CDCl_3$) δ (ppm) 56.09, 63.42, 115.12, 117.89, 118.60, 119.52, 127.48, 127.90, 128.80, 138.16, 152.15, 155.36, 165.44

IR: $\nu_{C=N}$ = 1634 cm^{-1}, ν_{C-O} = 1160 cm^{-1}, $\nu_{C-O\ (ether)}$ = 1028 $^{cm-1}$, $\nu_{O-H\ (intramolecular)}$ = 2847-3090 cm^{-1}

LC-MS (CH_3CN:H_2O (1:1 *v/v*)): $t_{r\ PDA}$ = 1.93 min, $t_{r\ 254\ nm}$ = 1.93 min; [**L**^{6}+H]$^+$ *m/z*$_{calc}$ = 242.1, *m/z*$_{exp}$ = 242.1

ESI-MS (MeOH; + 50 V): [**L**^{6}+H]$^+$ *m/z*$_{calc}$ = 242.1, *m/z*$_{ecp}$ = 242.1

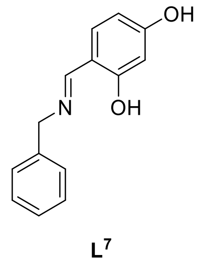

L^7

2-[[(phenylmethyl)imino]phenyl]-5-hydroxy-phenol:

Prepared from the *general procedure **A*** from 2,4-dihydroxybenzaldehyde (Sigma Aldrich, 98%) and benzylamine to give 2-[[(phenylmethyl)imino]phenyl]-5-hydroxy-phenol **L^7** (792.9 mg, 3.49 mmol, **48%**) as an orange powder. Reaction time: 2 hours at reflux.

Optimization of the conditions[176]

2,4-dihydroxybenzaldehyde (505.7 mg, 3.66 mmol, 1 equiv.) and benzylamine (411 mg, 419.4 µL, 3.84 mmol, 1.05 equiv.) were dissolved in dry THF (5 mL) and 4Å molecular sieves (4.0 g) were added to remove formed water during the reaction. The mixture was reflux for 2 hours. Molecular sieves were removed by filtration and the solution was then evaporated. The obtained product was recrystallized from toluene:MeOH (1:1 *v/v*). Finally, 2-[[(phenylmethyl)imino]phenyl]-5-hydroxy-phenol **L^7** was obtained (282.6 mg, 1.24 mmol, **34%**) as an orange powder.

Characterization

^{1}H-NMR (400 MHz, $(CD_3)_2CO$) δ (ppm) 4.77 (s, 2H), 6.32 (d, *J* = 2.4 Hz, 1H), 6.39 (dd, *J* = 8.4 Hz, *J* = 2.4 Hz, 1H), 7.25 (d, *J* = 8.4 Hz, 1H), 7.28-7.36 (m, 5H), 8.53 (s, 1H)

^{13}C-NMR (75 MHz, $(CD_3)_2CO$) δ (ppm) 63.01, 103.59, 107.85, 113.13, 128.06, 128.7, 129.50, 134.38, 140.22, 162.64, 166.56, 206.21

IR: $\nu_{C=N}$ = 1594 cm^{-1}, $\nu_{C\text{-}O}$ = 1165 cm^{-1}

LC-MS ($CH_3CN:H_2O$ (1:1 *v/v*)): $t_{r\ PDA}$ = 1.59 min, $t_{r\ 254\ nm}$ = 1.60 min; [**L^7**+H]$^+$ m/z_{calc} = 228.1, m/z_{exp} = 228.1

ESI-MS (MeOH; + 100 V): [**L^7**+H]$^+$ m/z_{calc} = 228.1, m/z_{exp} = 228.1

II.5.2.2. Synthesis and characterization of the metal complexes

Metal salts (provider, quality) used for the syntheses are listed below:

Cobalt(II) acetate (Co(acetate)$_2$), Alfa Aesar, > 98%, anhydrous
Cobalt(II) acetate, tetrahydrate (Co(acetate)$_2$.4H_2O), Alfa Aesar, 98%
Cobalt(II) chloride, hexahydrate ($CoCl_2.6H_2O$), Sigma, 98.0-102.0%
Cobalt(II) perchlorate, hexahydrate ($Co(ClO_4)_2.6H_2O$), Fluka, cryst., purum. p.a.
Cobalt(II) sulfate, heptahydrate ($Co(SO_4)_2.7H_2O$), Prolabo, p.a. for analysis

Manganese(II) acetate, tetrahydrate (Mn(acetate)$_2$.4H_2O), Janssen, > 99%, min 22.5% Mn
Manganese(II) chloride, tetrahydrate ($MnCl_2.4H_2O$), Alfa Aesar, 99.0%, cryst.
Manganese(II) perchlorate, hydrate ($Mn(ClO_4)_2.xH_2O$), Aldrich, 99%
Manganese(II) sulfate, heptahydrate ($Co(SO_4)_2.7H_2O$), Merck, cryst.

II.5.2.2.1. First strategy of synthesis

General procedure **C** for preparation of cobalt(II) and manganese(II) complexes:[145,146]

The ligand (**L^1-L^7**) (2 equiv.) was dissolved in an appropriate solvent. After complete dissolution, the cobalt(II) or the manganese(II) salt (1 equiv.) was added and the solution was stirred at r.t. or was heated over a given period.

---

[176] Chesnut, R. W.; Cesati, R. R.; Cutler, C. S.; Pluth, S. L.; Katzenellenbogen, J. A. *Organometallics* **1998**, *17* (22), 4889–4896.

General procedure **D** for preparation of cobalt(II) and manganese(II) complexes using a one pot route:

The aldehyde (2 equiv.) and the benzylamine (2 equiv.) were dissolved in an appropriate solvent. After complete dissolution, the cobalt(II) or the manganese(II) salt (1 equiv.) was added and the solution was stirred at r.t. or under heating.

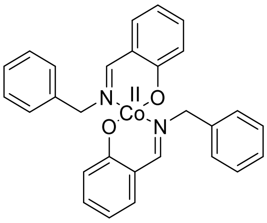

1Co

***Bis*{2-[[(phenylmethyl)imino]methyl]-phenolato} cobalt(II):**

Prepared from the *general procedure **C*** from 2-[[(phenylmethyl)imino]methyl]-phenol **L**^{1}. The following Table II-21 depicts the experimental conditions (solvent, temperature) and the metal salts that were used.

Table II-21: Screening of conditions for bis*{2-[[(phenylmethyl)imino]methyl]-phenolato} cobalt(II)* ***1Co*** *synthesis from 2-[[(phenylmethyl)imino]methyl]-phenol* ***L**^{1}**.*

Entry	Cobalt(II) salt, reactant	Solvent	Duration	T (°C)	Work-up	Results
1	$CoCl_2.6H_2O$	EtOH	1 h	r.t.	Slowly evaporated for 5 days then filtered and washed with cold EtOH	Co^{III}(**L**^{1})$_3$
2*	Co(acetate)$_2$ + $NaHCO_3$ (4 equiv.)	Degassed EtOH	15 min	78 °C	Precipitated with degassed distilled water, filtered and washed with EtOH	**L**^{1}
3	$Co(SO_4)_2.7H_2O$ + 0.1 M NaOH (pH adjusted to 7-8)	H_2O	1.5 h	100 °C	Filtrated and washed with H_2O	Co^{III}(**L**^{1})$_3$

* under argon atmosphere

Prepared from the *general procedure **D*** from 2-hydroxybenzaldehyde and benzylamine. The following Table II-22 depicts the experimental conditions (solvent, temperature) and the metal salts that were used.

Table II-22: Screening of conditions for bis*{2-[[(phenylmethyl)imino]methyl]-phenolato} cobalt(II)* ***1Co*** *one-pot synthesis from 2-hydroxybenzaldehyde and benzylamine.*

Entry	Cobalt(II) salt, reactant	Solvent	Duration	T (°C)	Work-up	Results
1	$CoCl_2.6H_2O$	CD_3OD		r.t.	Filtrated and washed with cold EtOH	$Co^{III}(\mathbf{L^1})_3$
2	Co(acetate)$_2$	EtOH	2 h at 50 °C then 1 h at r.t.		Filtrated and washed with cold EtOH	$Co^{III}(\mathbf{L^1})_3$
3	Co(acetate)$_2$	$EtOH:H_2O$ (9:1 *v/v*)*	1 h	r.t.	Slowly evaporated for 5 days	$Co^{III}(\mathbf{L^1})_3$
4	$Co(ClO_4)_2.6H_2O$	EtOH	55.5 h	r.t.	Filtrated and washed with cold EtOH	$Co^{III}(\mathbf{L^1})_3$
5	$Co(SO_4)_2.7H_2O$	EtOH	55.5 h	r.t.	Filtrated and washed with cold EtOH	L + $Co^{II}(\mathbf{L^1})_2$ +$Co^{III}(\mathbf{L^1})_3$**
6	**Co(acetate)$_2$**	**Solvent-free*** **	**15 min**	**r.t.**	**Filtrated and washed with cold MeOH**	**$Co^{II}(\mathbf{L^1})_2$ (87%)**

* **L**^{1} was dissolved in EtOH. After dissolution, cobalt(II) salt, previously solubilised in water was added to the mixture.

** Results confirmed by HRMS

*** Salicylaldehyde and benzylamine were placed to react without solvent to give the corresponding ligand. After 2 hours of reaction, the cobalt(II) salt freshly dissolved in a small volume of MeOH was added to the mixture.

Characterization

IR: $\nu_{C=N}$ = 1604 cm^{-1}, ν_{C-O} = 1188 cm^{-1}
ESI-MS (EtOH, + 250 V): [**1Co**+Na]$^+$ m/z_{calc} = 502.1, m/z_{exp} = 502.2
HRMS: [$Co^{III}(\mathbf{L^1})_2$]$^+$ m/z_{calc} = 479.1169, m/z_{exp} = 479.1138
[**1Co**+Na]$^+$ m/z_{calc} = 502.1068, m/z_{exp} = 502.1041
[**1Co**+K]$^+$ m/z_{calc} = 518.0807, m/z_{exp} = 518.0773
Microanalysis: calc: 70.14% C, 5.05% H, 5.84% N; found: 70.35% C, 5.01% H, 5.90% N
EPR: - *Measurements done at r.t. as a powder and in solution (toluene):* no signal was recorded due to the too fast relaxation times of cobalt(II) species.

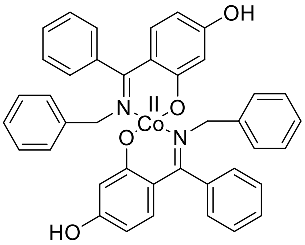

2Co

Bis{2-[phenyl[(phenylmethyl)imino]methyl]-5-hydroxy-phenolato} cobalt(II):

Prepared from the *general procedure* ***C*** from 2-[phenyl[(phenylmethyl)imino]methyl]-5-hydroxy-phenol **L**^{2}. The following Table II-23 depicts the experimental conditions (solvent, temperature) and the metal salt that was used.

Table II-23: Screening of conditions for bis*{2-[phenyl[(phenylmethyl)imino]methyl]-5-hydroxy-phenolato} cobalt(II)* ***2Co*** *synthesis from 2-[phenyl[(phenylmethyl)imino]methyl]-5-hydroxy-phenol* ***L²*.**

Entry	Cobalt(II) salt, reactant	Solvent	Duration	T (°C)	Work-up	Results
1	Co(acetate)$_2$	EtOH	2 h	50 °C	Filtrated and washed with cold EtOH	Not desired product*
2	Co(acetate)$_2$	EtOH	16.5 h	50 °C	Slowly evaporated for 5 days	No isolated product

* Results confirmed by microanalysis

Characterization

The targeted complex **2Co** was not obtained.

A first batch of *bis*{2-[phenyl[(phenylmethyl)imino]methyl]-5-hydroxy-phenolato} cobalt(II) **2Co-1** was provided by Clariant and analyzed.

Characterization

ESI-MS (dioxane:H_2O (1:1 *v/v*); + 235 V): $[\mathbf{L^2}+H]^+$ m/z_{calc} = 304.1, m/z_{exp} = 304.2
$[\mathbf{2Co\text{-}1}+H]^+$ m/z_{calc} = 664.2, m/z_{exp} = 664.3

Microanalysis: **2Co-1** calc: 72.39% C, 4.86% H, 4.22% N; found: 78.55% C, 5.58% H, 4.55% N
L² calc: 79.19% C, 5.65% H, 4.62% N
If it is considered that the sample is only composed of complex **2Co-1** and ligand **L²**, **2Co-1**:**L²** 1:9 calc: 78.51% C, 5.57% H, 4.58% N

A second batch of *bis*{2-[phenyl[(phenylmethyl)imino]methyl]-5-hydroxy-phenolato} cobalt(II) **2Co-2** was re-synthesized and provided by Clariant.

2,4-dihydroxybenzophenone (64.20 g, 299.69 mmol, 1 equiv.) and toluenesulfonic acid monohydrate (0.03 equiv.) were dissolved at r.t. in toluene (100 g). Benzylamine (1.1 equiv.) was added to the solution at 29 °C. The formed water during the reaction was removed by a water separation system. The very viscous solution was stirred at r.t. for one night. Then cobalt(II) acetate tetrahydrate (0.5 equiv.) was added and the mixture was heated at 85 °C for 5 hours. The yellow-orange resultant suspension was filtered and washed with EtOH. The obtained product was then washed with water and dried under vacuum. *Bis*{2-[phenyl[(phenylmethyl)imino]methyl]-5-hydroxy-phenolato} cobalt(II) **2Co-2** was obtained as a light-green powder.

Characterization

ESI-MS (dioxane:H_2O (1:1 *v/v*); + 235 V): $[\mathbf{L^2}+H]^+$ m/z_{calc} = 304.1, m/z_{exp} = 304.2
$[\mathbf{2Co\text{-}2}+H]^+$ m/z_{calc} = 664.2, m/z_{exp} = 664.3

Microanalysis: **2Co-2** calc: 72.39% C, 4.86% H, 4.22% N; found: 77.25% C, 5.47% H, 4.45% N
L² calc: 79.19% C, 5.65% H, 4.62% N
If it is considered that the sample is only composed of complex **2Co-2** and ligand **L²**, **2Co-2**:**L²** 28:72 calc: 77.29% C, 5.43% H, 4.51% N

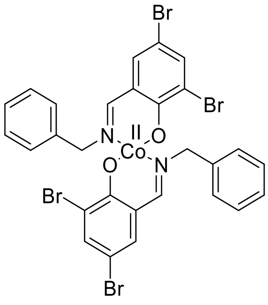

3Co

Bis{2-[[(phenylmethyl)imino]phenyl]-4,6-dibromo-phenolato} cobalt(II):

Prepared from the *general procedure **C*** from 2-[[(phenylmethyl)imino]phenyl]-4,6-dibromo-phenol **L³**. The following Table II-24 depicts the experimental conditions (solvent, temperature) and the metal salt that was used.

Table II-24: Screening of conditions for bis*{2-[[(phenylmethyl)imino]phenyl]-4,6-dibromo-phenolato} cobalt(II)* ***3Co*** *synthesis from 2-[[(phenylmethyl)imino]phenyl]-4,6-dibromo-phenol* ***L³.***

Entry	Cobalt(II) salt, reactant	Solvent	Duration	T (°C)	Work-up	Results
1[145]	$CoCl_2.6H_2O$	EtOH	1 h	r.t.	Slowly evaporated for 10 days	$Co^{III}(\mathbf{L^3})_3$

Characterization

The targeted complex **3Co** was not obtained.

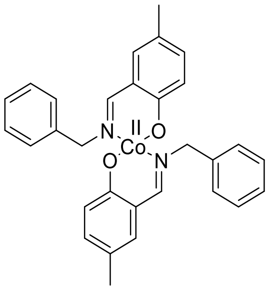

4Co

Bis{2-[[(phenylmethyl)imino]phenyl]-4-methyl-phenolato} cobalt(II):

Prepared from the *general procedure **C*** from 2-[[(phenylmethyl)imino]phenyl]-4-methyl-phenol **L⁴**. The following Table II-25 depicts the experimental conditions (solvent, temperature) and the metal salt that was used.

Table II-25: Screening of conditions for bis*{2-[[(phenylmethyl)imino]phenyl]-4-methyl-phenolato} cobalt(II)* ***4Co*** *synthesis from 2-[[(phenylmethyl)imino]phenyl]-4-methyl-phenol* ***L⁴.***

Entry	Cobalt(II) salt, reactant	Solvent	Duration	T (°C)	Work-up	Results
1[146]	$CoCl_2.6H_2O$	EtOH	30 min	r.t.	Slowly evaporated for 10 days	$Co^{III}(\mathbf{L^4})_3$

Characterization

The targeted complex **4Co** was not obtained.

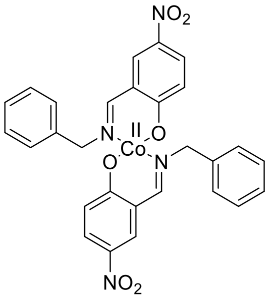

5Co

Bis{2-[[(phenylmethyl)imino]phenyl]-4-nitro-phenolato} cobalt(II):

Prepared from the *general procedure **C*** from 2-[[(phenylmethyl)imino]phenyl]-4-nitro-phenol **L**^{5}. The following Table II-26 depicts the experimental conditions (solvent, temperature) and the metal salt that was used.

Table II-26: Screening of conditions for bis*{2-[[(phenylmethyl)imino]phenyl]-4-nitro-phenolato} cobalt(II)* ***5Co*** *synthesis from 2-[[(phenylmethyl)imino]phenyl]-4-nitro-phenol **L**^{5}.*

Entry	Cobalt(II) salt, reactant	Solvent	Duration	T (°C)	Work-up	Results
1	$CoCl_2.6H_2O$	EtOH	3 h	80 °C	Cooled down to r.t., slowly evaporated for 4 days and washed with cold EtOH	Co^{III}(**L**^{5})$_3$

Characterization

The targeted complex **5Co** was not obtained.

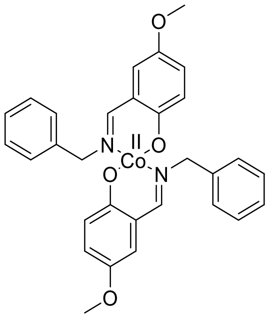

6Co

Bis{2-[[(phenylmethyl)imino]phenyl]-4-methoxy-phenolato} cobalt(II):

Prepared from the *general procedure **C*** from 2-[[(phenylmethyl)imino]phenyl]-4-methoxy-phenol **L**^{6}. The following Table II-27 depicts the experimental conditions (solvent, temperature) and the metal salts that were used.

Table II-27: Screening of conditions for bis{2-[[(phenylmethyl)imino]phenyl]-4-methoxy-phenolato} cobalt(II) ***6Co*** *synthesis from 2-[[(phenylmethyl)imino]phenyl]-4-methoxy-phenol* ***L^6.***

Entry	Cobalt(II) salt, reactant	Solvent	Duration	T (°C)	Work-up	Results
1	$CoCl_2.6H_2O$	EtOH	25.5 h	50 °C	Cooled down to r.t., filtered and washed with cold EtOH	$Co^{III}(\mathbf{L^6})_3$
2*	Co(acetate)$_2$	MeOH	10 min	r.t.	Rapidly cooled down, filtered and washed with cold MeOH	$Co^{III}(\mathbf{L^6})_3$
3*	Co(acetate)$_2$	MeOH:H_2O (1:1 *v/v*)	10 min	0 °C		**
4*	Co(acetate)$_2$	MeOH:H_2O (1:0.75 *v/v*)	5 min	0 °C	Filtrated and washed with cold MeOH	$\mathbf{L^6}$
5*	Co(acetate)$_2$	MeOH	5 min	r.t.	Solvent was evaporated	$\mathbf{L^6}$
6*	Co(acetate)$_2$	MeOH	5 min	r.t.	Pentane was added to precipitate obtained complex and solution was cooled down for one night at 4 °C, filtered and washed with cold MeOH	$Co^{III}(\mathbf{L^6})_3$
7	Co(acetate)$_2$	dioxane	10 min	r.t.	Cooled down for one night at 4 °C and slowly evaporated for 10 days	$Co^{III}(\mathbf{L^6})_3$

* under argon atmosphere

** **L^6** was not soluble in this reaction condition and reaction was stopped before reactants started to react.

Prepared from the *general procedure **D*** from 2-hydroxy-5-methoxybenzaldehyde and benzylamine. The following Table II-28 depicts the experimental conditions (solvent, temperature) and the metal salt that was used.

Table II-28: Screening of conditions for bis{2-[[(phenylmethyl)imino]phenyl]-4-methoxy-phenolato} cobalt(II) ***6Co*** *one-pot synthesis from 2-hydroxy-5-methoxybenzaldehyde and benzylamine.*

Entry	Cobalt(II) salt, reactant	Solvent	Duration	T (°C)	Work-up	Results
1	Co(acetate)$_2$	Solvent-free*	30 min	r.t.	Cooled down during one night at 4 °C, filtered and washed with cold MeOH	$Co^{III}(\mathbf{L^6})_3$

* 2-hydroxy-5-methoxybenzaldehyde and benzylamine were placed to react without solvent to give the corresponding ligand (2 hours at 60 °C). After this time, cobalt(II) salt previously dissolved in MeOH was added.

Characterization

The targeted complex **6Co** was not obtained.

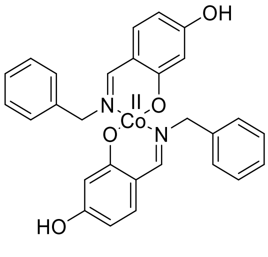

7Co

_Bis_{2-[[(phenylmethyl)imino]phenyl]-5-hydroxy-phenolato} cobalt(II):

Prepared from the *general procedure **C*** from 2-[[(phenylmethyl)imino]phenyl]-5-hydroxy-phenol **L**^{7}. The following Table II-29 depicts the experimental conditions (solvent, temperature) and the metal salt that was used.

Table II-29 : Screening of conditions for bis*{2-[[(phenylmethyl)imino]phenyl]-5-hydroxy-phenolato} cobalt(II)* ***7Co*** *synthesis from 2-[[(phenylmethyl)imino]phenyl]-5-hydroxy-phenol* ***L**^{7}**.***

Entry	Cobalt(II) salt, reactant	Solvent	Duration	T (°C)	Work-up	Results
1	$CoCl_2.6H_2O$	MeOH	25 h	50 °C	Cooled down to r.t., filtered and washed with cold MeOH	Co^{III}(**L**^{7})$_3$

Characterization

The targeted complex **7Co** was not obtained.

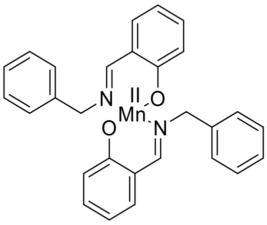

1Mn

Bis{2-[[(phenylmethyl)imino]methyl]-phenolato} manganese(II):

Prepared from the *general procedure **C*** from 2-[[(phenylmethyl)imino]methyl]-phenol **L**^{1}. The following Table II-30 depicts the experimental conditions (solvent, temperature) and the metal salt that was used.

Table II-30: Screening of conditions for bis*{2-[[(phenylmethyl)imino]methyl]-phenolato} manganese(II)* ***1Mn*** *synthesis from 2-[[(phenylmethyl)imino]methyl]-phenol* ***L**^{1}**.***

Entry	Manganese(II) salt, reactant	Solvent	Duration	T (°C)	Work-up	Results
1	$MnCl_2.4H_2O$	EtOH	23 h	50 °C	Slowly evaporated for 5 days	No isolated product
2	$MnCl_2.4H_2O$	EtOH:H_2O (9:1 *v/v*)*	1 h	r.t.	Cooled down in an ice bath	No isolated product

* **L**^{1} was dissolved in EtOH. After complete dissolution, manganese(II) salt, previously solubilised in water was added to the mixture.

Prepared from the *general procedure **D*** from 2-hydroxybenzaldehyde and benzylamine. The following Table II-31 depicts the experimental conditions (solvent, temperature) and the metal salts that were used.

Table II-31: Screening of conditions for bis*{2-[[(phenylmethyl)imino]methyl]-phenolato} manganese(II)* ***1Mn*** *one-pot synthesis from 2-hydroxybenzaldehyde and benzylamine.*

Entry	Manganese(II) salt, reactant	Solvent	Duration	T (°C)	Work-up	Results
1	Mn(acetate)$_2$.4H$_2$O	EtOH	2 h	50 °C	Filtrated	No isolated product
2	MnCl$_2$.4H$_2$O	EtOH	23 h	50 °C	Slowly evaporated for 5 days	**L^1**
3	MnCl$_2$.4H$_2$O	EtOH:H$_2$O (9:1 *v/v*)*	1 h	r.t.	Cooled down in an ice bath	No isolated product
4	Mn(ClO$_4$)$_2$.xH$_2$O	EtOH	55.5 h	r.t.		No isolated product
5	Mn(SO$_4$)$_2$.H$_2$O	EtOH	55.5 h	r.t.	Filtrated, washed with cold EtOH	L + Mn^{II}(**L^1**)$_2$ + Mn^{III}(**L^1**)$_3$**

* Ligand was dissolved in EtOH. After complete dissolution, cobalt(II) salt, previously solubilised in water was added to the mixture.

** Results confirmed by HRMS

Characterization

The targeted complex **1Mn** was not obtained.

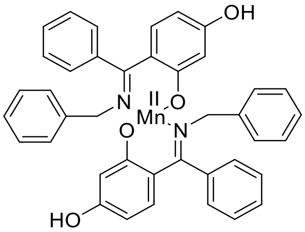

2Mn

Bis{2-[phenyl[(phenylmethyl)imino]methyl]-5-hydroxy-phenolato} manganese(II):

Prepared from the *general procedure* ***D*** from 2,4-dihydroxybenzophenone and benzylamine. The following Table II-32 depicts the experimental conditions (solvent, temperature) and the metal salt that was used.

Table II-32: Screening of conditions for bis*{2-[phenyl[(phenylmethyl)imino]methyl]-5-hydroxy-phenolato} manganese(II)* ***2Mn*** *one-pot synthesis from 2,4-dihydroxybenzophenone and benzylamine.*

Entry	Manganese (II) salt, reactant	Solvent	Duration	T (°C)	Work-up	Results
1	MnCl$_2$.4H$_2$O	EtOH	16.5 h	50 °C	Slowly evaporated for 5 days	No isolated product

Characterization

The targeted complex **2Mn** was not obtained.

II.5.2.2.2. Second strategy of synthesis

General procedure **E** for preparation of cobalt(II) and manganese(II) template complexes:[147]

Cobalt(II) or manganese(II) acetate (1 equiv.) was dissolved in EtOH by heating the solution at 70 °C for 20 minutes. After complete dissolution, the aldehyde (2 equiv.), previously dissolved in EtOH, was added dropwise at r.t. and the mixture was stirred at r.t. for one day. The obtained product was filtered, washed with chloroform and dried on a heat chamber at 70 °C for one day.

General procedure **F** for preparation of cobalt(II) and manganese(II) complexes:

The template complex (1 equiv.) (*i.e.* cobalt(II) or manganese(II) complex with aldehyde) and benzylamine (2.5 equiv., Alfa Aesar, > 98%) were condensed in an appropriate solvent under argon atmosphere. The mixture was stirred for 5 minutes at r.t.. The obtained product was filtered, washed with cold solvent and dried on a heat chamber at 70 °C for one day.

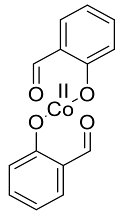

1aCo

***Bis*{2-formylphenolato} cobalt(II):**

Prepared from the *general procedure **E*** from 2-hydroxybenzaldehyde (Alfa Aesar, 99%) to give *bis*{2-formylphenolato} cobalt(II) **1aCo** (971 mg, 3.22 mmol, **54%**) as an orange-red powder.

Characterization

IR: $\nu_{C\text{-}O}$ = 1145 cm^{-1}, $\nu_{C=O\ \text{intramolecular}}$ = 1620 cm^{-1}

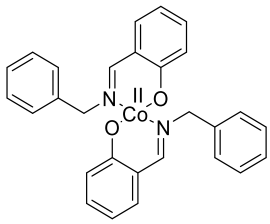

1Co

***Bis*{2-[[(phenylmethyl)imino]methyl]-phenolato} cobalt(II):**

Prepared from the *general procedure **F*** from *bis*{2-formylphenolato} cobalt(II) **1aCo** to give *bis*{2-[[(phenylmethyl)imino]methyl]-phenolato} cobalt(II) **1Co** (24.5 mg, 0.05 mmol, **15%**). Solvent: EtOH

Characterization

IR: $\nu_{C=N}$ = 1604 cm^{-1}, $\nu_{C\text{-}O}$ = 1145 cm^{-1}

ESI-MS (MeOH; + 150 V): [**1Co**+H]$^+$ m/z_{calc} = 480.1, m/z_{exp} = 480.3

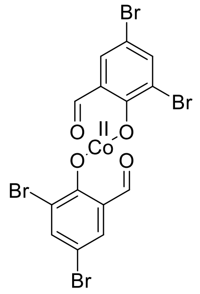

3aCo

Bis{2,4-dibromo-6-formylphenolato} cobalt(II):

Prepared from the *general procedure* ***E*** from 3,5-dibromosalicyladehyde (Aldrich, 98%) to give *bis*{2,4-dibromo-6-formylphenolato} cobalt(II) **3aCo** (2.699 g, 4.38 mmol, **73%**) as an orange-red powder.

Characterization

IR: $\nu_{C\text{-}O}$ = 1135 cm^{-1}, $\nu_{C=O\ \text{intramoléculaire}}$ = 1640 cm^{-1}, ν_{Br} = 719 cm^{-1}
ESI-MS (MeOH; + 300 V): [**3aCo**+Na]$^+$ *m/z*$_{\text{calc}}$= 639.6, *m/z*$_{\text{exp}}$ = 639.8

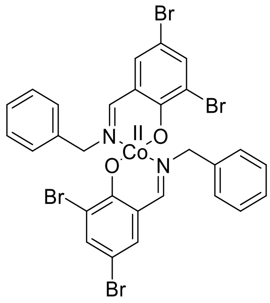

3Co

Bis{2-[[(phenylmethyl)imino]phenyl]-4,6-dibromo-phenolato} cobalt(II):

Prepared from the *general procedure* ***F*** from *bis*{2,4-dibromo-6-formylphenolato} cobalt(II) **3aCo** to give *bis*{2-[[(phenylmethyl)imino]phenyl]-4,6-dibromo-phenolato} cobalt(II) **3Co** (124.3 mg, 0.16 mmol, **96%**) as a yellow-orange powder. Solvent: CH_3CN.

Characterization

IR: $\nu_{C=N}$ = 1612 cm^{-1}, $\nu_{C\text{-}O}$ = 1141 cm^{-1}, ν_{Br} = 700 cm^{-1}
ESI-MS (MeOH; + 200 V): [**3Co**+H]$^+$ *m/z*$_{\text{calc}}$ = 795.8, *m/z*$_{\text{exp}}$ = 796.0

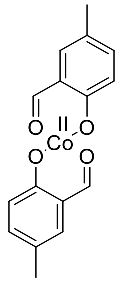

4aCo

***Bis*{2-formyl-4-methylphenolato} cobalt(II):**

Prepared from the *general procedure **E*** from 2-hydroxy-5-methylbenzaldehyde **L^4a** to give *bis*{2-formyl-4-methylphenolato} cobalt(II) **4aCo** (174 mg, 0.53 mmol, **33%**) as an orange powder.

Characterization

IR: $\nu_{C\text{-}O}$ = 1157 cm^{-1}, $\nu_{C=O\ \text{intramolecular}}$= 1639 cm^{-1}
ESI-MS (MeOH; + 150 V): [**4aCo**+H]$^+$ m/z_{calc} = 330.0, m/z_{exp} = 330.2

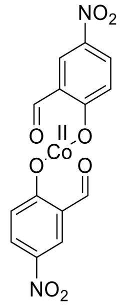

5aCo

***Bis*{2-formyl-4-nitrophenolato} cobalt(II):**

Prepared from the *general procedure **E*** from 2-hydroxy-5-nitrobenzaldehyde (Aldrich, 98%) to give *bis*{2-formyl-4-nitrophenolato} cobalt(II) **5aCo** (1.868 g, 4.78 mmol, **80%**) as a yellow-orange powder.

Characterization

IR: $\nu_{C\text{-}O}$ = 1135 cm^{-1}, $\nu_{C=O\ \text{intramolecular}}$ = 1640 cm^{-1}, ν_{NO_2}= 1245 and 1603 cm^{-1}

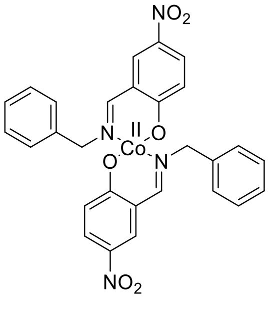

5Co

***Bis*{2-[[(phenylmethyl)imino]phenyl]-4-nitro-phenolato} cobalt(II):**

Prepared from the *general procedure **F*** from *bis*{2-formyl-4-nitrophenolato} cobalt(II) **5aCo** to give *bis*{2-[[(phenylmethyl)imino]phenyl]-4-nitro-phenolato} cobalt(II) **5Co** (268 mg, 0.47 mmol, **92%**) as an orange solid. Solvent: CH_3CN.

Characterization

IR: $\nu_{C=N}$ = 1625 cm^{-1}, $\nu_{C\text{-}O}$ = 1129 cm^{-1}, ν_{NO_2}= 1245 and 1596 cm^{-1}
ESI-MS (MeOH; + 400 V): [**5Co**+Na]$^+$ *m/z*$_{calc}$ = 592.1, *m/z*$_{exp}$ = 592.3

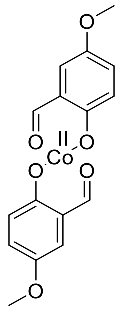

6aCo

***Bis*{2-formyl-4-methoxyphenolato} cobalt(II):**

Prepared from the *general procedure* ***E*** from 2-hydroxy-5-methoxybenzaldehyde to give *bis*{2-formyl-4-methoxyphenolato} cobalt(II) **6aCo** (1.449 g, 4.01 mmol, **67%**) as an orange powder.

Characterization

IR: $\nu_{C\text{-}O}$ = 1150 cm^{-1}, $\nu_{C=O\ \text{intramolecular}}$= 1635 cm^{-1}, $\nu_{C\text{-}O\ \text{ether}}$ = 1036 cm^{-1}
ESI-MS (MeOH; + 100 V): [**6aCo**+H]$^+$ *m/z*$_{calc}$ = 362.0, *m/z*$_{exp}$ = 362.1

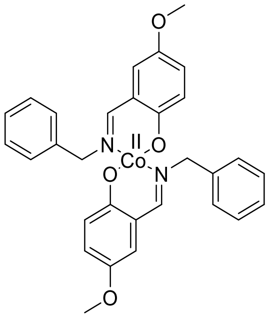

6Co

***Bis*{2-[[(phenylmethyl)imino]phenyl]-4-methoxy-phenolato} cobalt(II):**

Prepared from the *general procedure* ***F*** from *bis*{2-formyl-4-methoxyphenolato} cobalt(II) **6aCo** to give *bis*{2-[[(phenylmethyl)imino]phenyl]-4-methoxy-phenolato} cobalt(II) **6Co** (65 mg, 0.12 mmol, **22%**) as an orange solid. Solvent: CH_3CN.

Characterization

IR: $\nu_{C=N}$ = 1606 cm^{-1}, $\nu_{C\text{-}O}$ = 1146 cm^{-1}, $\nu_{C\text{-}O\ \text{ether}}$ = 1026 cm^{-1}
ESI-MS (MeOH; + 200 V): [Co^{III}(**L**^{6})$_2$]$^+$ *m/z*$_{calc}$= 539.1, *m/z*$_{exp}$ = 539.1 Complexes were probably oxidized quickly in methanol, acetonitrile or dioxane solution or also ionized by oxidation in ESI-MS conditions.

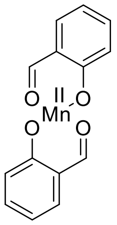

1aMn

***Bis*{2-formylphenolato} manganese(II):**

Prepared from the *general procedure **E*** from salicylaldehyde to give *bis*{2-formylphenolato} manganese(II) **1aMn** (1.258 g, 4.23 mmol, **71%**) as a yellow powder.

Characterization

IR: $\nu_{C\text{-}O}$ = 1155 cm^{-1}, $\nu_{C=O\ \text{intramolecular}}$ = 1647 cm^{-1}

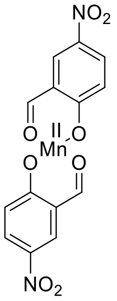

5aMn

***Bis*{2-formyl-4-nitroxyphenolato} manganese (II):**

Prepared from the *general procedure **E*** from 2-hydroxy-5-nitrobenzaldehyde to give *bis*{2-formyl-4-nitroxyphenolato} manganese (II) **5aMn** (565 mg, 1.46 mmol, **49%**) as a yellow-orange powder.

Characterization

IR: $\nu_{C\text{-}O}$ = 1174 cm^{-1}, $\nu_{C=O\ \text{intramolecular}}$ = 1639 cm^{-1}, ν_{NO_2}= 1242 and 1599 cm^{-1}

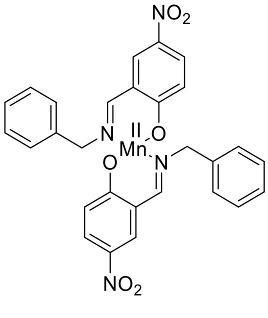

5Mn

***Bis*{2-[[(phenylmethyl)imino]phenyl]-4-nitro-phenolato} manganese(II):**

Prepared from the *general procedure **F*** from *bis*{2-formyl-4-nitroxyphenolato} manganese (II) **5aMn** to give *bis*{2-[[(phenylmethyl)imino]phenyl]-4-nitro-phenolato} manganese(II) **5Mn** (128 mg, 0.23 mmol, **88%**) as an orange solid. Solvent: EtOH.

Characterization

IR: $\nu_{C=N}$ = 1633 cm^{-1}, $\nu_{C\text{-}O}$ = 1178 cm^{-1}, ν_{NO_2} = 1244 and 1594 cm^{-1}

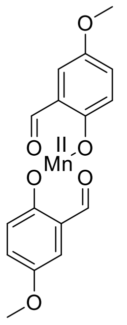

6aMn

***Bis*{2-formyl-4-methoxyphenolato} manganese (II):**

Prepared from the *general procedure **E*** from 2-hydroxy-5-methoxybenzaldehyde (Aldrich, 98%) to give *bis*{2-formyl-4-methoxyphenolato} manganese (II) **6aMn** (161 mg, 0.45 mmol, **23%**) as an orange powder.

Characterization

IR: $\nu_{C\text{-}O}$ = 1148 cm^{-1}, $\nu_{C=O\ \text{intramolecular}}$ = 1643 cm^{-1}, $\nu_{C\text{-}O\ \text{ether}}$ = 1027 cm^{-1}
ESI-MS (MeOH; + 100 V): [**6aMn**+H]$^+$ m/z_{calc} = 358.0, m/z_{exp} = 358.1

II.5.2.2.3. Characterization of the commercially available complexes

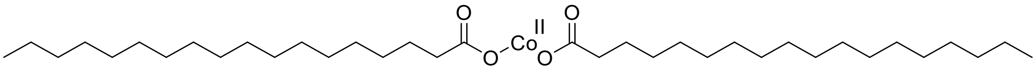

9Co

Cobalt(II) stearate:

Commercially available (Alfa Aesar, Co 9-10%) **9Co-1**

Characterization

Microanalysis: calc: 69.09% C, 11.27% H, 0.00% N; found: 66.72% C, 10.90% H, 0.00% N
EPR: - *Measurement at r.t. as a powder and in solution (in toluene):* no signal was recorded due to too fast relaxation times of cobalt(II) species.
- *Measurement at 4 K as a powder:* the recorded spectrum was characteristic of a high spin (S = 3/2) cobalt(II) species.

IR: $\nu_{\mathrm{C-H\ (CH_3)}}$= 2956 cm^{-1}, $\nu_{\mathrm{C-H\ asym.\ (CH_2)}}$ = 2916 cm^{-1}, $\nu_{\mathrm{C-H\ sym.\ (CH_2)}}$ = 2850 cm^{-1}, $\nu_{\text{stearic acid}}$ = 1690 cm^{-1}, $\nu_{\mathrm{COO^-\ asym.}}$ = 1557 cm^{-1}, $\delta_{\mathrm{C-H\ (CH_2)}}$= 1467 cm^{-1}, $\nu_{\mathrm{COO^-\ sym.}}$ = 1410 cm^{-1}, $\delta_{\mathrm{C-H\ (CH_2)}}$= 720 cm^{-1}

One batch of cobalt(II) stearate **9Co-2** was also provided by Clariant and was characterized.

Characterization

Microanalysis: calc: 69.09% C, 11.27% H, 0.00% N; found: 67.26% C, 10.99% H, 0.00% N
IR: $\nu_{\mathrm{C-H\ asym.\ (CH_2)}}$ = 2916 cm^{-1}, $\nu_{\mathrm{C-H\ sym.\ (CH_2)}}$ = 2850 cm^{-1}, $\nu_{\text{stearic acid}}$ = 1686 cm^{-1}, $\nu_{\mathrm{COO^-\ asym.}}$ = 1557 cm^{-1}, $\nu_{\mathrm{COO^-\ sym.}}$ = 1410 cm^{-1}

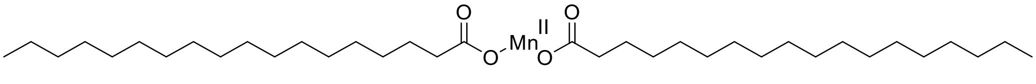

9Mn

Manganese(II) stearate:[126]

Stearic acid (1 equiv., 1.42 g, 5 mmol, Merck, ≥ 97%, for synthesis) was melted at 80-85 °C (melting point = 67-72 °C) and then sodium hydroxide (1 equiv. 0.25 M, 20 mL, 5 mmol, BDH AnalaR, ≥ 98%) was added dropwise under agitation for one hour. No purification of the obtained Na(stearate) was performed. A solution of manganese chloride hexahydrate (0.5 equiv., 0.2 M, 12.5 mL, 2.5 mmol, Alfa Aesar, 99.0%, cryst.) was prepared and added dropwise to the solution of sodium stearate, previously prepared. The reaction temperature was maintained at 80-85 °C with continuous stirring. The solid product was filtered and washed with hot water to remove sodium chloride. Finally, the manganese(II) stearate **9Mn-1** was dried under vacuum and obtained (**quantitative** yield) as a white powder.

Characterization

Microanalysis: calc: 69.53% C, 11.35% H, 0.00% N; found: 66.92% C, 11.12% H, 0.00% N

EPR: - *Measurement at r.t. as a powder:* broad line centred at *g* = 2.008 with a line width of 220 G, with an approximately Lorentzian form. This broad line can be attributed to low spin (S = ½) manganese(II) species.

- *Measurement at r.t. in solution:* any spectrum could be recorded because no appropriate solvent could be found until now to solubilize manganese(II) stearate **9Mn**.
- *Measurement at low temperature (4 to 15 K) as a powder:* the recorded signal was characteristic of a high spin (S = 5/2) manganese(II) species. By decreasing the temperature (from 15 to 4 K), the line width was increasing and *g* factor was changing. This comportment was due to a low ferromagnetic coupling with an ordering temperature comprised between 5 and 10 K. This ordering temperature was closely related to the synthesis way.

IR: $\nu_{\mathrm{C-H\ (CH_3)}}$= 2955 cm^{-1}, $\nu_{\mathrm{C-H\ asym.\ (CH_2)}}$ = 2917 cm^{-1}, $\nu_{\mathrm{C-H\ sym.\ (CH_2)}}$ = 2850 cm^{-1}, $\nu_{\text{stearic acid}}$ = 1686 cm^{-1}, $\nu_{\mathrm{COO^-\ asym.}}$ = 1563 cm^{-1}, $\delta_{\mathrm{C-H\ (CH_2)}}$= 1463 cm^{-1}, $\nu_{\mathrm{COO^-\ sym.}}$ = 1428 cm^{-1}, $\delta_{\mathrm{C-H\ (CH_2)}}$= 718 cm^{-1}

One batch of manganese(II) stearate **9Mn-2** was also provided by Clariant and was characterized.

Characterization

Microanalysis: calc: 69.53% C, 11.35% H, 0.00% N; found: 68.09% C, 11.13% H, 0.00% N

IR: $\nu_{\mathrm{C-H\ asym.\ (CH_2)}}$ = 2916 cm^{-1}, $\nu_{\mathrm{C-H\ sym.\ (CH_2)}}$ = 2850 cm^{-1}, $\nu_{\text{stearic acid}}$ = 1685 cm^{-1}, $\nu_{\mathrm{COO^-\ asym.}}$ = 1560 cm^{-1}, $\nu_{\mathrm{COO^-\ sym.}}$ = 1425 cm^{-1}

Optimization of the synthesis[153]

Stearic acid (2.994 g, 10 mmol, 1 equiv., Merck, ≥ 97%, for synthesis) was dissolved in MeOH and heated at 60 °C to favour a good solubility. A solution of tetramethylammonium hydroxide pentahydrate (1 equiv., Fluka, > 98%, purum) was added to the solution and the mixture was stirred for 15 minutes. Manganese(II) chloride, tetrahydrate (0.5 equiv., Alfa Aesar, 99.0%, cryst.), previously dissolved in MeOH, was then added dropwise with vigorous stirring. The white precipitate appearing with time was then filtered, washed with MeOH and dried on a heat chamber at 70 °C for one night. Manganese(II) stearate **9Mn-3** was then obtained (2.965 g, 4.77 mmol, **95%**) as a white powder.

Characterization

IR: $\nu_{\text{C−H asym. (CH}_2\text{)}}$ = 2914 cm^{-1}, $\nu_{\text{C−H sym. (CH}_2\text{)}}$ = 2849 cm^{-1}, $\nu_{\text{COO}^- \text{ asym.}}$ = 1569 cm^{-1}, $\nu_{\text{COO}^- \text{ sym.}}$ = 1411 cm^{-1} (less quantity compared to previous versions **9Mn-1** and **9Mn-2**)
Microanalysis: calc: 69.53% C, 11.35% H, 0.00% N; found: 66.86% C, 11.09% H, 0.83% N (due to the presence of remaining tetramethylammonium hydroxide)

Optimization of the purification conditions

- Filtration of the precipitate and washing with water

After having the white precipitate in the reaction mixture, it was filtered and washed with water.

Characterization

IR: $\nu_{\text{C−H asym. (CH}_2\text{)}}$ = 2917 cm^{-1}, $\nu_{\text{C−H sym. (CH}_2\text{)}}$ = 2850 cm^{-1}, $\nu_{\text{stearic acid}}$ = 1682 cm^{-1}, $\nu_{\text{COO}^- \text{ asym.}}$ = 1563 cm^{-1}, $\nu_{\text{COO}^- \text{ sym.}}$ = 1420 cm^{-1}

- Filtration of the precipitate and washing with MeOH

After having the white precipitate in the reaction mixture, it was filtered and washed three times with MeOH, for one hour each time.

Characterization

IR: $\nu_{\text{C−H asym. (CH}_2\text{)}}$ = 2914 cm^{-1}, $\nu_{\text{C−H sym. (CH}_2\text{)}}$ = 2849 cm^{-1}, $\nu_{\text{COO}^- \text{ asym.}}$ = 1569 cm^{-1}, $\nu_{\text{COO}^- \text{ sym.}}$ = 1413 cm^{-1}
Microanalysis: calc: 69.53% C, 11.35% H, 0.00% N; found: 69.20% C, 11.26% H, 0.00% N
EPR: - *Measurement at r.t. as a powder:* broad line centred at *g* = 2.008 with an approximately Lorentzian form. This broad line can be attributed to low spin (S = ½) manganese(II) species.

Chapter III:

Oxidation of organic additive models

III. Oxidation of organic additive models

This Ph.D. work was mainly aimed at unravelling the putative mechanism of complexation, oxygenation and activation of cobalt(II) complexes of interest for oxygen barriers applications. A putative mechanism was previously described by Cabani[108] (Scheme III-1). The different steps related to the metal catalysts (complexation and hydrolysis - steps **1** and **1’**, oxygenation - step **2** and activation - step **3**) have been then thoroughly examined in Chapter II. In this chapter, a step further will be reached by investigating the oxidation capacities of various substrates (step **6**). This is of crucial importance because, in the absence of sacrificial substrates, some of the cobalt(II) catalysts that we have considered were shown to undergo, in the course of the oxidation/activation processes, a conversion into more stable cobalt(III) trischelate species (*i.e.* seen in the previous chapter). These trivalent metal trischelates complexes are not reactive towards oxygen scavenging. The substrates, also called additives or sacrificial additives, should undergo a fast metal-catalysed oxidation in the presence of the activated metal catalysts to scavenge oxygen in a definitive manner.

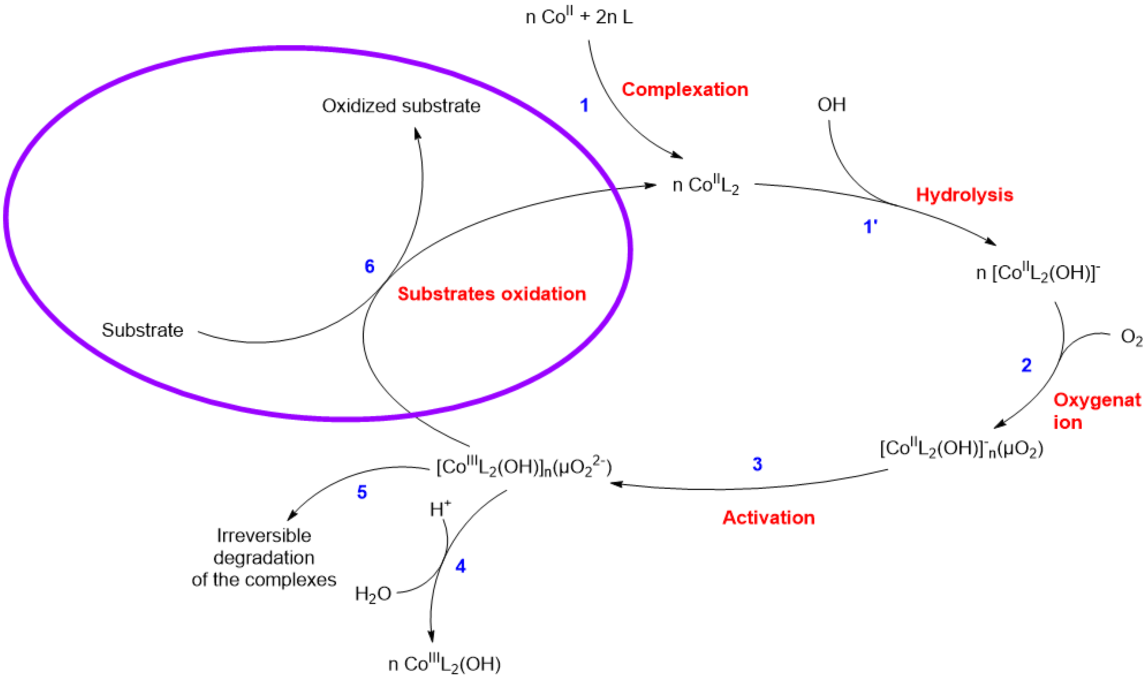

n Co^{II} + 2n L
1
Complexation
n $Co^{II}L_2$
OH
Hydrolysis
1'
n $[Co^{II}L_2(OH)]^-$
O_2
2
Oxygenation
$[Co^{II}L_2(OH)]^-_n(\mu O_2)$
3
Activation
$[Co^{III}L_2(OH)]_n(\mu O_2^{2-})$
5
Irreversible degradation of the complexes
H^+
4
H_2O
n $Co^{III}L_2(OH)$
Oxidized substrate
6
Substrates oxidation
Substrate

*Scheme III-1: Putative mechanism of complexation, oxygenation and activation of cobalt(II) complexes. The main steps are noted **1** to **6**. Adapted from Cabani.*

III.1. Oxidation of substrates with either metal catalysts or strong oxidants

Oxidation of organic substrates can be carried out either by using a strong organic oxidant or by activation of oxygen assisted by metal catalysts. The metal-catalysed aerobic oxidation of substrates will be reviewed hereafter with metal catalysts of interest in the context of this project, namely cobalt(II)/manganese(II) Schiff bases complexes, cobalt(II) *bis*(acetylacetonate) and cobalt(II)/manganese(II) *bis*(stearate) (also called metal stearate).

III.1.1. Metal-catalysed aerobic oxidation

Interest was first focused on cobalt(II) and manganese(II) catalysts displaying either acetylacetonate, Schiff bases or stearate binding ligands, used to oxidize organic substrates.

III.1.1.1. Acetylacetonate complexes

In 2001, the group of Mastrorilli[117] described that, under the same experimental conditions, the use of the cobalt(II)(acac)$_2$ considerably enhanced the efficacies of alcohols oxidation with respect to the same experiments conducted in the absence of metal catalysts (*i.e.* improvement of the yields, (1): 4 to 96%, (2) 20 to 82% and (3) 22 to 82%, respectively, Scheme III-2).

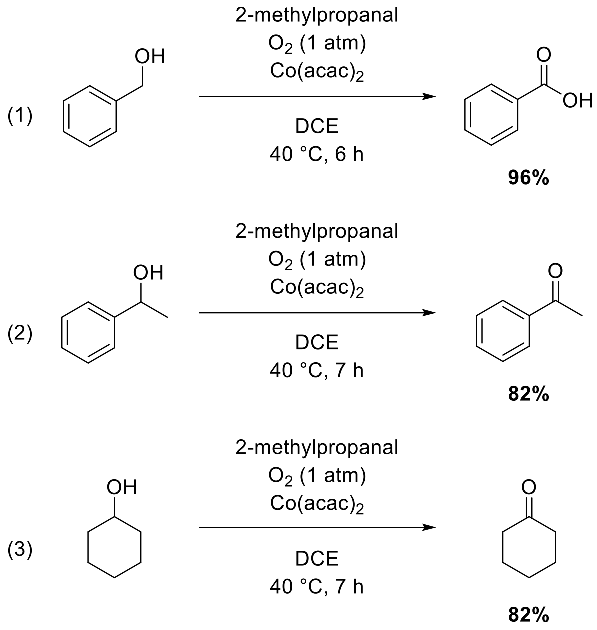
(1)
OH
2-methylpropanal
O2 (1 atm)
Co(acac)2
DCE
40 °C, 6 h
O
OH
96%
(2)
OH
2-methylpropanal
O2 (1 atm)
Co(acac)2
DCE
40 °C, 7 h
O
82%
(3)
OH
2-methylpropanal
O2 (1 atm)
Co(acac)2
DCE
40 °C, 7 h
O
82%

Scheme III-2: Oxidation of alcohols into ketones or carboxylic acid catalysed by cobalt(II)(acac)$_2$ and described by the group of Mastrorilli.

The same group demonstrated also in 2001[118] that in the presence of cobalt(II) catalyst (*i.e.* cobalt(II)(acac)$_2$), the oxidation of substituted phenols could be significantly improved as well. The yield of the desired product, 2,6-di-*tert*-butylcyclohexa-2,5-diene-1,4-dione, was enhanced from 1% to 61% by adding cobalt(II)(acac)$_2$ under the experimental conditions (Scheme III-3).

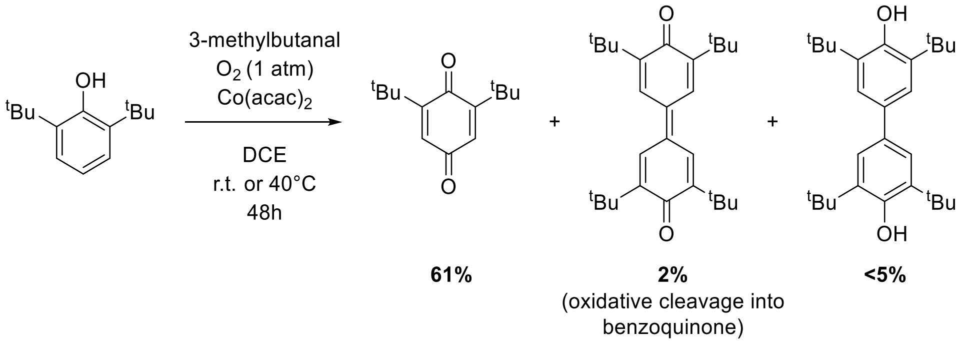
OH
tBu
tBu
3-methylbutanal
O2 (1 atm)
Co(acac)2
DCE
r.t. or 40°C
48h
O
tBu
tBu
O
61%
+
O
tBu
tBu
tBu
tBu
O
2%
(oxidative cleavage into benzoquinone)
+
OH
tBu
tBu
tBu
tBu
OH
<5%

*Scheme III-3: Oxidation of 2,6-di-*tert*-butylphenol catalysed by cobalt(II)(acac)$_2$ and described by the group of Mastrorilli.*

The use of cobalt(II)(acac)$_2$ as a versatile catalyst for the oxidation of a broad spectrum of substrates was highlighted six years before the work of the group of Mastrorolli by the reported investigation on the oxidation of α-hydroxyketones into α-diketones[121] (Scheme III-4).

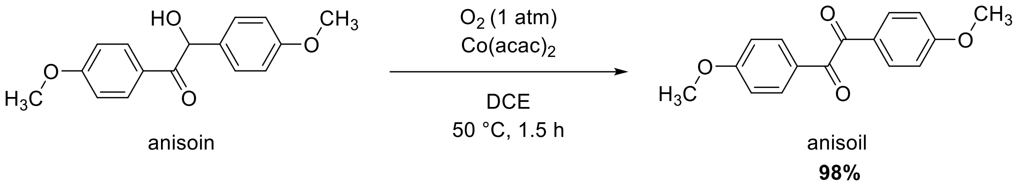

Scheme III-4: Oxidation of anisoin into anisoil catalysed by cobalt(II)(acac)$_2$ and described by Dell'Anna.

Similarly, in 1996 and 1997, the group of Ishii[115,119] also related the oxidation of alkanes using *N*-hydroxyphtalimide and cobalt(II)(acac)$_2$ into the corresponding ketones or di-carboxylic acids (Scheme III-5).

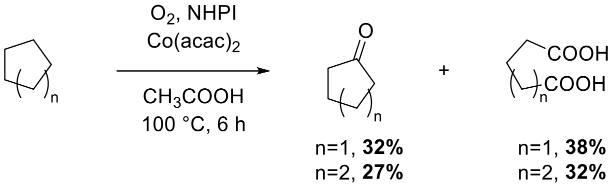

Scheme III-5: Oxidation of alkanes catalysed by cobalt(II)(acac)$_2$ described by Ishii, (NHPI: N*-hydroxyphtalimide).*

III.1.1.2. Schiff bases complexes

Another class of metal catalysts of interest in this Ph.D. work is the cobalt(II)/manganese(II) Schiff bases complexes. They are well known as efficient systems in catalysis and are most frequently quoted in the literature data than the acetylacetonate complexes.

For instance, oxidation of substituted phenols by cobalt(II)(salen) or derivatives was described in the literature.[71,72] More precisely, the oxidation of 2,6-di-*tert*-butylphenol or derivatives by cobalt(II)(salen) or derivatives was mainly related,[68,69,70,74,177] which is illustrated in Scheme III-6 for the oxidation of 2,6-di-*tert*-butylphenol at different temperatures performed by the group of Araki.[68]

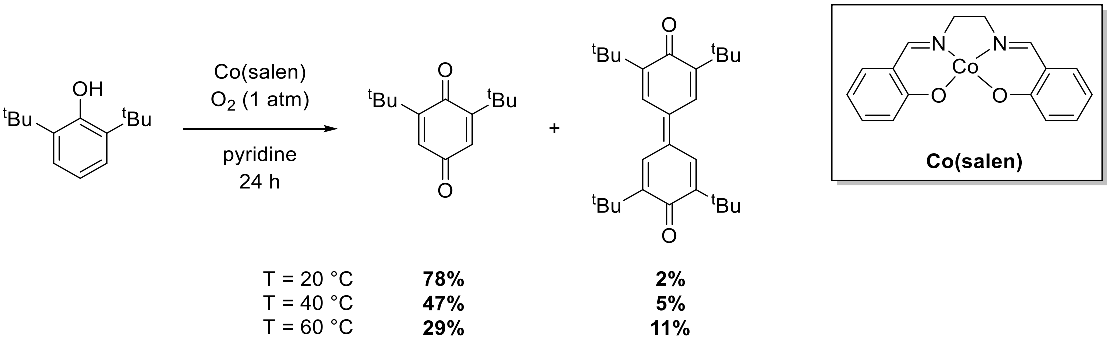

*Scheme III-6: Oxidation of 2,6-di-*tert*-butylphenol catalysed by cobalt(II)(salen) and described by the group of Araki.*

For its part, the group of Drago[77] reported in 1987 the oxidation of various alkenes into the corresponding alcohols and ketones. Scheme III-7 exemplifies the oxidation of hex-1-ene into hexan-2-one and hexan-2-ol catalysed by cobalt(II)SMDPT and oxygen.

---

[177] Nishinaga, A.; Tomita, H.; Matsuura, T. *Tetrahedron Lett.* **1979**, *31*, 2893–2896.

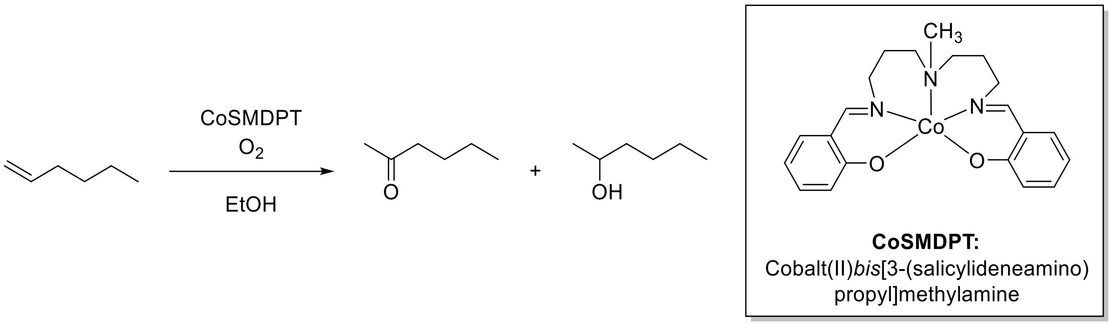
CoSMDPT
O_2
EtOH
O
OH
+
CH_3
N
N
N
Co
O
O
CoSMDPT:
Cobalt(II)*bis*[3-(salicylideneamino)
propyl]methylamine

Scheme III-7: Oxidation of hex-1-ene into hexan-2-one and hexan-2-ol catalysed by cobalt(II)SMDPT and described by the group of Drago.

The oxidative conversion of aldehydes can also be performed with the help of Schiff base cobalt(II) complexes and hydrogen peroxide as described by the group of Iwasawa.[78] An example of conversion of aldehyde into alcohol or peroxide can be seen on Scheme III-8.

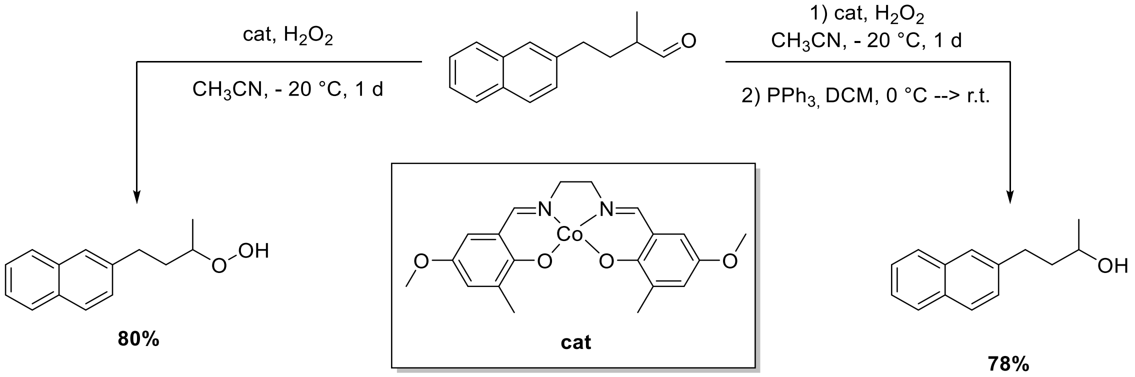
cat, H_2O_2
CH_3CN, - 20 °C, 1 d
1) cat, H_2O_2
CH_3CN, - 20 °C, 1 d
2) PPh_3, DCM, 0 °C --> r.t.
O
OH
80%
cat
OH
78%

Scheme III-8: Transformation of aldehyde into alcohol or hydroperoxide catalysed by cobalt(II) Schiff base complex and related by the group of Iwasawa.

Oxidation of amines has also been reported in the presence of cobalt(II)(salen) and derivatives with either oxygen or *tert*-butylhydroperoxide (*i.e.* TBHP).[69,79,80,81,82,83,84] For instance, the group of Jäger[69] related the oxidation of amine into nitroso or nitro groups. Two examples are described in Scheme III-9 with the support of Schiff base cobalt(II) or manganese(II) complexes.

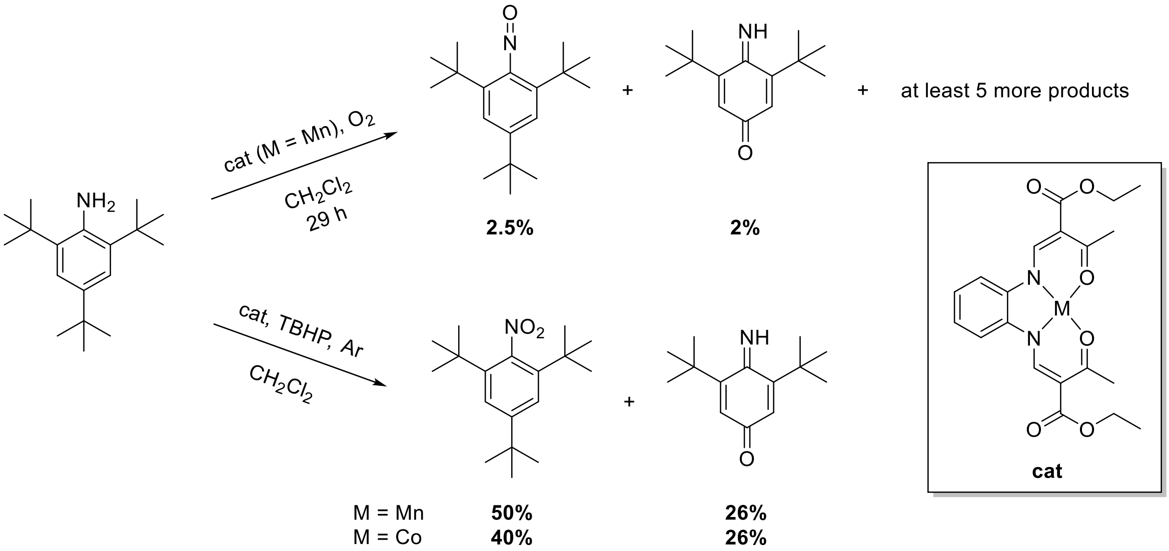
NH_2
cat (M = Mn), O_2
CH_2Cl_2
29 h
cat, TBHP, Ar
CH_2Cl_2
O
N
NH
O
+
+
at least 5 more products
2.5%
2%
NO_2
NH
O
+
M = Mn
M = Co
50%
40%
26%
26%
cat

*Scheme III-9: Oxidation of 2,4,6-tri-*tert*-butylaniline into 1,3,5-tri-*tert*-butyl-2-nitrosobenzene and 3,5-di-*tert*-butyl-4-iminocyclohexa-2,5-dien-1-one or 1,3,5-tri-*tert*-butyl-2-nitrobenzene and 3,5-di-*tert*-butyl-4-iminocyclohexa-2,5-dien-1-one catalysed by cobalt(II) and manganese(II) Schiff base catalysts and described by the group of Jäger; TBPH: *tert*-butylhydroperoxide.*

III.1.1.3. Stearate complexes

The last category of catalysts of interest that we would like to emphasize is the metal stearate complexes. The use of cobalt(II)/manganese(II) stearates as catalysts is by far less reported than the Schiff base or acac complexes mainly, due to their solubility issues.

Among the scarce investigations, cobalt(II) stearate was, however, employed either for the oxidation of linoleic acid,[123] hydrocarbons[124] or toluene (*i.e.* into benzoic acid)[125] (Scheme III-10).

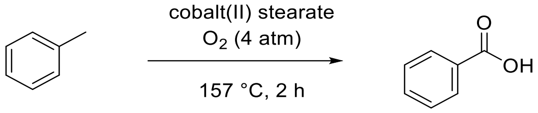

Scheme III-10: Oxidation of toluene into benzoic acid catalysed by cobalt(II) stearate as reported by Gizli.

It has also been reported that the degradation of HDPE can be catalysed either by cobalt(II) stearate[127] or by manganese(II) stearate.[126] It is the reason why the use of sacrificial additives is of crucial importance to preserve the integrity of the plastic materials.

III.1.2. Oxidation of organic additives of interest

After a brief review that related the use of given cobalt(II) or manganese(II) catalysts for the oxidation of a broad set of substrates, we will describe, in the following section, the oxidation, in the presence of selected metal catalysts, of several additives (*i.e.* organic substrates) of interest for Clariant (Scheme III-11). Before approaching the complexity of the masterbatches unit of Clariant (*i.e.* using simultaneously metal catalyst and additives in the solid state at high temperature), it was decided to focus, in a phased approach, on the oxidation of the sole additives. In this respect, the use of common oxidants as hydrogen peroxide (H_2O_2) or TBHP has been first tested. This approach would help us defining the class of additives that are more prone to easy oxidation and to establish a reactivity sequence. Oxidation of methylene benzylic or 2,2,6,6-tetramethylpiperidine (or TMP) functions has been realized. Model additives displaying such units have been therefore employed in this study (Scheme III-11). The synthesis and the characterization of the oxidized organic additives have been also performed and the proof of concept of oxidation of a selected additive in the presence of a given metal catalyst has been carried out at last.

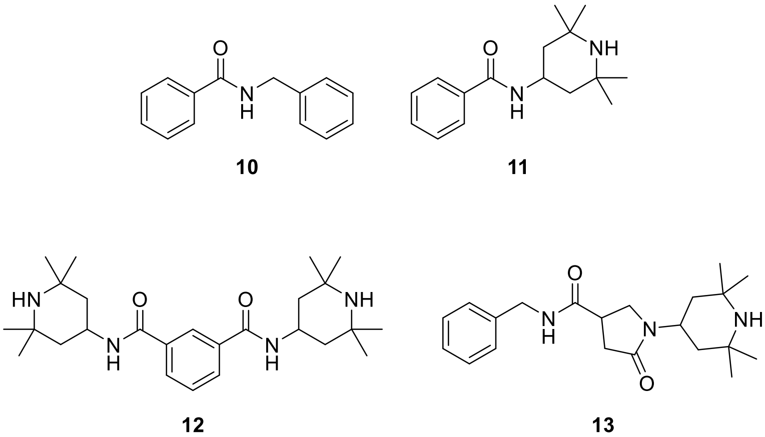

Scheme III-11: Organic model additives that have been investigated in this project.

III.2. Absorption spectrophotometry: a tool to monitor the oxidation of organic additives by oxidants

III.2.1. Oxidation of additives with H_2O_2 and TBHP

Three additives were selected (*N*-phenylmethylbenzamide **10**, *N*-(2,2,6,6-tetramethylpiperidin-4-yl)benzamide **11** and *N$_1$*,*N$_3$*-*bis*(2,2,6,6-tetramethylpiperidin-4-yl)-1,3-benzenedicarboxamide **12**) and were tested with 1 and 10 equivalents of H_2O_2 or TBHP during 3 days (Scheme III-12).

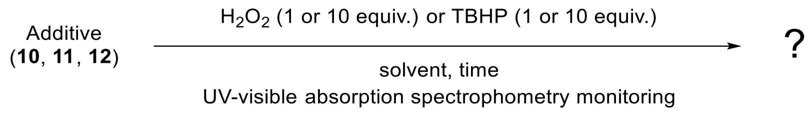
Additive
(**10**, **11**, **12**)
H_2O_2 (1 or 10 equiv.) or TBHP (1 or 10 equiv.)
solvent, time
UV-visible absorption spectrophotometry monitoring
?

*Scheme III-12: UV-visible absorption spectrophotometry monitoring of oxidation attempts of **10**, **11** and **12**.*

In fact, these oxidizing reagents were chosen because these two peroxides are commonly used and described in the literature as powerful oxidants in organic chemistry. The reactions were monitored by UV-visible absorption spectrophotometry.

For **10** (Figure III-1), no significant variations of the signal were observed after 3 days of oxidation, whether in the presence of H_2O_2 or TBHP as oxidants and whatever the number of equivalents (1 or 10 equiv.) added.

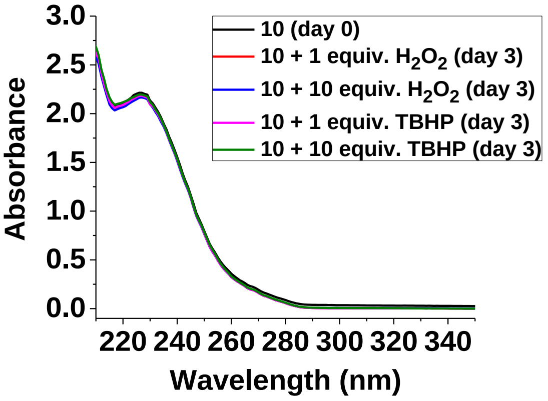

*Figure III-1: Oxidation of **10** with H_2O_2 (1 and 10 equiv.) and TBHP (1 and 10 equiv.) monitored by UV-visible absorption spectrophotometry; [**10**] = 9.70 x 10^{-5} M, solvent: CH_3CN:H_2O (1:1 v/v), l = 1 cm.*

For **11**, weak variations were observed after three days of reaction (Figure III-2) when using TBHP as oxidant and after a much longer time (about 20 days) when using H_2O_2 as oxidizing reagent (Figure III-3). However, the anticipated oxidation product for this type of model additives should be a nitroxide radical that is characterized by an absorption centred at ~ 450 nm. This absorption characteristics was not seen neither with TBHP (Figure III-2) nor with H_2O_2 (Figure III-3) leading us to conclude that **11** was not efficiently oxidized with these reagents under these experimental conditions.

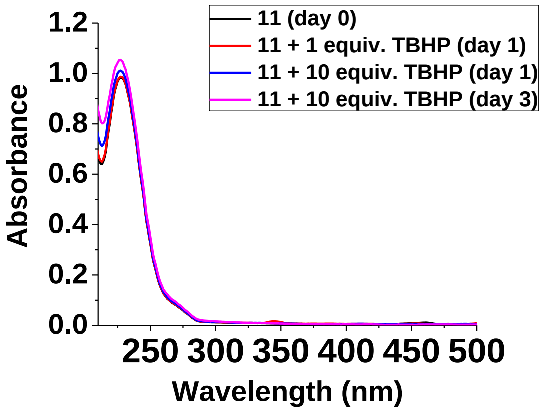

*Figure III-2: Oxidation of **11** with TBHP (1 and 10 equiv.) monitored by UV-visible absorption spectrophotometry; [**11**] = 1.05 x 10^{-4} M, solvent: $CH_3CN:H_2O$ (1:1 v/v), l = 1 cm.*

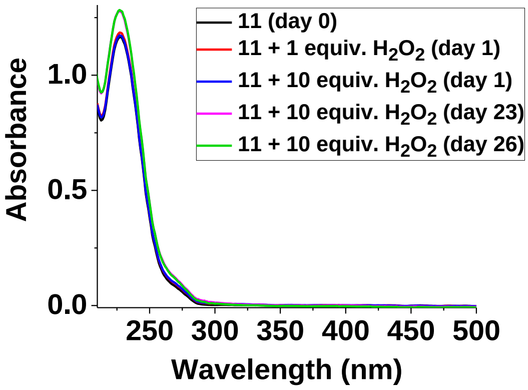

*Figure III-3: Oxidation of **11** with H_2O_2 (1 and 10 equiv.) monitored by UV-visible absorption spectrophotometry; [**11**] = 1.05 x 10^{-4} M, solvent: $CH_3CN:H_2O$ (1:1 v/v), l = 1 cm.*

With respect to the oxidation of **12** with H_2O_2 or TBHP monitored by UV-visible absorption mean (Figure III-4), the same observations, as previously done for **11**, can be drawn.

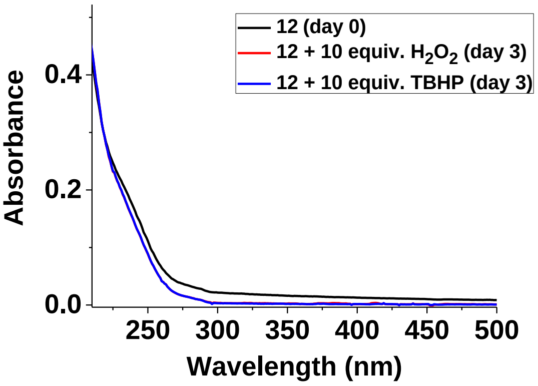

*Figure III-4: Oxidation of **12** with H_2O_2 (10 equiv.) and TBHP (10 equiv.) followed by UV-visible absorption spectrophotometry; [**12**] = 1.06 x 10^{-5} M, solvent: EtOH, l = 1 cm.*

It appeared that H_2O_2 or TBHP were not appropriate oxidants under these experimental conditions (*i.e.* efficiency and speed) to monitor with easiness the oxidation of the different additives.

III.2.2. Another alternative for the oxidation of the additives

The benzylic oxidation of *N*-phenylmethylbenzamide **10** into *N*-benzoylbenzamide **10.ox** (Scheme III-13) was reported in the literature[178,179,180,181,182,183,184] with yields ranging from 67 to 98%.

---

[178] Itoh, I.; Matsusaki, Y.; Fujiya, A.; Tada, N.; Miura, T.; Itoh, A. *Tetrahedron Lett.* **2014**, *55* (20), 3160–3162.

[179] Tada, N.; Ban, K.; Yoshida, M.; Hirashima, S.; Miura, T.; Itoh, A. *Tetrahedron Lett.* **2010**, *51* (47), 6098–6100.

[180] Nakayama, H.; Itoh, A. *Synlett* **2008**, No. 5, 675–678.

[181] Nicolaou, K. C.; Mathison, C. J. N. *Angew. Chem. Int. Ed.* **2005**, *44* (37), 5992–5997.

[182] Xu, L.; Zhang, S.; Trudell, M. L. *Chem. Commun.* **2004**, No. 14, 1668.

[183] Yu, H.; Chen, Y.; Zhang, Y. *Chin. J. Chem.* **2015**, *33* (5), 531–534.

[184] Yu, H.; Zhang, Y. *Eur. J. Org. Chem.* **2015**, *2015* (8), 1824–1828.

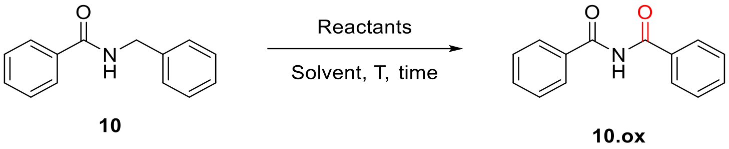

Scheme III-13:Oxidation of N-*phenylmethylbenzamide* ***10*** *into* N-*benzoylbenzamide* ***10.ox****.*

The related synthetic routes can be grouped into two categories: those using oxygen and photons (i.e. light) (Table III-1, Entries 1 to 3), and those employing metal catalysts (Table III-1, Entries 4 to 7).

The group of Itoh related the oxidation of **10** with molecular oxygen and a fluorescent lamp[178,179] (Table III-1, Entries 1 and 2) or a Xenon lamp[180] (Table III-1, Entry 3). Nevertheless, the use of fluorescent or Xenon lamp is not always easy to implement in a laboratory and not applicable in the context of this study.

Another synthetic route was described and used iodine catalyst[181] (Table III-1, Entry 4) or combination with chromium oxide[182] (Table III-1, Entry 5). The group of Yu described in 2015[183,184] the use of copper catalyst (Table III-1, Entries 6 and 7) for the efficient oxidation of **10**. From this brief literature survey, it therefore appeared that the oxidation of compound **10** is far of being an insurmountable problem, but the accessible methods usually relied on specific oxidizing reagents in combination with metal catalysts in most cases. Moreover, prior to the study of the oxidation of the organic additives in the presence of metal catalysts, our interest was focused on the oxidation of these additives by strong oxidants. Another synthetic strategy has therefore to be found.

Table III-1: Synthetic conditions of the oxidation of ***10*** *into* ***10.ox****.*

Entry	Reactants				Solvent	T (°C)	Time (h)	Yield (%)
1[178]	O_2	$h\nu$ (fluorescent lamp)	2-Cl-AQN (0.1 equiv.)		EtOAc	r.t.	70	**74**
2[179]	O_2	$h\nu$ (fluorescent lamp)	48% aq HBr (0.05 equiv.)	$Mg(OH)_2$ (0.025 equiv.)	EtOAc	r.t.	10	**95**
3[180]	O_2	$h\nu$ (500 W Xenon lamp)	I_2 (1.0 mol%)		EtOAc	r.t.	36	**67**
4[181]	DMP (2 equiv.)				PhF/DMSO	85	1	**98**
5[182]	H_5IO_6 (6 equiv.)	Ac_2O (6 equiv.)	CrO_3 (2.5 mol%)		CH_3CN	0	1	**92**
6[183]	CuBr (20 mol%)	TBHP (10 equiv.)	TEMPO (50 mol%)		CH_3CN	r.t.	8	**90**
7[184]	CuBr (20 mol%)	TBHP (9.0 equiv.)	$PhI(OAc)_2$ (50 mol%)	$CaCO_3$ (2.5 equiv.)	CH_3CN	r.t.	24	**75**

2-Cl-AQN: 2-chloroanthraquinone
DMP: Dess-Martin Periodinane
TEMPO: (2,2,6,6-tetramethylpiperidin-1-yl)oxyl

The oxidation of the secondary amine in the tetramethylpiperidine(TMP)-like compounds such as *N*-(2,2,6,6-tetramethylpiperidin-4-yl)benzamide **11**, N_1,N_3-*bis*(2,2,6,6-tetramethylpiperidin-4-yl)-1,3-benzenedicarboxamide **12** or 3-(*N*-phenylmethylcarboxamide)-1-(2,2,6,6-tetramethylpiperidin-4-yl)pyrrolidi-5-one **13** into corresponding nitroxide (*i.e.* TEMPO-like derivatives) is hardly described in the literature. In 2014, the group of Göbel[185] reported the preparation of *N*-[(2,2,6,6-tetramethylpiperidin-4-yl)oxy]benzamide **11.ox** from **11** under basic conditions (pH 10-12) with H_2O_2

---

[185] Seven, I.; Weinrich, T.; Gränz, M.; Grünewald, C.; Brüß, S.; Krstić, I.; Prisner, T. F.; Heckel, A.; Göbel, M. W. *Eur. J. Org. Chem.* **2014**, *2014* (19), 4037–4043.

in the presence of a catalytic amount of sodium tungstate in MeOH. As mentioned previously, the objective of this study in this section was to focus on the oxidation of the additives themselves without the use of any metal catalyst. However, in this reported study, sodium tungstate played the role of the metal catalyst. As done by the group of Rajca,[186] oxidation of 2,2,6,6-tetraethylpiperidin-4-ol into the corresponding nitroxide radical was performed in DCM with *meta*-chloroperoxybenzoic acid (designated as *m*-CPBA) (Scheme III-14). As this secondary amine is present on several model additives **11**, **12** and **13**), it was thus decided to use this protocol on the investigated additives.

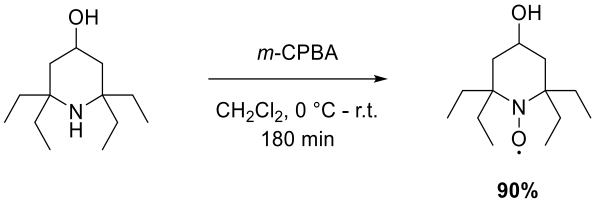

Scheme III-14: Oxidation of amine into nitroxide described by the group of Rajca.

III.2.2.1. Synthesis of the oxidized additives with meta-*chloroperoxybenzoic acid*

The four organic additives (**10**, **11**, **12** and **13**; although **10** is not based on TMP-like group,) were first oxidized with *m*-CPBA (2.2 equiv.) in DCM at r.t. for 3hours (Scheme III-15). The crude products were not purified and analysed by ESI-MS to evidence the formation of the oxidized products (Table III-2).

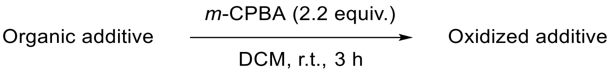

Scheme III-15: Oxidation of the organic additives with m-*CPBA.*

Interestingly, the benzylic oxidation of **10** into **10.ox** was observed under these experimental conditions (Table III-2, Entry 1). Regarding the oxidation of the secondary amines, **11**, was successfully transformed into the corresponding nitroxide **11.ox** (Table III-2, Entry 2). As **12** is bearing two secondary amine groups (*i.e.* TMP-like moiety), it can be oxidized once (mono-oxidized product, *N*^{1}-(2,2,6,6-tetramethylpiperidin-4-yl)-*N*^{3}-[(2,2,6,6-tetramethylpiperidin-4-yl)oxy]-1,3-benzenedicarboxamide **12.ox.a**) or twice (fully oxidized product, *N*^{1},*N*^{3}-*bis*[(2,2,6,6-tetramethylpiperidin-4-yl)oxy]-1,3-benzenedicarboxamide **12.ox.b**). The formation of the two oxidized products (**12.ox.a** and **12.ox.b**) was clearly characterized by ESI-MS (Table III-2, Entry 3). The last additive, **13**, displayed two different types of oxidation sites (secondary amine and benzylic position) leading to three potential oxidation products: oxidation of the TMP-like group into nitroxide (TEMPO-like) (3-(*N*-phenylmethylcarboxamide)-1-[(2,2,6,6-tetramethylpiperidin-4-yl)oxy]pyrrolidi-5-one **13.ox.a**), oxidation of the benzylic position (3-(*N*-benzoylcarboxamide)-1-(2,2,6,6-tetramethylpiperidin-4-yl)pyrrolidi-5-one **13.ox.b**) or a combination of both, it means oxidation of the amine and of the benzylic protons (3-(*N*-benzoylcarboxamide)-1-[(2,2,6,6-tetramethylpiperidin-4-yl)oxy]pyrrolidi-5-one **13.ox.c**). However, only the oxidation of the amine (**13.ox.a**) was observed by ESI-MS under these experimental conditions (Table III-2, Entry 4). To favour the oxidation of both sites of **13** (*i.e.* TMP-like and benzylic), the synthesis was repeated by increasing the amount of *m*-CPBA (4.4 equiv.), but the result was unaffected: only the oxidation of the TMP-like amine was detected by ESI-MS (**13.ox.a**).

---

[186] Paletta, J. T.; Pink, M.; Foley, B.; Rajca, S.; Rajca, A. *Org. Lett.* **2012**, *14* (20), 5322–5325

*Table III-2: Oxidation of the organic additives (**10**, **11**, **12** and **13**) with* m-CPBA.

Entry	Organic additive	Potential oxidized products	Observed products by ESI-MS
1	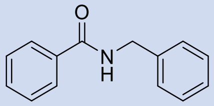 **10**	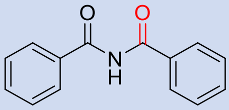 **10.ox**	[**10.ox**+Na]$^+$ m/z_{exp} = 248.1 m/z_{calc} = 248.1
2	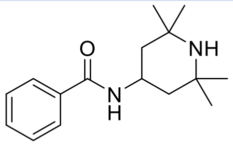 **11**	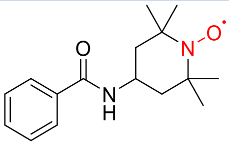 **11.ox**	[**11.ox***+Na]$^+$ m/z_{exp} = 298.2 m/z_{calc} = 298.2
3	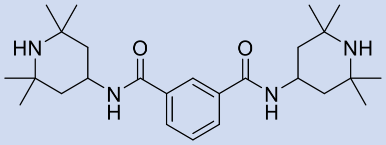 **12**	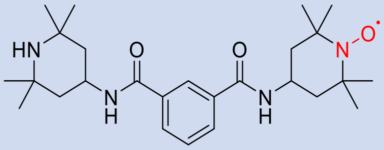 **12.ox.a** 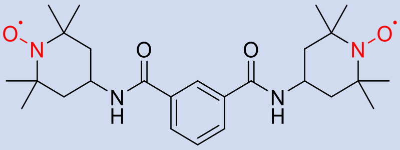 **12.ox.b**	[**12.ox.a***+H]$^+$ m/z_{exp} = 458.4 m/z_{calc} = 458.3 and [**12.ox.b****+H]$^+$ m/z_{exp} = 474.5 m/z_{calc} = 474.3 [**12.ox.b*****+Na]$^+$ m/z_{exp} = 495.5 m/z_{calc} = 495.3
4	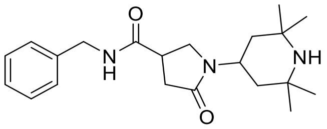 **13**	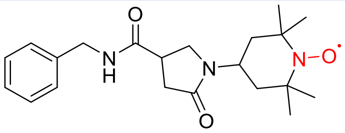 **13.ox.a** 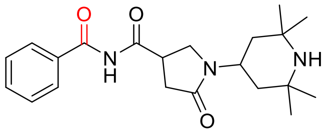 **13.ox.b** 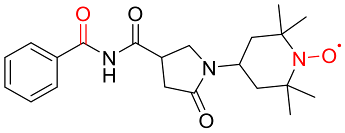 **13.ox.c**	[**13.ox.a**+Na]$^+$ m/z_{exp} = 395.4 m/z_{calc} = 395.2

* nitroxide radical was observed by ESI-MS as hydroxylamine
** one nitroxide radical was observed by ESI-MS as hydroxylamine
*** nitroxide radicals were observed by ESI-MS as hydroxylamines

The optimization of the syntheses and the purification of the obtained products were performed by Clariant to get some benchmarks of the oxidized compounds for our further studies. These pure oxidized products (**10.ox**, **11.ox**, **12.ox.b** and **13.ox.a**) were fully characterized by ESI-MS and EPR for the oxidized radical species (**11.ox**, **12.ox.b** and **13.ox.a**). In fact, as **11.ox**, **12.ox** and **13.ox** are carrying nitroxide radical groups, they are paramagnetic species and not suitable for NMR analysis. The recorded EPR spectra are defined by two main values, the *g* factor and the line width. The *g* factor is a positive number that characterizes the paramagnetic centre. It can be considered as a chemical shift as in NMR spectroscopy. The EPR spectra of the different compounds in hands were measured at r.t. directly on powder samples (Figure III-5). They displayed a transition centred at *g* ~ 2 that is characteristic of a nitroxide radical species (Table III-3). The study performed on the same samples in DCM solution at r.t. revealed more information (Figure III-6). In fact, the sub-structures were composed by three lines, corresponding to the hyperfine coupling between nitrogen atom (^{14}N, I = 1) and the unpaired electron. The *g* factor and the line width are given in Table III-3. For the biradical **12.ox.b** species, a magnetic coupling between the two radical was expected. In this case, the paramagnetic signature should be five lines with 1:2:3:2:1 intensities. Nevertheless, this sample presented only three lines of the same intensity, revealing no or very weak coupling between the two radical units, most likely due to the long distance between the two radical centres.

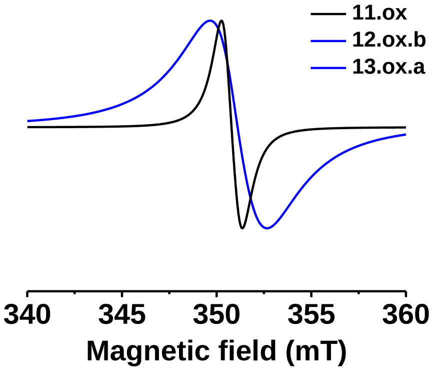

Figure III-5: EPR spectra of ***11.ox****,* ***12.ox.b*** *and* ***13.ox.a*** *at r.t. recorded on powders.*

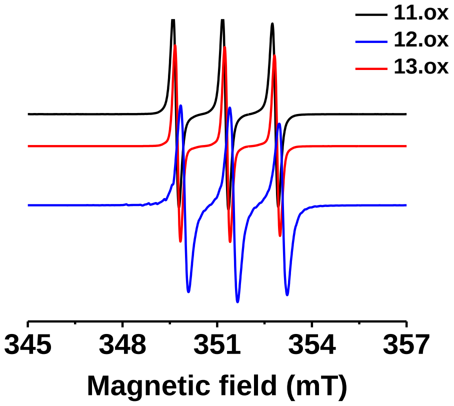

Figure III-6: EPR spectra of ***11.ox****,* ***12.ox.b*** *and* ***13.ox.a*** *at r.t. recorded on solutions; [****11.ox****] = 3.2 x* 10^{-3} *M, [****12.ox.b****] = 2.2 x* 10^{-3} *M, [****13.ox.a****] = 2.1 x* 10^{-3} *M, solvent: degassed DCM.*

Table III-3: EPR characterization of ***11.ox****,* ***12.ox.b*** *and* ***13.ox.a*** *at r.t. on powders and in DCM solutions.*

Oxidized additive	Powder measurements		Solution measurements	
	g factor	Line width (G)	*g* factor	Line width (G)
11.ox	2.006	15	2.005	1.6
12.ox.b	2.006	14	2.005	3.7
13.ox.a	2.005	30	2.005	1.6

III.2.2.2. Oxidation of additives with m-CPBA: kinetics monitoring by absorption spectrophotometry

The organic additives (**10**, **11**, **12** and **13**) and their corresponding oxidized additives (**10.ox**, **11.ox**, **12.ox.b** and **13.ox.a**) displayed marked difference in their UV-visible absorption spectra that allowed monitoring the course of the oxidation reaction as a function of time. In fact, the UV absorption of **10**, initially centred at 227 nm, underwent a bathochromic shift upon oxidation to 243 nm for **10.ox** as it can be observed on Figure III-7. For the additive containing the TMP-like amine moiety (**11**, **12** and **13**), no UV-visible spectral alteration was observed. However, their oxidized derivatives (**11.ox**, **12.ox.b** and **13.ox.a**) presented a broad absorption band in the visible region at ~ 450 nm (449 nm, Figure III-8; 447 nm, Figure III-9 and 449 nm, Figure III-10 for **11.ox**, **12.ox.b** and **13.ox.a**, respectively) that is characteristics of the nitroxide radicals. It is noteworthy that a weak absorption at 449 nm can be already seen for **11**, indicating that this additive was already partially oxidized. By a basic quantitative approach using the molar extinction coefficient (calibration) of **11.ox**, it was possible to evaluate that this additive **11** already contained ~ 10.5% of **11.ox** (mol%).

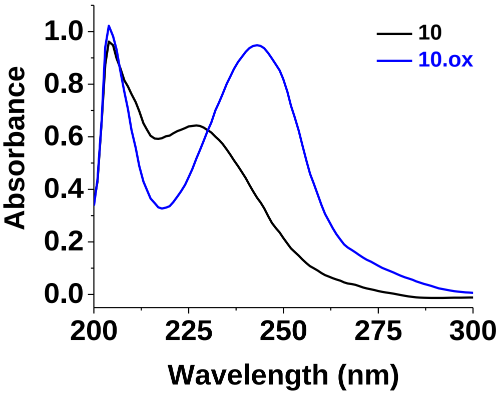

*Figure III-7: UV-visible absorption spectra of **10** and **10.ox**; [**10**] = [**10.ox**] = 2.0 x 10^{-5} M, solvent: MeOH, l = 1 cm.*

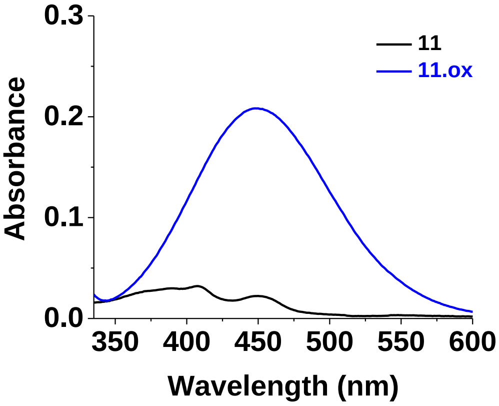

*Figure III-8: UV-visible absorption spectra of **11** and **11.ox**; [**11**] = [**11.ox**] = 2.0 x 10^{-2} M, solvent: MeOH, l = 1 cm.*

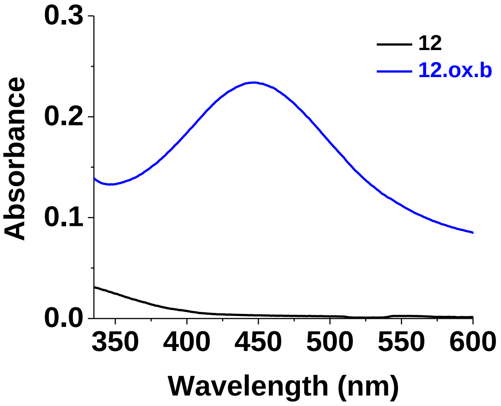

*Figure III-9: UV-visible absorption spectra of **12** and **12.ox.b**; [**12**] = [**12.ox.b**] = 2.0 x 10^{-2} M, solvent: MeOH, l = 1 cm.*

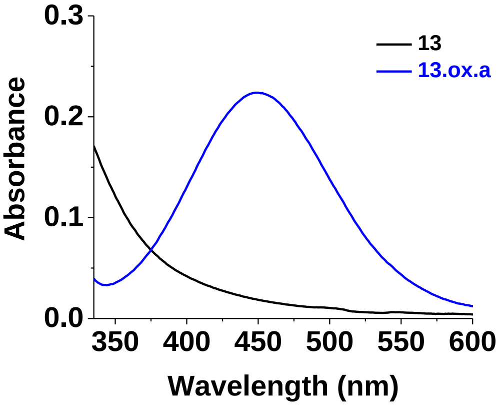

*Figure III-10: UV-visible absorption spectra of **13** and **13.ox.a**; [**13**] = [**13.ox.a**] = 2.0 x 10^{-2} M, solvent: MeOH, l = 1 cm.*

As noticeable spectral variations can be clearly observed between the starting organic additives **11**, **12** and **13** and their corresponding oxidized products, the monitoring of their oxidation reactions was performed by UV-visible absorption spectrophotometry. For example, Figure III-11 depicts the UV-visible absorption spectral variation of **11** in the presence of 5 equivalent of *m*-CPBA over time. An increase of the absorption at 450 nm can be observed in the course of the reaction and these variations are depicted in Figure III-12. The absorption at 450 nm (*i.e.* nitroxide absorption) followed an exponential variation as a function of time meaning that the reaction is first order with respect to the substrate (pseudo first-order conditions were used; [*m*-CPBA] >> [**11**]). The absorption variation with time was processed to obtain the half-life time of the oxidation reaction: $t_{1/2}$ = 1.8(2) min.

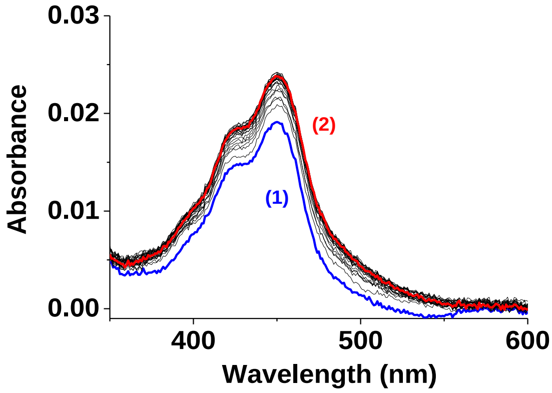

Figure III-11:UV-visible absorption spectrophotometric variations of ***11*** *with* m-CPBA *(5 equiv.) as a function of time;* ***(1)*** *t = 0,* ***(2)*** *t = 50 min, [****11****] = 7.71 x* 10^{-3}*M, solvent: EtOH, l = 1 cm.*

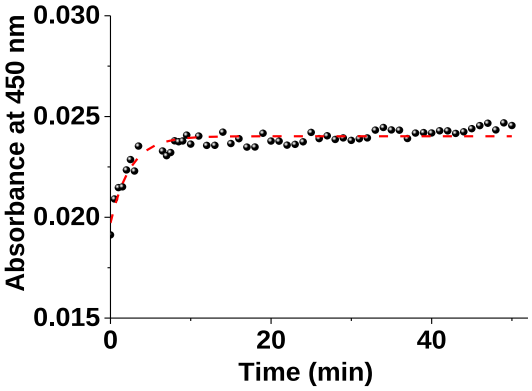

Figure III-12: Absorbance variation at 450 nm of ***11*** *with m-CPBA (5 equiv.) as a function of time; [****11****] = 7.71 x* 10^{-3}*M, solvent: EtOH, l = 1 cm.*

Using absorption spectrophotometry, the oxidation reactions of **11**, **12** and **13** were monitored in different solvents and with different [*m*-CPBA]/[substrate] ratios. For the sake of comparison, the results are gathered in Table III-4. Even though the oxidation kinetics seemed to be fast for all the additives, the reaction of **11** was not efficient (*i.e.* from 5 to 31% yield), but significantly higher than for the other additives (0.7 to 17% yield for the oxidation of **12** and 2 to 5% yield for the oxidation of **13**). Increase the concentration of *m*-CPBA had a real influence on the yield of the reaction: the more the amount of added *m*-CPBA was, the higher the yield was.

During the oxidation reaction of **12**, a two-step mechanism could be observed with a very first fast step followed by a second much slower one (*i.e.* proposed to be the successive oxidation of the two TMP-like units). The first step was too fast to be accurately processed (*i.e.* to determine the corresponding kinetics parameters). The yields given in Table III-4 for **12** are the overall yields (considering the two steps as a whole); the kinetics parameters ($t_{1/2}$) are given for the second slower step. If attention is paid on additives **11** and **12** that are closely related (*i.e.* **11** is carrying one reactive unit, whereas **12** possessed two), kinetics parameters cannot be straightforwardly compared as **12** revealed a two-step kinetics and only the kinetic parameters related to the second step were determined. However, in terms of effectiveness, oxidation of only one unit (**11**) led to the higher yields in ethanol. The solvent had also a clear impact on the oxidation reaction of our series of substrate (*i.e.* more efficient reactions in alcohols). In terms of speed of the reaction, the following sequence can be proposed: **12** (first oxidation) >> **13** > **11** >> **12** (second oxidation).

Table III-4: Yield and kinetics parameters for the oxidation of ***11****,* ***12*** *and* ***13*** *in the presence of* m-CPBA *in different solvents monitored by UV-visible absorption spectrophotometry.*

Solvent	*m*-CPBA (equiv.)	11		12*		13	
		Yield (%)	$t_{1/2}$ (min)	Yield (%)	$t_{1/2}$ (min)	Yield (%)	$t_{1/2}$ (min)
MeOH	25	5	6.9(2)	17	6.7(3)	5	2.5(3)
EtOH	3	*n.t.*	*n.t.*	0.7	231(77)	*n.t.*	*n.t.*
	5	28	1.8(2)	2	24(2)	2	0.30(4)
	10	31	2.6(2)	3	36(4)	2	0.19(5)
DCE	3	9	2.10(2)	5	~ 3500 (~ 58 h)	*n.t.*	*n.t.*

n.t.: not tested

** two-step mechanism: the first step was too fast to determine the corresponding kinetics parameters; yields are overall yields of the two steps; kinetics parameters are given for the second step*

The oxidized organic products being successfully synthesized and characterized, and their oxidation kinetics being determined, we then turned our efforts to monitor the aerobic oxidation of selected additives mediated by metal catalysts. Due to its good compromise between efficacy and speed, compound **11** was chosen for the following experiments.

III.3. Assisted-oxidation of organic additives with metal complexes

The interest of this study was to establish a proof-of-concept of the feasibility of the aerobic oxidation of organic additives by metal catalyst. As said previously, organic additive, **11**, was selected as well as two metal catalysts, the *bis*{2-[[(phenylmethyl)imino]methyl]-phenolato} cobalt(II) **1Co** and cobalt(II) stearate **9Co** (Scheme III-16). Substrate **11** was chosen because its efficient oxidation in ethanol in the presence of *m*-CPBA that is expected to facilitate the detection of oxidized product.

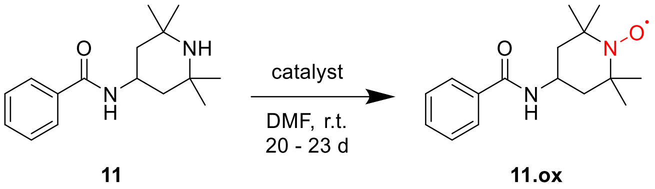

*Scheme III-16: Oxidation of **11** by metal catalyst.*

Substrate **11** was solubilised in dimethylformamide. When dissolved, the metal complex (**1Co** or **9Co**) was added and the reaction took place at r.t. for 23 and 20 days, in the presence of **1Co** and **9Co** respectively. After purification on column chromatography, the product was analysed by ESI-MS to evidence the formation of the oxidized product **11.ox**. Even though the product was not pure enough and cobalt(II) catalyst was remaining, the formation of the **11.ox** was proved by ESI-MS ([2x**11.ox**+H]$^+$ m/z_{exp} = 553.6, m/z_{calc} = 553.4). No further efforts were placed on the purification of the obtained products, as the proof-of-concept of the oxidation of the organic additives in the presence of metal catalyst was established.

It was proven that the four investigated additives (**10**, **11**, **12** and **13**) can be easily oxidized in the presence of *m*-CPBA. Following this investigation, it was then of interest to monitor the oxidation products of the considered additives mediated by the metal catalysts under aerobic conditions. In order to do so, one additive was selected (**11**) as well as two metal catalysts (**1Co** and **9Co**). Even though the synthesized products were not pure enough, it was proven that the organic additive could be oxidized in the absence of strong oxidant, and only in aerobic conditions with cobalt(II) catalyst.

To sum up, this chapter illustrated the possibility to oxidize substrates (model organic additive here) in the presence of a strong organic oxidant (*m*-CPBA) or in the presence of a metal catalyst (**1Co** or **9Co**). Even though these results were obtained in solution, it however constitutes a proof-of-concept of the oxidation of organic additives in the presence of the metal catalyst. To mimic the real conditions (polymeric matrix) of these systems, the same approach will be performed in the solid-state in the following chapter.

III.4. Experimental section

III.4.1. Analytical equipments used in this study

III.4.1.1. Nuclear Magnetic Resonance spectroscopy - NMR

Objectives and means: *NMR analyses were carried out to characterize the intermediates and the final compounds that were synthesized in this work.*

NMR spectra were recorded on Bruker Avance III HD (400 MHz for ^1H analysis) with BBFO probe with solvent peaks as reference. Solvent used for NMR analysis was chloroform-*d* ($CDCl_3$, Aldrich, 99.8 atom% D). Chemical shifts (δ) are expressed in ppm relative to TMS. Multiplicity is indicated as s (singlet), d (doublet), t (triplet), q (quartet), m (multiplet), dd (doublet of doublets). Coupling constant (*J*) values are given in hertz (Hz).

III.4.1.2. Electrospray Ionization-Mass Spectrometry - ESI-MS

Objectives and means: *ESI-MS analyses were carried out to characterize the intermediates and the final compounds that were synthesized in this work.*

ESI-MS analyses were carried out on an Agilent Technologies 6120 quadrupole equipped with an electrospray (ESI) interface. The sample solutions were continuously introduced into the spectrometer source with a syringe pump (Kd Scientific) at a flow rate of 800 $\mu L.h^{-1}$. For electrospray ionization, the drying gas was heated at 250 °C and its flow was set at 6 $L.min^{-1}$. The capillary exit voltage was set at 5 kV and the skimmer voltage was varied to optimize the signal responses. The cone voltage applied for each sample will be detailed in this chapter for each of the experiments. Scanning was performed over the maximum *m/z* scale from *m/z* 100 to 1500. Solvents used for ESI-MS analyses are high quality solvents (methanol, VWR, HPLC grade; acetonitrile, Sigma Aldrich, CHROMASOLV® for HPLC or VWR, ≥ 99.95%, for HPLC; and degassed water).

III.4.1.3. UV-visible absorption spectrophotometry

Objectives and means: *UV-visible absorption spectrophotometry measurements (characterization and kinetics of the oxidation rate) were carried out to monitor the oxidation of organic additive models (monomeric form) in solution by strong oxidants. This allowed us evaluating their potential to be easily (or not) oxidized and establishing a reactivity sequence. The aim of that study was to use the most interesting models in terms of oxidation capacity with the most promising metal catalysts.*

UV-visible absorption spectrophotometric measurements were performed using solvents of spectrophotometric grade (acetonitrile (CH_3CN), VWR, ≥ 99.95%, for HPLC or Sigma Aldrich, CHROMASOLV® for HPLC; degassed water; ethanol (EtOH), VWR, ≥ 99.7%, absolute or Carlo Erba, ≥ 99.9%, anhydrous; 1,2-dichloroethane (DCE), Afla Aesar, > 99.7%, spectrophotometric grade, stabilized with amylene; and methanol (MeOH), Merck, UVASOL® for spectroscopy). The UV-visible absorption spectra were recorded using either a Varian CARY 50 or an Agilent CARY 5000 spectrophotometer. Measurements were performed with suprasil quartz cells displaying optical pathlength of 10 mm. The baseline was recorded in the corresponding solvent prior to any measurements. Scanning was usually performed at a scan rate of 200 $nm.min^{-1}$.

Monitoring of the organic additive models oxidation using strong oxidants: oxidation of **10**, **11** and **12** by H_2O_2 (Sigma Aldrich, 30% in water w/w) or TBHP (Fluka, ~ 70% in water, solution purum) (1 or 10 equiv.) was monitored by UV-visible absorption spectrophotometry in CH_3CN:H_2O (1:1 *v/v*) or in EtOH solvents mixtures. Solutions were freshly prepared and measured. After 3 days of reaction, the solutions were re-measured.

Monitoring and kinetics of organic additive models oxidation by a strong oxidant: oxidation of **10, 11**, **12** and **13** by *m*-CPBA (Aldrich, 77%) (0 to 25 equiv.) was measured by UV-visible absorption spectrophotometry in different solvents. The solutions were freshly prepared and kinetic profiles of the oxidation reactions were measured (from 10 minutes to 10 hours).

III.4.1.4. Microanalysis

Objectives and means: *microanalyses (C, H, N) were performed to characterize the synthetic organic compounds.*

Elemental analyses were performed on a Flash 2000 from ThermoFisher Scientific.

III.4.1.5. Electron Paramagnetic Resonance spectroscopy - EPR

Objectives and means: *EPR measurements were carried out to evaluate the paramagnetic character of the synthesized compounds.*

EPR measurements were performed on a Bruker EMX spectrometer X-band equipped with a 4119 HS-W1 cavity (high sensitivity). Measurements were performed at r.t..

III.4.2. Oxidation of organic additive models by strong oxidants (H_2O_2, TBHP) monitored by UV-visible absorption spectrophotometry

Objectives and means: *the capacities of organic additive models (monomeric pattern of potential polymeric additives designed by Clariant) to be oxidized efficiently and rapidly by strong organic oxidants (H_2O_2 (Sigma Aldrich, 30% in water* w/w*) and TBHP (Fluka, ~ 70% in water, solution purum)) was investigated in solution by UV-visible absorption spectrophotometric means.*

- Oxidation of *N*-phenylmethylbenzamide **10**

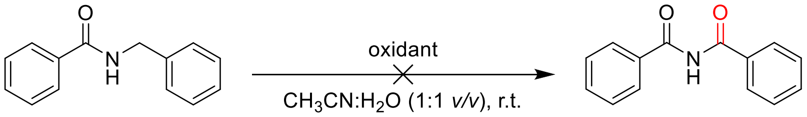

10 **10.ox**

UV-visible absorption spectra were recorded on *N*-phenylmethylbenzamide **10** with each oxidant (H_2O_2 and TBHP) considered in this work. The spectrophotometric experiments were conducted at r.t. with two different stoichiometries ([oxidant]/[**10**] = 1 and 10 equiv.) in $CH_3CN:H_2O$ (1:1 *v/v*) solvents mixture just after the preparation and after 3 days of reaction. No oxidation of the benzylic position was evidenced under these experimental conditions.

- Oxidation of *N*-(2,2,6,6-tetramethylpiperidin-4-yl)benzamide **11**

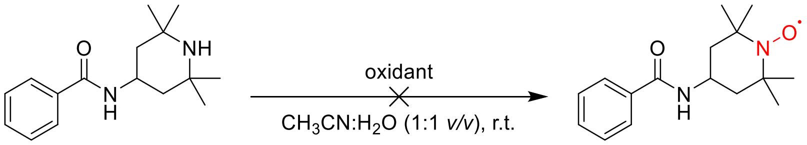

11 **11.ox**

UV-visible absorption spectra were recorded on *N*-(2,2,6,6-tetramethylpiperidin-4-yl)benzamide **11** with each oxidant (H_2O_2 and TBHP) considered in this work. The spectrophotometric experiments were conducted at r.t. with two different stoichiometries ([oxidant]/[**11**] = 1 and 10 equiv.) in $CH_3CN:H_2O$ (1:1 *v/v*) solvents mixture just after the preparation and after 3 days of reaction. No oxidation of the secondary amine was evidenced under these experimental conditions.

- Oxidation of *N*^{1},*N*^{3}-*bis*(2,2,6,6-tetramethylpiperidin-4-yl)-1,3-benzenedicarboxamide **12**

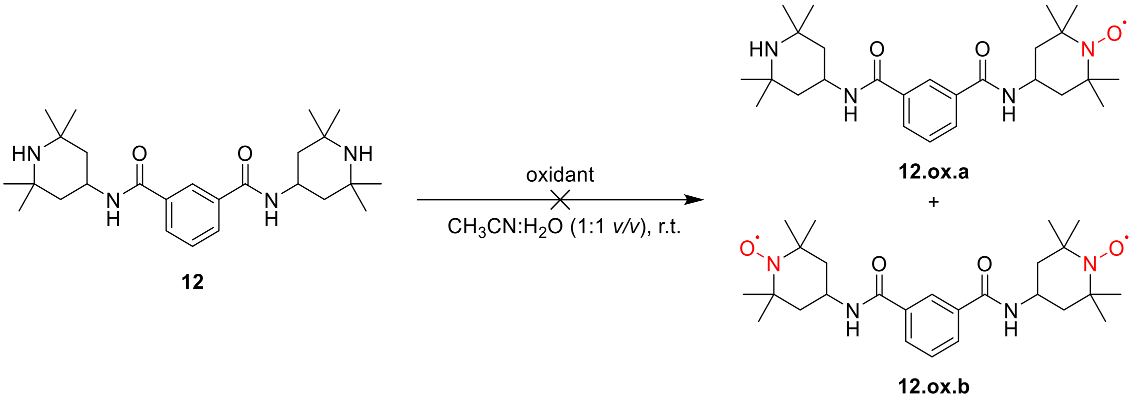

UV-visible absorption spectra were recorded on *N*^{1},*N*^{3}-*bis*(2,2,6,6-tetramethylpiperidin-4-yl)-1,3-benzenedicarboxamide **12** with each oxidant (H_2O_2 and TBHP) considered in this work. The spectrophotometric experiments were conducted at r.t. with only one stoichiometry ([oxidant]/[**12**] = 10 equiv.) in EtOH just after the preparation and after 3 days of reaction. No oxidation of the secondary amine was evidenced under these experimental conditions.

III.4.3. Oxidation kinetics of organic additive models by strong oxidant (*m*-CPBA) monitored by UV-visible absorption spectrophotometry

Objectives and means*: the capacities of organic additives models (monomeric pattern of potential polymeric additives designed by Clariant) to be oxidized efficiently and rapidly by strong organic oxidants was investigated in solution by UV-visible absorption spectrophotometric means. The preliminary study conducted with H_2O_2 and TBHP demonstrated the need to employ a more efficient oxidizing reagent. Meta-chloroperoxybenzoic acid* m-CPBA *(Aldrich, 77%) was found to be an interesting reagent in combination with compounds* ***10****,* ***11****,* ***12*** *and* ***13****. The following* Table III-5 *depicts the experimental conditions (solvent, [oxidant]/[compound] ratio...) and the time needed to reach the end of the reaction.*

*Table III-5: Kinetics of organic additives **10 – 13** oxidation monitored by UV-visible absorption spectrophotometry with* m-*CPBA (0 to 25 equiv.) in different solvents (MeOH, DCE, EtOH) for different times (10 min-5 h).*[186]

Solvent ***m*-CPBA (equiv.)** **Additive**	**MeOH**	**DCE**			**EtOH**			
	25	**2.2**	**3**	**4.4**	**0**	**3**	**5**	**10**
10	*n.d.*	10 h	*n.d.*	10 h	*n.d.*	*n.d.*	*n.d.*	*n.d.*
11	40 min	2.5 h + 5 h	1 h	2.5 h	10 min	*n.d.*	1 h	1 h
12	1 h	*n.d.*	1 h	*n.d.*	20 min	1 h	1 h	1 h
13	50 min	*n.d.*	*n.d.*	*n.d.*	30 min	*n.d.*	20 min	20 min

n.d.: not determined

III.4.4. Synthesis of the oxidized organic additive models

Solvents (provider, quality) used for the syntheses are listed below:

Dichloromethane (DCM), Sigma Aldrich, ≥ 99.9% (GC), puriss. p.a., ACS reagent or Honeywell, ≥ 99% (GC), puriss.

Diethyl ether, VWR, 100.0%, AnalaR Normapur or Sigma Aldrich, ≥ 99.5% (GC)

General procedure **G** for oxidation of organic additives:[186]

The organic additive model (1 equiv.) was dissolved in DCM and the solution was cooled down with an ice bath. Then, a solution of *m*-CPBA (2.2 equiv., Aldrich, 77%) was added dropwise over 15-20 minutes and the mixture was stirred at r.t. for 3 hours. The solvent was removed by evaporation. The resulting solid was dissolved in diethyl ether and washed four times with saturated aqueous sodium bicarbonate solution, then two times with brine. After drying over magnesium sulfate, evaporation of the solvent in rotary evaporator gave the final product.

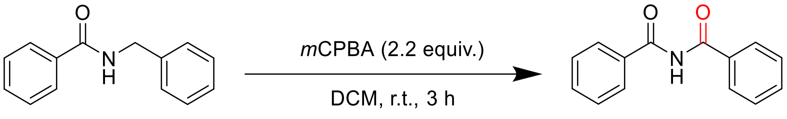

10 **10.ox**

The oxidized product **10.ox** was prepared from the *general procedure* ***G*** from *N*-phenylmethylbenzamide **10**.

The crude product was not purified but was analyzed by ESI-MS to evidence the formation of oxidized product *N*-benzoylbenzamide **10.ox**.

Characterization

ESI-MS (CH_3CN; + 125 V): [**10**+Na]$^+$ m/z_{calc} = 234.1, m/z_{exp} = 234.1
[**10.ox**+Na]$^+$ m/z_{calc} = 248.1, m/z_{exp} = 248.1

Optimization of the synthesis and purification (done by Clariant)

N-phenylmethylbenzamide **10** (2.00 g, 9.47 mmol, 1 equiv.) was dissolved in acetonitrile. TEMPO (0.5 equiv.), CuBr (0.2 equiv.) and TBHP 70% (10 equiv.) were added to the solution. The mixture was stirred at r.t. for 5 days.[187]

The unreacted peroxides were quenched by sodium bisulphite until the peroxide test indicated the absence of peroxide in the solution. This step led to two layers. The yellow aqueous layer was removed and EtOAc was added to the colourless organic layer. This layer was then washed three times with a 1 M sodium hydroxide solution, then once with chlorhydric acid. Solvent was removed, and the crude product was recrystallized (solubilization in MeOH and addition of water to precipitate the targeted product). *N*-benzoylbenzamide **10.ox** was obtained (1.14 g, 5.06 mmol, **53%**).

Characterization

^{1}H-NMR (400 MHz, $CDCl_3$) δ (ppm) 7.49-7.54 (m, 4H), 7.60-7.64 (m, 2H), 7.86-7.89 (m, 4H), 8.89 (s, 1H)
ESI-MS (MeOH; + 130 V): [**10.ox**+Na]$^+$ m/z_{calc} = 248.1, m/z_{exp} = 248.1
Microanalysis: calc: 74.65% C, 4.92% H, 6.22% N; found: 74.60% C, 4.91% H, 6.27% N

---

[187] Yu, H.; Chen, Y.; Zhang, Y. *Chin. J. Chem.* **2015**, *33* (5), 531–534.

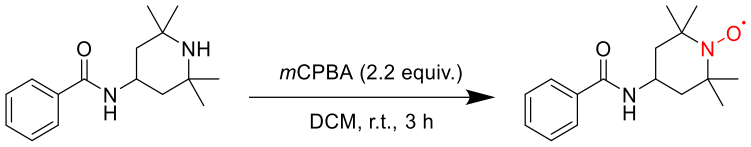

11 **11.ox**

The oxidized product **11.ox** was prepared from the *general procedure* ***G*** from *N*-(2,2,6,6-tetramethylpiperidin-4-yl)benzamide **11**.

The crude product was not purified but was analyzed by ESI-MS to evidence the formation of oxidized product *N*-[(2,2,6,6-tetramethylpiperidin-4-yl)oxy]benzamide **11.ox**.

Characterization

ESI-MS (CH_3CN; + 125 V): [**11**+H]$^+$ m/z_{calc} = 261.2, m/z_{exp} = 261.2
[**11.ox**+Na]$^+$ m/z_{calc} = 298.2, m/z_{exp} = 298.2

Optimization of the synthesis (done by Clariant)

General procedure ***H*** for oxidation of organic additives:

The organic additive model (2.00 g, 1 equiv.) was dissolved in methanol. An aqueous solution of sodium carbonate (2.3 equiv.) was added to the solution. Sodium tungstate monohydrate (0.056 equiv.) was then added to the solution and a solution of H_2O_2 30% (3.1 equiv.) was added dropwise. The mixture was stirred at r.t. overnight. The remaining peroxides were quenched by sodium bisulphite until the peroxide test indicated the absence of peroxide in the solution. The suspension was filtered and washed three times with water.

The oxidized product **11.ox** was prepared from the *general procedure* ***H*** from *N*-(2,2,6,6-tetramethylpiperidin-4-yl)benzamide **11**.

N-[(2,2,6,6-tetramethylpiperidin-4-yl)oxy]benzamide **11.ox** was obtained (1.80 g, 6.54 mmol, **85%**).

Characterization

ESI-MS (MeOH; + 125 V): [**11**+H]$^+$ m/z_{calc} = 261.2, m/z_{exp} = 261.2
[**11.ox**+Na]$^+$ m/z_{calc} = 298.2, m/z_{exp} = 298.3

EPR: - *Measurement at r.t. as a powder*: line centered at g = 2.006 with a line width of 15 G, characteristic of nitroxide radicals.
- *Measurement at r.t. in solution (DCM):* sub-structure composed by three transitions, corresponding to hyperfine coupling between nitrogen atom (^{14}N, I = 1) and the unpaired electron. These lines were characterized by a g factor of 2.005 and a line width of 1.6 G.

Microanalysis: **11.ox (N-O$^\bullet$)** calc: 69.79% C, 8.42% H, 10.17% N
11.ox (N-OH) calc: 69.53% C, 8.75% H, 10.14% N
found: 67.28% C, 8.48% H, 9.88% N

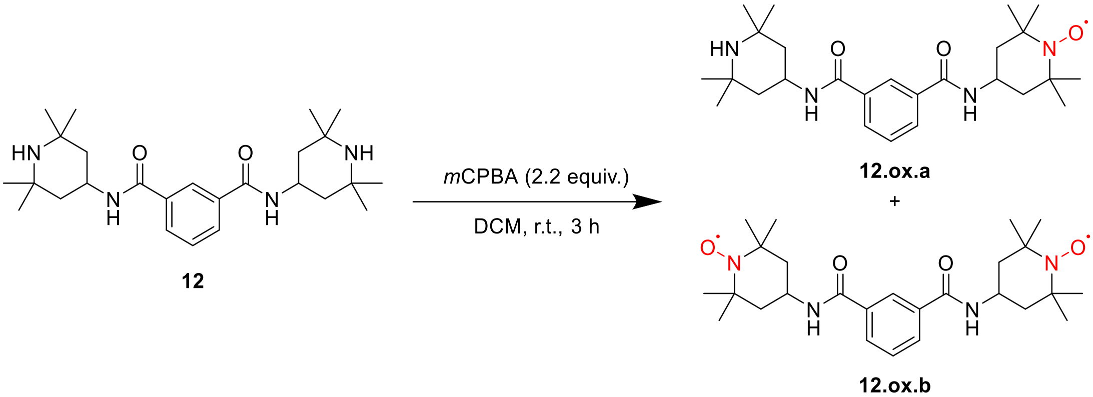

The oxidized products were prepared from the *general procedure **G*** from *N¹,N³-bis*(2,2,6,6-tetramethylpiperidin-4-yl)-1,3-benzenedicarboxamide **12**.

The crude product was not purified and just analyzed by ESI-MS to evidence the formation of oxidized products *N¹*-(2,2,6,6-tetramethylpiperidin-4-yl)-*N³*-[(2,2,6,6-tetramethylpiperidin-4-yl)oxy]-1,3-benzenedicarboxamide **12.ox.a** and *N¹,N³-bis*[(2,2,6,6-tetramethylpiperidin-4-yl)oxy]-1,3-benzenedicarboxamide **12.ox.b**.

Characterization

ESI-MS (CH_3CN:H_2O 2:1 *v/v*; + 150 V): [**12.ox.a**+H]$^+$ m/z_{calc} = 458.3, m/z_{exp} = 458.4
[**12.ox.b (N-O$^•$ + N-OH)**+H]$^+$ m/z_{calc} = 474.3, m/z_{exp} = 474.5
[**12.ox.b**+Na]$^+$ m/z_{calc} = 495.3, m/z_{exp} = 495.5

Optimization of the synthesis (done by Clariant)

The oxidized products were prepared from the *general procedure **H*** from *N¹,N³-bis*(2,2,6,6-tetramethylpiperidin-4-yl)-1,3-benzenedicarboxamide **12** (sodium carbonate (4.66 equiv.), sodium tungstate monohydrate (0.112 equiv.), solution of H_2O_2 30% (6.26 equiv.)).

N¹,N³-bis[(2,2,6,6-tetramethylpiperidin-4-yl)oxy]-1,3-benzenedicarboxamide **12.ox.b** was obtained (0.85 g, 1.80 mmol, **40%**).

Characterization

ESI-MS (MeOH; + 100 V): [**12.ox.b**+Na]$^+$ m/z_{calc} = 495.3, m/z_{exp} = 495.4

EPR: - *Measurement at r.t. as a powder*: line centered at g = 2.006 with a ray width of 14 G, characteristic of nitroxide radicals.
- *Measurement at r.t. in solution (DCM):* sub-structure composed by three lines, corresponding to hyperfine coupling between nitrogen atom (^{14}N, I = 1) and the unpaired electron. These rays were characterized by a g factor of 2.005 and a line width of 3.7 G. If the two nitroxide radicals were coupling between them, the paramagnetic signature should be 5 lines with 1:2:3:2:1 intensities. In this sample, this signature was not revealed, due to very low coupling between the two radicals in reason of the distance between them.

Microanalysis: **12.ox.b (2 N-O$^•$)** calc: 66.07% C, 8.53% H, 11.85% N
12.ox.b (N-O$^•$ + N-OH) calc: 65.93% C, 8.73% H, 11.83% N
12.ox.b (2 N-OH) calc: 65.79% C, 8.92% H, 11.80% N
found: 56.32% C, 7.35% H, 10.10% N

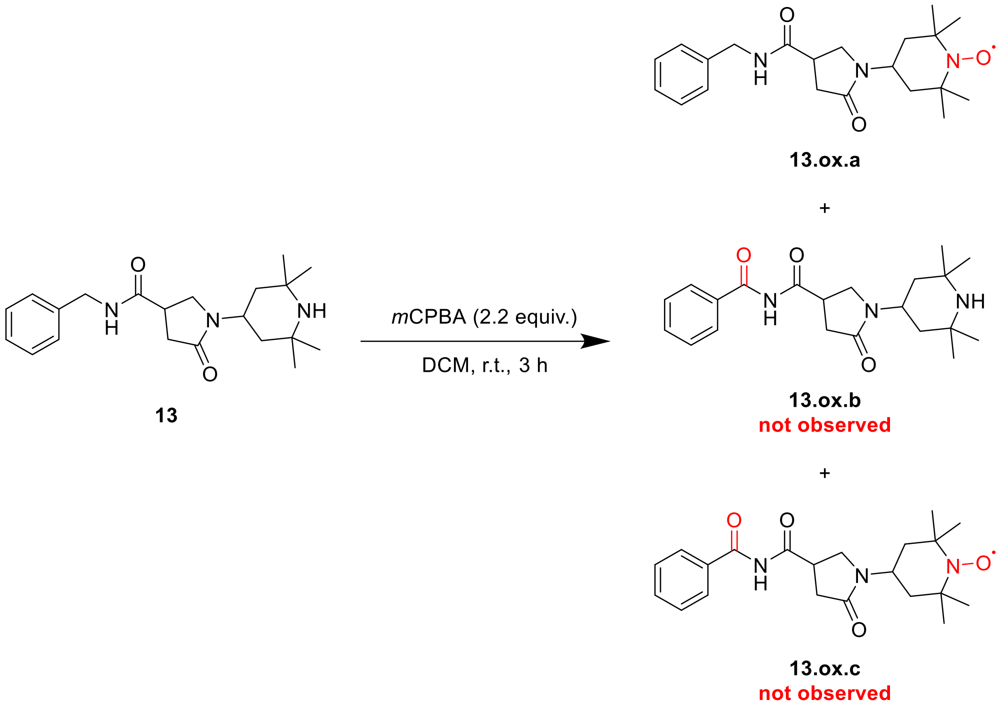

13 **13.ox.a** **13.ox.b** not observed **13.ox.c** not observed

The oxidized products were prepared from the *general procedure* ***G*** from 3-(*N*-phenylmethylcarboxamide)-1-(2,2,6,6-tetramethylpiperidin-4-yl)pyrrolidi-5-one **13**.

The crude product was not purified but analyzed by ESI-MS to evidence the formation of oxidized products 3-(*N*-phenylmethylcarboxamide)-1-[(2,2,6,6-tetramethylpiperidin-4-yl)oxy]pyrrolidi-5-one **13.ox.a**, 3-(*N*-benzoylcarboxamide)-1-(2,2,6,6-tetramethylpiperidin-4-yl)pyrrolidi-5-one **13.ox.b** and 3-(*N*-benzoylcarboxamide)-1-[(2,2,6,6-tetramethylpiperidin-4-yl)oxy]pyrrolidi-5-one **13.ox.c**.

Characterization

ESI-MS (CH_3CN:H_2O 2:1 *v/v*; + 200 V): [**13**+H]$^+$ m/z_{calc} = 358.3, m/z_{exp} = 358.3
[**13**+Na]$^+$ m/z_{calc} = 380.2, m/z_{exp} = 380.3
[**13.ox.a**+Na]$^+$ m/z_{calc} = 395.2, m/z_{exp} = 395.4

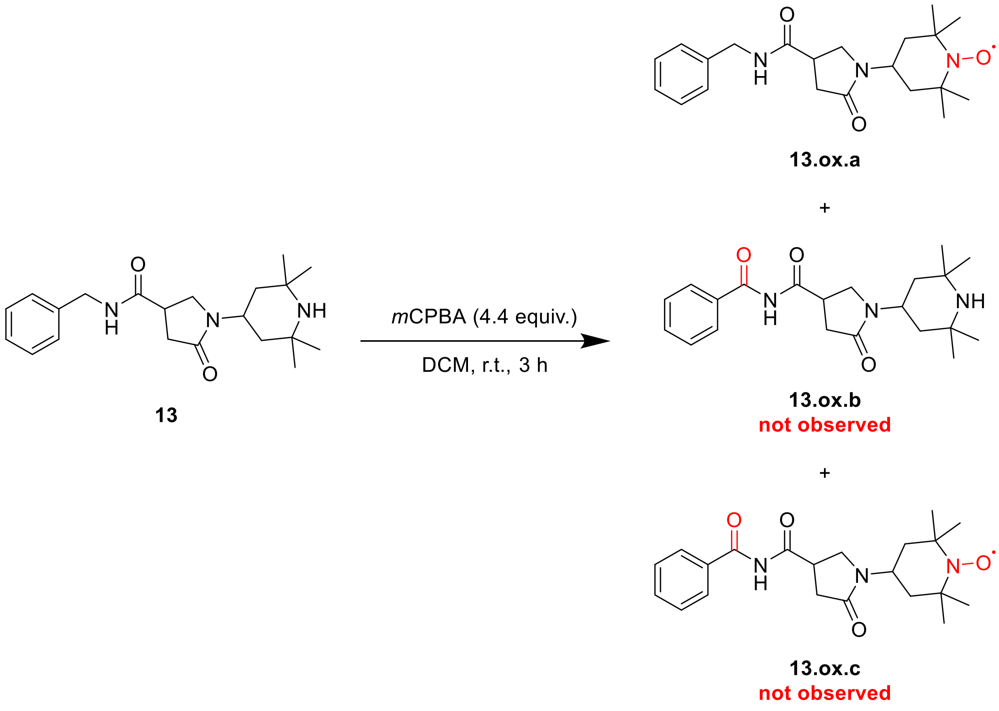

13 **13.ox.a** **13.ox.b** not observed **13.ox.c** not observed

The crude product was not purified but analyzed by ESI-MS to evidence the formation of oxidized products **13.ox.a**, **13.ox.b** and **13.ox.c**.

Characterization

ESI-MS (MeOH; + 200 V): [**13**+H]$^+$ m/z_{calc} = 358.3, m/z_{exp} = 358.3
[**13**+Na]$^+$ m/z_{calc} = 380.2, m/z_{exp} = 380.3
[**13.ox.a**+H]$^+$ m/z_{calc} = 373.2, m/z_{exp} = 373.3
[**13.ox.a**+Na]$^+$ m/z_{calc} = 395.2, m/z_{exp} = 395.3

Optimization of the synthesis (done by Clariant)

The oxidized products were prepared from the *general procedure **H*** from 3-(*N*-phenylmethylcarboxamide)-1-(2,2,6,6-tetramethylpiperidin-4-yl)pyrrolidi-5-one **13**.

3-(*N*-phenylmethylcarboxamide)-1-[(2,2,6,6-tetramethylpiperidin-4-yl)oxy]pyrrolidi-5-one **13.ox.a** only was obtained.

Characterization

ESI-MS (MeOH; + 150 V): [**13.ox.a**+Na]$^+$ m/z_{calc} = 395.2, m/z_{exp} = 395.4

EPR: - *Measurement at r.t. as a powder*: line centered at *g* = 2.002 with a line width of 30 G, characteristic of nitroxide radicals.
- *Measurement at r.t. in solution (DCM):* sub-structure composed by three lines, corresponding to hyperfine coupling between nitrogen atom (^{14}N, I = 1) and the unpaired electron. These lines were characterized by a *g* factor of 2.005 and a line width of 1.6 G.

Microanalysis: **13.ox.a (N-O$^\bullet$)** calc: 67.71% C, 8.12% H, 11.28% N
13.ox.a (N-OH) calc: 67.53% C, 8.37% H, 11.25% N
found: 67.44% C, 7.90% H, 11.29% N

III.4.5. Oxidation of organic additive models by metal catalyst

Solvents (provider, quality) used for the syntheses are listed below:

Cyclohexane, VWR, 100%, GPR Rectapur or Sigma Aldrich, ≥ 99.5% (GC), puriss. p.a., ACS reagent
Dimethylformamide (DMF), Sigma Aldrich, ≥ 99.5% (GC), puriss., absolute, over molecular sieve
Ethyl acetate (EtOAc), VWR, 99.9%, GPR Rectapur or Sigma Aldrich, ≥ 99.5% (GC), puriss. p.a., ACS reagent

General procedure ***I*** for oxidation of organic additives:

Cobalt(II) catalyst (1 equiv.) was dissolved in DMF (10 mL). After complete dissolution, a solution of *N*-(2,2,6,6-tetramethylpiperidin-4-yl)benzamide **11** (100 mg, 1 equiv.) in DMF (10 mL) was added. The mixture was stirred at r.t.. The solvent was removed by evaporation and the crude product was purified on column chromatography.

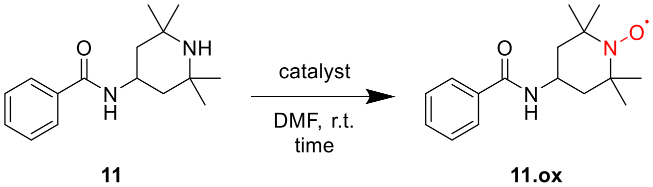

11 **11.ox**

The oxidized product **11.ox** was prepared from the *general procedure **I*** from *N*-(2,2,6,6-tetramethylpiperidin-4-yl)benzamide **11** and cobalt(II) stearate **9Co-1** (Alfa Aesar, 9-10% Co). Reaction time: 23 days. Purification: column chromatography: cyclohexane:EtOAc (9:1 *v/v*). The product was not pure enough and was analyzed by ESI-MS to evidence the formation of the oxidized additive *N*-[(2,2,6,6-tetramethylpiperidin-4-yl)oxy]benzamide **11.ox**.

ESI-MS (MeOH; + 125 V): [2 x **11.ox (N-OH)**+H]$^+$ m/z_{calc} = 553.4, m/z_{exp} = 553.6

The oxidized product was prepared from *general procedure **I*** from *N*-(2,2,6,6-tetramethylpiperidin-4-yl)benzamide **11**, cobalt(II) perchlorate, hexahydrate (1 equiv., Fluka, cryst., purum. p.a.) and 2-[[(phenylmethyl)imino]methyl]-phenol **L^1** (2 equiv.). Reaction time: 20 days. Purification: column chromatography: EtOAc. The product was not pure enough and was analyzed by ESI-MS to evidence the formation of the oxidized additive *N*-[(2,2,6,6-tetramethylpiperidin-4-yl)oxy]benzamide **11.ox**.

ESI-MS (MeOH; + 125 V): [2 x **11.ox (N-OH)**+H]$^+$ m/z_{calc} = 553.4, m/z_{exp} = 553.6

Chapter IV:

Polymeric additives oxidation

IV. Polymeric additives oxidation

The aim of this industrial collaboration with Clariant was to provide help through a fundamental approach to develop innovative oxygen barriers (*i.e.* resulting from the synergistic and subtle combination of metal catalysts and additives) for food and drinks preservation in plastic packaging, and to gain a deeper knowledge of their mechanism of action.

In the first chapter, a focus has been directed to the preparation, the characterization and the evaluation of the physico-chemical properties of cobalt(II) and manganese(II) complexes, including systems prepared from Schiff base ligands. A particular attention has been paid on the reactivity in solution such as the oxygenation and the subsequent activation processes of these metal catalysts.

In a next step, the thorough study of organic additives models (*i.e.* bearing benzylic and/or TMP-like oxidable functions) in solution demonstrated that their oxidation could be performed by strong oxidants, but also and perhaps the most important in the frame of this project, by metal catalysts (section III.3). Interestingly, model compound **11** was shown to be oxidized under aerobic conditions in the presence of two cobalt(II) catalysts (**1Co** and **9Co**). This clearly established the proof-of-concept of possible oxidation of organic additives in the presence of metal catalysts under aerobic conditions.

However, oxygen barriers for foods and drinks preservation will be introduced into plastic films or plastic bottles. To mimic the real conditions as much as possible, a solid-state study has to be therefore undertaken.

Several polymeric additives were tested in a preliminary approach by Clariant and two new polymeric additives drew our attention as promising potential systems with improved oxygen scavenging capacities with respect to the organic additives previously studied in Chapter III (**10**, **11**, **12** and **13**). Therefore, a particular interest has been devoted in this chapter to these two polymeric additives, Dercolyte S 125 (noted **14**) and a polytetrahydrofuran derivative (namely polyTHF noted **15**) whose chemical structures are depicted in Scheme IV-1.

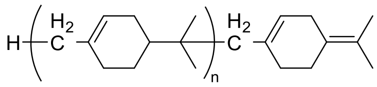

Dercolyte S 125

14

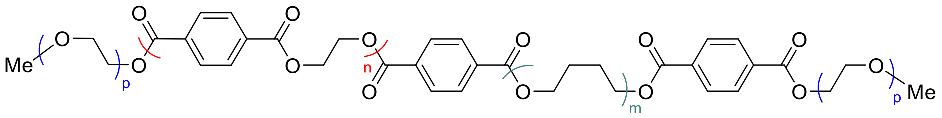

polytetrahydrofuran derivative

15

Scheme IV-1: Polymeric additives investigated in this Ph.D. work.

The oxidation of these two polymeric additives will be studied in solid-state, either alone or in combination with cobalt(II) or manganese(II) catalysts (*i.e.* to assess the impact of the metal catalysts). An appropriate analytical strategy has to be set up to properly monitor the oxidation reactions, to quantify their efficacies, and to evaluate their corresponding kinetics parameters.

The second objective, though not least important, was to elucidate the nature of the oxidation product(s) that are formed in the course of the oxidation processes. For that, a set of complementary solid-sate or solution analytical techniques has been fruitfully employed.

IV.1. Analytical approach for polymeric additives oxidation monitoring and selection of metal catalysts

As previously stated, the main objective was to easily monitor, in the solid-state, the aerobic oxidation of two polymeric additives. The solid-state studies are indeed more complicated to set up as they are more difficult to follow. The most popular analytical techniques usually employed to follow a chemical reaction in solution - *e.g.* gas or liquid chromatography, NMR, mass spectrometry to cite a few - are not adapted for solid-state analyses as the integrity of the samples has to be maintained during the reaction. Other analytical methods can be devoted to the solid-state analyses (*e.g.* SEM, XPS...), but their routine use is by far not obvious, and often quite expensive.

FTIR was hereafter selected as the most technically effective solution to follow the oxidation of the additives in the solid-state. In fact, it is easy to set up, not expensive, it can provide precise information on the nature of the chemical functions and on the reaction kinetics, and consume small amount of products.

Potassium bromide pellets was the first basic method that was envisaged to monitor the oxidation of the additives by FTIR. The targeted samples were mixed with potassium bromide (5:95 *w/w*) and the potassium bromide pellets were prepared with the use of a hydraulic press. Even though it consumed only a small amount of the samples, the pellets were nevertheless fragile (*i.e.* temperature sensitive and sensible to repeated handlings). Besides, it was not possible to process the potassium bromide pellets with all the polymeric samples provided by Clariant because of their aspect, stickiness and shape. In addition, these pellets were not stable at high temperatures. As the samples were subjected to heating to speed up the oxidation process as well as to mimic the extrusion step (*i.e.* thermo-mechanical manufactured process by which a softened plastic material - homogenous mixture of PET, additive and catalyst etc. - is forced through a shaped metal piece or a die to produce a continuous film of the product), it was therefore not possible to study the oxidation reaction of the polymeric samples at higher temperature. Last but not least, once the potassium bromide pellet was prepared, it was not possible to recover the sample from potassium bromide for other complementary solution analyses (*e.g.* microanalyses, NMR...).

In a second approach, the use of glass strips was considered to not consume the product. As it can be seen on Figure IV-1, the absorption of the glass (**1**) was found to be significantly important especially in the fingerprint region (1500-500 cm^{-1}) which precludes the use of these glass strips. However, as a test, the metal catalyst **2Co** was sandwiched between two glass strips and its FTIR signature was measured without (**2**) and with (**3**) an applied pressure, respectively. Without any pressure (**2**), no FTIR signal could be observed, whereas with an applied pressure (**3**), only the glass absorption was again measured. This approach to monitor the oxidation of the polymeric samples was therefore skipped.

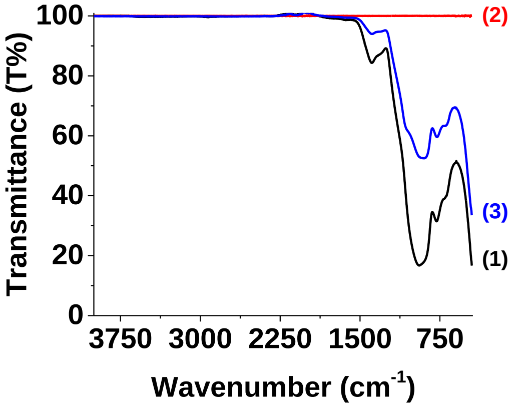

Figure IV-1: FTIR spectra; ***(1)*** *two glass strips with applied pressure,* ***(2) 2Co*** *sandwiched between two glass strips without applied pressure,* ***(3) 2Co*** *sandwiched between two glass strips with applied pressure.*

Even though the conventional route to measure FTIR spectra consumed relative amounts of the samples at each regular measurement, it was, however, decided to use this strategy to monitor the oxidation reactions of the selected polymeric additives over time. Additive **14** and catalyst were mixed together as powders in a 1:35 ratio (catalyst:additive *w/w*) in compliance with the requirements from Clariant. The prepared samples were stored at r.t. and at 70°C, and FTIR measurements were recorded at regular intervals. For this first preliminary screening approach, 7 catalysts were selected, namely 5 cobalt(II) complexes previously prepared from the synthesized Schiff base ligands (*i.e.* **1Co**, **2Co-2**, **3Co**, **5Co**, **6Co** (II.3), the cobalt(II) stearate **9Co-1** (*i.e.* from Alfa Aesar)) and the manganese(II) stearate **9Mn-1** (*i.e.* synthesized in the laboratory, section II.5.2.2.3).

Figure IV-2 first displays the FTIR spectra recorded for samples prepared from **14** and **1Co** (*i.e.* **1Co**:**14**, 1:35 *w/w*) that were stored at r.t.. No significant variation could be observed, meaning that the additive was not oxidized under these experimental conditions.

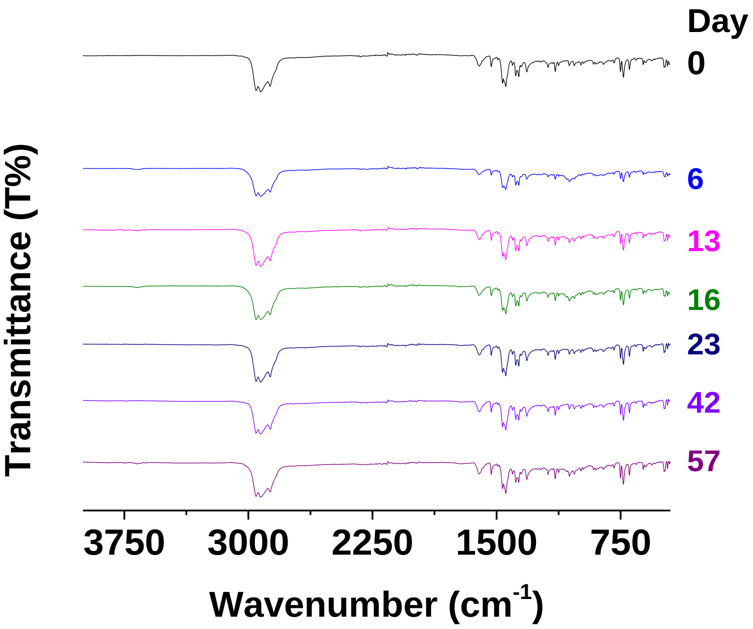

Figure IV-2: Oxidation of ***14*** *in the presence of* ***1Co*** *(****1Co****:****14****, 1:35* w/w*) monitored by FTIR; the samples were stored at r.t..*

On the other hand, Figure IV-3 displays the FTIR spectra recorded for **14** in the presence of **1Co** for samples that were stored at 70 °C. An absorption band centred at 1715 cm^{-1} and seemingly arising from the formation of carbonyl functions was gradually increasing over time.

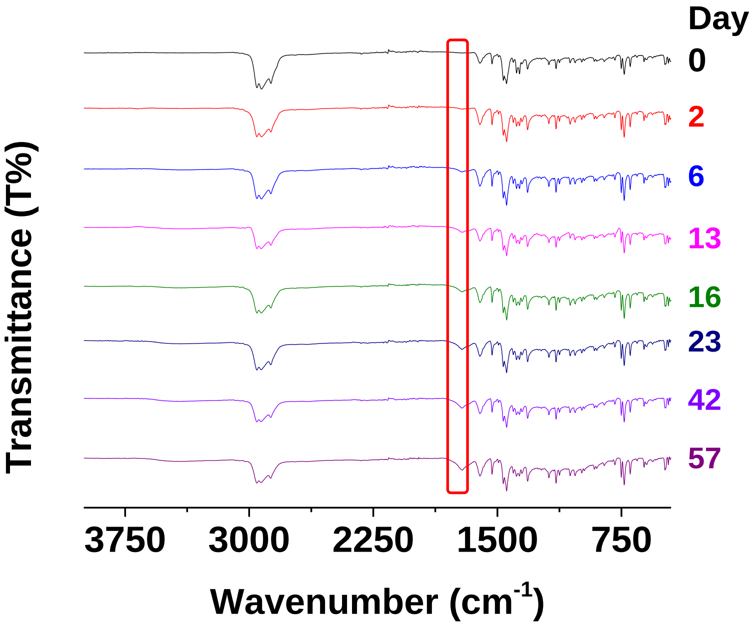

*Figure IV-3: Oxidation of **14** in the presence of **1Co** (**1Co**:**14**, 1:35* w/w*) probed by FTIR; the samples were stored at 70 °C.*

For Dercolyte S 125 **14**, the absorption peak (bending vibrations/scissoring mode δ_{CH}) centered at 1462 cm^{-1} was used as the internal reference (*i.e.* no variation of this signal was observed whatever the oxidation state of Dercolyte S 125 **14**) and the absorption peak centered at 1715 cm^{-1} (stretching $\nu_{C=O}$) was normalized and used to monitor the oxidation process as a function of time. After processing of these FTIR data, the percentage of formation of the oxidized products could be accurately evaluated. Figure IV-4 displays the normalized area measured at 1715 cm^{-1} and the effectiveness of the different catalysts on the oxidation of additive **14** can be thus compared. Firstly, it can be clearly observed that the additive underwent an aerobic thermal-catalysed oxidation at 70 °C regardless of the tested system. Surprisingly, it was also observed that the additive **14** was oxidized, even in the absence of any metal catalyst (*i.e.* reference experiment). The most promising metal catalyst was undeniably the cobalt(II) stearate **9Co-1**, far above the other catalysts herein considered, whether in terms of quantity of the oxidized products formed during the reaction (Figure IV-4) or of kinetics (*i.e.* speed) of the oxidation reaction (Table IV-1).

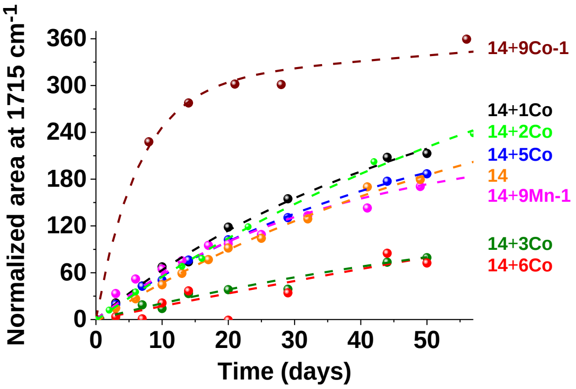

*Figure IV-4: Normalized area at 1715 cm^{-1} representing the oxidation of **14** at 70 °C with the different metal catalysts considered in this work. The dash lines correspond to the first order processing of the data.*

*Table IV-1: Half-life time of the oxidation reaction of **14** in the presence of different metal catalysts at 70 °C assessed by FTIR measurements.*

Sample	**$t_{1/2}$ (day)**
14	46(2)
14+1Co	25(3)
14+2Co	57(14)
14+3Co	33(11)
14+5Co	23(2)
14+6Co	*n.d.*
14+9Co-1	4.4(0.5)
14+9Mn-1	20(2)

n.d.: not determined with accuracy

These results stand in contrast with the solution studies (Chapter II). It was indeed shown that the cobalt(II) complexes with the Schiff bases ligands were more efficient in terms of oxygenation/activation. However, it was also demonstrated that these complexes were converted to their cobalt(III) trischelates upon aerobic oxidation. This likely explains the inability of theses metal complexes to efficiently assist the oxidation of Dercolyte S 125 **14**. Furthermore, even successful, the preparation of the Schiff base cobalt(II) complexes (**1Co**, **2Co**, **3Co**, **5Co** and **6Co**) remained difficult and not applicable to a large scale synthesis for industrial purposes (*i.e.* unless compound **1Co**). Until now, despite many attempts, **2Co** was not obtained as a pure complex (*i.e.* the complex **2Co-1**, that was tested, was provided by Clariant and was found to be mixture of 10% of the cobalt(II) complex and 90% of the starting ligand; proportions evaluated by microanalysis, section II.5.2.2.1). Last but not least, they are not approved by the regulation authorities so far, while **9Co** and **9Mn** are tolerated in plastics formulations for food and drink preservation. The regulatory approvals by the adequate authorities are time-consuming and costly procedures. For all these reasons and in compliance with Clariant, the solid-state studies have been thereafter focused on the two stearate metal catalysts **9Co** and **9Mn**.

IV.2. Investigation on Dercolyte S 125 14 oxidation

IV.2.1. Preliminary investigations of oxidation in the solid state

The preliminary FTIR measurements on the oxidation of additive **14** demonstrated a strong catalytic activity of **9Co-1**, whereas **9Mn-1** seemingly slowed down the oxidation reaction of **14** with respect to **14** taken alone. One of the reasons could be the dispersity of the samples, in particular the particle sizes of the additives or the catalysts.

To test this hypothesis, SEM measurements were first performed on three samples, the fresh additive **14**, the additive **14** alone having undergone oxidation at 70 °C over 112 days and the additive **14** having undergone oxidation at 70 °C in the presence of **9Co-1** over 89 days (*i.e.* **9Co**:**14**, 1:35 *w/w*). Figure IV-5 displays images of the surface of the fresh polymeric additive **14** and as anticipated, the sample was not homogenous in terms of particle size (*i.e.* between ~ 1 and 150 μm). In addition, the surface seemed to be smooth. As the polymeric samples had a great tendency to store the electrons, it was difficult to get more information on the surface. After being stored at 70 °C, the morphology of the sample was found to be comparable to the fresh one (Figure IV-6) and the heterogeneousness of the particle sizes remained the same (*i.e.* between ~ 1 and 150 μm).

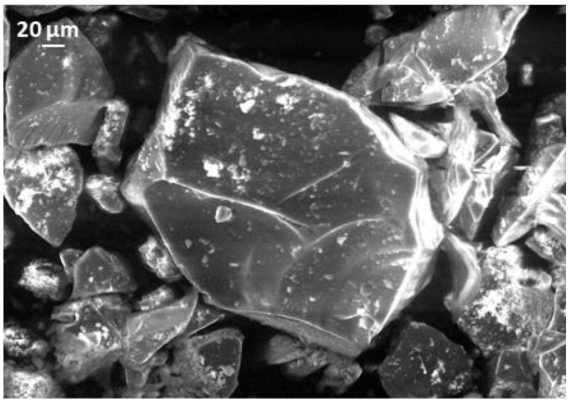

*Figure IV-5: SEM image of fresh **14**.*

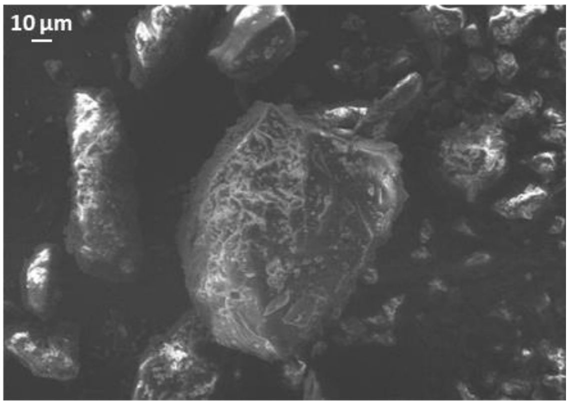

*Figure IV-6: SEM image of **14** after oxidation at 70 °C.*

When **14** was oxidized in the presence of **9Co-1** at 70 °C, the morphology of the sample was slightly different than the samples treated in the absence of metal catalyst (Figure IV-7) and the sample heterogeneity remained the same. To obtain precise information on the surface of the samples, complementary analyses are required. However, as it was not the purpose of this study, only the particle size distribution of the samples was evaluated.

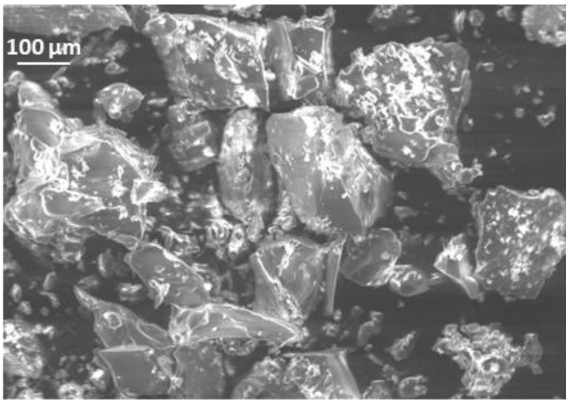

*Figure IV-7: SEM image of **14** after oxidation with **9Co-1** at 70 °C.*

To go even farther in this approach, Energy Dispersive X-ray Spectroscopy (EDS) coupled to SEM allowed determining the nature of the elements and their relative proportions. This type of measurement was performed for the three same samples and the oxygen content was found to significantly increase when the sample was stored at 70 °C compared to that kept at r.t.: ~ 6.4% *versus* ~ 3.2% (Figure IV-8 and Figure IV-9). In the presence of **9Co-1**, the same effect was observed (Figure IV-10).

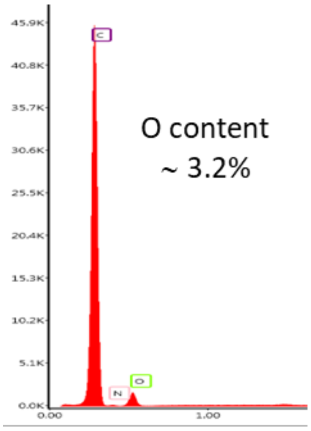

*Figure IV-8: SEM-EDS analysis of fresh **14**.*

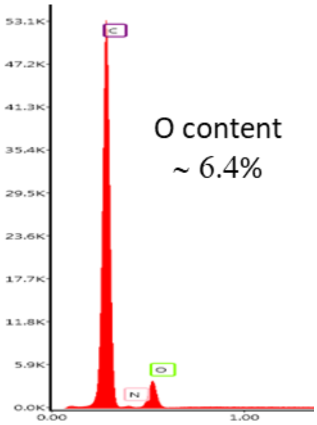

*Figure IV-9: SEM-EDS analysis of **14** after oxidation at 70 °C.*

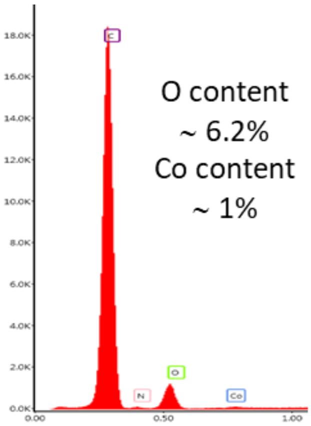

*Figure IV-10: SEM-EDS analysis of **14** after oxidation with **9Co-1** at 70 °C.*

SEM imaging allowed confirming the heterogeneity of the prepared samples in terms of particle size distribution. Coupled to EDS, it demonstrated a significant oxygen enrichment of the samples when these were stored at 70 °C, substantiating the first results obtained by FTIR.

IV.2.2. Particle size: a key role on the oxidation process?

It was now proven that the studied samples were not homogeneous in terms of particle size. For this reason, it was thus decided to evaluate the influence of particle size distribution of the catalysts and of the additive. In this regard, the additive and the catalysts were finely ground and sieved by hand separately. After having ground the additive **14**, its particle size distribution was evaluated by laser diffraction granulometry allowing determining the maximum of the Gaussian curve and the median value (d (0.5)) of the particle size distribution. The laser diffraction granulometry measurements showed a heterogeneous distribution of the particle sizes (Figure IV-11).

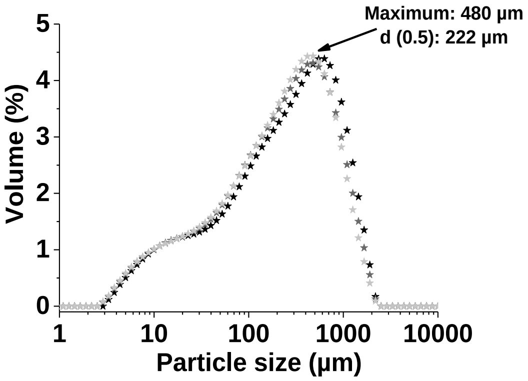

*Figure IV-11: Laser diffraction granulometry of **14** after grinding and before sieving.*

A sieving of the ground sample was thus performed between through different sieves (149, 100, 50 and 42 µm). Three fractions were collected (Figure IV-12): **fraction 1** that corresponds to the particle sizes between 100 and 150 µm, **fraction 2** between 50 and 100 µm and **fraction 3** between 42 and 50 µm. Their particle size distributions were measured once again by laser diffraction granulometry (Figure IV-13) and displayed more homogeneous particle size distributions.

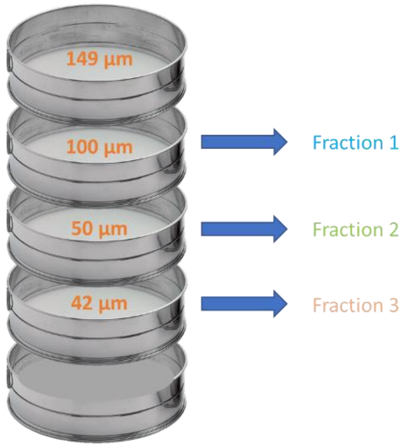

*Figure IV-12: Sieving protocol of **14**.*

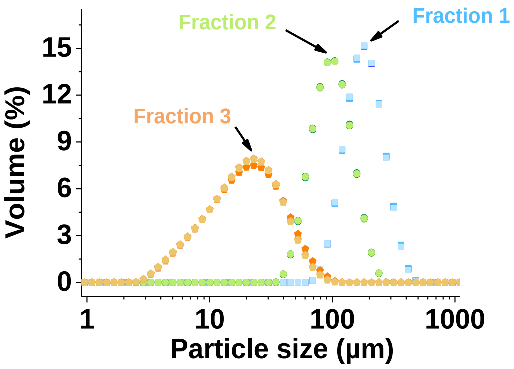

*Figure IV-13: Laser diffraction granulometric analysis of **14** after sieving.*

The parameters of the different fractions of **14** are gathered in Table IV-2.

*Table IV-2: Laser diffraction granulometry data after sieving **14**.*

Fraction	Gaussian curve maximum (µm)	d (0.5) (µm)
14-F1	182	169
14-F1'*	138	157
14-F2	105	92
14-F3	30	18

* A second biggest particle size distribution of **14** was prepared

The same approach was applied on each of the two catalysts of interest, **9Co** and **9Mn**. It should be mentioned that, from now on, the two catalysts that will be discussed were provided by Clariant (**9Co-2** and **9Mn-2**). They were ground and sieved through the same sieves. Their particle size distribution parameters are displayed in Table IV-3.

*Table IV-3: Laser diffraction granulometric data of **9Co-2** and **9Mn-2** after the sieving process.*

Sample	Collected fraction (µm)	Gaussian curve maximum (µm)	d (0.5) (µm)
9Co-2-F1	100-149	158	154
9Co-2-F2	50-100	105	94
9Co-2-F3	42-50	53	51
9Co-2-F4	< 42	26	19
9Mn-2-F1	100-149	138	133
9Mn-2-F2	50-100	120	82
9Mn-2-F3	42-50	60	56
9Mn-2-F4	< 42	30	23

IV.2.2.1. Influence of the additive particle size distribution

In a first step, the influence of the additive particle size distribution was assessed while fixing that of the catalyst. For the two catalysts of interest, **9Co** and **9Mn**, the smallest particle size distribution was used (**9Co-2**-F4 and **9Mn-2**-F4, Table IV-3). Each particle size distribution of the additive **14** (*i.e.* **14**-F1, **14**-F2 and **14**-F3, Table IV-2) was studied either alone at r.t. and at 70 °C or in combination with the fraction 4 of the metal stearates (**9Co-2**-F4 or **9Mn-2**-F4) at both temperatures, leading to eighteen samples (Figure IV-14).

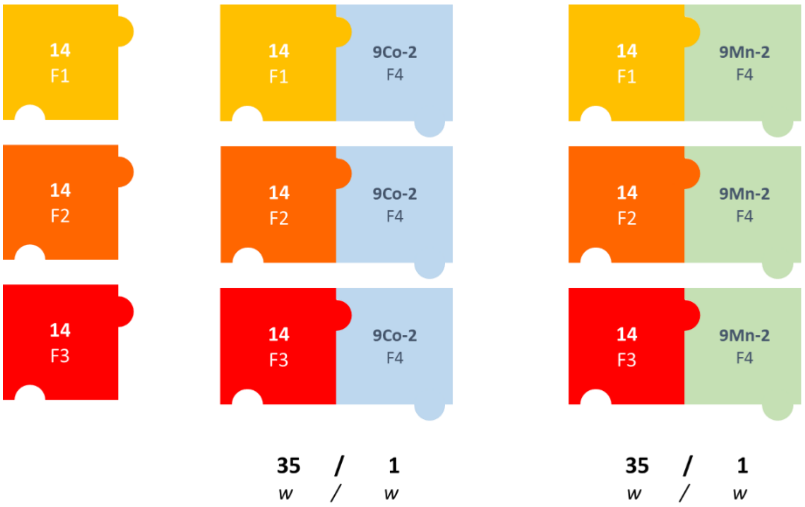

*Figure IV-14: Different combinations for the study of the influence of the additive particle size distribution on the oxidation process of **14**.*

The catalyst and the additive were mixed together in a 1:35 (*w/w*) ratio. FTIR spectra were measured on the different samples at regular intervals over 201 days of storage. Figure IV-15 displays the FTIR spectra of the fraction 1 of the additive (**14**-F1) before the oxidation (*black line*), after 201 days of oxidation at r.t. (*red line*) and at 70 °C (*blue line*). It clearly evidenced the formation over time of carbonyl bonds centred at 1715 cm^{-1} (stretching $\gamma_{C=O}$) and also of alcohols (centred at about 3450 cm^{-1}, stretching γ_{O-H}). As the formation of carbonyls was more easily discernible, the kinetic parameters of the oxidation reaction were quantified with respect to this characteristic band.

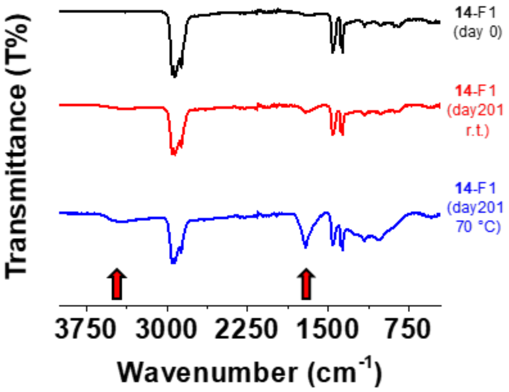

Figure IV-15: FTIR spectra of ***14****-F1 before the aerobic oxidation (day 0) and after 201 days of oxidation at r.t. and at 70°C.*

After processing the data, the kinetics parameters of the oxidation reaction of the additive **14** can be evaluated. Whereas no significant oxidation of **14** was observed when the samples were stored at r.t., large variations were observed for the samples stored at 70 °C (Figure IV-16, Figure IV-17 and Figure IV-18). It is important to mention that the FTIR and kinetic data are the results of experiments performed in duplicate or triplicate.

For the polymeric additive **14** used alone, its particle size distribution did not affect the kinetics and the efficacy of the oxidation reaction (Figure IV-16 and Table IV-4, see below).

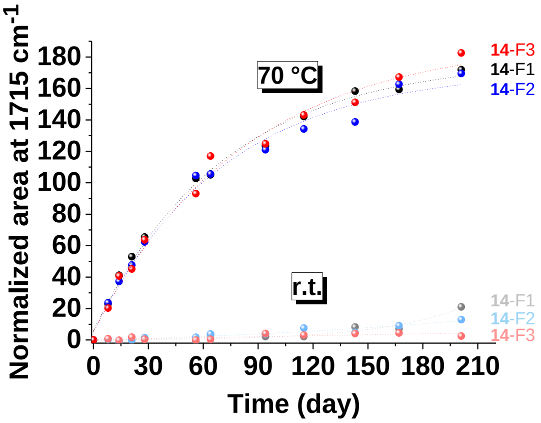

Figure IV-16: Normalized area at 1715 cm^{-1} illustrating the oxidation reaction of the three-different particle size distributions of ***14*** *alone at r.t. and at 70 °C.*

By contrast, a clear impact of the additive particle size distribution in the presence of the cobalt(II) catalyst **9Co-2** or the manganese(II) catalyst **9Mn-2** was observed in terms of efficacy (Figure IV-17 and Figure IV-18), but not in terms of speed (*i.e.* kinetics, Table IV-4). In fact, it appeared that the biggest particle size distribution allowed generating a higher amount of oxidized products with time in the presence of **9Co-2** (Figure IV-17), while the opposite situation was observed with **9Mn-2** (Figure IV-18).

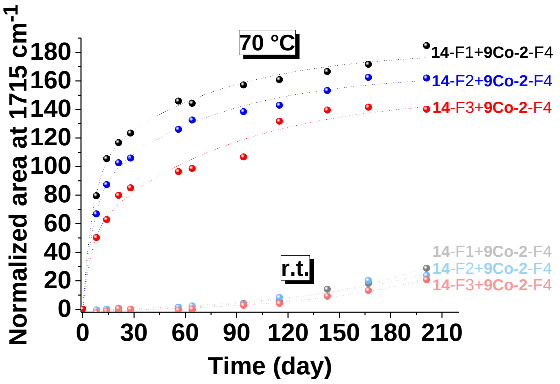

*Figure IV-17: Normalized area at 1715 cm^{-1} illustrating the oxidation process of the three different particle size distributions of **14** with **9Co-2**-F4 at r.t. and at 70 °C.*

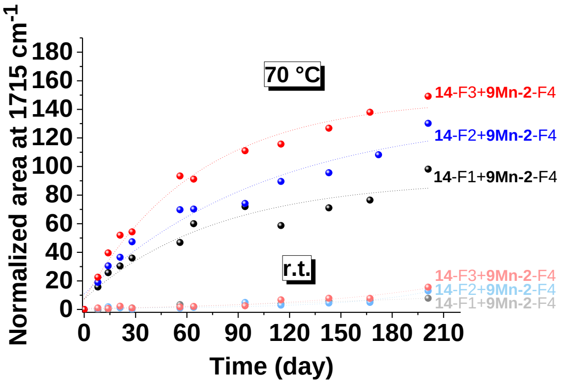

*Figure IV-18: Normalized area at 1715 cm^{-1} illustrating the oxidation process of the three different particle size distributions of **14** with **9Mn-2**-F4 at r.t. and at 70 °C.*

If only one particle size distribution of the additive **14** is now only taken into account, the efficacies of the catalysts can be compared. Figure IV-19 indeed displays the results obtained for the largest particle size distribution of additive **14** alone (**14**-F1) that are compared to those obtained with cobalt(II) catalyst (**9Co-2**-F4) and manganese(II) catalyst (**9Mn-2**-F4). It can be clearly demonstrated that the manganese(II) catalyst is by far less efficient that the cobalt(II) analogue and the additive alone (*i.e.* the oxidized product formation sequence is as follows: **9Co-2**-F4 > **14**-F1 >> **9Mn-2**-F4). After 201 days of experiment, the quantities of oxidized product formed for **9Co-2**-F4/**14**-F1 and **14**-F1 alone were almost the same. The main impact of the **9Co-2** catalyst, and to a lesser extent of **9Mn-2**, was to significantly speed up the oxidation reaction rate of Dercolyte S 125 **14**. The combination of **9Mn-2** led to much lower amount of oxidized species of **14** formed after 201 days of experiment.

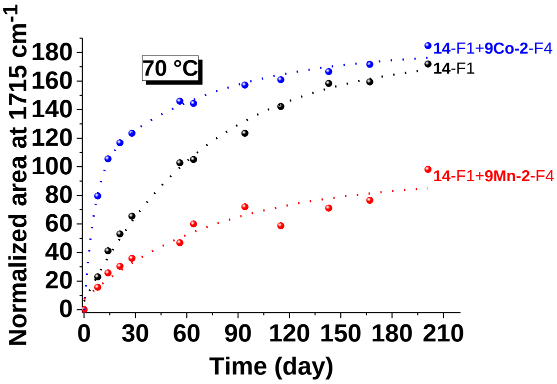

*Figure IV-19: Normalized area at 1715 cm^{-1} describing the oxidation process of **14** alone, with **9Co-2**-F4 and with **9Mn-2**-F4 as a function of time at 70 °C.*

If we now compare the kinetics parameters, no marked influence of the particle size distribution within a same category (*i.e.* additive **14** alone, additive **14** with cobalt(II) catalyst **9Co-2** and additive **14** with manganese(II) catalyst **9Mn-2**) can be seen (Table IV-4). It is noteworthy that, whereas **9Mn-2** did not improve the efficiency of the oxidation reaction with respect to additive **14** taken alone, it however sped up the oxidation reaction rate by a factor of ~ 5. Similarly, **9Co-2** catalysed the oxidation of the polymeric additive **14** (*i.e.* the oxidation process was found to be at least 12 times faster than **14** taken alone) as well as it significantly improved the efficiency of the reaction.

*Table IV-4: Half-life times (given in days) of the different oxidation reactions of the polymeric additive **14** at 70 °C.*

	$t_{1/2}$ (days)		
	No catalyst	+**9Co-2**-F4	+**9Mn-2**-F4
14-F1	50(4)	4.1(7)	12(6)
14-F2	50(7)	4.3(8)	11(4)
14-F3	58(10)	4(2)	19(3)

IV.2.2.2. Influence of the catalyst particle size distribution

Once the additive particle size distribution was evaluated, the same type of experiments was reproduced to evaluate the influence of the catalyst particle size distribution. The four different fractions of **9Co-2** and **9Mn-2** (Table IV-3) were mixed in a 1:35 (*w/w*) ratio with a fixed particle size distribution of the polymeric additive **14** (F1', Table IV-2) as shown in Figure IV-20.

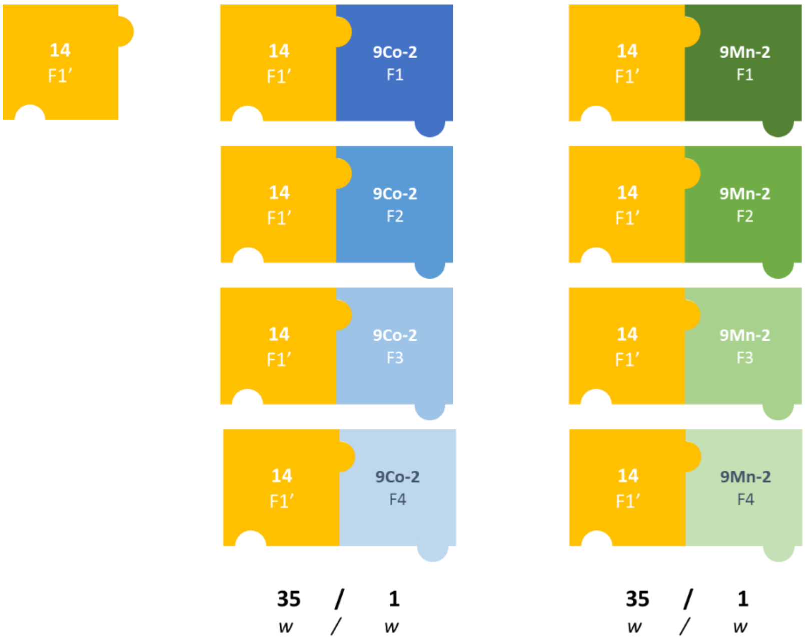

*Figure IV-20: Different combinations used for the study of the influence of the catalyst particle size distribution on the oxidation process of **14**.*

After 139 days of aerobic reaction, no oxidation was observed at r.t. in the solid-state for the different examined samples (Figure IV-21 and Figure IV-22), thus confirming the previous results. At higher temperature (70 °C), no marked effect of the particle size distribution of the catalyst was observed both for **9Co-2** (Figure IV-21) and for **9Mn-2** (Figure IV-22).

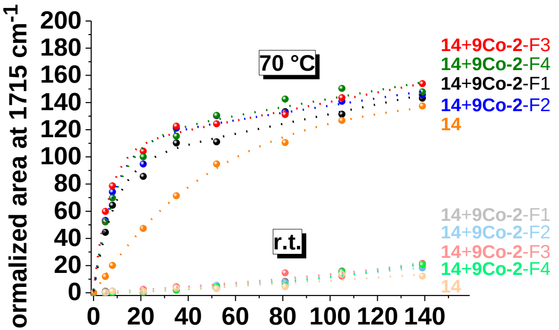

*Figure IV-21: Normalized area at 1715 cm^{-1} illustrating the oxidation process of **14** with the four different particle size distributions of **9Co-2** at r.t. and at 70 °C.*

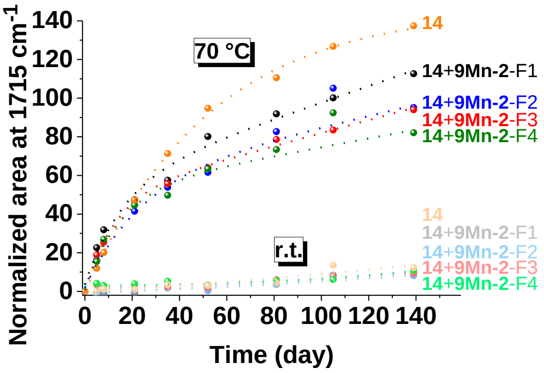

*Figure IV-22: Normalized area at 1715 cm^{-1} describing the oxidation process of **14** with the four different particle size distributions of **9Mn-2** at r.t. and at 70 °C.*

In terms of kinetics (Table IV-5), both metal catalysts sped up the oxidation kinetics of **14** with a marked effect for the cobalt(II) stearate **9Co-2**. The particle size distribution of each of the catalysts did not influence significantly the kinetics parameters within the given errors.

Table IV-5: Half-life times (given in days) of the different oxidation reactions at 70 °C.

	$t_{1/2}$ (day) 14-**F1'**		$t_{1/2}$ (day) 14-**F1'**
No catalyst	36(2)	**No catalyst**	36(2)
+9Co-2-F1	6(1)	**+9Mn-2**-F1	12(6)
+9Co-2-F2	6(1)	**+9Mn-2**-F2	17(9)
+9Co-2-F3	4.6(3)	**+9Mn-2**-F3	9(1)
+9Co-2-F4	6(1)	**+9Mn-2**-F4	10(3)

To sum up, no aerobic oxidation of **14** took place at r.t. in the absence or in the presence of the catalyst, in contrast to what was observed at 70 °C, thus suggesting a "thermal/metal catalyst" effect on the Dercolyte S 125 polymeric additive **14**. It has been also observed that the particle size distribution of the catalyst did not influence the efficacy and the kinetics of the oxidation reaction of the polymer. By contrast, even though the particle size distribution of the additive did not influence the kinetics of the oxidation reaction in the presence of a metal catalyst, it affected its efficacy.

IV.2.3. "Extrusion" process: an activation stage for the metal catalysts?

During the industrial process, masterbatches are extruded (*i.e.* see above for a definition) to form the desired plastic films or bottles. During this step, the polymers are heated at high temperature in a low air environment. It was therefore decided to mimic these extrusion conditions by heating the samples at 100 °C for 10 minutes under argon atmosphere and by exposing them to air before they reached the r.t..

For that, the additive **14** (**14**-F1', Table IV-2) was mixed with cobalt(II) (**9Co-2**-F4, Table IV-3) or manganese(II) (**9Mn-2**-F4, Table IV-3) stearate catalysts or studied alone. The prepared samples were maintained under an argon atmosphere and heated at 100 °C for 10 minutes (Figure IV-23). After this period, the samples were then placed under air atmosphere before reaching r.t.. They were afterwards stored at r.t. or at 70 °C and were measured at regular intervals by FTIR to monitor the oxidation process over 139 days.

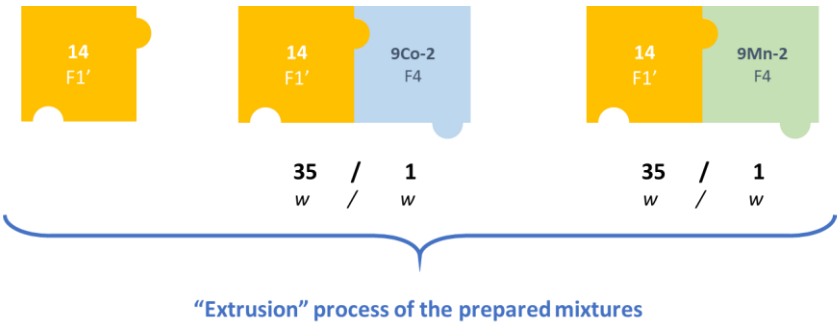

*Figure IV-23: Different combinations of interest for the study of the influence of the "extrusion" process on the oxidation process of **14**.*

At first glance, the major difference was the enhancement of the additive oxidation at r.t., although it remained less efficient and slower than at 70 °C (Figure IV-24). Secondly, the cobalt(II) stearate **9Co-2** was still found to be the most efficient catalyst either in terms of efficacy or kinetics. Last but not least, it was observed (Figure IV-24) for the manganese(II) catalyst **9Mn-2** a more efficient and faster process during the first month of reaction with respect to the oxidation of **14** lacking the metal catalyst.

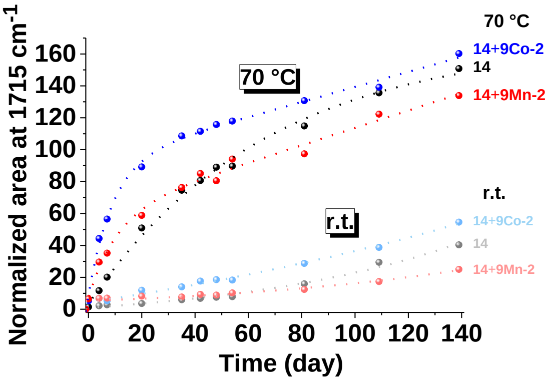

*Figure IV-24: Normalized area at 1715 cm^{-1} representing the oxidation of **14**, with **9Co-2** and **9Mn-2** at r.t. and at 70 °C after 10 minutes of "extrusion".*

The half-life times of the oxidation processes were calculated and are presented in Table IV-6. The oxidation kinetics of **14** with **9Mn-2** was found to be faster (*i.e.* a significant enhancement of the oxidation products can be seen during the first month of reaction). For **9Co-2** catalyst, no influence of the "*extrusion*" on the rate of the reaction could be evidenced (Table IV-6).

Table IV-6: Half-life times (given in days) of the different oxidation reactions at 70 °C after no and ten minutes of "extrusion".

Conditions / **Sample**	**$t_{1/2}$ (day)** No "*extrusion*" **70 °C**	**$t_{1/2}$ (day)** 10 min "*extrusion*" **70 °C**
14-F1'	36(2)	46(3)
14-F1'+**9Co-2**-F4	6(1)	6.3(6)
14-F1'+**9Mn-2**-F4	10(3)	7(1)

The time of "*extrusion*" was varied from 10 minutes (Figure IV-24) to 30 minutes (Figure IV-25) and to 1 hour (Figure IV-26). Surprisingly, it was clearly observed that the rise of the "*extrusion*" time (from 10 minutes to 1 hour) lessened the efficacy of the cobalt(II) catalyst **9Co-2**.

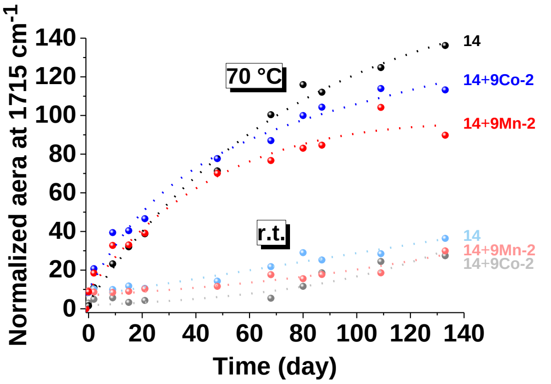

*Figure IV-25: Normalized area at 1715 cm^{-1} describing the oxidation reaction of **14**, with **9Co-2** and **9Mn-2** at r.t. and at 70 °C following an "*extrusion*" *process of 30 minutes.*

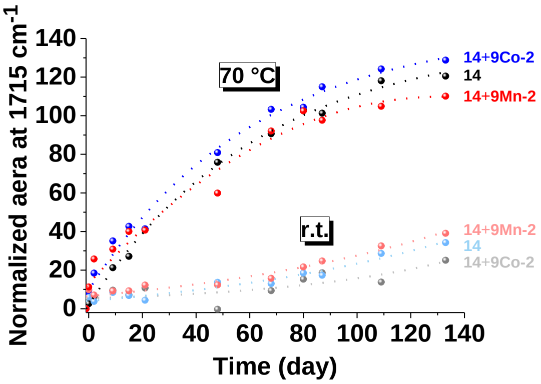

*Figure IV-26: Normalized area at 1715 cm^{-1} showing the oxidation reaction of **14**, with **9Co-2** and **9Mn-2** at r.t. and at 70 °C following an "*extrusion*" *process of 1 hour.*

With respect to the polymeric additive **14** taken alone, it was observed that neither an "*extrusion*" treatment nor the time of this process affected its oxidation efficacy (Figure IV-27).

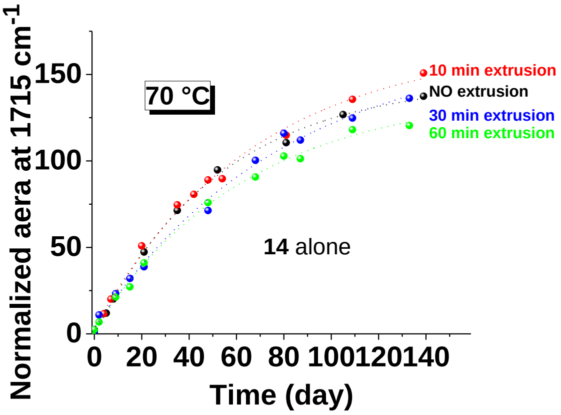

*Figure IV-27: Normalized area at 1715 cm^{-1} representing the oxidation reaction of **14** at 70 °C after 0, 10, 30 and 60 minutes of "*extrusion*".

In the presence of a metal catalyst, the observations stood in sharp contrast. With **9Co-2** (Figure IV-28), following an "*extrusion*" of 10 minutes, the performance of the catalyst on the oxidation reaction remained nearly the same. However, increasing the "*extrusion*" time to 30 minutes or 1 hour had a deleterious effect on the efficacy of the oxidation reaction of **14**.

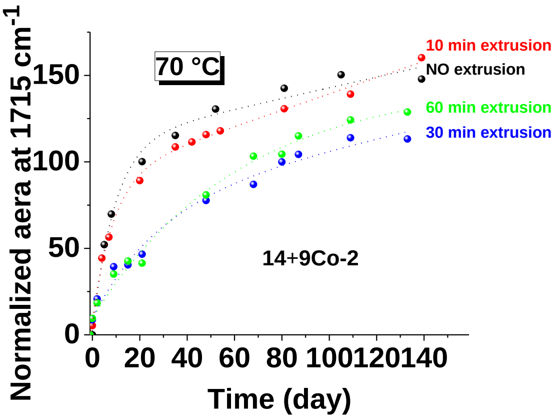

*Figure IV-28: Normalized area at 1715 cm^{-1} illustrating the oxidation of **14** with **9Co-2** at 70 °C after 0, 10, 30 and 60 minutes of "*extrusion*".

By contrast, for the manganese(II) catalyst **9Mn-2** (Figure IV-29), and whatever the time of “*extrusion*”, the efficacy of the oxidation reaction of **14** was improved (*i.e.* with the strongest effect after ten minutes of *“extrusion”*).

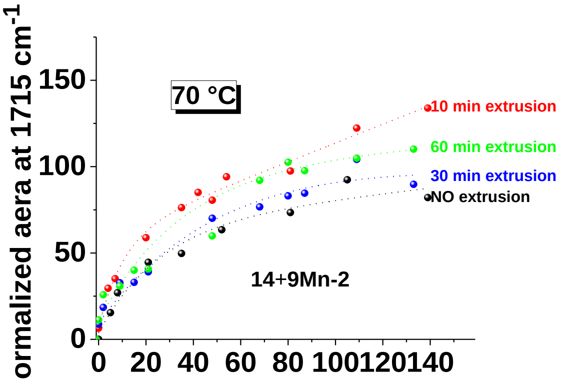

*Figure IV-29: Normalized area at 1715 cm^{-1} representing the oxidation of **14** with **9Mn-2** at 70 °C after 0, 10, 30 and 60 minutes of “*extrusion*”.*

If we now focus on the kinetics parameters of these oxidation reactions (Table IV-7), the reaction was slowed down following an “*extrusion*” process when **14** was considered alone. With **9Co-2**, the oxidation kinetics of **14** was not affected after 10 minutes of “*extrusion*”, but was significantly slowed down when the “*extrusion*” time was expanded. The same conclusions can be drawn for the **9Mn-2** catalyst.

*Table IV-7: Half-life times (given in days) of the different oxidation reactions at 70 °C after 0, 10, 30 and 60 minutes of “*extrusion*”.*

Conditions / Sample	$t_{1/2}$ (day) No “*extrusion*” 70 °C	$t_{1/2}$ (day) 10 min “*extrusion*” 70 °C	$t_{1/2}$ (day) 30 min “*extrusion*” 70 °C	$t_{1/2}$ (day) 60 min “*extrusion*” 70 °C
14-F1’	36(2)	46(3)	58(10)	43(3)
14-F1’+**9Co-2**-F4	6(1)	6.3(6)	17(9)	35(17)
14-F1’+**9Mn-2**-F4	10(3)	7(1)	~ 35*	~ 35*

* Estimated value

We demonstrated that heating the mixture for 10 minutes (mimicking the “*extrusion*” process) had little to no effect on the oxidation of **14** with **9Co-2**. Increasing the “*extrusion*” time lowered both the efficacy and kinetics of the oxidation reaction. The same conclusions can be drawn for **9Mn-2**. However, even after an “*extrusion*” of 1 hour, the oxidation efficacy was found to be improved. In a next experiment, only the catalyst was “extruded” for 10 minutes under argon atmosphere following the protocol previously described. The mixtures with the additive **14** were prepared afterwards (Figure IV-30) and the oxidation process was analysed using the same analytical means and under the identical experimental conditions (*i.e.* r.t. or 70 °C; catalyst:**14** 1:35 *w/w*).

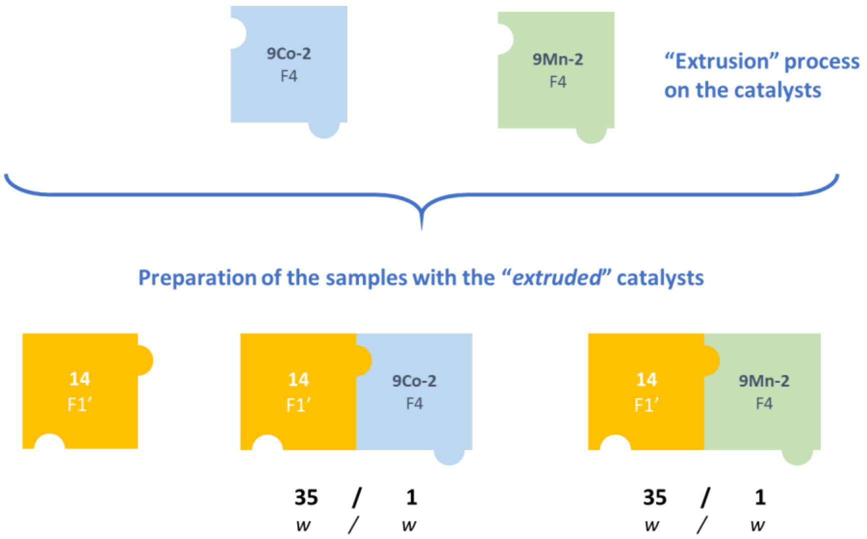
9Co-2
F4
9Mn-2
F4
"Extrusion" process on the catalysts
Preparation of the samples with the "*extruded*" catalysts
14
F1'
14
F1'
9Co-2
F4
14
F1'
9Mn-2
F4
35 / 1
w / w
35 / 1
w / w

Figure IV-30: Different combinations of interest for the study of the influence of the catalyst "extrusion" process on the oxidation process of ***14****.*

The samples were stored either at r.t. or at 70 °C, and FTIR measurements were performed at regular intervals over 164 days. Figure IV-31 displays the progress of the oxidation reaction (*i.e.* rise of the carbonyl bond peak area at 1715 cm^{-1}) over time and showcased, as previously, the significantly improved efficacy at 70 °C in the presence of **9Co-2** catalyst in contrast to **9Mn-2**. As described previously, oxidation of **14** was observed at r.t. following a limited heating of the catalyst.

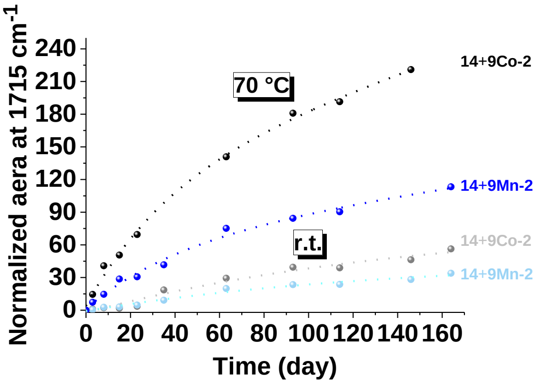

Figure IV-31: Normalized area at 1715 cm^{-1} *representing the oxidation process of* ***14*** *in the presence of either* ***9Co-2*** *or* ***9Mn-2*** *at r.t. and at 70 °C after 10 minutes of catalyst "extrusion" at 100 °C.*

If we now compared all the experiments that were performed following an "*extrusion*" treatment in the presence of **9Co-2**, the oxidation process related to Dercolyte S 125 **14** was significantly improved in terms of efficacy following a heating at 100°C during 10 minutes of only the metal catalyst (*in blue*, Figure IV-32) prior the mixture preparation and far ahead of the 10 minutes of "*extrusion*" of the additive/catalyst mixture (*in red*, Figure IV-32) and of the no extruded sample (*in black*, Figure IV-32).

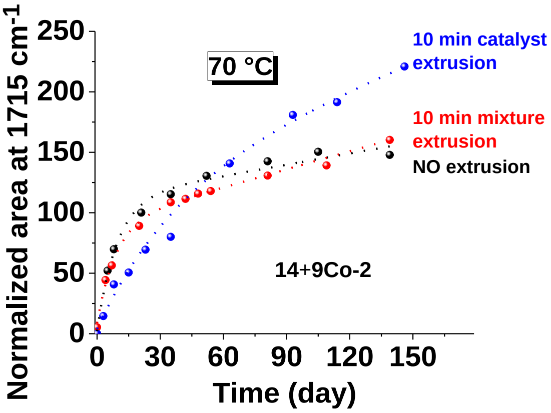

*Figure IV-32: Normalized area at 1715 cm^{-1} representing the oxidation of **14** with **9Co-2** at 70 °C after 0 or 10 minutes of “*extrusion*” of the catalyst/**14** additive and after 10 minutes of “*extrusion*” of only the catalyst.*

For the manganese(II) catalyst, even though the efficacy was improved when the catalyst was extruded for 10 minutes (*in blue*, Figure IV-33), the best results were obtained when the additive/catalyst mixture was extruded for 10 minutes (*in red*, Figure IV-33).

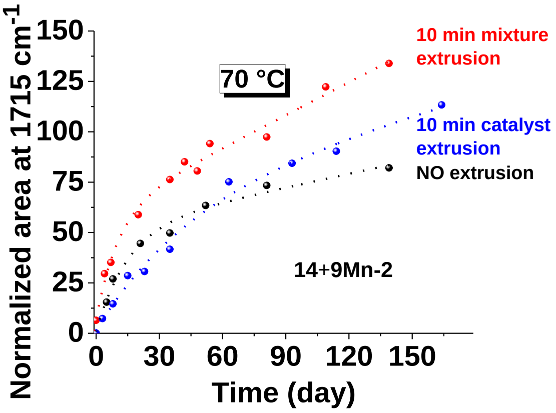

*Figure IV-33: Normalized area at 1715 cm^{-1} representing the oxidation of **14** with **9Mn-2** at 70 °C after 0 or 10 minutes of “*extrusion*” of the catalyst/**14** additive and 10 minutes of “*extrusion*” of only the catalyst.*

Table IV-8 now depicts the kinetic parameters (half-life times of the oxidation reaction evaluated by FTIR) of the above-described experiments. Very interestingly, extruding the mixture over 10 minutes had a weak to no impact on the performance of the oxidation process of **14** whatever the metal catalyst used. By contrast, heating only the catalyst (**9Co-2** or **9Mn-2**) for 10 minutes drastically slowed down the oxidation reaction of **14** that was monitored over more than 130 days. These experiments clearly demonstrated the marked impact of heating either the catalyst or the mixture on the oxygenation/oxidation properties of the system. These experiments were of crucial interest for understanding the manufacturing processes of the masterbatches unit of Clariant. Depending whether efficacy or rapidity (or both) is targeted, the catalyst or the mixture (0/10 minutes) “*extrusion*” can be proposed. For the manganese(II) catalyst, we clearly demonstrated that “*extrusion*” (*i.e.* of the catalyst/additive mixture) used along the manufacturing stage might improve significantly the properties of the material either in terms of efficacy or kinetics.

Table IV-8: Half-life times (given in days) of the different oxidation reactions at 70 °C after 0, 10 minutes of “extrusion” *of the mixture or of only the catalyst.*

	$t_{1/2}$ **(day)**		
Conditions / **Sample**	No “*extrusion*” **70 °C**	10 min “*mixture extrusion*” **70 °C**	10 min “*catalyst extrusion*” **70 °C**
14-F1’+**9Co-2**-F4	6(1)	6.3(6)	23(8)
14-F1’+**9Mn-2**-F4	10(3)	7(1)	35(17)

Even though the best results in terms of efficacy were obtained when only the **9Co-2** was extruded, the kinetics was slower. Depending whether efficacy or rapidity is preferred, catalyst “*extrusion”* or 0 or 10 minutes of “*extrusion*” should be favoured.

For the manganese(II) systems, either in terms of efficacy or in terms of kinetics, the “*extrusion*” of the additive/catalyst ratio remained the best approach.

IV.2.4. Potential coordination of the catalyst along the oxidation process with the oxidized polymeric additive or one of its precursors

Upon oxidation, we demonstrated that the additive displayed new functions such as carbonyl or alcohols (see above). These new functions might constitute potential binding sites for cobalt(II) or manganese(II) coordination and could provide explanations of the peculiar behaviour emphasized for the examined systems (*i.e.* **9Co-2**/**14** *versus* **9Mn-2**/**14**). To test this possibility, we undertook new experiments that were monitored by FTIR spectroscopy. As previously described in Chapter II (II.3.1.3), the IR absorbance at 1560 cm^{-1} in **9Co-2** and **9Mn-2** arose from the symmetric vibration stretching of the carboxylate group coordinated to the metal ion (*i.e.* cobalt(II) or manganese(II)). To monitor a possible decoordination of the carboxylate group from the metal centre, the catalyst/additive ratio was varied (1:1, 2:1, 3:1 and 1:2, *w/w*) to emphasize whether decoordination of carboxylate group, and so coordination to the oxidized additive, occurred or not. The additive **14** (fraction F1, Table IV-2) was mixed with cobalt(II) stearate **9Co-2** (fraction F4, Table IV-3) or manganese(II) stearate **9Mn-2** (fraction F4, Table IV-3) in the targeted ratios. The prepared samples were stored at r.t. or at 70 °C and FTIR measurements were performed at regular intervals over a period of 135 days. Whatever the studied system (catalyst, catalyst/additive ratio), the same trends were observed and only the results for the catalyst/additive 1:2 (*w/w)* ratio will be hereafter thoroughly described. When the **14**/**9Co-2** system was studied, no variation of the band centred at 1560 cm^{-1} was observed at r.t. (*in red*, Figure IV-34) and at 70 °C (*in blue*, Figure IV-34) suggesting the absence of interaction between the oxidized additive and the metal centre. However, at 70 °C, an intensity increase of the bands centred at 1410 and 1706 cm^{-1} was observed, suggesting the formation of polymeric species of the cobalt(II) catalyst. When considering the **14**/**9Mn-2** system, no decoordination of the carboxylate and no coordination to the oxidized additive were observed both at r.t. (*in red*, Figure IV-35) or at 70 °C (*in blue*, Figure IV-35).

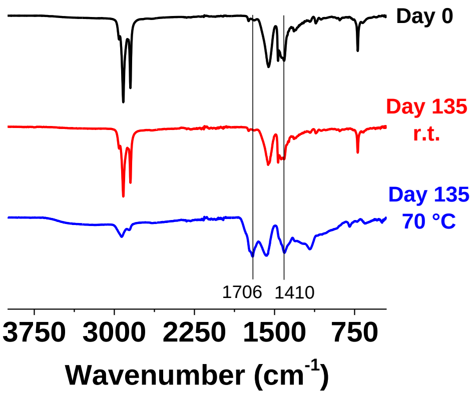

*Figure IV-34: FTIR spectra of **14:9Co-2** (1:2 w/w).*

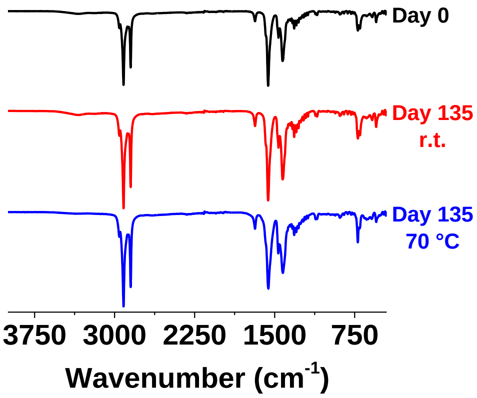

*Figure IV-35: FTIR spectra of **14:9Mn-2** (1:2 w/w).*

Whatever the tested ratio and the studied catalyst (**9Co-2** or **9Mn-2**), the oxidized product or its precursors were not coordinated to the metal centre during the oxidation process as no decoordination of the carboxylate from the stearate could be observed.

IV.2.5. Catalyst impurities poisoning of the oxidation reaction?

As previously discussed, **9Mn-1** and **9Mn-2** were not fully pure and were found to contain residual stearic acid. It is noteworthy that the manganese(II) stearate samples mostly used in this work were provided by Clariant or from commercial source. They cannot be purified or re-synthesized by the industrialist because of the large scale of catalysts regularly used and of the associated costs. Therefore, efforts were put to the evaluation of the impurities impacts on the catalytic activities of the metal complexes and to search for strategies to overcome these potential issues if any. The results obtained from the previous solid-state studies demonstrated a lower catalytic activity of **9Mn** compared to **9Co**. It was thus decided to first investigate whether the potential acidity, due to the residual stearic acid, could explain the lower efficacy of **9Mn-1** (or **9Mn-2**) with respect to **9Co**. For that, the polymeric additive **14** (fraction F1', Table IV-2) was mixed with **9Mn-2** catalyst (fraction F4, Table IV-3) and calcium oxide (*i.e.* used as a base to trap the residual acidity) as described in Figure IV-36 (catalyst:base:additive 0.5:0.5:35 *w/w/w*). The aim of this approach was to evaluate if the addition of a base could improve the efficacies of the corresponding commercial metal catalysts.

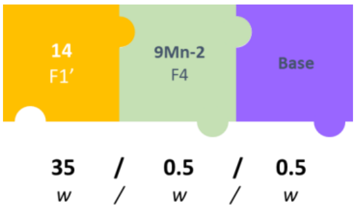

*Figure IV-36: Combinations employed to evaluate the potential "*decontamination*" of **9Mn-2** by CaO for the oxidation of **14**.*

The samples were stored under aerobic conditions at r.t. and at 70 °C over a period of 63 days. FTIR measurements were performed at regular intervals and were compared to those previously obtained for the **14/9Mn-2** system. Figure IV-37 first shows that the presence of a base significantly enhanced the efficacy of the **9Mn-2** catalyst at r.t. but worsened it at 70 °C. In addition to the lower efficacies, the oxidation reactions were also slowed down (Table IV-9).

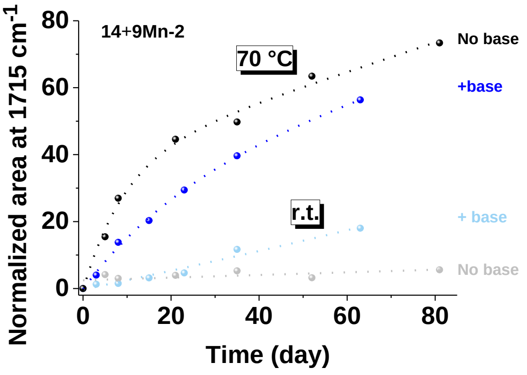

Figure IV-37: Normalized area at 1715 cm^{-1} describing the oxidation of ***14*** *by* ***9Mn-2*** *at r.t. and 70 °C in the absence and presence of a base (*i.e. *CaO).*

Table IV-9: Half-life times (given in days) of the different oxidation reactions of ***14*** *at 70 °C by* ***9Mn-2*** *in the absence and in the presence of calcium oxide.*

Conditions **Sample**	**$t_{1/2}$ (day)**	
	Without base	With base
14-F1'+**9Mn-2**-F4	7(2)	17(12)

To go a step further and assess how free stearic acid can influence the catalytic activity of a metal catalyst, it was put forward to "*contaminate*" the cobalt(II) catalyst **9Co** by addition of stearic acid. Different mixtures of additive **14** (fraction F1', Table IV-2) with cobalt(II) stearate **9Co-2** (fraction F4, Table IV-3) and stearic acid were prepared with the following catalyst:stearic acid:additive ratios: 0:1:35, 0.5:0.5:35 and 0.9:0.1:35 (*w/w/w*). These mixtures were stored at r.t. and at 70 °C and were measured by FTIR at regular intervals over a period of 63 days (Figure IV-38).

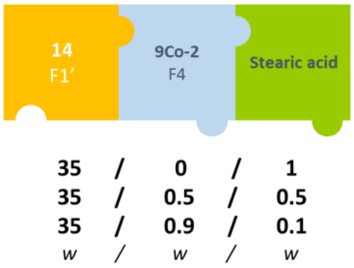

Figure IV-38: Different combinations of interest for the study of the "contamination" of ***9Co-2*** *on the oxidation process of* ***14****.*

The progress of the oxidation reactions of Dercolyte S 125 **14** over time (*i.e.* formation of the carbonyl bond at 1715 cm^{-1}) under the different experimental conditions is shown in Figure IV-39. At 70 °C and in the presence of a catalyst:stearic acid 0:1 (*w/w*) ratio (*in blue*, Figure IV-39) the efficacy of the oxidation reaction was worse than the additive **14** used alone (*in grey*, Figure IV-39) thus demonstrating that addition of only free stearic acid had a negative impact on the aerobic oxidation of **14**. When the catalyst:stearic acid ratio was modified to 1:1 (*in red*, Figure IV-39), the efficacy of the oxidation reaction was about the same than the additive **14** alone. Last but not least, modifying the ratio to catalyst:stearic acid 9:1 (*w/w*) (*in green*, Figure IV-39) gave comparable results than the **14**/**9Co-2** mixture lacking stearic acid (*in black*, Figure IV-39).

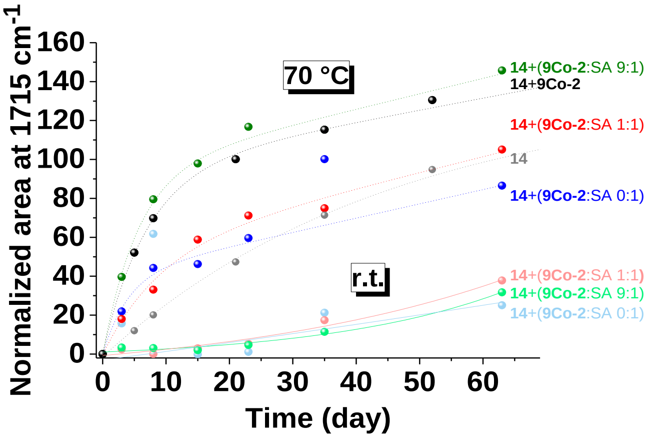

*Figure IV-39: Normalized area at 1715 cm^{-1} representing the oxidation of **14** with **9Co-2** at r.t. and at 70 °C in the absence and in the presence of stearic acid (SA).*

To some extent, the higher the amount of stearic acid was, the less efficient the oxidation reaction was. However, whatever the ratio used, the presence of stearic acid did not influence significantly the rate of the oxidation reaction (Table IV-10). This set of experiments demonstrated that the residual presence of stearic acid (*i.e.* as seen for the manganese(II) and cobalt(II) stearate provided by Clariant) is not a major issue since it does not markedly alter the catalytic properties of the cobalt(II) complexes.

Table IV-10: Half-life times (given in days) of the oxidation reactions at 70 °C in the absence and presence of stearic acid.

Conditions / Sample	$t_{1/2}$ (day)			
	9Co:SA 1:0	**9Co**:SA 9:1	**9Co**:SA 1:1	**9Co**:SA 0:1
	70 °C	70 °C	70 °C	70 °C
14-F1'+**9Co-2**-F4	4.9(7)	3.9(9)	6(3)	3(1)

SA: stearic acid

To complete this study and confirm the inertness of stearic acid (*i.e.* residual amounts) with respect to the catalytic activities of the divalent metal complexes, we turned our efforts to a potential "*decontamination*" by calcium oxide of **14**/**9Co-2** samples containing (*i.e.* deliberately added) stearic acid (Figure IV-40). We have shown previously (*i.e.* for the manganese(II) system) that the presence of base deleteriously affected the oxidation efficacy (Figure IV-37) but had no to weak impact on the reaction kinetics (Table IV-9). Far from being beneficial to improve the oxidation reaction of **14** with **9Mn**, the addition of CaO used to trap the free stearic acid had indeed a negative effect when the samples were stored at 70 °C. At r.t., addition of calcium oxide was shown to enhance the efficiency of the oxidation reaction by the manganese(II) complex.

The same conclusions can be drawn for the cobalt(II) catalyst (Figure IV-41) that was combined to free stearic acid and calcium oxide (Figure IV-40). The addition of base adversely affected the efficiency of the oxidation of Dercolyte S 125 **14**, while no effect was seen on the reaction kinetics (Table IV-11). To sum up, residual amounts of stearic acid present in **9Mn** or **9Co** (*i.e.* provided a presence of less than 10%) do not influence the catalytic properties of the metal complexes. While moderate, a positive effect can be observed at r.t. if a base such calcium oxide is used. At 70 °C, CaO had however a deleterious effect (Figure IV-41). Due to the lack of time, we did not evaluate the potential impact of other bases. CaO is indeed a peculiar reactant that can trap water to lead to the formation of calcium hydroxide (*i.e.* exothermic reaction) and further to calcium carbonate in the presence of CO_2. Its reactivity most likely explains its detrimental effect on the oxidation reaction of Dercolyte S 125 **14**.

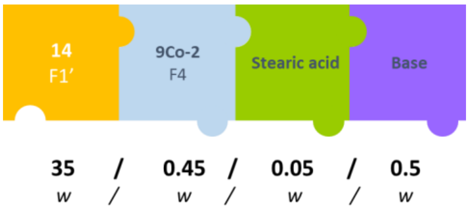

*Figure IV-40: Combinations used to test the "decontaminating" potential of CaO with **9Co-2** "poisoned" with free stearic acid.*

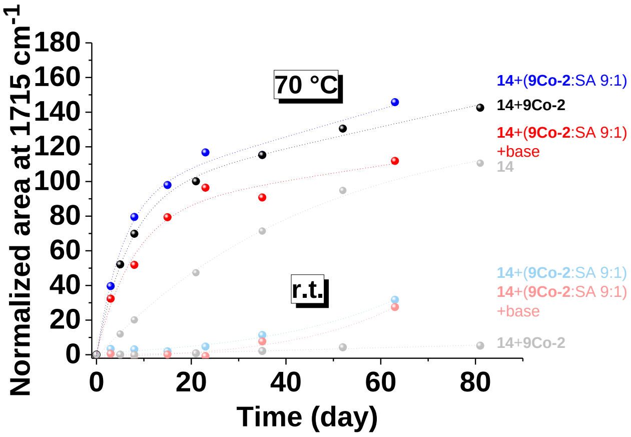

*Figure IV-41: Normalized area at 1715 cm^{-1} illustrating the oxidation of **14** with **9Co-2** at r.t. and at 70 °C in the presence of stearic acid (SA) and calcium oxide (base).*

*Table IV-11: Half-life times (given in days) of the different oxidation reactions of **14** at 70 °C in the presence of stearic acid and calcium oxide.*

Conditions		t$_{1/2}$ (day)	
Sample	**9Co**	**9Co**:SA 9:1	**9Co**:SA 9:1 + Base
14-F1'+**9Co-2**-F4	4.9(7)	3.9(9)	5(2)

IV.2.6. Elucidation of the nature of the oxidized product(s)

As it was thoroughly described in the previous section, FTIR spectra of the "fresh" additive **14** (*in black,* Figure IV-42) and after oxidation at 70 °C for 307 days (*in red*, Figure IV-42) clearly evidenced the formation of characteristic signals that originated from the aerobic oxidation process: an FTIR absorption centred at 1715 cm^{-1} that is characteristics of carbonyl groups and another one centred at ~ 3450 cm^{-1} that likely reflects the formation of alcohol functions. Significant spectral variations also occurred in the FTIR fingerprint region of the compound but were not considered due to the intricacy of this spectral range (1400-500 cm^{-1}). For further development of this oxygen barriers systems based innovative polymeric additives, it was however of importance to characterize as much as possible the oxidation products derived from aerobic oxidation of Dercolyte S 125 **14**.

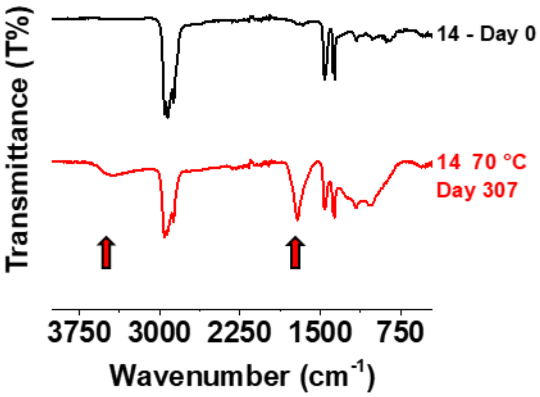

*Figure IV-42: FTIR spectra of fresh additive **14** and oxidized one.*

It has been initially proposed, that the oxidation of the additive **14** took place in the α position of the double carbon-carbon bond (*i.e.* allylic oxidation) leading to alcohols and/or carbonyl functions (Scheme IV-2).

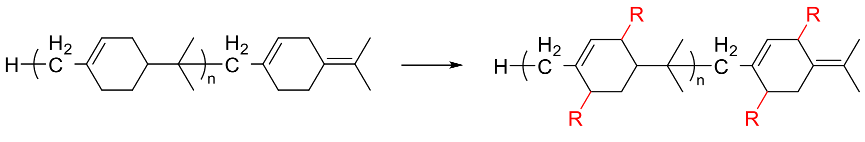

14

R = O or OH

*Scheme IV-2: Proposed metal catalyst-assisted aerobic oxidation route of the polymeric additive **14**.*

To obtain more information, the presence of carbonyl (C=O) and alcohol (C-OH) functions during the oxidation process of Dercolyte S 125 **14** was ascertained by XPS measurements. Significant oxygen enrichment of **14** samples that experienced thermal oxidation was clearly evidenced at the beginning of this project by SEM-EDS (Figure IV-8, Figure IV-9 and Figure IV-10) measurements. XPS survey scans (Figure IV-43) further confirmed this property.

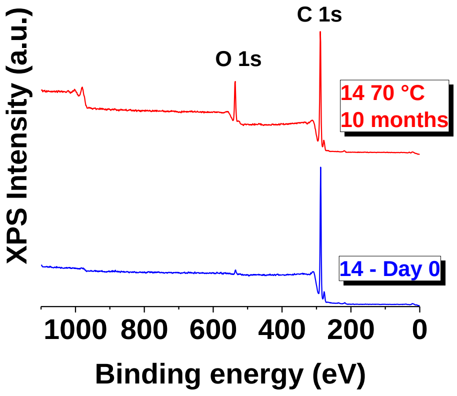

*Figure IV-43: XPS survey scans of **14**.*

When interest was focused on the C 1s electrons, no major difference was observed at first glance between the two samples of **14** (day 0, *in blue*, Figure IV-44 and after ten months at 70 °C, *in red*, Figure IV-44). Nevertheless, after spectra deconvolution, it appeared, as expected (*i.e.* Dercolyte S 125 **14** is a carbon rich polymer with a theoretical raw formula of $(C_{10}H_{15})_n$), that the spectrum of the fresh **14** contributed of up to 92% in the C 1s scan (C-C bond binding energy of 285 eV) of the oxidized additive and that the remaining 8% were most likely due to carbon-oxygen bonds (C-O bond binding energy at ~ 287 eV and C=O bond binding energy at ~ 289 eV, Figure IV-45).[188,189]

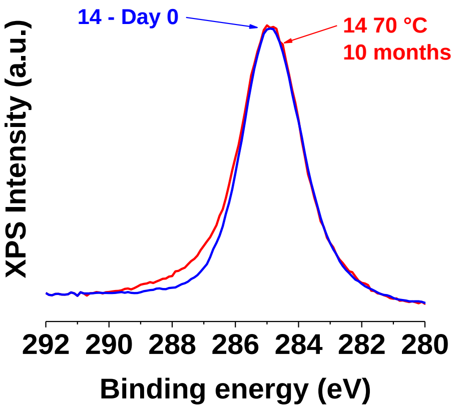

*Figure IV-44: XPS C 1s scans of **14**.*

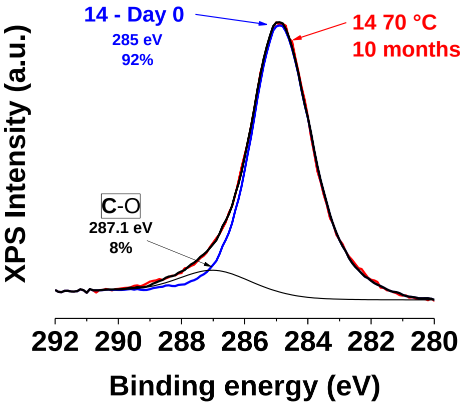

*Figure IV-45: XPS – deconvolution of C 1s scans of **14**.*

With respect to the O 1s scans of **14** (Figure IV-46), the enrichment in oxygen of the oxidized additive was clearly evidenced (*i.e.* Dercolyte S 125 **14** was already partially oxidized but at a low level). The deconvolution of the signal (Figure IV-47) demonstrated a contribution of only 12% of the initial additive to the oxidized additive. The remaining signal was due mainly to single carbon-oxygen bonds that contributed of up to 57% (C-O bond binding energy at ~ 533 eV) and carbon-oxygen double bonds for 31% (C=O bond binding energy at ~ 531.5-532 eV).

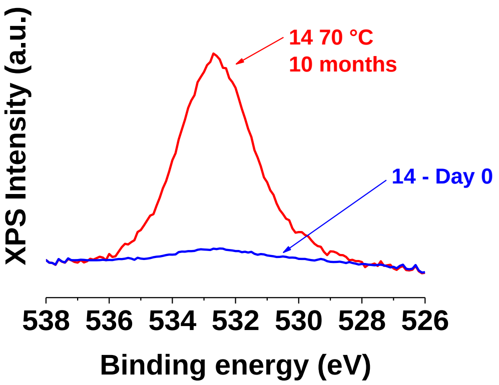

*Figure IV-46: XPS O 1s scans of **14**.*

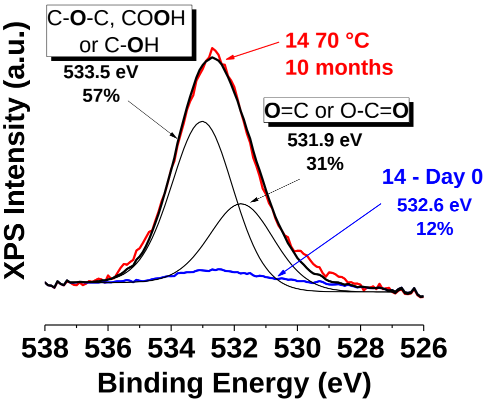

*Figure IV-47: XPS – deconvolution of O 1s scans of **14**.*

Elemental analyses of different samples of the additive **14** along the oxidation period were next measured and the corresponding results are gathered in Table IV-12. After 10 days of oxidation at 70 °C, an oxygen enrichment of 3.4% was measured with respect to the initial compound; it increased to 11.6% after 4.5 months of aerobic oxidation at 70°C (*i.e.* no catalyst was added to these samples to allow an accurate determination). In addition, to evidence an extensive oxidation of the polymeric additive, these analyses also demonstrated that **14** was partially oxidized from the outset.

*Table IV-12: Microanalyses results for **14** samples along the oxidation process.*

	%N	%C	%H	%O
Fresh **14**	0	86.7	11.5	**1.8**
14 after 10 days of oxidation at 70 °C	0	83.9	11.0	**5.2**
14 after 4.5 months of oxidation at 70 °C	0	77.0	9.6	**13.4**

---

[188] Datsyuk, V.; Kalyva, M.; Papagelis, K.; Parthenios, J.; Tasis, D.; Siokou, A.; Kallitsis, I.; Galiotis, C. *Carbon* **2008**, *46* (6), 833–840.

[189] https://xpssimplified.com/elements/carbon.php (accessed Dec 17, 2017).

With respect to the additive **14** and assuming in a first approach allylic oxidation, two carbon positions per unit might potentially be affected, *i.e.* the two positions in the α position of the carbon-carbon double bond. To estimate the number of oxidized positions as well as the nature of the oxidation product(s) (alcohol and/or ketone), a theoretical approach (elemental analysis) was undertook by assuming mono-oxidation of half of the units or mono-oxidation of all the units, and double oxidation of half of the units or all of the units (Figure IV-48).

If the oxidized products correspond to ketone or alcohol formation, the calculated elemental analyses demonstrated comparable values which preclude any definitive assignment. However, from the XPS and FTIR data, one can suggest that the aerobic oxidation of the polymeric additive **14** led to distribution of ketone and alcohols functions (*i.e.* assuming an equal distribution of carbonyls and alcohols, oxygen contents were shown to range between those of the ketone or alcohols products). Therefore, it can be suggested that after 10 days of oxidation (%O: 5.2%, Table IV-12), half of the units of the additive **14** were mono-oxidized (*green circle*, Figure IV-48). After 4.5 months of oxidation (%O: 13.4%, Table IV-12), the oxidized additive is in average somewhere between mono-oxidation of all the units, and mono-oxidation of all the units and bis-oxidation of half of the units of the polymer (*red circle*, Figure IV-48).

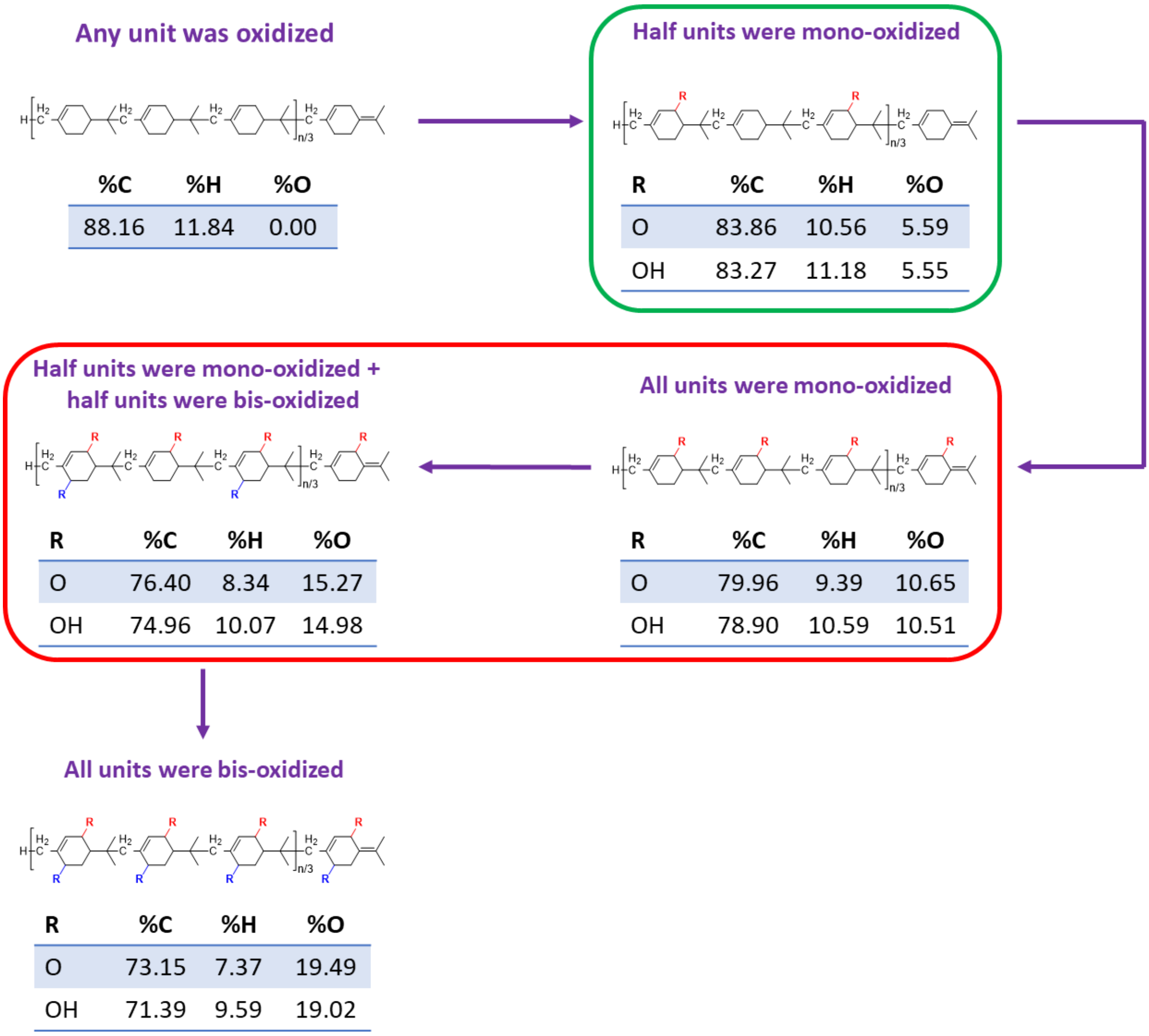
Any unit was oxidized
Half units were mono-oxidized
All units were mono-oxidized
Half units were mono-oxidized + half units were bis-oxidized
All units were bis-oxidized
H
H_2
C
n/3
R

%C	%H	%O
88.16	11.84	0.00

R	%C	%H	%O
O	83.86	10.56	5.59
OH	83.27	11.18	5.55

R	%C	%H	%O
O	79.96	9.39	10.65
OH	78.90	10.59	10.51

R	%C	%H	%O
O	76.40	8.34	15.27
OH	74.96	10.07	14.98

R	%C	%H	%O
O	73.15	7.37	19.49
OH	71.39	9.59	19.02

*Figure IV-48: Models for the calculation of the theoretical elemental analyses of putative oxidized species of the polymeric additive **14**.*

To go a step further and rule out the possibility of oxidative cleavage, size exclusion chromatography (SEC) analyses were performed on the three same samples. The results are gathered in Figure IV-49, Figure IV-50 and Table IV-13. It appeared that considering the weight average molecular weight ($\overline{M}w$), the number average molecular weight ($\overline{M}n$) or the dispersity (Đ), the additive **14** did not undergo an obvious cleavage upon thermal aerobic oxidation. The number of repetitive units is in average 7 with a high dispersity. The average molecular weight found in this work ($\overline{M}w$ = 2200 g.mol^{-1}) was found to be close to that given by the different providers ($\overline{M}w$ = 2500 g.mol^{-1}).

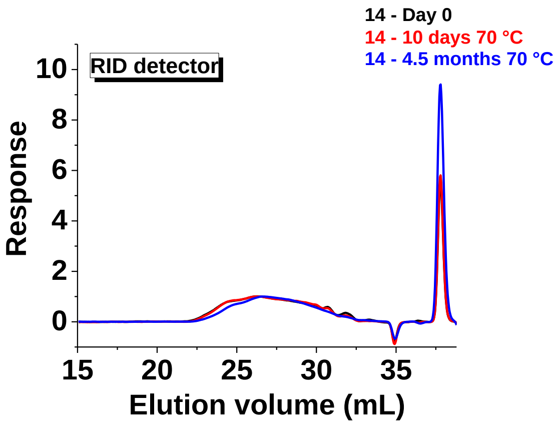

*Figure IV-49: SEC measurements of non-oxidized **14** before (black) and after 10 days (red) and 4.5 months (blue) of oxidation at 70 °C - refractive index detector (RID).*

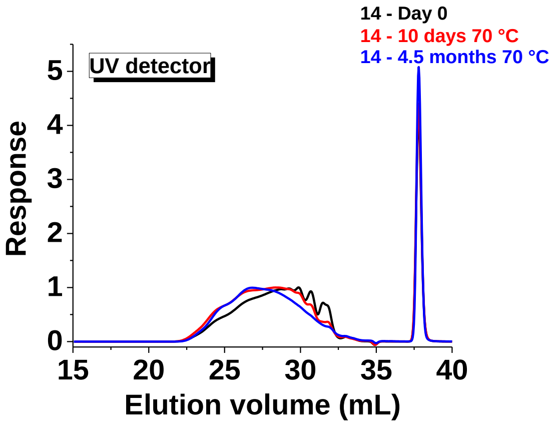

*Figure IV-50: SEC measurements of non-oxidized **14** before (black) and after 10 days (red) and 4.5 months (blue) of oxidation at 70 °C - UV detector.*

*Table IV-13: SEC data measured for the samples of the polymeric additive **14**.*

Sample	$\overline{M}n$ (g.mol^{-1})	$\overline{M}w$ (g.mol^{-1})	Đ
Fresh **14**	2200	1100	2.1
14 after 10 days of oxidation at 70 °C	2200	1100	1.9
14 after 4.5 months of oxidation at 70 °C	1900	1000	1.8

EPR measurements were performed to ensure that the oxidized products were not radical species (see previous chapter). This was clearly confirmed by the EPR, as no signal was clearly evidenced.

Last but not least, we recorded NMR spectra on “fresh” and oxidized (10 months of thermal aerobic oxidation at 70 °C) samples of Dercolyte S 125 **14**. Unexpectedly, no ^{13}C signals of the polymer could be measured despite many attempts at high concentrations in $CDCl_3$. On the other hand, the ^{1}H NMR spectra (Figure IV-51) of the polymeric additive **14** in solution were not easy to interpret due to severe line broadening of the proton signals due to the polymeric nature of the sample. Nevertheless, some conclusions could be drawn. For instance, the vinylic protons centred at 5.25 ppm of the oxidized **14** disappeared upon oxidation.

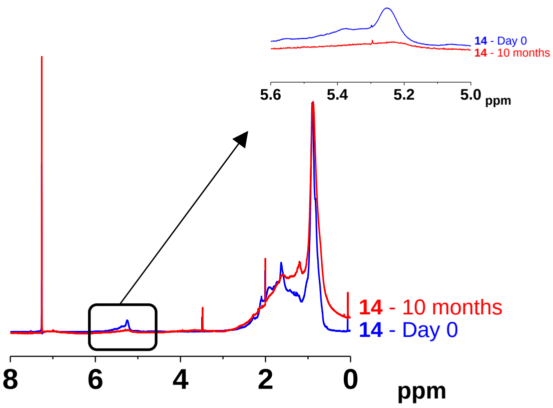

*Figure IV-51: ^{1}H NMR of **14**, $CDCl_3$, 400 MHz.*

Therefore, the formation of alcohols/ketones in the α position of the C=C double bond (*i.e.* following allylic oxidation) cannot be the sole potential oxidation products. Epoxidation of the C=C double bond can be therefore also suggested as described on Scheme IV-3.

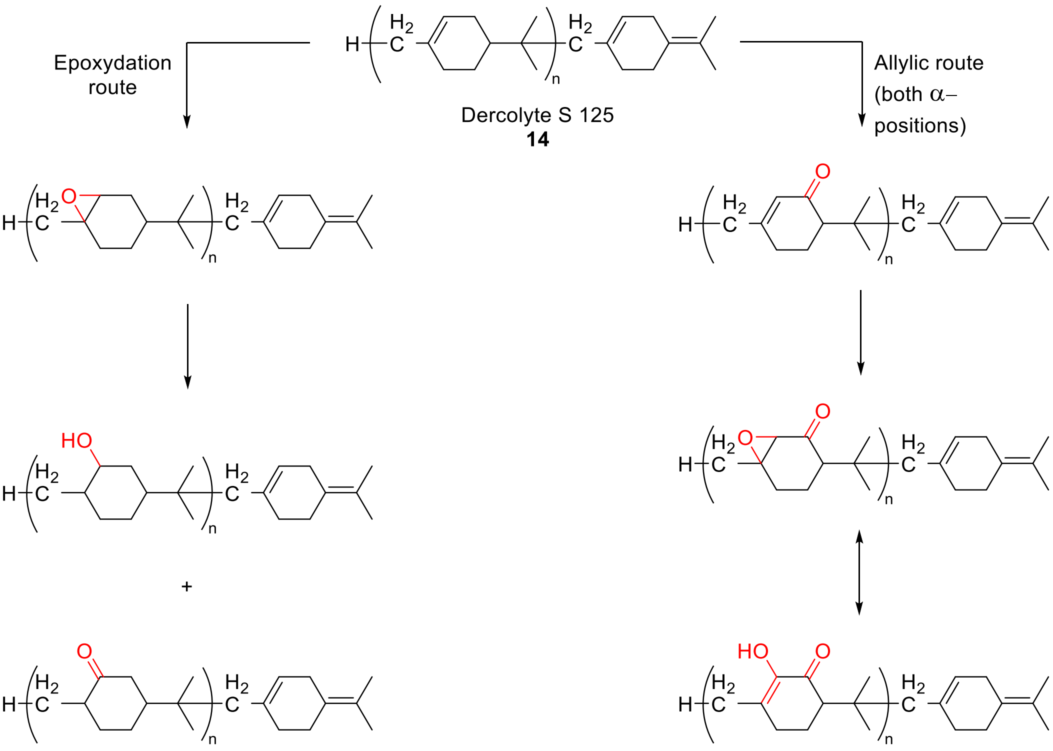

Scheme IV-3: Suggested oxidized products among other and their putative mechanism of formation. For the allylic oxidation, the two α-positions can be involved. As an example, only the products resulting from one α-position are described in the scheme.

To sum up, it has been clearly demonstrated by this extensive study that the cobalt(II) complex (**9Co**) was the most efficient catalyst (*i.e.* with respect to manganese(II) catalyst **9Mn** and the Schiff base complexes) allowing the fastest oxidation reaction of the homopolymer Dercolyte S 125 **14** ($t_{1/2}$ ~ 3 days with a catalyst/additive ratio of 1:35 *w/w*). The additive **14** displays more than one oxidable position per unit, making it a relevant candidate for oxygen barrier applications. In addition, even though it was difficult to properly elucidate the exact nature of the oxidation product(s) (*i.e.* epoxidation is likely an oxidation route), the polymeric additive **14** did not undergo evident cleavage along the oxidation process and therefore kept its integrity.

IV.3. Study of the oxidation of polyTHF 15

The same solid-state approach than that executed for the homopolymeric additive Dercolyte S 125 **14** was performed on a second copolymeric additive (resulting from the condensation of PEG, PET and polyTHF) designed and developed by Clariant that we have designated as polyTHF **15** (Scheme IV-4).

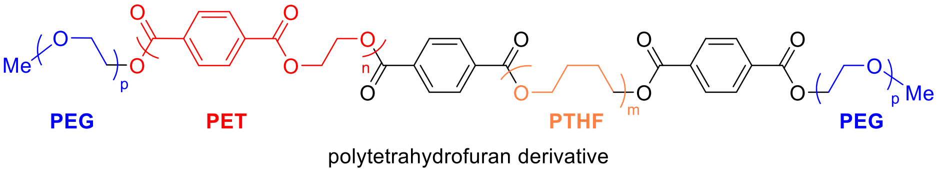

15

*Scheme IV-4:Chemical structure of the polymeric additive **15**.*

The oxidation of this polymeric additive was studied alone and in the presence of metal catalysts (*i.e.* cobalt(II) stearate **9Co-2** and manganese(II) stearate **9Mn-2** provided by Clariant, and a manganese(II) stearate **9Mn-3**, whose synthesis and purity were optimised in the laboratory, section II.3.1.3). To stick as closely to the previous experiments done with the polymeric additive **14** and also to work with homogeneous particle size distributions of both the additive and the catalysts, compound **15** and the metal complexes were all sieved separately, and their distribution checked by laser diffraction granulometry (Table IV-14).

*Table IV-14: Laser diffraction granulometry results after sieving of **15** and the targeted metal catalysts.*

Fraction	Gaussian curve maximum (µm)	d (0.5) (µm)
15-1-F1*	169	159
15-2-F1*	239	264
9Co-2-F4	26	19
9Mn-2-F4	30	23
9Mn-3-F4	23	3

* two different batches of **15** were studied

IV.3.1. Oxidation of polyTHF 15 monitored by FTIR

Before going further with the FTIR kinetic monitoring, it was of importance to characterize as much as possible the different FTIR absorptions of the PolyTHF compound **15** (Figure IV-52). The FTIR spectrum of **15** was fully attributed and the corresponding attributions are depicted in Figure IV-52. The PolyTHF **15** was mostly characterized by five intense absorptions, namely the alkyl or aryl stretching bands $\nu_{C\text{-}H}$ (~ 3000 cm^{-1}), the aryl out-of-plane bending or the alkyl C-H rocking bands (726 cm^{-1}), the ester (~ 1100 cm^{-1}) and ether (~ 1250 cm^{-1}) stretching $\nu_{C\text{-}O}$ bands, and importantly the ester carbonyl (1715 cm^{-1}) $\nu_{C=O}$ band.

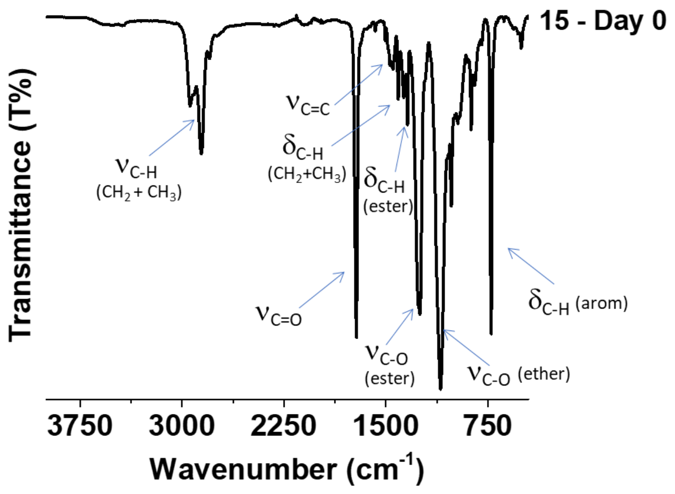

*Figure IV-52: Attributed FTIR spectrum of **15**.*

The oxidation of polyTHF **15** was firstly monitored at r.t. on the additive alone, or in combination with **9Co-2**, **9Mn-2** and **9Mn-3** (Figure IV-53).

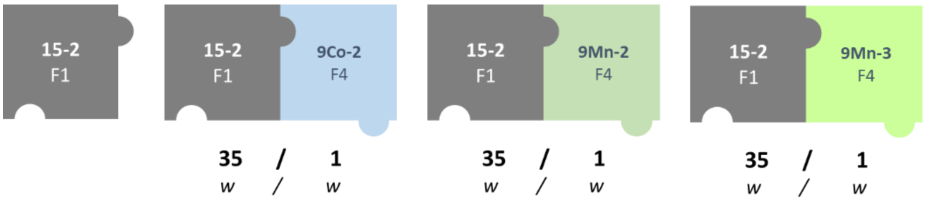

*Figure IV-53: Different combinations of interest for the study of the oxidation process of **15** at r.t.*

The samples were monitored by FTIR at regular intervals. After 48 days of monitoring at r.t., the formation of new functions was clearly observed (Figure IV-54): alcohol-type (~ 3425 cm^{-1}), carbonyl (broadening of the band centred at 1715 cm^{-1}) and ether (intensity increase of the peak centred at 1250 cm^{-1}) absorptions. The C-H_{ar} bending absorption at 726 cm^{-1} is seemingly not affected thus suggesting that aerobic oxidation does not affect the aromatic subunits of **15**.

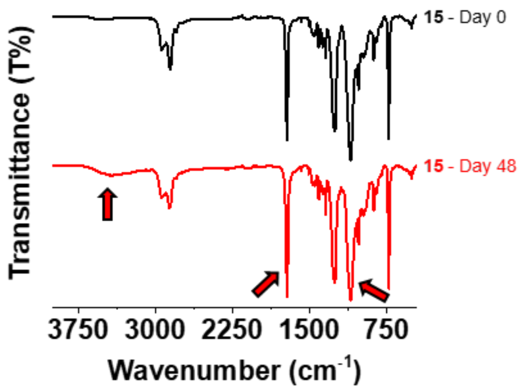

*Figure IV-54: FTIR spectra of **15** at day 0 and after 48 days of aerobic oxidation at r.t..*

Similarly to Dercolyte S 125 **14**, it was decided to focus on the FTIR absorption centred at 1715 cm^{-1} (*i.e.* relative to the C=O functions). The results for the four different combinations (*i.e.* additive/catalyst mixtures) are gathered in Figure IV-55. Contrary to Dercolyte S 125 **14** (*i.e.* no oxidation at r.t.), a slow oxidation of the polyTHF **15** was observed at r.t.. The oxidation reaction was markedly improved by addition of metal catalysts. Cobalt(II) stearate **9Co-2** was found to be still the best catalyst either in terms of quantity of oxidized products formed *(i.e.* a maximum is reached after a week followed by a slow decrease of the signal) or in terms of kinetics (*i.e.* the reaction is finished after less than 10 days). The two manganese(II) stearate **9Mn-2** (*i.e.* provided by Clariant) and **9Mn-3** (*i.e.* prepared in the laboratory, sections II.3.1.3 and II.5.2.2.3) presented both valuable catalytic activities but were found to be far less efficient than the cobalt(II) analogue. If the two manganese(II) stearate are compared, **9Mn-3**, whose synthesis and purity were optimized, displayed much better reactivity than **9Mn-2**.

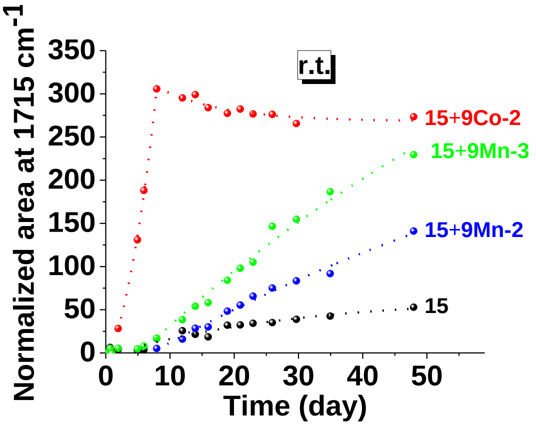

*Figure IV-55: Normalized area at 1715 cm^{-1} describing the oxidation of **15** either alone or with **9Co-2, 9Mn-2** or **9Mn-3** at r.t..*

In terms of kinetic properties, at r.t., the two manganese(II) catalysts seemed to markedly slow down the oxidation reaction of **15** as shown in Table IV-15. By contrast, cobalt(II) catalyst **9Co-2** markedly sped up the oxidation reaction of **15** (*i.e.* by a factor of 3).

*Table IV-15: Estimated half-life times of the different oxidation reactions of **15** monitored by FTIR at r.t. (given in days).*

Sample	$t_{1/2}$ (day)
15-2-F1	~ 17
15-2-F1+**9Co-2**-F4	5(1)
15-2-F1+**9Mn-2**-F4	~ 69
15-2-F1+**9Mn-3**-F4	~ 58

IV.3.1.1. Optimization of the catalyst:additive ratio

An investigation was then focused on the evaluation of the relevant catalyst:additive ratio for the **15/9Co-2** combination. For that, four different ratios were tested: 1:9, 1:35, 1:42.5 and 1:99 (catalyst: additive *w/w*). The prepared samples were stored at r.t. and were measured at regular intervals by FTIR (Figure IV-56) over about 20 days with a higher sampling frequency.

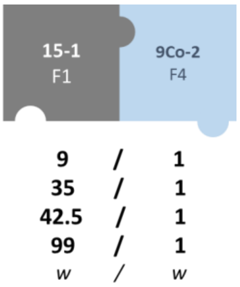

*Figure IV-56: Different combinations used to evaluate the catalyst/ratio influence on the oxidation process of **15** at r.t..*

The reaction seemed to be finished after about 5 days and higher the catalyst:additive ratio, more efficient the oxidation of **15** was. Nevertheless after 17 days, the difference between the different catalyst:additive ratio was not so significant.

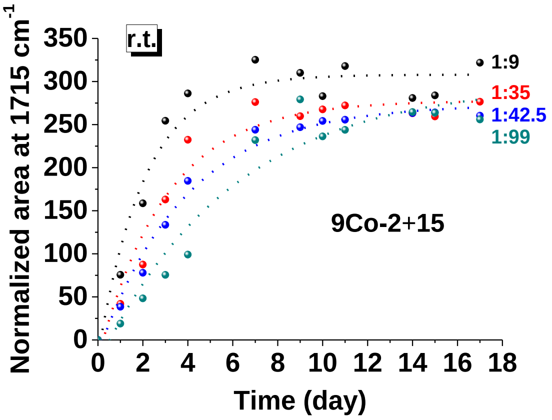

*Figure IV-57: Normalized area at 1715 cm^{-1} showing the progress of the oxidation reaction of **15** with **9Co-2** at r.t. with different catalyst:additive ratios.*

This first observation was confirmed by the kinetics parameters that were determined (Table IV-16 and Figure IV-58). Whatever the catalyst:additive ratio studied, the oxidation reaction was found to be fast. Moreover, the higher the proportion of cobalt(II) catalyst was, the more efficient and the faster the oxidation of **15** was. It is noteworthy that the polyTHF **15** was more prone to aerobic oxidation than Dercolyte S 125 **14** at r.t. in the presence of **9Co-2**. Importantly, the oxidation reaction was completed at r.t. after a few days of reaction, while the polymeric additive **14** was found to be almost inert under the same experimental conditions.

*Table IV-16: Half-life times of the different oxidation reactions of **15** at r.t. in the presence of **9Co-2** with different catalyst:additive ratios (given in days).*

Sample	Catalyst:additive ratio	$t_{1/2}$ (day)
15-1-F1 +**9Co-2**-F4	1:9	1.4(2)
15-1-F1 +**9Co-2**-F4	1:35	2.7(3)
15-1-F1 +**9Co-2**-F4	1:42.5	2.1(4)
15-1-F1 +**9Co-2**-F4	1:99	4(1)

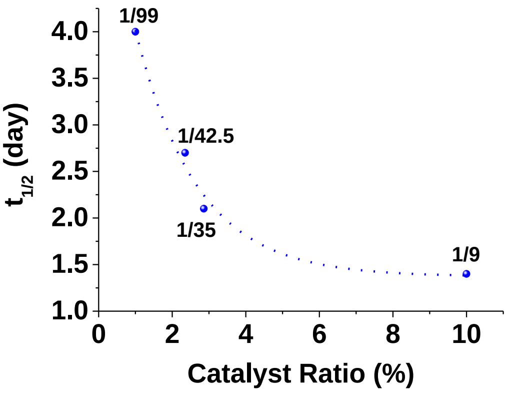

*Figure IV-58: Half-life times of the oxidation reaction of **15** in the presence of **9Co-2** at r.t. as a function of the catalyst:additive ratio.*

IV.3.1.2. Influence of the temperature on the metal-catalysed oxidation process of 15

The influence of the temperature on the oxidation efficiency of **15** was thereafter investigated. The polyTHF **15** was studied either alone or in combination with **9Co-2**, **9Mn-2** or **9Mn-3** (catalyst:additive 1:35 *w/w*) as illustrated in Figure IV-59.

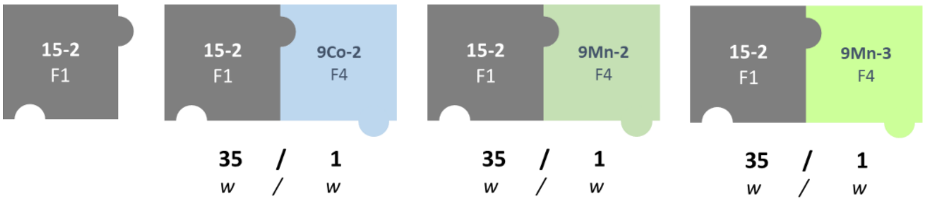

*Figure IV-59: Different mixtures prepared for the study of the oxidation process of **15** at 70 °C.*

The prepared samples were stored at 70 °C and monitored at regular intervals by FTIR. After 48 days of monitoring at 70 °C, the formation of new functions was clearly observed (**15** alone, Figure

IV-60 and **15** in the presence of **9Co-2**, Figure IV-61): alcohol-type (~ 3425 cm^{-1}), carbonyl (broadening of the band centred at 1715 cm^{-1}) and ether (intensity increase of the peak centred at 1250 cm^{-1}) absorptions. Concomitantly, vanishing of specific absorptions also occurred such as the C-H stretching absorption (ν_{C-H}) at 2860-2950 cm^{-1}, indicating most likely an oxidation of the methylene protons.

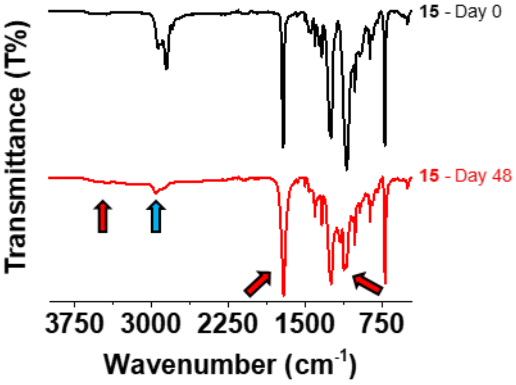

*Figure IV-60: FTIR spectra of **15** at day 0 and after 48 days of aerobic oxidation at 70 °C.*

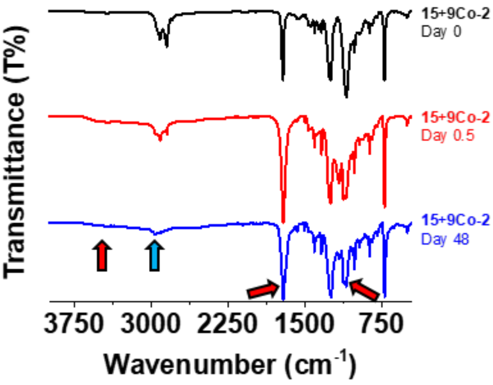

*Figure IV-61: FTIR spectra of **15** at day 0 and after 0.5 and 48 days of aerobic oxidation with **9Co-2** at 70 °C.*

The C-H$_{ar}$ bending absorption at 726 cm^{-1} is seemingly not affected thus suggesting that aerobic oxidation does not affect the aromatic subunits of **15**. These observations can be drawn for all the combinations studied at 70 °C and appeared more rapidly in the presence of metal catalyst (after only 0.5 day, Figure IV-61).

Whatever the studied combination, the oxidation reactions were found to be even more efficient and faster at 70 °C (Figure IV-62) than at r.t. (Figure IV-55). For instance, the oxidation reaction polyTHF **15** reached a maximum after less than three weeks with appreciable amount of oxidized products with respect to the experiment conducted at r.t.. The oxidation profiles measured for the oxidation of **15** in the presence of the metal catalysts was similar with a striking different behaviour (*i.e.* biphasic kinetic process) with respect to that measured in the absence of metal catalyst (*i.e.* mono-exponential variation). An efficiency sequence can be proposed on the basis of the amount of oxidized products formed at the end of the oxidation process (*i.e.* after 40 days of reaction): **15** ~ **15+9Co-2** >> **15+Mn-2** ~ **15+Mn-3**. We will discuss more in detail the putative oxidation mechanism that can be suggested.

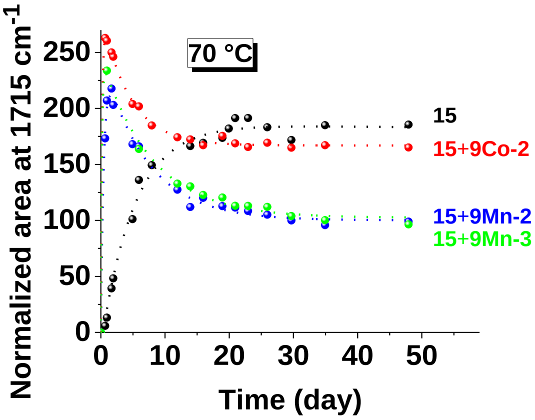

*Figure IV-62: Normalized area at 1715 cm^{-1} representing the oxidation of **15** either alone or with **9Co-2**, **9Mn-2** or **9Mn-3** at 70 °C.*

If we now take into account the kinetic parameters (Table IV-17), we can be clearly observed a significant catalytic effect of both the cobalt(II) and manganese(II) catalysts (Figure IV-62). The oxidation reaction of **15** indeed followed a biphasic mechanism. In the presence of **9Co** or **9Mn** at 70 °C, the first step was found to be very fast (*i.e.* completed in less than 2-3 days) and is followed by a much slower second step that is likely indicative of a loss of carbonyl functions as the monitored band is related to the C=O absorption. This might suggest an oxidative cleavage triggered by high temperature (*i.e.* not obviously observed for the experiments carried out at r.t., Figure IV-55) of the polymer along the oxidation process. In the absence of metal catalyst, the oxidation reaction is slowed down and the oxidation/degradation steps appeared concerted (*i.e.* **15** is continuously degraded throughout the oxidation process) thus explaining the presence of only one rate-limiting step.

Table IV-17: Half-life times of the different oxidation reactions of ***15*** *at r.t. and at 70 °C (given in days).*

	$t_{1/2}$ (day)		
	r.t.	70 °C	
Sample		1st step	2nd step
15-**2**-F1	~ 17	3.6(4)	
15-**2**-F1+**9Co**-**2**-F4	5(1)	0.13(2)	3.3(2)
15-**2**-F1+**9Mn**-**2**-F4	~ 69	0.32(3)	5.1(5)
15-**2**-F1+**9Mn**-**3**-F4	~ 58	<< 0.2	8.3(8)

IV.3.2. Elucidation of the nature of the oxidation product(s)

As described above, FTIR spectroscopy evidenced signatures of the formation of alcohol, carbonyl and ether along the oxidation process of **15**. The formation of these oxygenated functions was confirmed by XPS measurements on a sample of **15** that underwent thermal oxidation in the absence of any metal catalyst to not interfere with the analyses. At first glance, the XPS survey scans (Figure IV-63) did not reveal major differences.

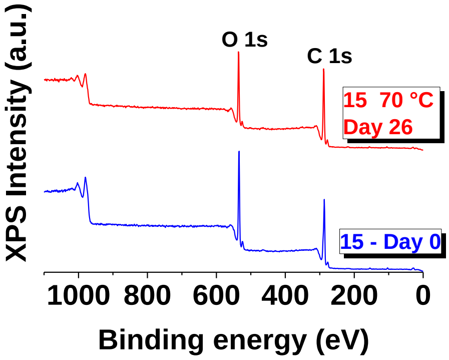

Figure IV-63: XPS survey scans of ***15****.*

Nevertheless, when examining more in detail in C 1s and O 1s scans, formation of new bonds at typical binding energies was observed. This is for instance the case for the C 1s scans (Figure IV-64) with the formation of a new chemical bond characterized by a binding energy of ~ 289 eV (characteristics of C=O bond binding energy at ~ 289 eV). When the signal was deconvoluted (Figure IV-65), it appeared that the initial polymer **15** contributed of up to 68% in the C 1s scan for the oxidized sample. The remaining contributions were attributed to single carbon-carbon bonds (binding energy of ~ 285 eV, 17%) and C=O bonds (binding energy of ~ 289 eV, 15%).

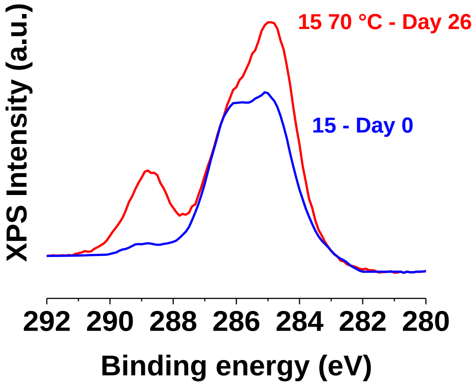

*Figure IV-64: XPS C 1s scans of **15**.*

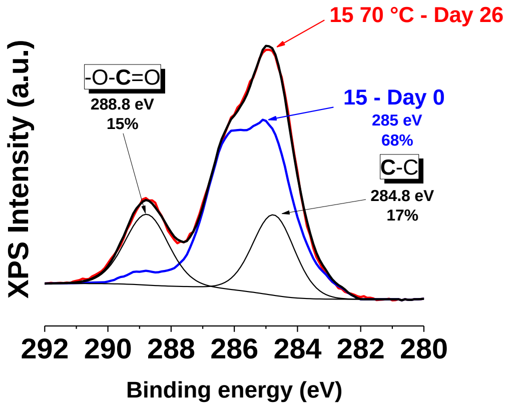

*Figure IV-65: XPS – deconvolution of C 1s scans of **15**.*

If we now focus on the O 1s scans (Figure IV-66), we can clearly observe that the intensity and the bandwidth of the oxidized sample of **15** were much higher than for the non-oxidized one. Deconvolution of the O 1s signal (Figure IV-67) indicated that the non-oxidized sample contributed of up to only 27% in the oxidized polymer. The major contributions originated mainly from newly C-O (31%) and C=O (42%) formed bonds along the thermal aerobic oxidation.

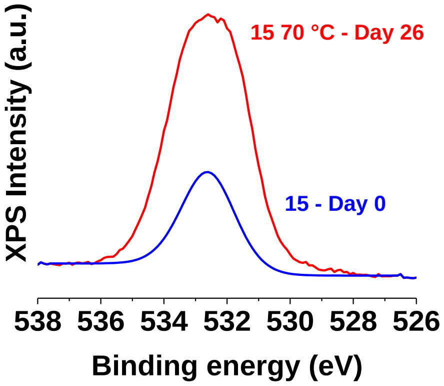

*Figure IV-66: XPS O 1s scans of **15**.*

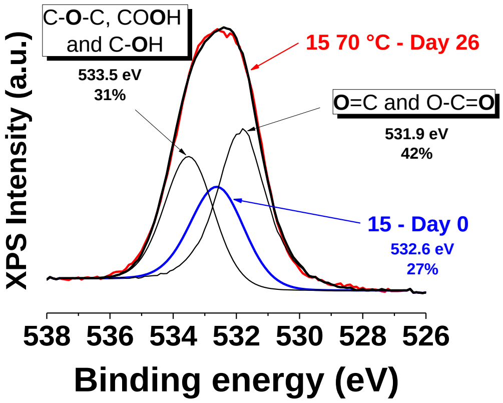

*Figure IV-67: XPS – deconvolution of O 1s scans of **15**.*

Elemental analysis further confirmed on oxygen enrichment of 9% of the polyTHF sample **15** after aerobic oxidation (Table IV-18). The same approach than that conducted with the homopolymer Dercolyte S 125 **14** is ruled out due to the presence of different repetitive units within the copolymer **15** and the lack of knowledge on its composition.

*Table IV-18: Microanalyses results for **15** samples along the oxidation process.*

	%N	%C	%H	%O
Fresh **15**	0	62.4	7.8	**29.8**
15 after 26 days of oxidation at 70 °C	0	55.9	5.3	**38.8**

To go a step further in the understanding of the oxidation mechanism of the polyTHF **15**, NMR experiments were carried out in $CDCl_3$. The ^1H NMR spectrum of the non-oxidized polymeric additive **15** was relatively easy to interpret compared to that of the first homopolymer, Dercolyte S 125 **14**. The different ^1H signals were easily attributed (*i.e.* 2D COSY and HSQC experiments were carried out to confirm the protons assignment) and are labelled in Figure IV-68. It is noteworthy that at this stage we do not have any information on the number of repetitive units and, so, on the polymer chain length and molecular weight.

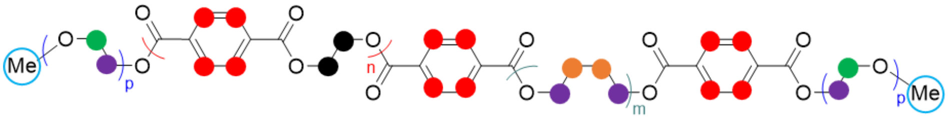

polytetrahydrofuran derivative
15

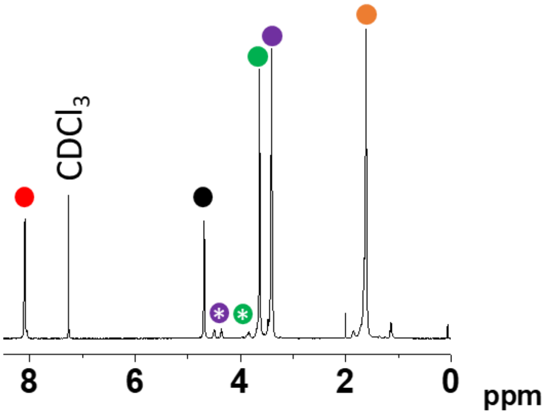

Figure IV-68: ^{1}H NMR spectrum of non-oxidized ***15*** *measured in CDCl$_3$ at 500 MHz.*
** indicated terminal residues of the polymer.*

When the ^{1}H NMR spectrum of the non-oxidized additive **15** was compared to that measured on a sample that experienced extended oxidation at 70 °C (Figure IV-69), the first striking observation was the disappearance of most of the CH$_2$ signals supporting extensive oxidation at these positions (*i.e.* *violet*, *green* and *orange* positions belonging to the polytetrahydrofuran- and PEG-subunits, Figure IV-68 and Scheme IV-4). Some CH$_2$ of the ethylene glycol-type moieties connecting to the terephtalate subunits (*i.e.* belonging to the PET-type units) were not affected by the oxidation process (*black* position, Figure IV-68).

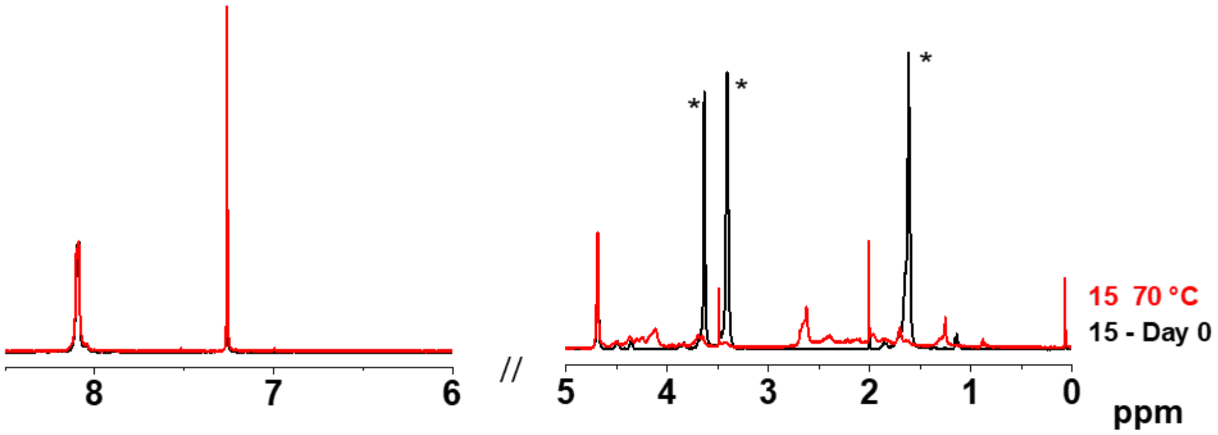

Figure IV-69: ^{1}H NMR spectra of non-oxidized polyTHF ***15*** *before (black) and after (red) prolonged oxidation at 70 °C recorded in CDCl$_3$ at 500 MHz.*

Further analysis of the ^{13}C NMR revealed other valuable information. On thermally-assisted oxidation of the copolymer **15**, ^{13}C NMR signals (Figure IV-70) were found to be lacking (*i.e.* exclusively those associated to the CH$_2$ lose on the ^{1}H NMR spectra on the oxidized sample) most likely due to an oxidative cleavage of compound **15** with gas release such as CO, CO$_2$...(*i.e.* the masterbatches of Clariant in Pogliano, Italia informed us that CO$_2$ generation was observed on oxidation of the PolyTHF **15**).

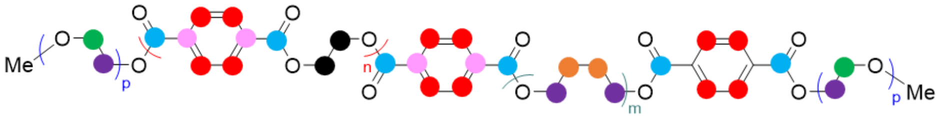

polytetrahydrofuran derivative
15

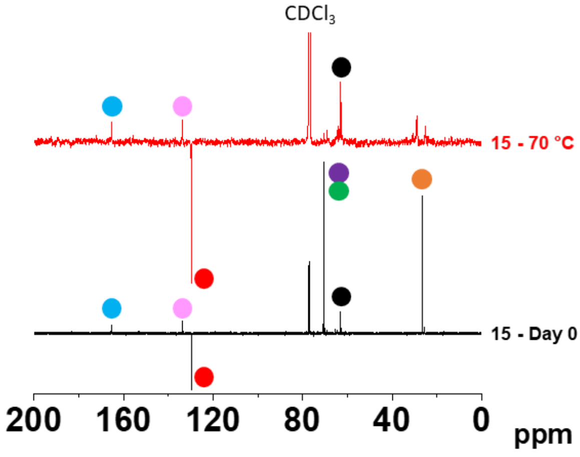

*Figure IV-70: ^{13}C DEPT NMR spectra of non-oxidized polyTHF **15** before (black) and after (red) prolonged oxidation at 70 °C recorded in $CDCl_3$ at 500 MHz.*

SEC analyses were therefore performed on the two same samples to ascertain the suggested thermal-oxidative cleavage revealed from our previous measurements. The SEC measurements with a refractive index (Figure IV-71) or UV detector (Figure IV-72) display a shift to the higher retention time along the oxidation of **15** thus clearly demonstrating the presence of much smaller molecular lengths.

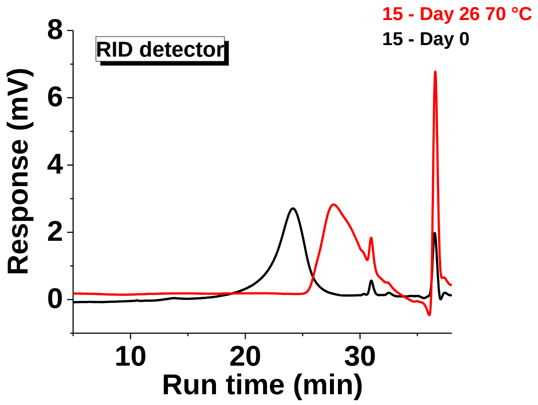

*Figure IV-71: SEC measurements of non-oxidized polyTHF **15** before (black) and after (red) prolonged oxidation at 70 °C - refractive index detector (RID).*

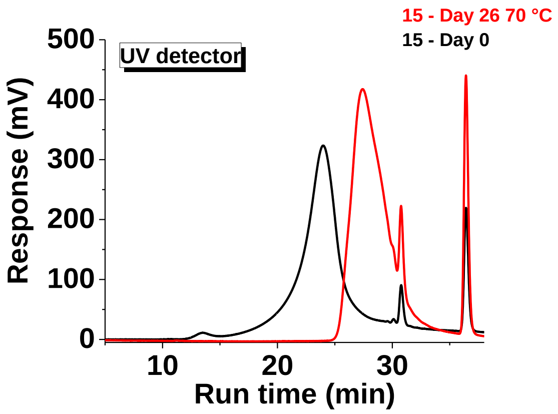

*Figure IV-72: SEC measurements of non-oxidized polyTHF **15** before (black) and after (red) prolonged oxidation at 70 °C - UV detector.*

The results are gathered on Table IV-19. They clearly indicated an extensive cleavage during the oxidation of the highly dispersed copolymer **15** into much shorter fragments with a significant improvement of the dispersity factor, as already suggested by FTIR and NMR.

*Table IV-19: SEC results for the **15** samples.*

Sample	$\overline{\mathrm{M}}$n (g.mol^{-1})	$\overline{\mathrm{M}}$w (g.mol^{-1})	Đ
Fresh **15**	18 800	46 100	49.8
15 after oxidation at 70 °C	2 700	4 500	1.6

The polymeric additive **15** underwent oxidation process both at r.t. and at 70 °C either alone or in the presence of metal catalysts. The catalytic activity of the investigated metal complexes was clearly demonstrated, with a key advantage for the cobalt(II) one as already observed with Dercolyte S 125 **14**. From the characterization of the oxidized products conducted by FTIR, microanalysis, XPS, SEC and NMR, it was clearly shown that the integrity of the polymer was not maintained on oxidation and that the copolymer **15** underwent extended oxidative cleavage (Scheme IV-5). Nevertheless, at this stage of this study, the precise elucidation of the nature of the oxidation products remained delicate and risky.

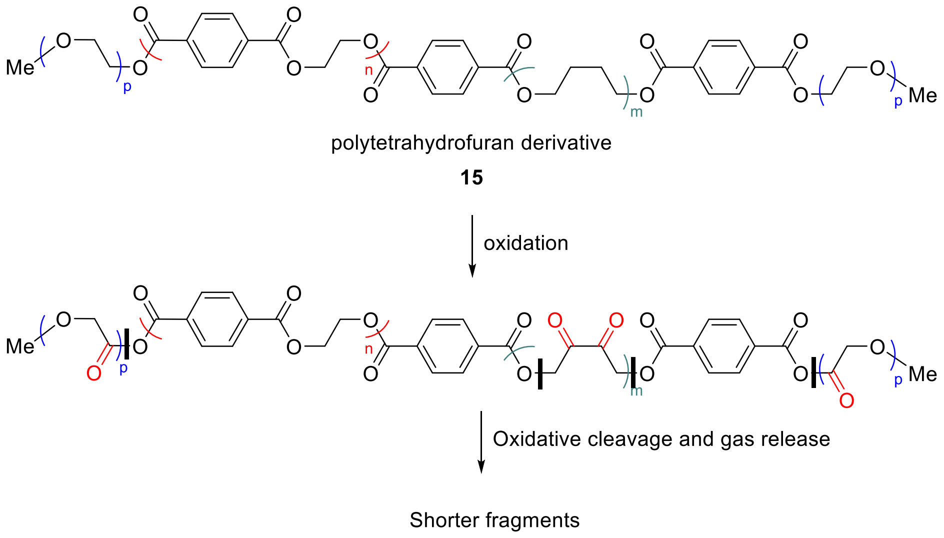
polytetrahydrofuran derivative
oxidation
Oxidative cleavage and gas release
Shorter fragments
Me
O
p
n
m

15

*Scheme IV-5: Putative oxidation sites and products formed from oxidative cleavage of **15**. The bold black lines indicate the potential cleavage points.*

It has been shown in the literature[190] that aerobic thermo-oxidation of polyethylene may lead to the formation of alkyl free radicals.

$$\left.\begin{array}{l} \mathrm{RH} \xrightarrow{\Delta,\ O_2} \mathrm{ROOH} \\ \mathrm{ROOH} \xrightarrow{\Delta,\ h\nu} \mathrm{RO}^{\bullet} + {}^{\bullet}\mathrm{OH} \end{array}\right\} \text{Hydroperoxides formation and cleavage}$$

$$\left.\begin{array}{l} \mathrm{ROOH} + \mathrm{M}^{2+} \longrightarrow \mathrm{M}^{3+} + {}^{-}\mathrm{OH} + \mathrm{RO}^{\bullet} \\ \mathrm{ROOH} + \mathrm{M}^{3+} \longrightarrow \mathrm{M}^{2+} + \mathrm{H}^{+} + \mathrm{ROO}^{\bullet} \end{array}\right\} \text{Metal catalyst reaction with hydroperoxides}$$

$$\left.\begin{array}{l} \mathrm{HO}^{\bullet} + \mathrm{RH} \longrightarrow \mathrm{H_2O} + \mathrm{R}^{\bullet} \\ \mathrm{R}^{\bullet} + \mathrm{O_2} \longrightarrow \mathrm{ROO}^{\bullet} \\ \mathrm{ROO}^{\bullet} + \mathrm{RH} \longrightarrow \mathrm{ROOH} + \mathrm{R}^{\bullet} \\ \mathrm{ROOH} \longrightarrow \mathrm{RO}^{\bullet} + {}^{\bullet}\mathrm{OH} \\ \mathrm{RO}^{\bullet} + \mathrm{RH} \longrightarrow \mathrm{ROH} + \mathrm{R}^{\bullet} \end{array}\right\} \text{Oxidation of polyethylene}$$

Scheme IV-6: Putative thermo-oxidative degradation of HDPE that may account for our observations (from Maryudi[190])

Once the alkyl radicals are formed (Scheme IV-6), they may react rapidly with oxygen and generate alkylperoxy free radicals ($\mathrm{ROO}^{\bullet}$). These radicals may then abstract hydrogen from the polymer to lead to hydroperoxides (ROOH). At the high temperatures, hydroperoxides rapidly cleave to form alkoxy and hydroxyl radicals. These compounds may in turn rapidly abstract hydrogen from the polymer to form more alkyl radicals. The alkoxy radical ($RO^\bullet$) being unstable will decompose spontaneously to form ketones, aldehydes, etc. and these carbonyl compounds might undergo further oxidation to produce acids, esters and to some extent volatile derivatives. Following this mechanism, metal complexes may catalyse the hydroperoxide decomposition step of the oxidation mechanism. This putative mechanism may account for our observations for the copolymer **15** and explains the catalytic effect of **9Co** leading to extensive oxidation and cleavage. This will be investigated more in detail.

---

[190] Maryudi, M.; Hisyam, A.; Yunus, R. M.; Bag, M. D. H. *Int. J. Eng. Res. Appl.* **2013**, *3* (2), 1156–1165.

In conclusion, using a fruitful panoply of complementary analytical tools, we gain deeper insights on the oxidation mechanism of two different polymers (*i.e.* the homopolymer **14** and the copolymer **15**) dedicated to the same industrial application (*i.e.* oxygen barriers for packaging). The catalytic properties of cobalt(II) and manganese(II) complexes were assessed and the choice fell on cobalt(II) stearate which undoubtedly displayed the highest catalytic activities whatever the additive combined. With respect to these two polymeric systems (**14** and **15**), studies conducted at the solid-state were realised to come as close as possible to the real conditions of the manufacturing of plastic films or bottles (*e.g.* "*extrusion*" process, composition...). The efficacy and the kinetics parameters of the cobalt(II) and manganese(II) catalysts on the oxidation of the polymeric additives were evaluated by FTIR, and different conditions were mimicked, especially those of the "*extrusion*" process.

In contrast to the additive Dercolyte S 125 **14**, the copolymeric additive **15** underwent oxidation either at r.t. or at 70 °C. Its oxidation kinetics was found to be much faster with respect to the oxidation of **14**, especially when associated with **9Co-2** at r.t. or at 70°C.

Tentative efforts were also devoted to the precise elucidation of the oxidation products for each of the additives by complementary analytical techniques (FTIR, SEC, XPS, microanalysis, NMR...). Even though it was difficult to characterize properly the oxidation products, it was demonstrated that the homopolymer **14** was not degraded throughout the oxidation process and that the alkene moiety is most likely one of the important reaction site. For the highly dispersed copolymer **15**, oxidation catalysed by metal stearates most likely took place at many sites and subsequently led to cleavage and generation of much smaller fragments, those stability, migration and potential toxicity have to be evaluated.

IV.4. Experimental section

IV.4.1. Analytical equipments used in this study

IV.4.1.1. Nuclear Magnetic Resonance spectroscopy - NMR

Objectives and means: *NMR analyses were carried out to characterize either the polymeric additives or the final polymeric additive compounds resulting from oxidation with or without metal catalysts.*

NMR spectra were recorded on Bruker Avance III HD 400 MHz with BBFO probe or a Bruker Avance III HD 500 MHz with "Prodigy" CPPBBO probe spectrometer with solvent peaks as reference. Solvent used for NMR analyses was chloroform-*d* ($CDCl_3$, Aldrich, 99.8 atom% D). Chemical shifts (δ) are expressed in ppm relative to TMS. Multiplicity is indicated as s (singlet), d (doublet), t (triplet), q (quartet), m (multiplet), dd (doublet of doublets). Coupling constant (*J*) values are given in hertz (Hz).

IV.4.1.2. Fourier Transform Infrared spectroscopy - FTIR

Objectives and means: *FTIR measurements were carried out to characterize the final products resulting from aerobic oxidation of the polymeric additives with or without metal catalysts (at r.t. or at 70 °C). The kinetics of oxidation was also evaluated by FTIR measurements thus providing valuable parameters to assess the efficacy of both the metal catalysts and the polymeric additives (displaying different chemical patterns).*

FTIR spectra were recorded neat on a Perkin Elmer FTIR Spectrometer Spectrum Two or on a Thermo Scientific Nicolet 380 FT-IR Spectrometer (used only to measure infra-red spectra on KBr pellets). Spectra were analysed using *Spectrum* software from PerkinElmer and indexed thanks to Parikh V.M. book.[165]

IV.4.1.3. Microanalysis

Objectives and means: *microanalyses (C, H, N) were performed to evaluate the extent of oxidation of the polymeric additives after aerobic treatments with or without catalysts at r.t. or at 70 °C.*

Elemental analyses were performed on a Flash 2000 from ThermoFisher Scientific.

IV.4.1.4. Electron Paramagnetic Resonance spectroscopy - EPR

Objectives and means: *EPR measurements were carried out to evaluate the paramagnetic character of the polymeric additives before and after aerobic treatment with or without the catalysts at r.t. or at 70 °C.*

EPR measurements were performed on a Bruker spectrometer EMX X-band equipped with a 4119 HS-W1 cavity (high sensitivity). An ESR cryostat (Oxford Instruments) was used for the low temperature measurements.

IV.4.1.5. Laser diffraction granulometry

Objectives and means: *for the sake of comparison, granulometry measurements were performed to characterize the particle size distribution of the investigated samples (polymeric additives and metal catalysts).*

Laser diffraction granulometry measurements were performed on a Malvern Instruments Mastersizer 2000 equipped with a *small volume dispersion unit* Hydro 2000SM controlled by a *dispersion unit controller.*

Depending on the particle size distribution, different technologies are available to measure particle size (Figure IV-73).[191] For our application, the laser diffraction detection was selected.

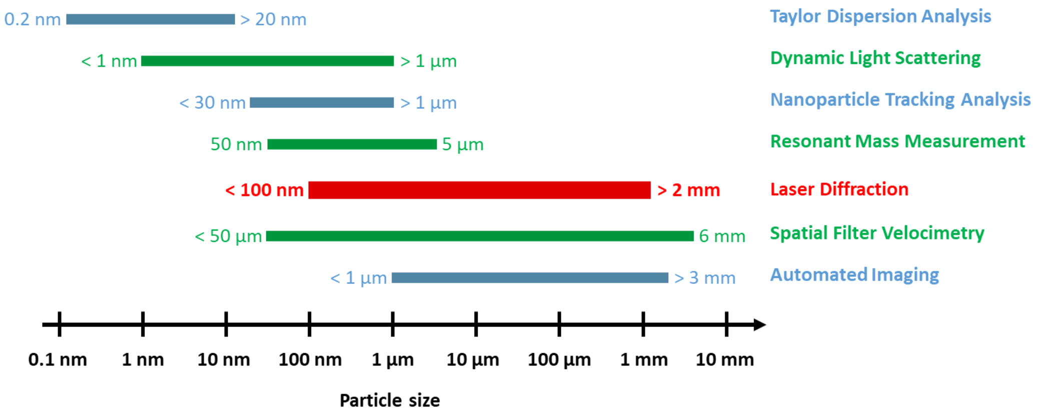

Figure IV-73: Different technologies to measure particle size.

The principle of particle size measurement by laser diffraction is based on a laser beam crossing a dispersed particulate sample. The measure of the angular variation in intensity of the scattered light allows determining the particle size of the sample. The larger the particle size is, the smaller the angles relative to the laser beam are, and on the contrary the smaller particle sizes will scatter the light with larger angles. This angular scattering intensity is then related to the particle size (Mie theory of light scattering). The result is given as a volume equivalent sphere diameter.

A sample analyzed by laser diffraction granulometry will be then characterized by four parameters (given in µm):

- The maximum of the Gaussian curve.
- d (0.1), the first decile: 10% of the sample present a particle size distribution lower than this maximum value.
- d (0.5), the median value: 50% of the sample present a particle size distribution lower than this value, and 50% higher than this maximum value.
- d (0.9), the 9th decile: 10% of the sample present a particle size distribution higher than this maximum value.

These values provide valuable information of the Gaussian curve form. In fact, the more the curve ideal is, the closer the values of the maximum of the Gaussian curve and d (0.5) will be.

IV.4.1.6. Scanning Electron Microscopy - SEM

Objectives and means: *scanning electron microscopy was used to obtain information on the topography and morphology of the investigated samples. This technique was mainly used for the study of the polymeric additive Dercolyte S 125* ***14****. In addition to these important parameters, elemental analysis was performed to evaluate the degree of oxidation of the samples.*

SEM measurements were performed with the help of a Zeiss GeminiSEM 500 microscope. The principle of this technique is based on an electron beam going through an electron retarder (electrons are slowed down to minimize surface alteration) before reaching the sample surface. Electrons are extracted from the surface and go through an electron booster before being analyzed in the detector. This allows giving topographic and morphologic information of the sample.

---

[191] https://www.malvern.com/ (accessed Oct 19, 2017).

EDS can be used in addition to SEM to obtain semi-quantitative elemental analysis in a very specific area of the sample. EDS measurements were performed on an EDAX apparatus. These two combined techniques allow determining proportion of given elements in a given area of interest.

IV.4.1.7. Size Exclusion Chromatography - SEC

Objectives and means: *size exclusion chromatography was used to evaluate the average polymer length as well as the type of dispersity. These experiments were conducted to evaluate the level of oxidative breakage upon aerobic oxidation of the polymeric additives.*

SEC measurements in THF were performed on Shimadzu chromatography system (pump: LC20-AD, inline degasser: DGU-20A, automatic injector: SIL-20A, column oven: CTO-20A at 35 °C, refractometric detector: RID-10A, UV detector: SPD-20A, flow rate: 1 mL.min^{-1}). Calibration was first performed with PS (10 Polymer Lab. standards from 162 to 20 650 g.mol^{-1}). Analyses were performed in THF (liquid chromatography quality) thanks to four monoporosity PLGel columns assembled in series (50 Å, 100 Å, 500 Å and 1000 Å) allowing separation from 100 to 600 000 g.mol^{-1}. Samples were dissolved in THF and filtered on 0.45 µm PTFE filter (Captiva, Agilent) prior to SEC analyses.

SEC measurements in chloroform were performed on Shimadzu Prominence LC-20 chromatography system (pump: LC20-AD, inline degasser: DGU-20A, automatic injector: SIL-20A, column oven: CTO-20A, refractometric detector: RID-10A, UV detector: SPD-20A, flow rate: 1 mL.min^{-1}). Calibration was first performed with PS (10 Polymer Lab. standards from 162 to 20 650 g.mol^{-1}). Analyses were performed in chloroform (liquid chromatography quality) thanks to a PLGel precolumn (5 µm) and four PLGel columns assembled in series (two 5 µm MIXED-C and one 5µm 100 Å) allowing separation from 580 to 1 650 000 g.mol^{-1}. Samples were dissolved in chloroform and measured at a concentration of 5 mg.mL^{-1}.

IV.4.1.8. X-ray Photoelectron Spectroscopy - XPS

Objectives and means: *XPS is a surface-sensitive spectroscopic tool that determines the elemental composition of a solid sample as well as the chemical and electronic states of the elements that compose this material. In our investigations, the XPS analyses were mainly performed to evaluate the nature of the chemical bonds in the different considered samples. This technique was also of crucial interest to evaluate the level of oxidation as well as to characterize in the solid state the oxidized products of the polymeric additives, Dercolyte S 125* ***14*** *and polytetrahydrofuran derivative (namely, polyTHF)* ***15*** *additives.*

XPS analyses were performed on a Thermo-VG Scientific spectrometer equipped with a CLAM4 (MCD) hemispherical electron analyzer. By irradiating a material with a beam of X-rays, one 1s electron is extracted from the upper layer (0 to 10 nm of the material) and is photo-ejected (Figure IV-74). This signal is then analyzed in terms of the kinetics and the number of electrons that are photo-ejected (Figure IV-75). XPS requires ultra-high vacuum (UHV; $P < 10^{-9}$ mbar) conditions.

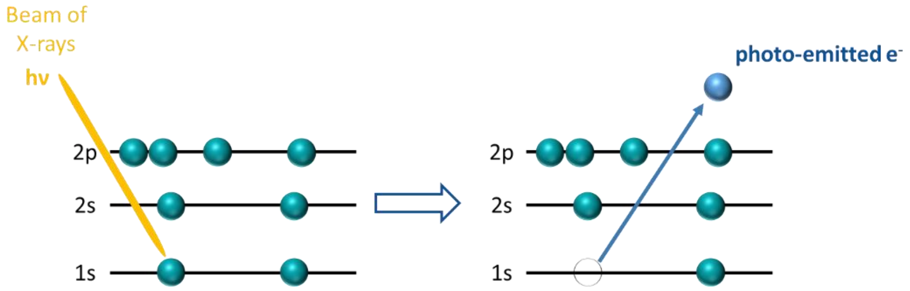
Beam of
X-rays
hν
2p
2s
1s
photo-emitted e-
2p
2s
1s

Figure IV-74: XPS principle.

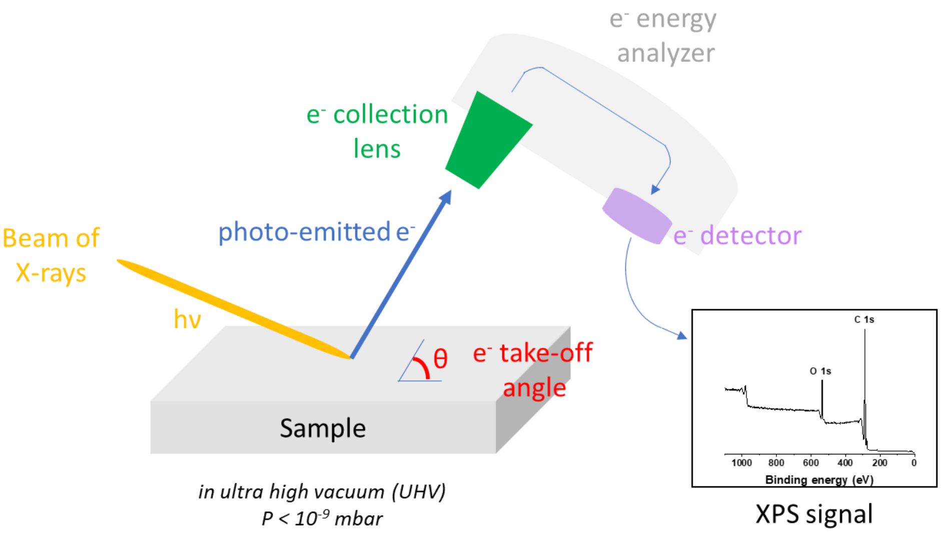
e- energy
analyzer
e- collection
lens
Beam of
X-rays
hν
photo-emitted e-
e- detector
θ
e- take-off
angle
Sample
in ultra high vacuum (UHV)
P < 10-9 mbar
C 1s
O 1s
1000
800
600
400
200
0
Binding energy (eV)
XPS signal

Figure IV-75: XPS equipment.

IV.4.2. General experimental protocols for setting up FTIR measurements

IV.4.2.1. Preparation of the KBr pellets for FTIR measurements

General procedure ***J*** for the preparation of the KBr pellets for FTIR measurements:

KBr was first finely ground. The sample (5% by weight) was added to KBr. The mixture was then finely ground together and placed into a Specac hydraulic press (applied pressure: 10 tons) to form the pellet. Pellet was stored at r.t. and was analyzed by FTIR at given intervals.

Three types of pellets were prepared following the *general procedure **J***:

- With the metal catalyst *bis*{2-[[(phenylmethyl)imino]methyl]-phenolato} cobalt(II) **1Co** alone (5% by weight).
- With the monomeric additive *N*-(3,3,5,5-tetramethylpiperidin-4-yl)benzamide **11** alone (5% by weight).
- With the metal catalyst *bis*{2-[[(phenylmethyl)imino]methyl]-phenolato} cobalt(II) **1Co** (0.5% by weight) combined to *N*-(3,3,5,5-tetramethylpiperidin-4-yl)benzamide **11** (4.5% by weight) (catalyst/additive/KBr 0.5:4.5:95 *w*/*w*/w and catalyst/additive 1:10 *w*/w).

These pellets were measured by FTIR just after the preparation (Day 0) and after storage at r.t. for 5, 8 and 22 days. However, this approach was discarded because of the stability and weakness of the KBr pellets especially when the material is stored at higher temperature as well as the large amount of compounds required. Last but not least, recovery of the sample for other analytical experiments (microanalysis, NMR…) was not possible when mixed with KBr.

IV.4.2.2. Use of glass strips for FTIR measurements

Glass strips were tested to analyze samples by FTIR and to avoid sample consumption during measurement. As said before, the KBr pellet approach was discarded due to major disadvantages (weakness of the pellet especially for repeated handlings and measurements, difficulty to operate at higher temperature…).

To properly assess this method, FTIR spectra of glass strips were firstly measured without any sample under the following conditions: (*i*) one or two superimposed glass strips without any applied pressure (no absorption was observed); (*ii*) one or two superimposed glass strips with applied pressure (strong absorption of the glass was observed). Thus, FTIR spectra of two superimposed glass strips containing a sample sandwiched between them were recorded: without pressure (no absorption was observed) or with pressure (strong absorption of the glass was still observed without any evidence for the sample).

Lastly, no glass strip was used and the FTIR spectra were recorded directly on the samples. FTIR spectra were of significance and reproducible. It was demonstrated that the measurements can be done without the need of glass strip/pressure or the use of KBr pellet. However, using this approach it was not possible to recover the material because of the small amount needed for the measurement which was removed from the diamond (FTIR instrument) by washing.

IV.4.2.3. Oxidation of the polymeric additives monitored by FTIR spectroscopy

General procedure ***K*** for monitoring the oxidation of the polymeric additives by FTIR spectroscopy:

The metal catalyst and the polymeric additive (catalyst/additive 1:35 *w/w*, unless otherwise stated) were mixed together in the solid-state. The metal catalyst and/or the polymeric additive, taken separately, were also analyzed by the same analytical technique. The prepared samples were stored both at r.t. and at 70 °C (unless otherwise stated) and analyzed by FTIR just after the preparation (Day 0) and at regular intervals over the storage period.

IV.4.2.4. Sieving of the samples

General procedure ***L*** for sample sieving:

The metal catalyst and the polymeric additive were finely ground and sieved separately on different size sieves (Tamisor or Saulas 224 µm, 149 µm, 100 µm, 50 µm and 42 µm sieves, depending on the targeted particle size) and analyzed by laser diffraction granulometry.

IV.4.2.5. Mimicking the "extrusion" process of the samples

General procedure ***M*** for sample "extrusion":

To stick as close as possible to the real conditions, the extrusion process performed during the industrial production of the material was mimicked in the laboratory. Two different protocols were used:

M1: The mixtures were prepared (metal catalyst alone, polymeric additive alone, and catalyst/additive mixtures (1:35 *w/w*), maintained under inert atmosphere (argon) and heated at 100 °C for 10, 30 or 60 minutes. After this so called "extrusion", they were then exposed to air before reaching r.t.. For this type of experiments, one FTIR measurement was first performed on the freshly prepared samples just before the "extrusion" (designated as Day 0 - initial) and just after the "extrusion" (designated as Day 0). The samples were then stored at r.t. and at 70 °C and analyzed by FTIR at regular intervals over the storage period.

M2: The metal catalyst alone was first kept under inert atmosphere (argon) and heated at 100 °C for 10 minutes. It was then exposed to air before reaching r.t.. The samples were then prepared (metal catalyst alone, polymeric additive alone and catalyst/additive mixtures (1:35 *w/w*)) using the treated catalyst. The samples were stored at r.t. and at 70 °C and analyzed by FTIR once just after "extrusion" process of the catalyst (designated as Day 0) and then at regular intervals over the storage time.

IV.4.2.6. Interpretation of the FTIR data

General procedure ***N*** for infrared data interpretation:

For Dercolyte S 125 (noted **14**) systems, the absorption peak (bending vibrations/scissoring mode δ_{CH}) centered at 1462 cm^{-1} was used as the reference (*i.e.* no variation of this signal whatever the oxidation state of Dercolyte S 125 **14**) and the absorption peak centered at 1715 cm^{-1} (stretching $\gamma_{C=O}$) was used to monitor the oxidation process as a function of time.

For polytetrahydrofuran derivative (namely polyTHF and noted **15**) systems, the absorption peak centered at 726 cm^{-1} (bending vibrations/rocking mode δ_{CH}) was used as the reference (*i.e.* no variation of this signal whatever the oxidation state of polyTHF **15**) and the absorption peak centered at 1715 cm^{-1} (stretching $\gamma_{C=O}$) was used to monitor the oxidation process as a function of time.

Each peak (reference signal and the peak of interest) was integrated thanks to *Spectrum* software from PerkinElmer and the area of the peaks of interest was normalized with respect to the area of the reference peak. The value of the area measured for the peak of interest at day 0 (just after the preparation of the sample) was set to 0. The data were then processed using *Origin* software with the following models: (*i*) mono-exponential (Equation IV-1), (*ii*) mono-exponential with signal drift (Equation IV-2) or (*iii*) bi-exponential (Equation IV-3).

$$y = p_1 + p_2 \exp(-p_3 x)$$

Equation IV-1: Mono-exponential model.

$$y = p_1 + p_2 \exp(-p_3 x) + p_4 x$$

Equation IV-2: Mono-exponential with signal drift model.

$$y = p_1 + p_2 \exp(-p_3 x) + p_4 \exp(-p_5 x)$$

Equation IV-3: Bi-exponential model.

For the comparison purposes, the half-life times of the oxidation reactions ($t_{1/2}$) were calculated as follows (Equation IV-4), where k_{obs} is the first order reaction rate constant, (*i.e.* p_3 parameter in the above models):

$$t_{1/2} = \frac{\ln 2}{k_{obs}} = \frac{\ln 2}{p_3}$$

Equation IV-4: Half-life time calculation (k_{obs}: reaction rate constant).

IV.4.3. Setting up of experiments for Dercolyte S 125 14 oxidation monitored by FTIR

IV.4.3.1. Preliminary experiments with polymeric additives in the presence of metal catalyst

Objectives and means: *this study was conducted to assess the relevance of FTIR technique to monitor the oxidation process of additives (monomeric additive* ***11*** *and polymeric additive* ***14****) and to quantify the process.*

Samples were prepared following the *general procedure* ***K*** with a 1:10 (catalyst/additive *w/w*) ratio. For this study, the selected additives were *N*-(3,3,5,5-tetramethylpiperidin-4-yl)benzamide **11** and Dercolyte S 125 **14**. The chosen metal catalysts were *bis*{2-[[(phenylmethyl)imino]methyl]-phenolato} cobalt(II) **1Co**, *bis*{2-[phenyl[(phenylmethyl)imino]methyl]-5-hydroxy-phenolato} cobalt(II) **2Co-1** (first batch provided by Clariant) and cobalt(II) **9Co-1** and manganese(II) **9Mn-1** stearates.

The combinations that were considered in this work are depicted in Table IV-20. FTIR spectra were recorded at regular intervals on the samples that were stored at r.t. and at 70 °C.

Table IV-20: Different combinations monitored in this study (in italics, period of storage and monitoring)

Catalyst **Additive**	No catalyst	**1Co**	**2Co-1**	**9Co-1**	**9Mn-1**
No additive		√ *40 d*	√ *40 d*	√ *122 d*	√ *122 d*
11	√ *57 d*	√ *57 d*	√ *57 d*	*n.t.*	*n.t.*
14	√ *145 d*	√ *57 d*	√ *57 d*	√ *122 d*	√ *122 d*

n.t.: not tested

IV.4.3.2. Influence of the particle size distribution of the samples

IV.4.3.2.1. Influence of the particle size distribution of the additives

***Objectives and means**: this study was conducted to evaluate the importance of the particle size distribution of a polymeric additive (Dercolyte S 125 **14**) on the oxidation process (kinetics and efficiency of the reaction), the particle size distribution of the metal catalyst (**9Co-2** or **9Mn-2**) being maintained. FTIR analytical technique was privileged in this investigation.*

For this study, only one additive (Dercolyte S 125 **14**) and two metal catalysts (cobalt(II) stearate **9Co-2** and manganese(II) stearate **9Mn-2**) were investigated. The samples were first ground and sieved following the *general procedure **L***. Three different particle size distributions were selected for the polymeric additive Dercolyte S 125 **14** (100-149 µm, 50-100 µm and < 42 µm) and only one for each of the metal catalysts (< 42 µm) that was kept constant for all the prepared combinations with the polymeric additive.

Table IV-21: Granulometry results of the sieved samples.

Sample	**Particle size distribution**	**Gaussian curve max. (µm)**	**d (0.1) (µm)**	**d (0.5) (µm)**	**d (0.9) (µm)**
Dercolyte S 125 **14**	1st	182	108	169	265
	2nd	105	57	92	147
	3rd	30	6.5	18	41
Cobalt(II) stearate **9Co-2**		26	1.3	19	47
Manganese(II) stearate **9Mn-2**		30	8.7	23	50

The different combinations of this study that were tested over 201 days following the *general procedure **K*** are presented in Table IV-22. FTIR spectra were recorded at regular intervals on the samples that were stored at r.t. and at 70 °C.

Table IV-22: Different combinations monitored in this study over 201 days.

Catalyst **Additive**	No catalyst	**9Co-2** (1 particle size)	**9Mn-2** (1 particle size)
No additive		√	√
14 (3 particle sizes)	√	√	√

IV.4.3.2.2. Influence of the particle size distribution of the metal catalyst

Objectives and means: *this study was conducted to evaluate the importance of the particle size distribution of the metal catalyst (**9Co-2** or **9Mn-2**) on the oxidation process (kinetics and efficiency of the reaction), the size distribution of the polymeric additive (Dercolyte S 125 **14**) being kept constant. FTIR analytical techniques was also privileged in this investigation.*

For this study, only one additive (Dercolyte S 125 **14**) and two metal catalysts (cobalt(II) stearate **9Co-2** and manganese(II) stearate **9Mn-2**) were selected. The samples were ground and sieved following the *general procedure **L***. In this case, only one particle size distribution was selected for the polymeric additive Dercolyte S 125 **14** (100-149 µm) and four particle size distributions were prepared for each of the metal catalysts **9Co-2** and **9Mn-2** (100-149 µm, 50-100 µm, 42-50 µm and < 42 µm).

Table IV-23: Granulometry results on the sieved samples.

Sample	Particle size distribution	Gaussian curve max. (µm)	d (0.1) (µm)	d (0.5) (µm)	d (0.9) (µm)
Dercolyte S 125 **14**		138	102	157	244
Cobalt(II) stearate **9Co-2**	1st	158	104	154	228
	2nd	105	58	94	153
	3rd	53	34	51	78
	4th	26	1.3	19	47
Manganese(II) stearate **9Mn-2**	1st	138	8	133	196
	2nd	120	49	82	125
	3rd	60	37	56	86
	4th	30	8.7	23	50

The different combinations tested in this study following the *general procedure **K*** and over a period of 139 days are presented in Table IV-24. FTIR spectra were recorded at regular intervals on the samples that were stored at r.t. and at 70 °C.

Table IV-24: Different combinations monitored in this study over 139 days.

Catalyst **Additive**	No catalyst	**9Co-2** (4 particle sizes)	**9Mn-2** (4 particle sizes)
No additive		√	√
14 (1 particle size)	√	√	√

IV.4.3.3. Influence of the "extrusion" process

IV.4.3.3.1. Influence of the "extrusion" on the metal catalyst/polymeric additive combination

Objectives and means: *to mimic as much as possible the real conditions used for the production of the industrial masterbatches (Clariant), the influence of heating over a short period (so called* "extrusion" *process) on the metal catalyst/polymeric additive mixture was examined. This property was considered with a polymeric additive combined to either cobalt(II) or manganese(II) stearate with predefined particle size distributions and composition. Monitoring the oxidation process by FTIR technique was performed on these mixtures.*

For this study, one polymeric additive (Dercolyte S 125 **14**) and two metal catalysts (cobalt(II) stearate **9Co-2** and manganese(II) stearate **9Mn-2**) were selected. The samples were first ground and sieved following the *general procedure **L***. One particle size distribution was selected for the polymeric additive (Dercolyte S 125 **14**, 100-149 µm) and one particle size distribution was used for each of the metal catalysts (**9Co-2** or **9Mn-2**, < 42 µm).

Table IV-25: Granulometry results on the sieved samples.

Sample	Gaussian curve max. (µm)	d (0.1) (µm)	d (0.5) (µm)	d (0.9) (µm)
Dercolyte S 125 **14**	138	102	157	244
Cobalt(II) stearate **9Co-2**	26	1.3	19	47
Manganese(II) stearate **9Mn-2**	30	8.7	23	50

Combinations involving the metal catalysts (either cobalt(II) stearate **9Co-2** or manganese(II) stearate **9Mn-2**) and the polymeric additive (Dercolyte S 125 **14**) were prepared following the *general procedure **K*** and "extruded" following the *general procedure **M1*** for 10 minutes. The different combinations that were tested in this study over a period of 139 days are described in Table IV-26. FTIR spectra were recorded at regular intervals on the samples that were stored at r.t. and at 70 °C.

Table IV-26: Different combinations monitored in this study over 139 days.

Catalyst Additive	No catalyst	9Co-2	9Mn-2
14	√	√	√

IV.4.3.3.2. Influence of the "extrusion" time on the metal catalyst/polymeric additive combination

Objectives and means: *to mimic as much as possible the real conditions used for the production of the industrial masterbatches (Clariant), the influence of heating on the metal catalyst/polymeric additive mixture over various periods was examined. This property was examined with a polymeric additive combined to either cobalt(II) or manganese(II) stearate with predefined particle size distributions and composition. The oxidation process and subsequent influence of the "extrusion" time were examined by FTIR technique.*

For this investigation, one polymeric additive (Dercolyte S 125 **14**) and two metal catalysts (cobalt(II) stearate **9Co-2** and manganese(II) stearate **9Mn-2**) were employed. Firstly, the samples were ground and sieved following the *general procedure **L***. One particle size distribution was selected for the polymeric additive (Dercolyte S 125 **14**, 100-149 µm) and one particle size distribution was used for each of the metal catalyst **9Co-2** or **9Mn-2**, < 42 µm).

Table IV-27: Granulometry results on the sieved samples.

Sample	Gaussian curve max. (µm)	d (0.1) (µm)	d (0.5) (µm)	d (0.9) (µm)
Dercolyte S 125 **14**	138	102	157	244
Cobalt(II) stearate **9Co-2**	26	1.3	19	47
Manganese(II) stearate **9Mn-2**	30	8.7	23	50

The sample mixtures were prepared following the *general procedure **K*** and "extruded" following the *general procedure **M1*** for 10, 30 or 60 minutes. The different combinations that were tested in this study over a period of 133 days are presented in Table IV-28. FTIR spectra were recorded at regular intervals on the samples that were stored at r.t. and at 70 °C.

Table IV-28: Different combinations monitored in this study over 133 days.

Catalyst / Additive	*"Extrusion"* time (min)	No catalyst	9Co-2	9Mn-2
14	10	√	√	√
	30	√	√	√
	60	√	√	√

IV.4.3.3.3. Influence of the "extrusion" on the metal catalyst

Objectives and means: *to mimic as much as possible the real conditions used for the production of the industrial masterbatches (Clariant), the influence of heating only the metal catalyst over a short period was examined. This property was examined with a polymeric additive combined to either cobalt(II) or manganese(II) stearate with predefined particle size distributions and composition. The oxidation process and subsequent influence of the metal catalyst "extrusion" were examined by FTIR technique.*

Hereafter, one polymeric additive (Dercolyte S 125 **14**) and two metal catalysts (cobalt(II) stearate **9Co-2** and manganese(II) stearate **9Mn-2**) were used. The samples were first ground and sieved following the *general procedure **L***. One particle size distribution was selected for the polymeric additive (Dercolyte S 125 **14**, 100-149 µm) and one particle size distribution was used for each of the metal catalyst as well (**9Co-2** or **9Mn-2**, < 42 µm).

Table IV-29: Granulometry results on the sieved samples.

Sample	Gaussian curve max. (µm)	d (0.1) (µm)	d (0.5) (µm)	d (0.9) (µm)
Dercolyte S 125 **14**	138	102	157	244
Cobalt(II) stearate **9Co-2**	26	1.3	19	47
Manganese(II) stearate **9Mn-2**	30	8.7	23	50

The metal catalyst (**9Co-2** or **9Mn-2**) was first "extruded" for 10 minutes and the mixtures with the untreated polymeric additive (Dercolyte S 125 **14**) were then prepared following the *general procedure **M2***. The different combinations that were tested over a period of 164 days are presented in Table IV-30. FTIR spectra were recorded at regular intervals on the samples stored at r.t. and at 70 °C.

Table IV-30: Different combinations monitored in this study over 164 days.

Catalyst / Additive	9Co-2	9Mn-2
14	√	√

IV.4.3.4. Evaluating whether a coordination of the metal catalyst occurs during the oxidation process with the oxidized polymeric additive or one of its precursors?

Objectives and means: *as the oxidized state of the polymeric additive might contain sites for metal coordination, it was of interest to analyze if any metal binding of the catalyst occurred during the oxidation process. To evaluate this potential property, the polymeric additive was combined to either cobalt(II) or manganese(II) stearate. The composition of the mixture was significantly altered to emphasize whether coordination occurs or not. The oxidation process was examined by FTIR technique with a particular focus on the FTIR absorption of the metal catalyst.*

In this study, one polymeric additive (Dercolyte S 125 **14**) and two metal catalysts (cobalt(II) stearate **9Co-2** and manganese(II) stearate **9Mn-2**) were used. Firstly, the mixtures containing the samples were prepared following the *general procedure* ***K***, without any preliminary sieving. The catalyst/additive *w/w* ratio was varied in this study, thus allowing monitoring more easily the FTIR absorption at 1560 cm^{-1}, that is characteristic of the symmetric stretching of the carboxylate group of the metal catalyst (**9Co-2** or **9Mn-2**) coordinated to the metal ion. The different combinations that were tested in this study over a period of 135 days are presented in Table IV-31. FTIR spectra were recorded at regular intervals on the samples that were stored at r.t. and at 70 °C.

Table IV-31: Different combinations monitored in this study over 135 days.

Catalyst / **Additive**	Catalyst/additive ratio (*w/w*)	**9Co-2**	**9Mn-2**
14	1:1	√	√
	2:1	√	√
	3:1	√	√
	1:2	√	√

IV.4.3.5. Influence of the potential impurities arising from the metal catalyst on the oxidation process

Objectives and means: *the manganese(II) stearate catalyst was found to display a peculiar behavior with respect to its cobalt(II) analogue. It was thus of importance to check if any impurity originating from the metal catalyst might influence the speed and efficiency of the oxidation process. FTIR of manganese(II) stearate indeed clearly demonstrated the presence of free stearic acid which can act as a "polluting" partner. To evaluate this potential property, free stearic acid was intentionally added to the catalyst/additive mixture. A base in the form of calcium oxide was also used to evaluate if it can reverse the deleterious effect of the free stearic acid. The influence of addition of stearic acid and/or calcium oxide was examined by FTIR technique.*

For this study, one polymeric additive (Dercolyte S 125 **14**) and two metal catalysts (cobalt(II) stearate **9Co-2** and manganese(II) stearate **9Mn-2**) were used. As described above, the samples were thinly ground and sieved following the *general procedure* ***L***. One particle size distribution was selected for the polymeric additive (Dercolyte S 125 **14**, 100-149 µm) and one particle size distribution was used for each of the metal catalyst (**9Co-2** or **9Mn-2**, < 42 µm).

Table IV-32: Granulometry results on the sieved samples.

Sample	**Gaussian curve max. (µm)**	**d (0.1) (µm)**	**d (0.5) (µm)**	**d (0.9) (µm)**
Dercolyte S 125 **14**	182	108	169	265
Cobalt(II) stearate **9Co-2**	26	1.3	19	47
Manganese(II) stearate **9Mn-2**	30	8.7	23	50

The sample mixtures were prepared following the *general procedure* ***K***. Particularly, calcium oxide was added to the mixture containing Dercolyte S 125 **14** and manganese(II) stearate **9Mn-2**. On the other hand, stearic acid was added to a mixture made of Dercolyte S 125 **14** and cobalt(II) stearate **9Co-2**. Finally, calcium oxide was added to the Dercolyte S 125 **14** and cobalt(II) stearate **9Co-2** mixture that was previously "polluted" with free stearic acid. The different combinations that were tested in this study over a period of 63 days are presented in Table IV-33. FTIR spectra were recorded at regular intervals on the samples that were stored at r.t. and at 70 °C.

Table IV-33: Different combinations monitored in this study over 63 days.

Catalyst / Additive	9Co-2	9Mn-2	Calcium oxide (base)	Stearic acid	Catalyst/Base/Stearic acid/ Additive ratio
14		√	√		**0.5**:0.5:0:**35**
	√				**1**:0:0:**35**
	√			√	**0.9**:0:0.1:**35**
	√			√	**0.5**:0:0.5:**35**
				√	**0**:0:1:**35**
	√		√	√	**0.45**:0.5:0.05:**35**

IV.4.4. Setting up of experiments for the oxidation of the polytetrahydrofuran derivative (polyTHF) additive 15 monitored by FTIR

IV.4.4.1. Preliminary experiments with the polymeric polyTHF additive in the presence of metal catalyst

Objectives and means: *this study was mainly conducted to assess the relevance of FTIR technique to monitor the oxidation process of the polyTHF additive* ***15*** *in the presence of metal catalysts and to quantify that process.*

One polyTHF polymeric additive (first batch of the polytetrahydrofuran derivative **15-1** provided by Clariant) and three metal catalysts (cobalt(II) stearate **9Co-2** and manganese(II) stearate **9Mn-2** and **9Mn-3**) were considered in this study. The samples were first finely ground and sieved following the *general procedure* ***L***. One particle size distribution was selected for the polymeric additive (polyTHF **15-1**, 149-224 µm) and one particle size distribution was used for each of the metal catalysts (**9Co-2**, **9Mn-2** and **9Mn-3**, < 42 µm). The **9Mn-3** catalyst was re-synthesized in the laboratory and its purity was carefully checked (section II.5.2.2.3).

Table IV-34: Granulometry results on the sieved samples.

Sample	Gaussian curve max. (µm)	d (0.1) (µm)	d (0.5) (µm)	d (0.9) (µm)
PolyTHF **15-1**	169	46	159	325
Cobalt(II) stearate **9Co-2**	26	1.5	19	43
Manganese(II) stearate **9Mn-2**	34	10	27	54
Manganese(II) stearate **9Mn-3**	23	0.5	2.5	33

Different additive/catalyst combinations were investigated in this study following the *general procedure* ***K*** over a short period of 14 days at r.t.. These combinations are depicted Table IV-35. FTIR spectra were recorded at regular intervals.

Table IV-35: Different combinations monitored in this study over 14 days.

Catalyst / Additive	No catalyst	9Co-2	9Mn-2	9Mn-3
15-1	√	√	√	√

IV.4.4.2. Influence of the catalyst/additive ratio on the efficiency and speed of the additive oxidation

Objectives and means: *the aim of this study was to evaluate the appropriate additive/catalyst ratio for fast and efficient oxidation of the polyTHF polymeric additive* ***15*** *in the presence of either cobalt(II) or manganese(II) catalyst. The oxidation process was monitored using FTIR analytical technique.*

Hereafter, one polymeric additive (first batch polyTHF **15-1**) and one metal catalyst (cobalt(II) stearate **9Co-2**) were employed. Firstly, the samples were finely ground and sieved following the *general procedure **L***. One particle size distribution was selected for the polymeric additive (polyTHF **15-1**, 149-224 µm) and one particle size distribution was used for the metal catalyst (**9Co-2**, < 42 µm).

Table IV-36: Granulometry results on the sieved samples.

Sample	Gaussian curve max. (µm)	d (0.1) (µm)	d (0.5) (µm)	d (0.9) (µm)
PolyTHF **15-1**	169	46	159	325
Cobalt(II) stearate **9Co-2**	26	1.5	19	43

The different mixtures were prepared following the *general procedure **K***. Nevertheless, catalyst/additive *w/w* ratios were varied for this study. The different combinations tested in this study for 14 days of storage at r.t. are presented in Table IV-37.

Table IV-37: Different combinations monitored in this study over 14 days.

Catalyst Additive	9Co-2	Catalyst/additive ratio
15-1	√	1:99
	√	1:42.5
	√	1:35
	√	1:9

IV.4.4.3. Influence of the temperature on the oxidation process of the polyTHF additive 15 with or without metal catalyst

Objectives and means: *the study was undertaken to evaluate the effect of the temperature during the storage on the oxidation of the polyTHF polymeric additive in the presence (or in the absence) of either cobalt(II) or manganese(II) stearate catalyst. The oxidation process was monitored by FTIR analytical technique. The temperature was set at 70 °C.*

For this study, one polymeric additive (second batch of polyTHF **15-2**) and three metal catalysts (cobalt(II) stearate **9Co-2** and manganese(II) stearate **9Mn-2** and **9Mn-3**) were considered. The samples were finely ground and sieved following the *general procedure **L***. One particle size distribution was selected for the polymeric additive (polyTHF **15-2**, 149-224 µm) and one particle size distribution for each of the metal catalysts (**9Co-2**, **9Mn-2** and **9Mn-3**, < 42 µm). The **9Mn-3** catalyst was re-synthesized in the laboratory and its purity was carefully checked (section II.5.2.2.3).

Table IV-38: Granulometry results on the sieved samples.

Sample	Gaussian curve max. (µm)	d (0.1) (µm)	d (0.5) (µm)	d (0.9) (µm)
PolyTHF **15-2**	239	149	264	448
Cobalt(II) stearate **9Co-2**	26	1.5	19	43
Manganese(II) stearate **9Mn-2**	34	10	27	54
Manganese(II) stearate **9Mn-3**	23	0.5	2.5	33

Different additive/catalyst combinations were tested following the *general procedure* ***K*** for this study that was carried over 48 days. These data are presented in Table IV-39.

Table IV-39: Different combinations monitored in this study over 48 days.

Catalyst **Additive**	No catalyst	**9Co-2**	**9Mn-2**	**9Mn-3**
15-2	√	√	√	√

IV.4.5. Characterization of the polymeric additives and their oxidation products

Objectives and means: *it was of importance not only to monitor and quantify the oxidation process of the polymeric additives in the absence and in the presence of the metal catalysts, but also to tentatively characterize the structure, nature and oxidation sites of the polymers. This characterization step therefore relies on analytical techniques mainly devoted to solids.*

IV.4.5.1. Characterization of Dercolyte S 125 14 *and its oxidation products*

IV.4.5.1.1. Microanalysis

Microanalyses were performed on the polymeric additive Dercolyte S 125 **14** that was subjected to different storage conditions (Day 0, 10 days and 4.5 months at 70 °C). The results are presented in Table IV-40. The aim of this analysis was mainly focused on the determination of oxygen enrichment of the polymeric additive. For the sake of accuracy and significance, only the sample stored at 70 °C and lacking the metal catalyst was considered.

Table IV-40: Microanalysis results for samples of Dercolyte S 125 ***14****.*

Sample (storage time at 70 °C)		**% C**	**% H**	**% N**
Dercolyte S 125 **14** (0)	*calc*	*88.16*	*11.84*	*0.00*
	found	86.71	11.49	0.00
Dercolyte S 125 **14** (10 days)	*found*	83.90	10.95	0.00
Dercolyte S 125 **14** (4.5 months)	*found*	77.04	9.62	0.00

IV.4.5.1.2. SEC analysis

The SEC analyses were performed on the same three samples (Dercolyte S 125 **14** stored at 70 °C for 0, 10 days and 4.5 months). The results are gathered in Table IV-41. This study was performed to first determine the nature of the polymer and then evaluate the degree of potential cleavage into smaller fragments upon oxidation. This aspect is of crucial importance especially for polymeric additives devoted to food conservation. Here also, only the samples lacking the metal catalysts were considered.

Table IV-41: SEC results for samples of Dercolyte S 125 ***14****.*

Sample (storage time at 70 °C)	$\overline{\mathrm{M}}\mathrm{w}$ (g.mol^{-1})	$\overline{\mathrm{M}}\mathrm{n}$ (g.mol^{-1})	**Đ**
Dercolyte S 125 **14** (0)	2247	1060	2.12
Dercolyte S 125 **14** (10 days)	2199	1124	1.96
Dercolyte S 125 **14** (4.5 months)	1907	1041	1.83

IV.4.5.1.3. XPS

Carbon 1s (Table IV-42) and oxygen 1s (Table IV-43) scans were recorded on two Dercolyte S 125 **14** samples (Day 0 and after 10 months of storage at 70 °C). The initial sample (Day 0) was used as a reference to analyze the sample that was stored at 70 °C over 10 months. This analysis was conducted to determine the nature of the oxidation sites (alcohols, carbonyl, carboxylic…) and contributed to give further insights into the structure and nature of the oxidized compounds of Dercolyte S 125 **14**.

Table IV-42: Carbon 1s scan of Dercolyte S 125 ***14*** *samples – contribution of the day 0 sample (285 eV) and of the C-O characteristic bond (287.1 eV) for the sample stored over 10 months at 70 °C.*

Sample (storage time at 70 °C)	Dercolyte S 125 **14** (Day 0)	**C-O bond** (287.1 eV)
Dercolyte S 125 **14** (10 months)	92%	8%

Table IV-43: Oxygen 1s scan of Dercolyte S 125 ***14*** *samples – contribution of the day 0 sample and of the CO characteristic bonds for the sample stored over 10 months at 70 °C.*

Sample (storage time at 70°C)	Dercolyte S 125 **14** (Day 0)	**C-O-C, COOH, C-OH bonds*** (533.5 eV)	**O=C, O-C=O bonds*** (531.9 eV)
Dercolyte S 125 **14** (10 months)	12%	57%	31%

* not possible to distinguish these types of bonds of C-O or C=O bonds

IV.4.5.1.4. EPR

EPR spectra of two samples were recorded at r.t. and at very low temperature, namely Dercolyte S 125 **14** (Day 0 and after 4 months at 70 °C). The results are gathered in the Table IV-44. This study was performed to test whether the oxidation products of Dercolyte S 125 **14** contain radical sites.

Table IV-44: EPR results for the Dercolyte S 125 ***14*** *samples.*

Sample	**Storage time / temperature**	**Measurement temperature**	**Result**
Dercolyte S 125 **14**	Day 0	r.t.	No signal
	Day 0	4 K	No signal
	4 months/70 °C	r.t.	No signal
	4 months/70 °C	4 K	No signal

IV.4.5.1.5. SEM imaging

SEM analyses were performed on three Dercolyte S 125 **14** samples, namely:

- Dercolyte S 125 **14**, day 0.
- Dercolyte S 125 **14**, after 90 days at 70 °C.
- Dercolyte S 125 **14** + cobalt(II) stearate **9Co-1** (catalyst/additive 1:9 *w/w*), after 67 days at 70 °C.

These SEM measurements were performed on Dercolyte S 125 **14** samples that were not previously sieved before the study. The results are summarized in Table IV-45. The initial aim of this study (*i.e.* that was initiated at the beginning of this Ph.D. thesis) was to get information on the morphology of the polymeric additive material as well as to monitor the oxygen levels at the surface just after the preparation of the sample and after a long period of heating at 70 °C.

Table IV-45: SEM results for the Dercolyte S 125 ***14*** *samples.*

Sample (storage time at 70 °C)	**Morphology**	**Oxygen content (%)**
Dercolyte S 125 **14** (0)	• Not homogeneous sample • Not easy to have information on surface (**14** stores electrons)	~ 3.2%
Dercolyte S 125 **14** (90 days)	Comparable morphology to Dercolyte S 125 **14** (Day 0)	~ 6.4%
Dercolyte S 125 **14** + Co(II) stearate (67 days)	• Not homogeneous sample • Different morphology compared to Dercolyte S 125 **14** alone	~ 6.2%

IV.4.5.1.6. NMR analysis

Two samples of Dercolyte S 125 **14** were analyzed by ^{1}H NMR to characterize the initial sample (day 0) and a sample that was stored at 70 °C over a period of 10 months. The NMR spectra before and after the aerobic treatment of the sample at 70 °C clearly demonstrated that an oxidation process occurred.

NMR Characterization of 14 (Day 0)

^{1}H-NMR (400 MHz, $CDCl_3$) δ (ppm) 0.90 (s), 1.20-2.32 (m), 5.25-5.56 (m)

NMR Characterization of 14 (10 months at 70 °C)

^{1}H-NMR (400 MHz, $CDCl_3$) δ (ppm) 0.87 (s), 1.09-2.29 (m)

IV.4.5.2. Characterization of the polyTHF 15 and its oxidation products

IV.4.5.2.1. Microanalysis

Microanalyses were performed on samples of polyTHF **15-2** that were subjected to different storage conditions (Day 0 and 26 days at 70 °C). The results are depicted in Table IV-46. The aim of this analysis was mainly focused on the determination of oxygen enrichment of the polymeric additive. For the sake of significance, only the sample stored at 70 °C and lacking the metal catalyst was considered.

Table IV-46: Microanalysis results for polyTHF ***15-2*** *samples.*

Sample (storage time at 70 °C)	**% C**	**% H**	**% N**
PolyTHF **15-2** (0)	62.40	7.83	0.00
PolyTHF **15-2** (26 days)	55.89	5.31	0.00

N.B.: even though the patterns that constitute the polyTHF **15-2** are known, the theoretical contents of C, H, N could not be calculated because the composition is unknown.

IV.4.5.2.2. SEC analysis

The SEC analyses were performed on the two samples (PolyTHF **15** stored at 70 °C for 0 and 26 days). The results are gathered in Table IV-41. This study was performed to first determine the nature of the polymer and then evaluate the degree of potential cleavage into smaller fragments upon oxidation. This aspect is of crucial importance especially for polymeric additives devoted to food conservation. Here also, only the samples lacking the metal catalysts were considered.

*Table IV-47: SEC results for samples of PolyTHF **15**.*

Sample (storage time at 70 °C)	$\bar{M}w$ (g.mol^{-1})	$\bar{M}n$ (g.mol^{-1})	Đ
PolyTHF **15** (0)	46 100	18 800	49.8
PolyTHF **15** (26 days)	4 500	2 700	1.6

IV.4.5.2.3. XPS analysis

Carbon 1s (Table IV-48) and oxygen 1s (Table IV-49) scans were recorded on two polyTHF **15-2** samples (Day 0 and after 26 days at 70 °C). The initial sample (Day 0) was used as a reference to analyse the sample that was maintained at 70 °C over 26 days. This analysis was conducted to determine the nature of the oxidation sites (alcohols, carbonyl, carboxylic…) and contributed to give further insights into the structure and nature of the oxidized compounds of polyTHF **15-2**.

*Table IV-48: Carbon 1s scan of the polyTHF **15-2** – contribution of the day 0 sample and of the C-C and O-C=O characteristic bonds for the sample stored over 26 days at 70 °C.*

Sample (storage time at 70 °C)	PolyTHF **15-2** (Day 0)	**C-C bond** (284.8 eV)	**-O-C=O bond** (288.8 eV)
PolyTHF **15-2** (26 days)	68%	17%	15%

*Table IV-49: Oxygen 1s scan of the polyTHF **15-2** – contribution of the day 0 sample and of the CO characteristic bonds for the sample stored over 26 days at 70 °C.*

Sample (storage time at 70 °C)	PolyTHF **15-2** (Day 0)	**C-O-C, COOH, C-OH bonds*** (533.5 eV)	**O=C, O-C=O bonds*** (531.9 eV)
PolyTHF **15-2** (26 days)	27%	31%	42%

* not possible to distinguish these types of bonds

IV.4.5.2.4. NMR analysis

Two samples of polyTHF **15-2** were analyzed by NMR (^{1}H and ^{13}C) to characterize the initial sample (day 0) and a sample that was stored at 70 °C over a period of 26 days. The NMR spectra before and after the aerobic treatment of the sample at 70 °C clearly demonstrated that an oxidation process occurred.

NMR Characterization of 15-2 (Day 0)

^{1}H-NMR (500 MHz, CDCl$_3$) δ (ppm) 1.61 (s), 3.41 (s), 3.64 (d), 3.82-3.88 (m), 4.34-4.37 (m), 4.44-4.51 (m), 4.68 (s), 8.09-8.11 (m)

^{13}C DEPT-NMR (126 MHz, CDCl$_3$) δ (ppm) 25.76, 26.49, 26.65, 63.16, 70.70, 70.76, 129.73, 129.78, 129.87, 133.85, 165.58

NMR Characterization of 15-2 (26 days at 70 °C)

^{1}H-NMR (500 MHz, CDCl$_3$) δ (ppm) 1.25 (m), 1.71 (s), 2.62-2.69 (m), 3.49 (s), 3.65-3.70 (m), 4.12-4.50 (m), 4.69 (s), 8.10 (s)

^{13}C DEPT-NMR (126 MHz, CDCl$_3$) δ (ppm) 25.37, 29.17, 63.19, 129.89, 133.87, 165.6

General conclusion

General conclusion

The main objective of this Ph.D. work was to get a deeper insight into the mechanism of action of oxygen barriers in plastics (*i.e.* composed of metal catalysts and sacrificial additives) for food and drinks preservation.

We have first and foremost investigated the physico-chemical properties of the metal catalysts in solution. Schiff base cobalt(II) and manganese(II) complexes, as well as cobalt(II) and manganese(II) stearates, were selected. The protonation constants and behaviour (*i.e.* stability) of the ligands have been successfully determined by UV-visible absorption spectrophotometry *versus* pH titrations, and have been clearly related to their affinities (*i.e.* determined as well in this work) for the metal centres (*i.e.* cobalt(II)). **1Co** appeared as one of the best promising system for oxygenation and activation. The successful preparation of these Schiff base cobalt(II) complexes was achieved by original synthetic strategies such as a one-pot solvent free synthesis or a “template” approach (*i.e.* synthesis of metallic precursors followed by condensation with benzylamine).

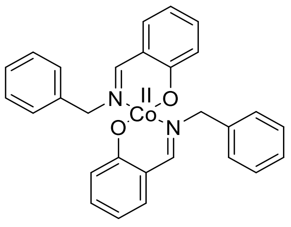

1Co

The oxygenation/activation stages of these metal catalysts were then evaluated by different but complementary analytical tools (*e.g.* UV-visible absorption spectrophotometry, oximetry, ESI-MS, ^{1}H NMR, cyclic voltammetry) to monitor their processes, evaluate their kinetics, and determine the nature of their products. While the methoxy-substituted Schiff base cobalt(II) complex **6Co** displayed the fastest oxygenation/activation in solution, a cobalt(III) trischelate species (*i.e.* inactive catalyst) was formed along the oxygenation/activation stages. These cobalt(III) trischelate species were found to not be anymore active towards oxygen binding. Even though their oxygenation/activation activities were not among the most effective, **2Co** and **9Co** were clearly evidenced to be the most promising systems as a result of the exclusive formation of cobalt(III) bischelates in solution under aerobic conditions.

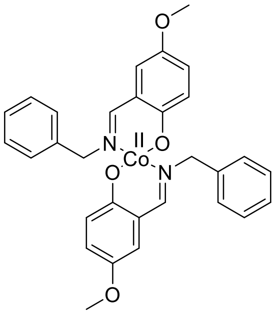

6Co

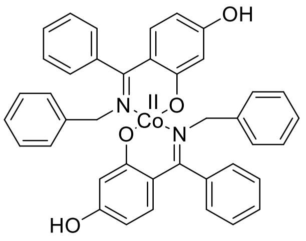

2Co

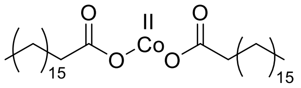

9Co

Following a physico-chemical survey in solution on these metal catalysts, the oxidation of the model organic additives was then assessed in solution by using classical organic oxidants (*e.g.* hydrogen peroxide, *tert*-butylhydroperoxide, *meta*-chloroperoxybenzoic acid), and their oxidation products fully characterized. To get a more definitive assessment of their reactivity in solution, their oxidation kinetic parameters were determined using absorption spectrophotometry. Finally, the oxidation in solution of the best promising organic additive **11** in the presence of one of the two selected cobalt(II) catalysts (**1Co** and **9Co**) was successfully achieved, thus establishing a proof-of-concept of the aerobic oxidation of additives by metal catalysts.

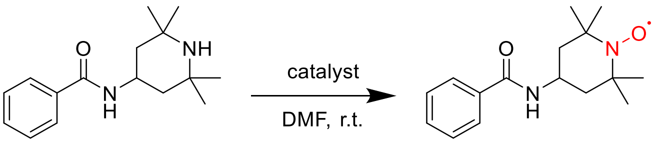

11 **11.ox**

Since the feasibility of the oxidation of the additives in solution by metal catalyst was clearly established, the main objective was then to be as close as possible from the real conditions (*i.e.* plastic films or bottles) and solid-state studies of the oxidation of the additives were undertaken. To monitor properly this oxidation stage, FTIR was found to be a relevant analytical tool. The aerobic (*i.e.* thermal or not) oxidation of two polymeric additives (the homopolymer Dercolyte S 125 **14** and the copolymer **15** designated as PolyTHF) was studied in the presence or in the absence of the metal catalyst under various experimental conditions (*e.g.* influence of the temperature, of the particle size distribution of the catalyst and/or the additive, of the pre-activation of the samples by an "*extrusion*" process, of the purity of the metal catalysts…). In contrast to the polymeric additive Dercolyte S 125 **14**, the copolymeric additive **15** underwent oxidation either at r.t. or at 70 °C. Its oxidation kinetics was found to be much faster with respect to that of **15**, especially when associated with **9Co** at r.t. or at 70 °C.

Last but not least, efforts have also been made on the elucidation of the oxidised products of **14** and **15**. Even a broad spectrum of different but complementary analytical tools were employed (*e.g.* FTIR, elemental analysis, XPS, SEC, NMR), their characterization remained challenging. It has been clearly demonstrated that the homopolymer **14** did not undergo oxidative cleavage even after intensive oxidation. The alkene residue was shown to be likely an important oxidation reaction site. For the highly dispersed copolymer **15**, oxidation catalysed by metal stearates took place at many sites and subsequently led to cleavage and generation of much smaller fragments.

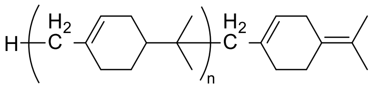

Dercolyte S 125

14

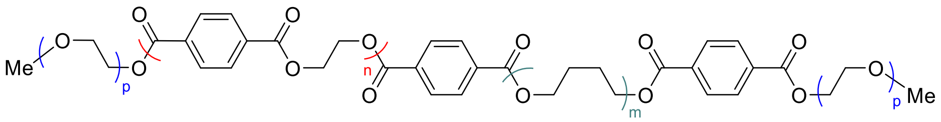

polytetrahydrofuran derivative

15

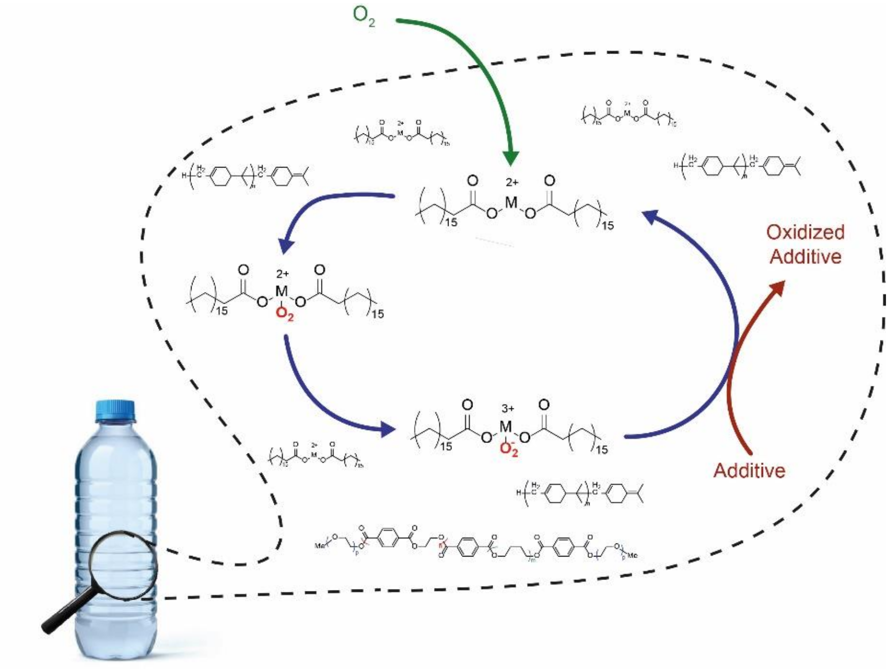

The speed and the effectiveness of the oxidation of the polymeric additives were shown to be highly dependent on the nature of the selected catalysts (*i.e.* **9Co** was found to be more efficient than its manganese(II) analogue **9Mn**). As a result of the different sensitivity to oxygen of food products, optimisation of the catalyst/additive combination and formulation (*i.e.* in terms of selected catalyst, nature of the additive, catalyst/additive ratio….) could meet the specific needs of different types of foodstuffs. As a perspective of this project, an extensive study could be directed to the real conditions (*i.e.* packaging filled of foodstuffs) where the effects of the oxygen barriers could be directly evaluated on food contents displaying a broad spectrum of sensitivity to oxygen (*e.g.* vitamin, lipid, fat, hop…).

List of molecules

List of molecules

Ligands

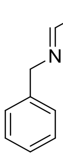

L^1

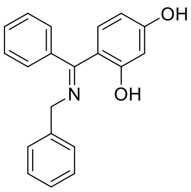

L^2

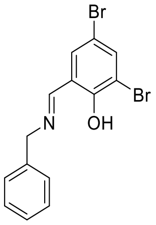

L^3

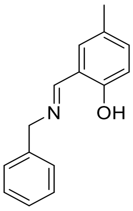

L^4

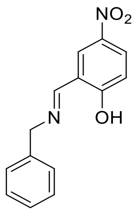

L^5

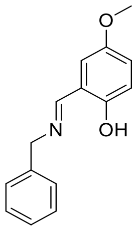

L^6

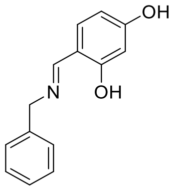

L^7

Cobalt(II) complexes

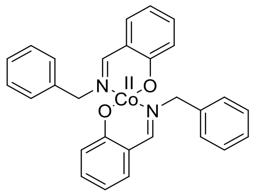

1Co

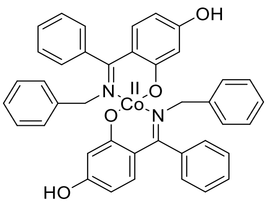

2Co

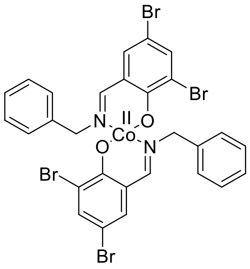

3Co

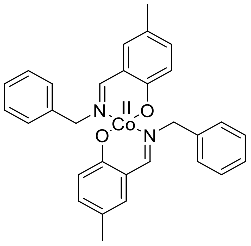

4Co

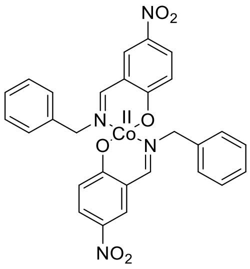

5Co

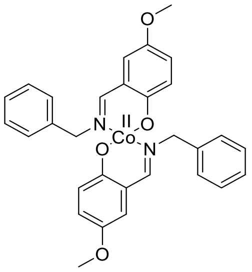

6Co

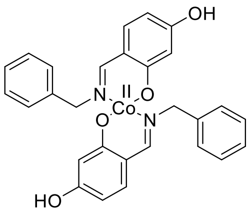

7Co

Cobalt(II) template complexes

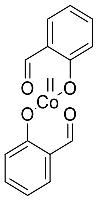

1aCo

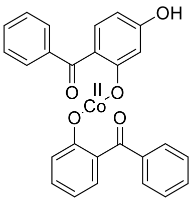

2aCo

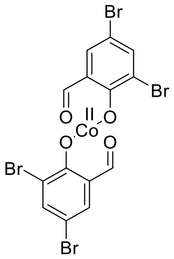

3aCo

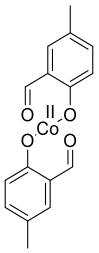

4aCo

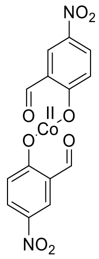

5aCo

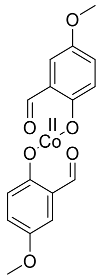

6aCo

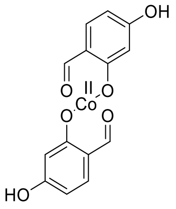

7aCo

Manganese(II) complexes

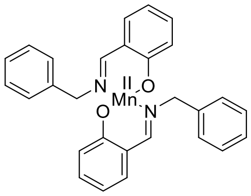

1Mn

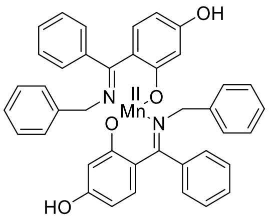
OH
N
II
Mn
O
O
N
HO

2Mn

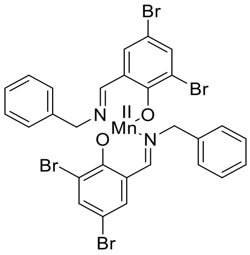
Br
Br
N
II
Mn
O
O
N
Br
Br

3Mn

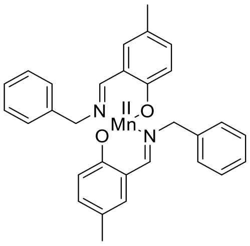

4Mn

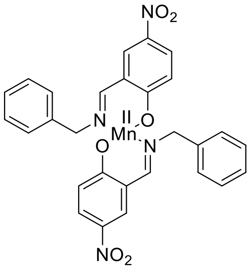
NO2
N
II
Mn
O
O
N
NO2

5Mn

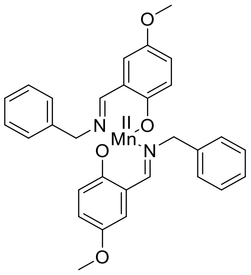
O
N
II
Mn
O
O
N
O

6Mn

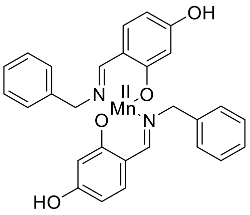
OH
N
II
Mn
O
O
N
HO

7Mn

Manganese(II) template complexes

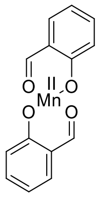

1aMn

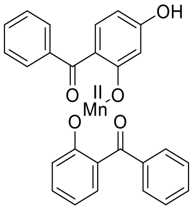
OH
O
II
Mn
O
O
O

2aMn

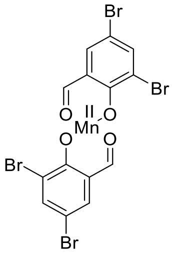
Br
Br
O
II
Mn
O
O
O
Br
Br

3aMn

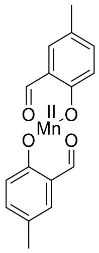

4aMn

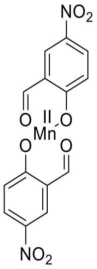
NO2
O
II
Mn
O
O
O
NO2

5aMn

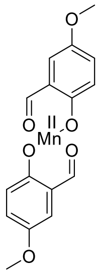
O
O
II
Mn
O
O
O
O

6aMn

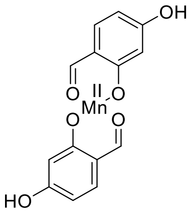
OH
O
II
Mn
O
O
O
HO

7aMn

Commercially available complexes

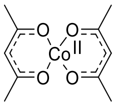

8Co

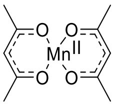

8Mn

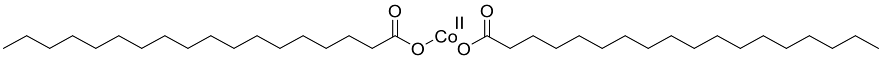

9Co

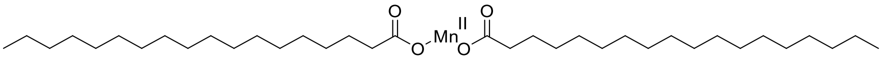

9Mn

Organic Additive Models

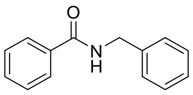

10

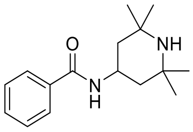

11

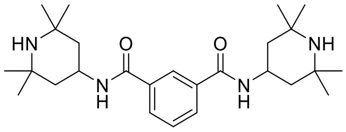

12

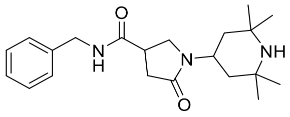

13

Oxidized Organic Additive Models

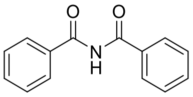

10.ox

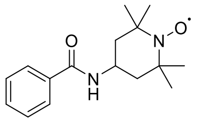

11.ox

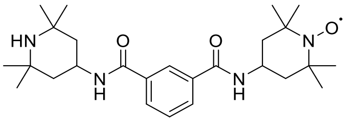

12.ox.a

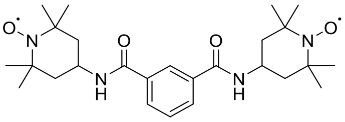

12.ox.b

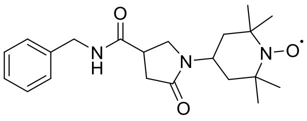

13.ox.a

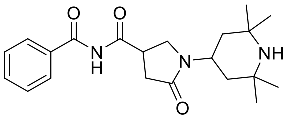

13.ox.b

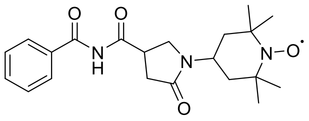

13.ox.c

Polymeric Additives

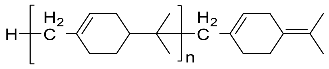

14

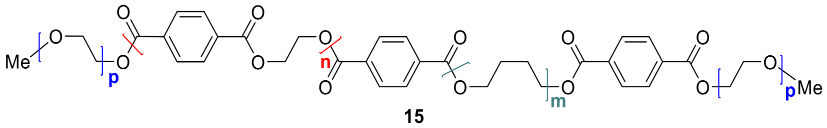

15

UNIVERSITÉ DE STRASBOURG

Angéline CHERBONNEL

CLARIANT

Study of the Mechanism of Action of Metallic Active Oxygen Barriers Applied in Polymers for Food and Drinks Preservation

Résumé

Les plastiques sont devenus les matériaux les plus utilisés pour la préservation de denrées alimentaires. Malgré leurs nombreux avantages (transparence, prix, modularité, propriété barrière aux gaz), leur imperméabilité à l'oxygène doit être sans cesse améliorée afin d'éviter aux denrées de subir diverses réactions d'oxydation et ainsi prolonger leurs durées de conservation. Pour cela, une solution envisageable consiste à combiner à des polymères, des catalyseurs métalliques pour piéger l'oxygène. Cette possibilité a été étudiée dans cette thèse. Après un premier chapitre introductif, le deuxième décrit les propriétés physico-chimiques des différents catalyseurs métalliques sélectionnés (stabilité, constantes de protonation, constante de complexation envers le cobalt(II) et le manganèse (II), capacité d'oxygénation, électrochimie). Le troisième chapitre est consacré à leur utilisation en tant qu'oxydant métallique de substrats organiques. Enfin le quatrième et dernier chapitre présente une étude à l'état solide de l'oxydation de polymères en présence de catalyseurs métalliques. Une large part de ce dernier chapitre a été consacrée à la caractérisation des produits d'oxydation.

Mots clés : **oxygénation, catalyseur métallique, polymère, piégeur à oxygène, physico-chimie, chimie analytique**

Abstract

Plastics are becoming the most used material for food and drinks preservation. Despite their numerous advantages (transparency, price, modularity, gas barrier property), their oxygen barrier properties have to be improved to avoid hazardous oxidation reactions to foods and drinks and so to increase their shelf-life. One alternative to solve this problem is to combine polymers and metal catalysts to scavenge oxygen. This possible strategy was investigated during this Ph.D. project. After a first introductive chapter, the second depicts the physico-chemical properties of selected metal catalysts (stability, protonation constants, complexation constants towards cobalt(II) and manganese(II), oxygenation capacity, electrochemistry). The third chapter is devoted to their use as powerful oxidant of organic substrate. Finally, the last chapter is dedicated to a solid-state study of polymer oxidation in the presence of metal catalysts. A large part of this last chapter has been devoted to the thorough elucidation of the nature/structure of the oxidized product(s).

Key words: **oxygenation, metal catalyst, polymer, oxygen scavenger, physico-chemistry, analytical chemistry**